

https://dspace.org/

Fabrication of Fouling Resistant and Operationally Stable Nanocomposite Membranes for BTEX Wastewater Treatment

Enemuo, Ngozi Doris

2024-11
University of the Witwatersrand, Johannesburg
https://hdl.handle.net/10539/48635

Enemuo, Ngozi Doris. (2024). Fabrication of Fouling Resistant and Operationally Stable Nanocomposite Membranes for BTEX Wastewater Treatment. [PhD thesis, University of the Witwatersrand, Johannesburg]. WIReDSpace. https://hdl.handle.net/10539/48635

Downloaded from a DSpace repository. https://dspace.org/

Fabrication of Fouling Resistant and Operationally Stable Nanocomposite Membranes for BTEX Wastewater Treatment



WITS
UNIVERSITY

Ngozi Doris Enemuo

A Thesis submitted to the Faculty of Science for the degree of Doctor of Philosophy, University of the Witwatersrand, Johannesburg

NOVEMBER 2024

DECLARATION

I declare that this thesis is my own unaided work. It is being submitted for the Degree of Doctor of Philosophy at the University of the Witwatersrand, Johannesburg. It has not been submitted before for any degree or examination at any other University.

Candidate signature:  Date: 20th November 2024

ABSTRACT

This thesis details the fabrication of a fouling-resistant and operationally stable membrane developed for removing BTEX (benzene, toluene, ethylbenzene, and xylene) from wastewater. BTEX is among the top major organic contaminants that have been reported to pollute the aquatic system. BTEX contaminants in the water bodies are detrimental to both humans and aquatic organisms, as exposure to these contaminants could result in mild or severe health complications. With the major source of these contaminants originating from anthropogenic activities, especially the discharge of poorly treated industrial wastewater, it is essential to continuously explore better means of ensuring effective treatment of BTEX-contaminated wastewater before discharge to the environment.

Membrane technology offers a low-cost, easy, and effective approach to removing such organic contaminants from wastewater. However, due to the hydrophobic nature of most membrane materials, there is a high fouling rate during the treatment process as a result of the interaction between the hydrophobic membrane and the hydrophobic organic contaminants. The fouling of the membrane leads to the deterioration of its properties, resulting in a severe decline in membrane performance. Addressing the issue of such membrane fouling is often done through hydrophilic modification, which entails using hydrophilic modifiers to enhance the hydrophilic property of the membrane. Once the membrane's hydrophilicity is enhanced, the interaction between the membrane and the organic contaminants is reduced, thereby minimizing the fouling rate of the membrane during the treatment process and ensuring that the membrane maintains its performance for a longer duration. Therefore, the goal of this study was to fabricate a fouling-resistant membrane by incorporating biogenic-synthesized iron oxide nanoparticles and polyvinyl alcohol (PVA) as hydrophilic modifiers to improve and maintain the membrane performance in the treatment of BTEX-contaminated water.

The first part of the study was to biogenically synthesize the iron oxide using the leaves, peels, and seeds extracts of the pomegranate and compare their properties and contributions in removing BTEX from contaminated wastewater. X-ray diffraction (XRD), Fourier transform infrared (FTIR), scanning electron microscopy (SEM), transmission electron microscopy (TEM), and Brunauer-Emmett-Teller (BET) were used to analyze the properties of the three different biogenic-synthesized iron oxide nanoparticles. The FTIR results showed that there is deposition of hydrophilic functional groups from the extracts to the synthesized nanoparticles, thus establishing that the biogenic-synthesized iron oxide nanoparticles have attached

hydrophilic functional groups, which is beneficial in their use as hydrophilic modifiers. From the FTIR spectra, the iron oxide nanoparticles synthesized using the leaves extract have a more intense peak of the hydrophilic functional groups, such as the -OH group; thus, it was selected as the nanoparticle used for the hydrophilic membrane modification. It was also established that the biogenic-synthesized iron oxide nanoparticles have the capacity to remove BTEX from wastewater, as indicated in the batch adsorption study. The findings of this part of the study are presented in **Paper 1**, which is fully discussed in Chapter 4 of this thesis.

In the second part of the study, the biogenic-synthesized iron oxide nanoparticles (NPs) (from the leaves extract of pomegranate) were blended into a polyvinylidene fluoride (PVDF) membrane, and the optimum blending amount of the NPs required for their optimum dispersion in the membrane was assessed. This was performed by varying the blending amounts of the NPs from 0.05 wt.% to 5.0 wt.%, and the ideal operating parameters were also identified. From the SEM and TEM images, the membrane modified with 1.0 wt.% of the NPs (denoted as PVDF 1.0) has the best dispersion of the NPs in the membrane matrix without agglomeration of the NPs. Among all the fabricated membranes, the PVDF 1.0 also has the lowest water contact angle (WCA) of 52^{o}, the lowest irreversible fouling (R_{ir}) of 18.3%, and the highest flux recovery ratio (FRR) of 81.3%. The PVDF 1.0 also performed better in the reusability test. Based on the properties and performance of PVDF 1.0, the optimum blending amount of the biogenic synthesized NPs in the PVDF membrane, using the fabrication conditions of this study, was established to be 1.0 wt%. The findings of this part of the study are presented in **Paper 2**, which is detailed in Chapter 5 of this thesis.

The third part of the study focused on further enhancing the membrane's hydrophilicity and antifouling ability to ensure its good operational stability under long-term BTEX filtration. This was done by utilizing the synergistic impact of biogenic-synthesized iron oxide NPs and PVA as good hydrophilic modifiers to improve the membrane's hydrophilicity and performance. Biogenic-synthesized NPs and PVA were blended into the membrane, and the properties and performance of the modified membrane were assessed (optimum amount, 1.0 wt% of the biogenic-synthesized NPs, was used as established in the second part of the study, that is, in Chapter 5). The WCA of the modified PVA-Fe_3O_4-PVDF membrane reduced to 40.5^{o}, and the R_{ir} also reduced to 2%, while the FRR increased to 98%. The performance of the membrane under long-term filtration showed that the modified membrane had fairly good operational stability, as the membrane maintained its flux for 84 hour without any significant

decline in flux. The findings of this section of the study are presented in **Paper 3**, which is discussed in Chapter 6 of this thesis.

The fourth part of the study investigated the reproducibility of some of the properties and performance of the modified PVA-Fe_3O_4-PVDF membrane. Ten more of the modified membranes were re-fabricated at different times, and their SEM, BTEX flux and BTEX rejection were analyzed. In terms of the SEM result, seven out of the ten re-fabricated membranes showed good dispersion of the NPs in the membrane matrix. The BTEX flux and rejection of the re-fabricated membrane were also fairly close to the originally reported value in Chapter 6 of this thesis. The findings of this section of the study are detailed in Chapter 7 of this thesis.

DEDICATION

This work is dedicated to my God, family and friends.

ACKNOWLEDGEMENTS

I want to thank my supervisors, Prof. Heidi Richards, Prof. Michael Daramola, and Dr. Lebea Nthunya, for their invaluable support and contributions during this study. Without your guidance, achieving the goals of this study would have been a mirage, and I appreciate the time, ideas, and support you provided, which necessitated the realization of the objectives of this study.

Thanks to the University of the Witwatersrand postgraduate merit funding and the Office of Research and Innovation for the financial support.

To all the staff and students in Environmental and Analytical Chemistry, thank you for your contributions during my progress presentation and the day-to-day discussions. Your suggestions have been beneficial in achieving this study's goals. Thank you also for the enabling and friendly environment you created in the group, which was emotionally rewarding to me during this study.

Lastly, I would like to express my gratitude to my family and friends for their moral and financial support and encouragement. Special thanks to Mr. Chionye Meremikwu, Mr. Emeka Enemuo, Dr. Orevaoghene Eterigho-Ikelegbe, Dr. Christopher Chukwuati, Dr.Onyinye Uwaezuoke, and Mrs. Chinwe Unuigbe for genuinely being my support during the stressful days of this journey. To my lovely kids, Michelle, Chioma, and Raphael, thank you for playing the “grown-up” kids’ role during the many days of my absence at home and when I could not make it home early to give you goodnight kisses. To every other friend and family that is not mentioned, know that you have been a pivotal part of my academic journey, and I am immensely grateful to you all.

PUBLICATION AND MANUSCRIPTS

This thesis is based on the following publication and manuscripts where the candidate was the principal author.

1. Comparative study of biogenic iron oxide nanoparticles from various extracts of pomegranate and their efficient application for removal of BTEX

Authors: Ngozi Enemuo, Heidi Richards, Michael Daramola

Manuscript submitted to the *Journal of Cleaner Production* (Manuscript no: JCLEPRO-D-24-28494)

2. Evaluation of the performance of Fe_3O_4-NPs/PVDF nanocomposite membrane for removal of BTEX from contaminated water

Authors: Ngozi Enemuo, Heidi Richards, Michael Daramola

Published in *Journal of Water Process Engineering* 60 (2024) 105185

https://doi.org/10.1016/j.jwpe.2024.105185

3. Preparation of hydrophilic PVDF membrane via blending with Fe_3O_4 nanoparticles and PVA for improved membrane performance in BTEX removal from wastewater

Authors: Ngozi Enemuo, Heidi Richards, Michael Daramola

Manuscript submitted to the *Journal of Environmental Chemical Engineering* (Manuscript no: JECE-D-24-11739)

CONFERENCE OUTPUTS

Membrane Modified with Biogenic-synthesized Fe_3O_4-NPs for BTEX Wastewater Treatment (3rd Commonwealth Chemistry Posters, virtual conference, 28 – 29 September 2022). Poster presentation

Fabrication of Fouling Resistant and Operationally Stable Nanocomposite Membranes for BTEX Wastewater Treatment (13th International Conference on Membranes and Membrane Processes, Chiba, Japan, 9th – 14th July, 2023). Poster presentation

Rethinking our Roles in Achieving the SDGs: A Case Study of the Biogenic-synthesized Iron Oxide Nanoparticles in BTEX Wastewater Treatment. (International Student Symposium on the Sustainable Development Goals: Implications for People and Planet, UNISA, South Africa, 18th – 19th November 2024). Oral Presentation.

CANDIDATE CONTRIBUTION TO ARTICLES

The principal author conducted the experiments, performed the data analysis, and wrote the first drafts of the published paper and manuscripts included in this thesis. The co-authors contributed to analyzing the data, revised the initial drafts of the articles, made suggestions to improve the articles, and supervised the principal author.

TABLE OF CONTENTS

DECLARATION i
ABSTRACT ii
DEDICATION v
ACKNOWLEDGEMENTS vi
PUBLICATION AND MANUSCRIPTS vii
CONFERENCE OUTPUTS viii
CANDIDATE CONTRIBUTION TO ARTICLES viii
TABLE OF CONTENTS ix
LIST OF FIGURES xiii
LIST OF TABLES xvi
ABBREVIATIONS AND NOMENCLATURE xvii
CHAPTER 1: Introduction 1
1.1 Background and motivation 1
1.2 Research hypothesis and questions 3
1.3 Aim and Objectives 4
1.4 Scope of the study 4
1.5 General approach 5
1.6 Novelty and scientific contribution to knowledge 5
1.7 Thesis layout 6
1.8 References 7
CHAPTER 2: Literature Review 12
2.1 Introduction 12
2.2 BTEX water contamination and treatment techniques 12
2.2.1 Description and physiochemical properties of BTEX 12
2.2.2 Sources of BTEX water contamination 13
2.2.3 Methods for treating BTEX wastewater 16
2.3 Hydrophilic modification of membranes for the treatment of organic-contaminated wastewater 18
2.3.1 Hydrophilic modification of membranes using inorganic nanoparticles 19
2.3.1.1 Biogenic-synthesized nanoparticles for hydrophilic modification of membranes 22
2.3.2 Hydrophilic modification of membranes using hydrophilic polymers 23
2.3.3 Hydrophilic modification using inorganic nanoparticles and hydrophilic polymers 24
2.4 Performance assessment of membranes 28
2.4.1 Membrane Flux 28

2.4.2 Membrane selectivity 29
2.4.3 Membrane anti-fouling tendency 30
2.5 References 31
CHAPTER 3: Materials and Experimental Procedures 46
3.1 Biosynthesis of iron oxide NPs 46
3.2 Fabrication of the Fe_3O_4 NPs and Fe_3O_4 NPs/PVA-modified membranes 46
3.3 Iron oxide NPs and membrane characterization 46
3.3.1 PXRD 46
3.3.2 FTIR 47
3.3.3 SEM 48
3.3.4 TEM 48
3.4 Membrane performance assessment 49
3.5 References 49
CHAPTER 4: Comparative study of biogenic iron oxide nanoparticles from various extracts of pomegranate and their efficient application for removal of BTEX 51
Abstract 51
4.1 Introduction 52
4.2 Experimental 54
4.2.1 Materials 54
4.2.2 Preparation of the extracts of the pomegranate 54
4.2.3 Synthesis of the Iron oxide NPs 55
4.3 Characterization of the pomegranate extracts and iron oxide NPs 56
4.4 Batch adsorption experiments 58
4.5 Results and discussion 59
4.5.1 Characterization of the pomegranate extracts 59
4.5.2 Characterization of the various iron oxide NPs 61
4.5.2.1 Powder X-ray Diffraction (PXRD) results 61
4.5.2.2 Chemical composition analysis 61
4.5.2.3 Morphological characterization 64
4.5.2.4 Textural properties of the FeNPs 64
4.5.2.5 Zeta potential results 66
4.5.3 BTEX adsorption study 67
4.5.3.1 Effect of solution pH on BTEX adsorption 67
4.5.3.2 Effect of adsorbent dosage 69
4.5.3.3 Effect of contact time and adsorption kinetics 71
4.5.3.4 Effect of initial concentration and adsorption isotherms 76

4.5.4 Possible adsorption mechanism 82
4.5.5 Regeneration of the biogenic-synthesized FeNPs 84
4.6 Conclusion 85
4.7 References 86
Chapter 5: Evaluation of the performance of Fe_3O_4-NPs/PVDF nanocomposite membrane for removal of BTEX from contaminated water 94
Abstract 94
5.1 Introduction 95
5.2 Experimental 97
5.2.1 Materials 97
5.2.2 Synthesis of Fe_3O_4-NPs 98
5.2.3 Fabrication of Fe_3O_4-NPs/PVDF membranes 98
5.3 Characterization of the leaves extract, Fe_3O_4-NPs, and the membranes 99
5.4 Membrane performance evaluation 100
5.5 Results and discussion 102
5.5.1 Phytochemical composition of the pomegranate leaf extract and characterization of the biosynthesized Fe_3O_4-NPs 102
5.5.2 Characterization of Fe_3O_4-NPs/PVDF membrane 109
5.5.3 Membrane performance evaluation 119
5.5.3.1 Pure water and BTEX permeation performance 119
5.5.3.2 BTEX removal from synthetic BTEX water 121
5.5.3.3 Antifouling and reusability study 124
5.6 Comparison with literature 126
5.7 Conclusion 127
5.8 References 127
Chapter 6: Preparation of hydrophilic PVDF membrane via blending with Fe_3O_4 nanoparticles and PVA for improved membrane performance in BTEX removal from wastewater 138
Abstract 138
6.1 Introduction 139
6.2 Experimental 143
6.2.1 Materials 143
6.2.2 Preparation of the hydrophilic-modified membrane 143
6.3 Characterization of the membrane 144
6.4 Membrane performance evaluation 145
6.5 Results and discussion 147
6.5.1 Fe_3O_4-NPs characterization 147

6.5.2 Membrane chemical composition 148
6.5.3 Membrane morphology 149
6.5.4 Membrane hydrophilicity, equilibrium water content, and porosity. 152
6.5.5 Membrane surface charge, thermal and mechanical stability 153
6.5.6 Permeance flux, separation, and antifouling performance of the membrane 156
6.5.7 Crossflow filtration performance 158
6.5.8 Stability of the modifiers in the membrane matrix 161
6.6 Comparison with similar studies 163
6.7 Conclusion 163
6.8 References 164
Chapter 7: Reproducibility study 174
7.1 Reproducibility studies of the properties and performance of the PVA-Fe_3O_4-PVDF membrane 174
CHAPTER 8: Conclusions and Recommendations 179
8.1 General conclusions 179
8.2 Recommendations 180
Appendix 181

LIST OF FIGURES

Figure 2. 1: Structure of the four compounds of BTEX. 13
Figure 2. 2: Typical example of petroleum leakage into the aquatic system (EPA, 2018). ... 14
Figure 2. 3: Typical industrial discharge of oil wastewater. (Available online at: https://cleanwater.org/publications/report-clean-water-act-regulation-oil-and-gas-wastewater-discharges) 15
Figure 2. 4: Depiction of adsorption of BTEX using carbon nanotubes (CNTs). (Anjum et al., 2019) 17
Figure 2. 5: Antifouling mechanism through hydration layer effect (Jhaveri & Murthy, 2016). 19
Figure 2. 6: Methods of incorporating inorganic nanoparticles into a membrane (Esfahani et al., 2019) 21
Figure 2. 7: Typical biosynthesis of NPs (Bhardwaj et al., 2020). 23
Figure 2. 8: Structure of some hydrophilic polymers showing their hydrophilic functional groups. 24
Figure 2. 9: Schematic depiction of dead-end and cross-flow filtration process (Paipuri, 2014). 29
Figure 2. 10: Schematic depiction of some of the membrane separation mechanisms (H. Zhang et al., 2022). 30
Figure 2. 11: Images of cleaned and fouled membrane (Dardor et al., 2021). 31
Figure 3. 1: Schematic representation of X-ray mechanism (ARPANSA, 2015)..... 47
Figure 3. 2: Schematic representation of FTIR mechanism (Bruker, 2019)..... 47
Figure 3. 3: Schematic depiction of the principle of SEM (SubsTech, 2015). 48
Figure 3. 4: Schematic depiction of the TEM principle. 49
Figure 4. 1: The experimental procedure for the synthesis of the iron oxide NPs. 56
Figure 4. 2: The prepared standards and pomegranate extracts for total phenolic content measurements. 58
Figure 4. 3: GC-MS chromatograms of the pomegranate leaves, peels, and seeds extract. ... 60
Figure 4. 4: (a,b,c) XRD patterns of the FeNPs, and (d,e,f) FTIR spectra of the FeNPs and the pomegranate extracts. 63
Figure 4. 5: SEM and TEM image of the FeNPs. 65

Figure 4. 6: The N_2 adsorption-desorption isotherms and pore size distributions (inset) of the FeNPs. 66
Figure 4. 7: Zeta potential of the FeNPs. 67
Figure 4. 8: Effect of solution pH on BTEX adsorption onto the FeNPs. 69
Figure 4. 9: Effect of FeNPs dosage on benzene adsorption. 70
Figure 4. 10: Linear fit for the pseudo-first-order kinetic model for BTEX adsorption on FeNPs. 73
Figure 4. 11: (a, b, c, d) Effect of contact time on BTEX adsorption on the FeNPs, and (e, f, g, h) their respective linear fit for pseudo-second-order kinetic model. 74
Figure 4. 12: (a, b, c, d) Effect of BTEX initial concentration on their adsorption on the FeNPs, and (e, f, g, h) their subsequent linear fit for Langmuir isotherm model. 80
Figure 4. 13: The linear fit of Freundlich isotherm model for BTEX adsorption on FeNPs. . 80
Figure 4. 14: Schematic diagram of the possible adsorption mechanism of BTEX on the FeNPs. 83
Figure 4. 15: Regeneration of the various FeNPs in BTEX adsorption. 85
Figure 5. 1: GC-MS chromatogram of the pomegranate leaves extract. 103
Figure 5. 2: (a) XRD pattern, (b) FTIR spectra, (c) SEM image, (d) TEM image, and (e) N_2 adsorption-desorption isotherm and pore size distribution (inset) of the Fe_3O_4-NPs. 108
Figure 5. 3: XPS spectra of the Fe 2p core level. 109
Figure 5. 4: The images of the PSF and PVDF membranes after exposure to BTEX solutions. PSF exposed to BTEX concentration of (a) 500 ppm, (b) 1000 ppm, and (c) 2000 ppm. PVDF exposed to BTEX concentration of (d) 500 ppm, (e) 1000 ppm, and (f) 2000 ppm..... 110
Figure 5. 5: SEM images of the before and after-exposure of PSF and PVDF membrane to BTEX solution. 110
Figure 5. 6: FTIR spectra of the fabricated membranes 112
Figure 5. 7: Cross-section SEM images of fabricated membranes with their respective EDX mapping images. 114
Figure 5. 8: Surface roughness images of the membranes. 115
Figure 5. 9: (a) Contact angle values as a function of the Fe_3O_4-NPs loadings and (b) zeta potential of the tested membranes..... 116
Figure 5. 10: (a) Stress-strain curves, and (b) TGA curves of the tested membranes. 119
Figure 5. 11: (a) Pure water flux and (b) BTEX flux of the tested membranes. 121
Figure 5. 12: Effect of TMP on the BTEX rejection of the membranes at (a) 100 kPa, (b) 300 kPa, and (c) 500 kPa. 123

Figure 5. 13: Effect of BTEX concentrations on membranes' rejection capacity. 124
Figure 5. 14: (a) fouling resistance of the membranes, (b) Fluctuation of the flux of pure water and BTEX water over time. 126
Figure 6. 1: The outcome of BTEX exposure of PES and PVDF membrane depicted by (a, d) photographs, (b, e) SEM image of membrane top surface, and (c, f) SEM image of membrane cross-section. 148
Figure 6. 2: FTIR spectra of PVDF, PVA, and PVA-Fe_3O_4-PVDF. 149
Figure 6. 3: SEM image of the (a) surface of pristine PVDF, (b) inner structure of pristine PVDF, (c) surface of PVA-Fe_3O_4-PVDF, (d) EDX mapping image of PVA-Fe_3O_4-PVDF, and the inner structure of PVA-Fe_3O_4-PVDF at magnification (e) 2.00 KX, (f) 10.00KX, (g) 40.00KX, and (h) 190.74KX. 151
Figure 6. 4: AFM images of the (a) pristine PVDF membrane, and (b) PVA-Fe_3O_4-PVDF membrane. 152
Figure 6. 5: (a) WCA, and (b) EWC and porosity of the pristine PVDF and PVA-Fe_3O_4-PVDF membrane. 152
Figure 6. 6: (a) surface zeta potentials, (b) TGA curves, and (c) stress-strain curves of the pristine PVDF and PVA-Fe_3O_4-PVDF membrane. 155
Figure 6. 7: (a) Permeate fluxes, (b) BTEX rejections, and (c) fouling ratios and cleaning efficiency of the membranes. 157
Figure 6. 8: Variation of (a) pure water flux, and (b) BTEX flux during the long-term filtration tests. 159
Figure 6. 9: Variation of the rejection of (a) benzene, (b) toluene, (c) ethylbenzene, and (d) xylene over long-term crossflow filtration. 160
Figure 6. 10: Reusability of the membrane. 161
Figure 6. 11: (a) SEM image, and (b) FTIR spectrum of the PVA-Fe_3O_4-PVDF membrane after long-term filtration test. 162
Figure 7. 1: The SEM image of the inner structure of the membranes shows the dispersion of the Fe_3O_4-NPs in the membrane matrix. 177

LIST OF TABLES

Table 2. 1: Some physical and chemical properties of the BTEX compounds. 13
Table 2. 2: Allowed levels of BTEX in water. 16
Table 2. 3: Studies on hydrophilic membrane modification using inorganic nanoparticles and hydrophilic polymers 26
Table 4. 1: Effect of FeNPs dosage on toluene, ethylbenzene, and xylene adsorption. 71
Table 4. 2: Kinetic pseudo-first and pseudo-second-order parameters of BTEX adsorption by the FeNPs. 76
Table 4. 3: Langmuir and Freundlich isotherm parameters of BTEX adsorption by the FeNPs. 80
Table 4. 4: Comparison of the adsorption capacities of various iron/iron oxide nanoparticles adsorbents in BTEX adsorption. 82
Table 5. 1: Some of the active phytochemicals in the pomegranate leaves extract with their compound name, retention time (R_T), and structure…….. 103
Table 5. 2: Composition of the fabricated membranes. 111
Table 5. 3: The thickness, porosity, EWC, and mean pore size of all the fabricated membranes. 117
Table 5. 4: Comparison of the performance of the Fe_3O_4-NPs/PVDF membrane with other studies in the literature 127
Table 6. 1: Comparison of the performance of the PVA-Fe_3O_4-PVDF membrane with other similar studies in the literature. 163
Table 7. 1: The reproducibility of the performance of the membranes 178

ABBREVIATIONS AND NOMENCLATURE

AFM	Atomic force microscopy
BET	Brunauer-Emmett-Teller
BSA	Bovine serum albumin
BTEX	Benzene, toluene, ethylbenzene, xylene
COD	Chemical oxygen demand
EDX	Energy-dispersive X-ray
FeNPs	Iron oxide nanoparticles
FTIR	Fourier transform infrared
GAE	gallic acid equivalents
GC-MS	Gas chromatography-mass spectroscopy
HA	Humic acid
NMP	N-Methyl-2-pyrrolidone
NPs	Nanoparticles
PAA	Polyacrylic acid
PEG	Polyethylene glycol
PEGMA	Poly(ethylene glycol)methyl ether methacrylate
PES	Polyethersulfone
PFO	Pseudo-first-order
PS	Polysulfone
PSO	Pseudo-second-order
PVA	Polyvinyl alcohol
PVDF	Polyvinylidene fluoride
PXRD	Powder X-ray diffraction

SEM	Scanning electron microscopy
TDS	Total dissolved solids
TEM	Transmission electron microscopy
VOCs	Volatile organic compounds
XPS	X-ray photoelectron spectroscopy

CHAPTER 1: Introduction

1.1 Background and motivation

The persistent global issue of the pollution of water bodies and contamination of usable water sources has intensified the need for continuous research on the control or mitigation of water pollution and contamination (Bastos et al., 2021; Schweitzer & Noblet, 2018). Water contaminants are mostly organic, inorganic, biological, and particulate matter; and are released into the water bodies through natural or anthropogenic activities (Madhav et al., 2020; Chin, 2012). Of most concern are the growing cases of contaminants in water bodies directly linked to various anthropogenic activities (Wang & Yang, 2016; Morin-Crini et al., 2022; Minnaar, 2020). The major sources of these contaminations are industrial discharge, used domestic products, agricultural and mining activities, power generation, and many more (Perk, 2013; Wang et al., 2019; Fayiga et al., 2018). For organic contaminants, industries play a major role in their high levels in water bodies by discharging untreated or poorly treated wastewater into the water bodies (Jones, 2013). According to the United Nations Environmental Program, one-seventh of the rivers in Africa, Asia, and Latin America are affected by grave organic pollution, which has been escalating for years (UNEP, 2020). The issue of organic pollution, specifically petroleum-based pollutant, has been reported in South Africa (Adeniji et al., 2017). Among the top organic contaminants found in water bodies are benzene, toluene, ethylbenzene, and xylene, collectively known as BTEX (Yu et al., 2022a). There are various means through which BTEX can be released into the water bodies, but the major source of release is the industrial discharge of petroleum-produced wastewater (Chen et al., 2022; Dórea et al., 2007; Shores et al., 2017). Exposure to BTEX-contaminated water can have severe health implications, including cancer, neurological complications, and reproductive health issues (USEPA, 2007). In addition, the presence of BTEX in the water bodies reduces the water quality and even the air quality through their volatilization from the water bodies to the surrounding atmosphere (Shores et al., 2017). With BTEX water contaminations arising from anthropogenic activities being on the increase (Thanigaivel et al., 2023), it is important to continuously develop ways of treating wastewater before discharge into water bodies.

Treatment methods such as advanced oxidative process (Bustillo-Lecompte et al., 2018; Jiménez et al., 2019), adsorption (Farsouni Eydi et al., 2019; Sobczyk et al., 2023), and membrane technology (Zha et al., 2015; Su et al., 2016) have been applied to remove BTEX from wastewater or contaminated water bodies. Among these conventional treatment methods,

membrane technology remains the most effective and efficient due to its good rejection of BTEX contaminants, ease of use, low cost, and ease of membrane fabrication, among others (Padaki et al., 2015; Younis et al., 2020; Zhang et al., 2019). The other BTEX wastewater treatment methods either are energy or cost-intensive or result in secondary pollution (Eke et al., 2007; Rawindran et al., 2017; Simões et al., 2020). Hence, membrane technology is presented as a viable treatment technique for the removal of BTEX from wastewater (Fayemiwo et al., 2017; Stefanakis, 2020). While membrane technology is a promising alternative for treating BTEX-contaminated wastewater, its usage is limited by the hydrophobic nature of most membrane materials (Younis et]al., 2020). With the membrane being hydrophobic, there is a strong interaction between the BTEX organic contaminant and the membrane, which leads to the fast accumulation of the contaminant on the membrane and, consequently, the fouling of the membrane (Zha et al., 2015). Hence, the application of membrane technology for BTEX removal usually involves hydrophilic modification of the membrane to minimize membrane fouling and maintain good membrane performance (Zha et al., 2015).

Very few studies have reported the hydrophilic modification of membrane for improved membrane performance in BTEX removal from wastewater. An internet search of previous studies on hydrophilic modification of membranes for BTEX removal from wastewater shows that there are a total of three studies that have been reported (Zha et al., 2015; Unuigbe et al., 2020; Makhani et al., 2022). Zha et al., (2015) utilized a hydrophilic polymer, cellulose acetate butyrate (CAB), to modify a polyethersulfone (PES) membrane for BTEX separation from produced wastewater. The PES/CAB membrane achieved a BTEX rejection of 84.6%, however, the antifouling test of the membrane performed between 0-5 hrs showed a significant decline in the BTEX flux, indicating severe fouling of the membrane under short-term filtration (Zha et al., 2015). Another hydrophilic modifier, tannin iron complex (TA-Fe^{III}), was used to improve the hydrophilicity and performance of the membrane, and a high BTEX removal of 93% was obtained (Makhani et al., 2022). However, the study did not provide any information on the antifouling performance of the membrane; hence effect of the TA-Fe^{III} in maintaining the membrane performance could not be ascertained (Makhani et al., 2022). Iron oxide nanoparticles were utilized by Unuigbe et al., (2020) to improve the performance of a PES membrane in treating BTEX-contaminated wastewater, and a BTEX rejection of 64.55% was obtained. The study also did not provide any information on the antifouling behaviour of the

membrane; hence the membrane's ability to maintain its performance due to the hydrophilic additive could not be ascertained.

Owing to the very limited studies on the hydrophilic modification of membranes for the treatment of BTEX-contaminated wastewater, it is important that new hydrophilic modifiers are explored for this purpose. The limited antifouling ability of the reported hydrophilic modified membranes in BTEX wastewater treatment necessitates the need to develop hydrophilic modified membranes with good antifouling ability under short-term and long-term applications. The health and environmental consequences of BTEX contamination of water bodies also highlight the need to develop membranes that have good potential to remove BTEX from wastewater before discharge.

This study explored the use of biogenic-synthesized iron oxide NPs as a hydrophilic modifier for membranes to remove BTEX from contaminated wastewater. Pomegranate extracts were used for the biosynthesis, and hydrophilic functional groups from the plant extract were deposited on the iron oxide NPs, thus enhancing their hydrophilic nature and improving the antifouling ability of the membrane modified with the NPs. To achieve even more enhanced antifouling performance, the synergistic impact of biogenic-synthesized iron oxide NPs and PVA were harnessed to improve the membrane performance under long-term filtration of BTEX wastewater. Thus, the blending of the two hydrophilic modifiers, that is, biogenic-synthesized iron oxide NPs and PVA, into the membrane was utilized to significantly improve the antifouling ability of the membrane and achieve good operational stability in terms of its long-term usage.

1.2 Research hypothesis and questions

The postulation of the following hypothesis led to the commencement of this study; 'blending biogenic-synthesized iron oxide NPs and PVA into a PVDF membrane enhances the membrane's hydrophilicity, reduces its fouling tendency and improves its long-term performance in BTEX removal'. This is inferred from the fact that making the membrane hydrophilic reduces the interaction between the membrane and the BTEX contaminants, and the two modifiers are highly hydrophilic materials. During the biosynthesis, hydrophilic functional groups such as the hydroxyl group are deposited on the biogenic-synthesized iron oxide NPs, which further enhances their hydrophilicity, thereby making it an ideal modifier for membrane modification. It was anticipated that the synergistic impact of the biogenic-

synthesized NPs and PVA would provide the membrane with improved properties that would enable the membrane to maintain its performance for a longer period.

This hypothesis led to the establishment of the following research question: Can an iron oxide nanocomposite membrane with high integrity and reproducibility be fabricated to remove BTEX from wastewater?

1.3 Aim and Objectives

The study aimed to fabricate antifouling and operationally stable membranes using biogenic-synthesized Fe_3O_4-NPs and PVA as the hydrophilic modifiers for the treatment of BTEX-contaminated wastewater. This was achieved by addressing the following objectives:

- Comparison of the biogenic synthesis of iron oxide nanoparticles using different parts of pomegranate and determining their contribution to BTEX removal from wastewater, as well as their subsequent use in PVDF modification.
- Fabricate fouling-resistant Fe_3O_4-NPs nanocomposite membranes and evaluate their performance in the removal of BTEX from wastewater.
- Investigate the synergistic impact of using biogenic-synthesized Fe_3O_4-NPs and PVA to achieve a high improvement in the antifouling and operational stability of membrane in treating BTEX-contaminated wastewater.
- Investigate the reproducibility of the reported features and performance of the PVA-Fe_3O_4-PVDF membranes by repeating the fabrication process and the performance analysis.

1.4 Scope of the study

The scope of this study was centered on developing an antifouling membrane for BTEX removal by first biogenically synthesizing one of the hydrophilic modifiers, that is, iron oxide NPs, and establishing its potential for BTEX removal. The biogenic-synthesized NPs and PVA were then blended into the membrane and fabricated via non-solvent-induced phase inversion. This was intended to reduce the hydrophobic-hydrophobic interaction between the BTEX organic contaminants and the membrane, thereby reducing its rapid fouling and ensuring its long-term improved performance. The modified membrane was applied in the removal of BTEX from synthetic wastewater in both dead-end filtration cell and cross-flow filtration setup.

The performance of the membrane under long-term filtration was assessed for 120 hours, and extending the duration of the BTEX filtration was not possible as we were granted limited access to the cross-flow filtration setup used for the test. However, the long-term filtration

results give a good indication of the membrane's ability to maintain its performance for a longer period of time.

1.5 General approach

First, the biogenic synthesis of iron oxide using the leaves, peels, and seeds extracts of the pomegranate was compared to determine their various physical properties and contribution to BTEX removal from wastewater. A report of this study was presented in **Paper 1**, which has been submitted to the Journal of Cleaner Production for evaluation and publication.

The optimum amount of the biogenic-synthesized Fe_3O_4-NPs for the PVDF membrane modification was established by fabricating the PVDF membranes using various amounts of the Fe_3O_4-NPs. The nanocomposite membranes were applied to remove BTEX from synthetic BTEX wastewater, and the membrane with the best Fe_3O_4 dispersion and performance was selected as the optimum membrane. This part of the study was reported in **Paper 2**, published in the Journal of Water Process Engineering.

The hydrophilicity of the optimum nanocomposite membrane was further enhanced by incorporating PVA into the membrane to further improve its antifouling ability and achieve operational stability during the treatment of BTEX wastewater. Performance tests were done under short-term and long-term durations, and the results of this part of the study were reported in **Paper 3**, which has been submitted to Separation and Purification Technology for evaluation and publication.

The reproducibility of the modified membrane was established by re-fabricating the membranes at different times and comparing their features and performance in BTEX wastewater treatment. This part of the study is reported in Chapter 7 of this thesis.

1.6 Novelty and scientific contribution to knowledge

The study aimed to contribute to addressing the issue of BTEX water contamination through the development of an effective treatment approach for BTEX removal from contaminated wastewater. In light of the limited study on the hydrophilic modification of membranes for BTEX wastewater treatment, this study presented a novel approach to harnessing the synergistic impact of biogenic-synthesized iron oxide NPs and PVA in developing a hydrophilic membrane with good antifouling behaviour and improved filtration performance in BTEX wastewater treatment.

This study achieved the well-dispersion of the biogenic-synthesized iron oxide NPs in the membrane matrix, thereby solving the problem of agglomeration reported in previous studies that utilized iron oxide NPs in membrane modification. The contribution of the biogenic-synthesized iron oxide to BTEX removal was assessed, thereby, for the first time, providing a comparative study on the potential of the biogenic-synthesized iron oxide NPs to remove BTEX from wastewater. The fabricated PVA-Fe_3O_4-PVDF membrane has high antifouling performance towards BTEX compared to other reported studies on BTEX treatment using membranes, and the membrane also exhibited fairly good performance during long-term crossflow filtration experiments. These attributes of the fabricated membrane highlight it as a membrane that can withstand fouling during its commercial use in the treatment of real BTEX-contaminated wastewater.

Therefore, the study can provide insights to other researchers on the effective utilization of biogenic-synthesized iron oxide NPs in membrane modification to remove several other organic contaminants from wastewater. Commercialization of the membrane may be feasible due to the fact that the membrane can withstand fouling for a considerable filtration duration, thereby contributing to providing solutions to properly remove BTEX from industrial wastewater before discharge to the water bodies.

1.7 Thesis layout

The thesis is presented as follows:

Chapter 1 introduces the prime aspects of the study, including the background and motivation, research hypothesis and questions, aims and objectives, the scope of the study, general approach, and novelty and scientific contribution to new knowledge.

Chapter 2 presents a short review of the previous studies reported on BTEX water contamination and treatment techniques. It also discusses the hydrophilic modification of membranes for the removal of organic contaminants such as BTEX from wastewater and the potential of biogenic-synthesized Fe_3O_4 NPs and PVA as hydrophilic modifiers in membranes.

Chapter 3 provides a short description of the materials and methods employed in this study; however, the corresponding articles in chapters 4, 5, and 6 provide detailed discussions of the materials and methods. Some of the characterization techniques are also briefly discussed.

Chapter 4 includes the reports presented in Paper 1 of this study which details the initial investigation of the potential of biogenic-synthesized iron oxide nanoparticles in BTEX removal from wastewater.

Chapter 5 presents the study and results reported in Paper 2 of this study which discussed the fabrication and performance assessment of Fe_3O_4-NPs/PVDF membrane in BTEX wastewater treatment.

Chapter 6 presents Paper 3 of this study which details the enhancement of the antifouling and operational stability of a PVDF membrane using biogenic-synthesized Fe_3O_4-NPs and PVA.

Chapter 7 is composed of the reproducibility study of some of the properties and performance of the modified membrane.

Chapter 8 outlines the conclusions derived from conducting this study, and the suggested future recommendations are also presented.

References

Bastos, M. I., Roebeling, P. C., Alves, F. L., & Villasante, S. (2021). *Water Pollution Threatening Marine, Coastal and Estuarine Systems: A Review of Environmental-Economic Approaches for the Assessment of Development Strategies*. 135–147. https://doi.org/10.2495/DMAN210111

Bustillo-Lecompte, C. F., Kakar, D., & Mehrvar, M. (2018). Photochemical treatment of benzene, toluene, ethylbenzene, and xylenes (BTEX) in aqueous solutions using advanced oxidation processes: Towards a cleaner production in the petroleum refining and petrochemical industries. *Journal of Cleaner Production*, *186*, 609–617. https://doi.org/10.1016/j.jclepro.2018.03.135

Chen, X., Sheng, Y., Wang, G., Guo, L., Zhang, H., Zhang, F., Yang, T., Huang, D., Han, X., & Zhou, L. (2022). Microbial compositional and functional traits of BTEX and salinity co-contaminated shallow groundwater by produced water. *Water Research*, *215*, 118277. https://doi.org/10.1016/j.watres.2022.118277

Chin, D. A. (2012). *Water-Quality Engineering in Natural Systems: Fate and Transport Processes in the Water Environment*. John Wiley & Sons.

Dórea, H. S., Bispo, J. R. L., Aragão, K. A. S., Cunha, B. B., Navickiene, S., Alves, J. P. H., Romão, L. P. C., & Garcia, C. A. B. (2007). Analysis of BTEX, PAHs and metals in the oilfield

produced water in the State of Sergipe, Brazil. *Microchemical Journal*, *85*(2), 234–238. https://doi.org/10.1016/j.microc.2006.06.002

Eke, P. E., Scholz, M., & Wallace, S. D. (2007). *Constructed Treatment Wetlands: Innovative Technology for Petroleum Industry*. SPE Annual Technical Conference and Exhibition. https://doi.org/10.2118/113644-STU

Enemuo, N., Richards, H., & Daramola, M. O. (2024). Evaluation of the performance of Fe3O4-NPs/PVDF nanocomposite membrane for removal of BTEX from contaminated water. *Journal of Water Process Engineering*, *60*, 105185. https://doi.org/10.1016/j.jwpe.2024.105185

Farsouni Eydi, E., Shariati, A., & Khosravi-Nikou, M. R. (2019). Separation of BTEX compounds (benzene, toluene, ethylbenzene and xylenes) from aqueous solutions using adsorption process. *Journal of Dispersion Science and Technology*, *40*(3), 453–463. https://doi.org/10.1080/01932691.2018.1472007

Fayemiwo, O., Moothi, K., & Daramola, M. (2017). BTEX compounds in water – future trends and directions for water treatment. *Water SA*, *43*(4), 602–613. https://doi.org/10.4314/wsa.v43i4.08

Fayiga, A. O., Ipinmoroti, M. O., & Chirenje, T. (2018). Environmental pollution in Africa. *Environment, Development and Sustainability*, *20*(1), 41–73. https://doi.org/10.1007/s10668-016-9894-4

Jiménez, S., Andreozzi, M., Micó, M. M., Álvarez, M. G., & Contreras, S. (2019). Produced water treatment by advanced oxidation processes. *Science of The Total Environment*, *666*, 12–21. https://doi.org/10.1016/j.scitotenv.2019.02.128

Jones, K. C. (2013). *Organic Contaminants in the Environment: Environmental Pathways & Effects*. Springer Science & Business Media.

Madhav, S., Ahamad, A., Singh, A. K., Kushawaha, J., Chauhan, J. S., Sharma, S., & Singh, P. (2020). Water Pollutants: Sources and Impact on the Environment and Human Health. In D. Pooja, P. Kumar, P. Singh, & S. Patil (Eds.), *Sensors in Water Pollutants Monitoring: Role of Material* (pp. 43–62). Springer. https://doi.org/10.1007/978-981-15-0671-0_4

Makhani, T., Sadare, O. O., Wagenaar, S., Moothi, K., Moutloali, R. M., & Daramola, M. O. (2022). Fabrication and performance evaluation of tannin iron complex (TA-FeIII/PES) UF membrane in treatment of BTEX wastewater. *Water SA*, *48*(4), Article 4.

Minnaar, A. (2020). Water Pollution and Contamination from Gold Mines: Acid Mine Drainage in Gauteng Province, South Africa. In K. Eman, G. Meško, L. Segato, & M. Migliorini (Eds.), *Water, Governance, and Crime Issues* (pp. 193–219). Springer International Publishing. https://doi.org/10.1007/978-3-030-44798-4_12

Morin-Crini, N., Lichtfouse, E., Liu, G., Balaram, V., Ribeiro, A. R. L., Lu, Z., Stock, F., Carmona, E., Teixeira, M. R., Picos-Corrales, L. A., Moreno-Piraján, J. C., Giraldo, L., Li, C., Pandey, A., Hocquet, D., Torri, G., & Crini, G. (2022). Worldwide cases of water pollution by emerging contaminants: A review. *Environmental Chemistry Letters*, *20*(4), 2311–2338. https://doi.org/10.1007/s10311-022-01447-4

Padaki, M., Surya Murali, R., Abdullah, M. S., Misdan, N., Moslehyani, A., Kassim, M. A., Hilal, N., & Ismail, A. F. (2015). Membrane technology enhancement in oil–water separation. A review. *Desalination*, *357*, 197–207. https://doi.org/10.1016/j.desal.2014.11.023

Perk, M. van der. (2013). *Soil and Water Contamination, 2nd Edition*. CRC Press.

Rawindran, H., Krishnan, S., & Sinnathambi, C. M. (2017). A Review on overboard CEOR discharged produced water treatment and remediation. *IOP Conference Series: Materials Science and Engineering*, *206*(1), 012086. https://doi.org/10.1088/1757-899X/206/1/012086

Schweitzer, L., & Noblet, J. (2018). Chapter 3.6—Water Contamination and Pollution. In B. Török & T. Dransfield (Eds.), *Green Chemistry* (pp. 261–290). Elsevier. https://doi.org/10.1016/B978-0-12-809270-5.00011-X

Shores, A., Laituri, M., & Butters, G. (2017). Produced Water Surface Spills and the Risk for BTEX and Naphthalene Groundwater Contamination. *Water, Air, & Soil Pollution*, *228*(11), 435. https://doi.org/10.1007/s11270-017-3618-8

Simões, A., Macêdo-Júnior, R., Santos, B., Silva, L., Silva, D., & Ruzene, D. (2020). Produced Water: An overview of treatment technologies. *International Journal for Innovation Education and Research*, *8*, 207–224. https://doi.org/10.31686/ijier.vol8.iss4.2283

Sobczyk, M., Muir, B., Skalny, M., Panek, R., Matusik, J., & Bajda, T. (2023). Fly ash-based zeolitic materials of different surface chemistry and texture: Insight into adsorption

performance and mechanisms of aqueous BTEX removal. *Journal of Environmental Chemical Engineering*, *11*(6), 111220. https://doi.org/10.1016/j.jece.2023.111220

Stefanakis, A. I. (2020). The Fate of MTBE and BTEX in Constructed Wetlands. *Applied Sciences*, *10*(1), Article 1. https://doi.org/10.3390/app10010127

Su, F., Lu, C., & Tai, J.-H. (2016). Separation of Benzene, Toluene, Ethylbenzene and P-Xylene from Aqueous Solutions by Carbon Nanotubes/Polyvinylidene Fluoride Nanocomposite Membrane. *Journal of Water Resource and Protection*, *8*(10), Article 10. https://doi.org/10.4236/jwarp.2016.810075

Thanigaivel, S., Vickram, S., Dey, N., Jeyanthi, P., Subbaiya, R., Kim, W., Govarthanan, M., & Karmegam, N. (2023). Ecological disturbances and abundance of anthropogenic pollutants in the aquatic ecosystem: Critical review of impact assessment on the aquatic animals. *Chemosphere*, *313*, 137475. https://doi.org/10.1016/j.chemosphere.2022.137475

UNEP. (2020). *UNEP*. Beat Pollution. http://www.unep.org/beatpollution/forms-pollution/freshwater

Unuigbe, C. F., Fayemiwo, O. M., & Daramola, M. O. (2020). Performance evaluation of iron nanoparticles infused polyethersulphone (Fe-NPs/PES) membrane during treatment of BTEX-contaminated wastewater. *Water and Environment Journal*, *34*(S1), 74–86. https://doi.org/10.1111/wej.12506

USEPA. (2023). *U.S. Environmental Protection Agency | US EPA*. https://www.epa.gov/

Wang, P., Yao, J., Wang, G., Hao, F., Shrestha, S., Xue, B., Xie, G., & Peng, Y. (2019). Exploring the application of artificial intelligence technology for identification of water pollution characteristics and tracing the source of water quality pollutants. *Science of The Total Environment*, *693*, 133440. https://doi.org/10.1016/j.scitotenv.2019.07.246

Wang, Q., & Yang, Z. (2016). Industrial water pollution, water environment treatment, and health risks in China. *Environmental Pollution*, *218*, 358–365. https://doi.org/10.1016/j.envpol.2016.07.011

Younis, S. A., Maitlo, H. A., Lee, J., & Kim, K.-H. (2020). Nanotechnology-based sorption and membrane technologies for the treatment of petroleum-based pollutants in natural ecosystems and wastewater streams. *Advances in Colloid and Interface Science*, *275*, 102071. https://doi.org/10.1016/j.cis.2019.102071

Yu, B., Yuan, Z., Yu, Z., & Xue-song, F. (2022). BTEX in the environment: An update on sources, fate, distribution, pretreatment, analysis, and removal techniques. *Chemical Engineering Journal*, *435*, 134825. https://doi.org/10.1016/j.cej.2022.134825

Zha, S., Yu, J., Zhang, G., Liu, N., & Lee, R. (2015). Polyethersulfone (PES)/cellulose acetate butyrate (CAB) composite hollow fiber membranes for BTEX separation from produced water. *RSC Advances*, *5*(128), 105692–105698. https://doi.org/10.1039/C5RA21185A

Zhang, Z., Du, X., Carlson, K. H., Robbins, C. A., & Tong, T. (2019). Effective treatment of shale oil and gas produced water by membrane distillation coupled with precipitative softening and walnut shell filtration. *Desalination*, *454*, 82–90. https://doi.org/10.1016/j.desal.2018.12.011

CHAPTER 2: Literature Review

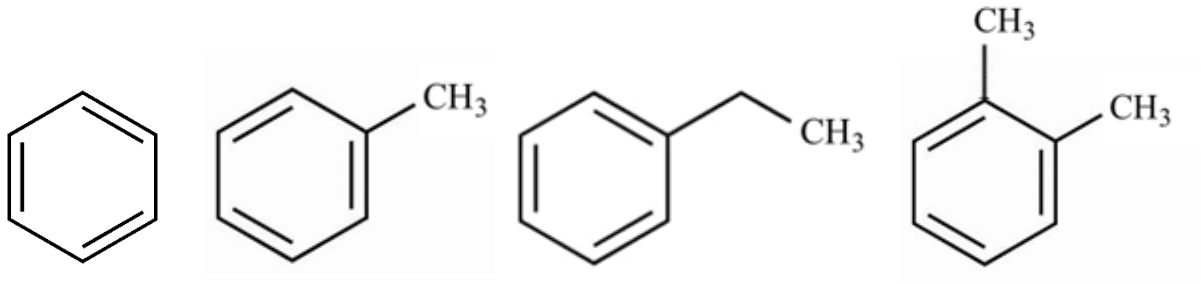
2.1 Introduction

This chapter reviews the literature on BTEX water contamination, including BTEX physiochemical properties, main sources of BTEX water contamination, and BTEX wastewater treatment techniques. It also discusses the hydrophilic modification of membranes as an approach to improving the membranes' antifouling tendency and maintaining their performance in the treatment of organic-contaminated wastewater.

2.2 BTEX water contamination and treatment techniques

2.2.1 Description and physiochemical properties of BTEX

Benzene, toluene, ethylbenzene, and xylene, collectively known as BTEX, are among the top representatives of volatile organic compounds (VOCs) and are major organic water contaminants of main concern (Yu et al., 2022a). As depicted in Figure 2.1, BTEX components are aromatic hydrocarbons that exist as liquids at room temperature (Liden et al., 2018). BTEX has moderate solubility in water (Alberici et al., 2002), and has been found in concentrations as high as 1000 mg/L in water bodies (Su et al., 2010). As monoaromatic hydrocarbons, BTEX has low boiling points (boiling points of BTEX are 80.1 ^{o}C, 110.6 ^{o}C, 136 ^{o}C, and 139^{o}C respectively), which makes them very volatile and, consequently, amplifies the chances of BTEX pollution of the atmosphere (Atamaleki et al., 2021). Thus, the threat of BTEX pollution is not limited to the aquatic environment but extends to the atmosphere (Duan. and Li, 2017). BTEX are also very toxic chemicals, and as a result, exposure to a BTEX-contaminated environment has associated health implications (USGS, 2006). In addition, BTEX contaminants can be transported by water and wind from one place to another and from one medium to another (US EPA, 2014). Moreover, BTEX can persist for a prolonged period in the environment, hence they are classified as persistent organic contaminants (Delzer, 1996; Varjani et al., 2017). Table 2.1 shows some of the physical and chemical properties of the BTEX compounds. Due to their physiochemical properties, which foster their accumulation in the environment, proper management of the sources of BTEX contamination is important to mitigate their presence in the environment, especially in the aquatic system.



Benzene Toluene Ethylbenzene Xylene

Figure 2. 1: Structure of the four compounds of BTEX.

Table 2. 1: Some physical and chemical properties of the BTEX compounds.

Parameters	Benzene	Toluene	Ethylbenzene	Xylene
Chemical formula	C_6H_6	$C_6H_5CH_3$	$C_6H_5CH_2CH_3$	$C_6H_4(CH_3)_2$
Polarity	Non-polar	Non-polar	Non-polar	Non-polar
Molecular weight (g/mol)	78.12	92.15	106.18	106.18
Density (g/mL)	0.876	0.867	0.867	0.868
Boiling point (°C)	80	111	136	138.5
Vapour pressure (25°C) (mmHg)	95	30	10	7
Solubility in water (20°C) (mg/L)	1780	500	150	150
Log k_{ow}	2.13	2.73	3.15	3.12

2.2.2 Sources of BTEX water contamination

BTEX can be released into the water bodies through natural and anthropogenic mediums (Duan & Li, 2017). Natural gas and petroleum deposits are the top natural ways by which BTEX is gradually released into the aquatic system (Delzer, 1996). Although natural sources contribute to the persistent occurrence of BTEX in the aquatic system, the BTEX contamination arising from anthropogenic is of most concern as there are high levels of contamination due to human activities (Yu et al., 2022a). Among the anthropogenic sources of BTEX contamination of the water bodies, petroleum-based contamination remains the major source of contamination (Duan & Li, 2017). Two of the key sources of such petroleum-based BTEX contamination are

petroleum leakage and petroleum-produced water discharge (Mohammadi et al., 2020; Duan & Li, 2017).

2.2.2.1 Petroleum leakage

Among the major composition of petroleum is BTEX. Unintended leakage of petroleum to the aquatic system constitutes high levels of BTEX in the water bodies (Liu et al., 2018). These leakages can occur due to poor storage of underground tankers, surface spills, and pipe leakage (Mohammadi et al., 2020). Many cases of petroleum oil spills, for instance, have been reported over the past years and have continued till the present time (Vanloocke et al., 1975; Overton et al., 2016; Li et al., 2023). On arrival of the petroleum leakages in the water bodies, some of constitutes evaporate into the atmosphere, while some reside or dissolve into the water thereby releasing BTEX as one of the contaminants. A typical example of petroleum leakage into the water body is shown in Fig. 2.2.

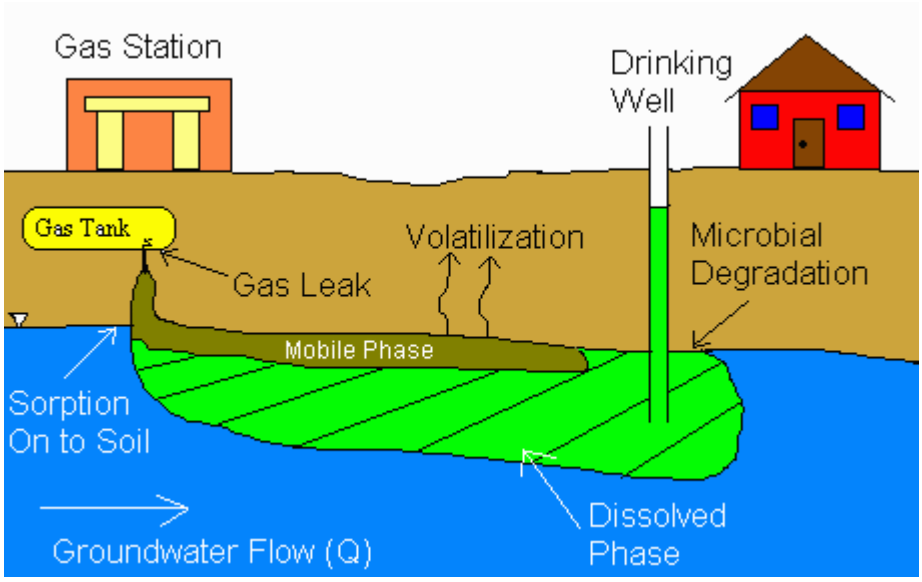


Figure 2. 2: Typical example of petroleum leakage into the aquatic system (EPA, 2018).

2.2.2.2 Petroleum-produced water discharge

The discharge of poorly treated petroleum-produced wastewater has been a constant threat to the pollution of the aquatic system (Ibiebele, 1986; Rozell & Reaven, 2012; Eldos et al., 2022). Fig. 2.3 depicts a typical discharge of petroleum-produced water discharge. With the consistent rise in the global human population, the demand for oil and petroleum-based products has been on the increase. This exacerbates the water pollution threats associated with the discharge of petroleum-based wastewater since more wastewater is generated from the growing industrial

activities. The incidence of petroleum-based pollution has been reported in South Africa and the country's rapid industrialization is contributing to such cases of water pollution (Adeniji et al., 2017). Most worrisome is the persistent cases of BTEX contamination often reported in the water bodies due to industrial discharge. For instance, in 2007, very high levels of BTEX were detected in the Houjing River of Taiwan, and one of the sources of the contamination was reported to be a nearby oil refinery (Lin et al., 2007). Eleven years later, Lee et al., (2018) measured the BTEX concentration of the same river and found high amounts of BTEX whose source was linked to industrial activities. Such repetitive cases of BTEX contamination call for more measures to address the issue of BTEX water contamination as exposure to BTEX has health and environmental adverse effects. Such health and environmental implications of BTEX exposure include cancer, neurological complications, reproductive issues, and poor air quality (Davidson et al., 2021; Sirotkin & Harrath, 2017). Measures such as regulation of BTEX levels in the aquatic systems have been stipulated by various authorities to curtail and control the pollution of water bodies by BTEX-contaminated wastewater. Table 2.2 shows the allowed levels of BTEX in both usable water and water bodies as regulated by the various authorities. The WHO, for instance, recommended the allowed levels of BTEX to be 10ppb, 700ppb, 300ppb, and 500ppb respectively (WHO, 2008). In addition, many techniques have also been developed for the removal or recovery of BTEX wastewater before discharge.



Figure 2. 3: Typical industrial discharge of oil wastewater. (Available online at: https://cleanwater.org/publications/report-clean-water-act-regulation-oil-and-gas-wastewater-discharges)

Table 2. 2: Allowed levels of BTEX in water

	WHO DWG[1] (ppb)	US NPDWS[2] (ppb)	ANZECC[3] (ppb)	ADWG[4] (ppb)
Benzene	10	5	600	1
Toluene	700	1000	180	800
Ethylbenzene	300	700	50	300
Xylene	500	10000	200	600

1. World Health Organisation Drinking Water Guidelines (WHO 2008); 2. United States National Primary Drinking Water Standards (USEPA 2003); 3. Australian and New Zealand Environment Conservation Council Environmental Protection Guidelines (ANZECC 2000), and 4. Australian Drinking Water Guidelines (NHMRC 2004).

2.2.3 Methods for treating BTEX wastewater

Various techniques have been developed to remove BTEX from wastewater before discharge. This includes advanced oxidation process (Bustillo-Lecompte et al., 2018b), adsorption (Anjum et al., 2019), and membrane technology (Unuigbe et al., 2020a). These techniques present potential solutions for addressing the issue of BTEX contamination of the aquatic system, however, they have associated disadvantages that limit their application in the treatment of BTEX-contaminated wastewater.

2.2.3.1 Advanced oxidation process

This process involves the degradation of the contaminants by in situ-generated reactive species, which facilitates the transformation of the contaminants to less toxic or non-toxic form and their mineralization, thereby resulting in their removal from the wastewater (Bustillo-Lecompte et al., 2018b). Bahmani et al., (2014) utilized UV/H_2O_2 in an advanced oxidation process to remove BTEX from contaminated water, and high BTEX removal efficiency was obtained. Hydroxyl and sulfate radical-based advanced oxidation process was also used to successfully degrade a significant amount of BTEX from wastewater (Fernandes et al., 2019). The degradation of BTEX using this process is often fast, however, the process is characterized by the high cost of the chemicals often used for the process, high energy consumption, and complex equipment (Rayaroth et al., 2023). In addition, the process sometimes generates toxic intermediates, which are usually more harmful than the BTEX (Rayaroth et al., 2023).

2.2.3.2 Adsorption

Removal of BTEX using the adsorption process is facilitated by the physicochemical surface interaction between the BTEX and the adsorbent material (Gusain et al., 2019). In this process, the contaminant gradually adsorbs on the adsorbent material through chemisorption or physisorption (Uddin et al., 2021). In chemisorption, the contaminant is adsorbed on the adsorbent through chemical interaction between the contaminant and the adsorbent material, while physical interaction such as Van der Waals and hydrogen bonding necessitates physisorption (Rasheed et al., 2020).

Many studies have been conducted using adsorption to remove BTEX from wastewater. Melaphi et al., (2023) successfully removed a significant amount of BTEX from wastewater by adsorbing the BTEX on activated carbon derived from macadamia nut shells. Another adsorbent material, ZSM-5 zeolite, was used to adsorb BTEX, and the BTEX detection limit was reduced as a result of being adsorbed on the ZSM-5 zeolite adsorbent (Megías-Sayago et al., 2020).

Using adsorption for the removal of BTEX from wastewater has many advantages, such as being relatively inexpensive, ease of application, and effective BTEX removal (Anjum et al., 2019). However, the adsorbents are rapidly filled with the BTEX, reducing their effectiveness in long-term use (Bina et al., 2014). Moreover, the regeneration of the adsorbent material is sometimes difficult, especially when the BTEX is adsorbed through chemisorption (Anjum et al., 2019). A typical adsorption of BTEX unto a nanomaterial is shown in Fig. 2.4.

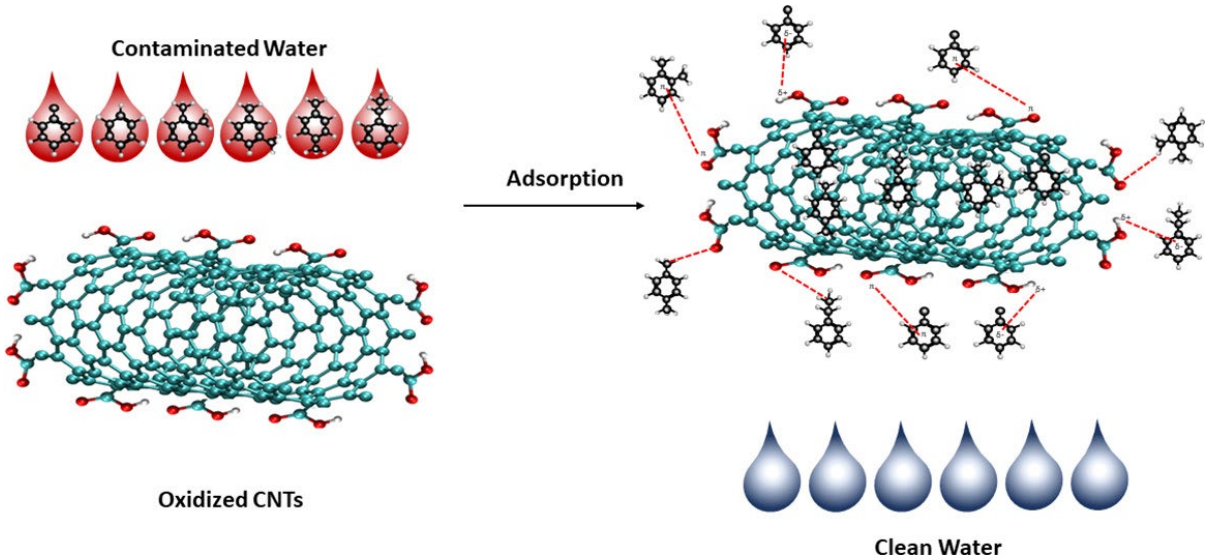


Figure 2. 4: Depiction of adsorption of BTEX using carbon nanotubes (CNTs). (Anjum et al., 2019)

2.2.3.3 Membrane technology

Among the treatment techniques, membrane technology has been established as a reliable and feasible approach for wastewater treatment due to its low cost, low energy requirement, high rejection of target contaminants, ease of membrane fabrication and application, and easy availability of membrane materials (Goh et al., 2020). Because of these attributes, membrane technology has gained much attention as a preferred treatment technique for the removal of organic contaminants from wastewater (Isawi, 2019; Zambianchi et al., 2017; Kim et al., 2018). The use of membrane technology in wastewater treatment involves applying a membrane acting as a barrier that prevents contaminants from passing through them while allowing water passage through the membrane (Ahmed et al., 2022). The principle of membrane separation is identical to that of the cell walls in the human body (Bishnoi, 2023). Membrane materials utilized for the separation can be polymeric or ceramic, and polymeric materials are mostly used because they are less costly and easier to fabricate (Warsinger et al., 2018).

The membrane materials for the fabrication of the membranes are mainly hydrophobic, and such materials are usually polymeric materials which include PS, PES, and PVDF (Singh & Hankins, 2016; Basile et al., 2015). For the treatment of organic-contaminated wastewater, the hydrophobic nature of the membranes enhances the hydrophobic interaction between the membrane and the organic contaminants resulting in the rapid accumulation of the contaminants on the membrane (Khanzada et al., 2020a). This causes fouling of the membrane and consequently reduces the membrane performance in the treatment of the wastewater (Khanzada et al., 2020a). Thus, for the removal of organic contaminants such as BTEX from wastewater using membrane technology, hydrophilic modification of the membrane is required to mitigate membrane fouling and achieve improved membrane performance (Subasi & Cicek, 2017).

2.3 Hydrophilic modification of membranes for the treatment of organic-contaminated wastewater

The aim of hydrophilic modification of membranes for the removal of organic contaminants is mainly to improve the fouling resistance of the membrane by suppressing the non-specific interaction of the contaminants and the membrane. This prevents the contaminants from attaching to the membrane, and as a result, membrane fouling is reduced while membrane performance is improved as depicted in Fig. 2.5 (Zhang et al., 2016a).

Various approaches are employed to improve the hydrophilicity of membranes for application in the removal of organic contaminants such as BTEX from wastewater (Ismail et al., 2020; Liu et al., 2011; Kochkodan & Hilal, 2015). One such approach is the blending of hydrophilic modifiers into the membrane (Kang & Cao, 2014). The hydrophilic modifiers are broadly categorized into two classes: inorganic nanoparticles and hydrophilic polymers (Kang & Cao, 2014). These hydrophilic modifiers possess hydrophilic properties that are transferred into the membrane, thereby enhancing the membrane hydrophilicity and subsequent reduction in membrane fouling (Akram et al., 2018). There are different mechanisms by which the fouling reduction is achieved, through (1) low-surface-energy effect which occurs via repelling the foulant by reducing interaction intensity. (2) active interaction/reaction effect, which occurs via foulant oxidation by decomposing the accumulated foulant, and (3) hydration layer effect, which occurs via preventing direct contact of foulant and membrane by the formation of hydration layer on the membrane surface (Zhao et al., 2018).

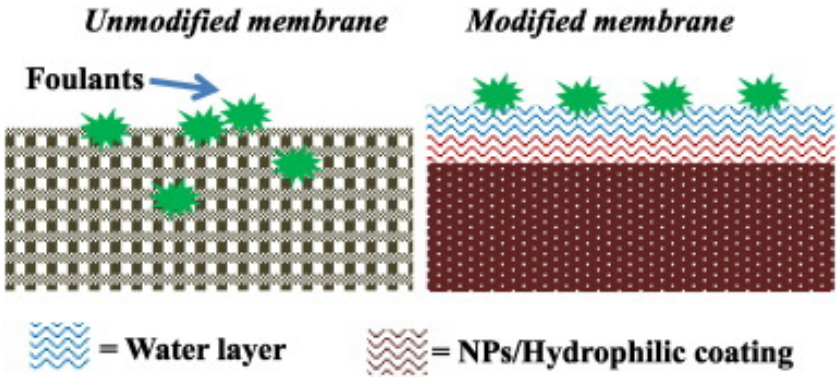


Figure 2. 5: Antifouling mechanism through hydration layer effect (Jhaveri & Murthy, 2016).

2.3.1 Hydrophilic modification of membranes using inorganic nanoparticles

Nanoparticles are nano-sized particles having a size measurement of 1-100 nm in at least one of its dimensions (Wiesenthal et al., 2011). Due to their nano size, they possess properties different from their bulk counterpart (Schmid, 2011). For instance, a significant fraction of their atoms are located at their surfaces, thus making their chemical reactivity higher than their bulk counterpart (Schmid, 2011). Such unique characteristics of the nanoparticles are beneficial in their application for hydrophilic modification of membranes. This is because the interaction of the membrane and the nanoparticles is maximized. Thus, the desirable attributes of the nanoparticles are infused into the membrane, thereby achieving improved membrane modification (Al Aani et al., 2017a).

Inorganic nanoparticles are intrinsically hydrophilic, hence they are mostly used for membrane modification to improve hydrophilicity in the treatment of organic-contaminated wastewater (Jhaveri & Murthy, 2016). Subsequently, the fouling resistance of the membrane is improved due to the hydration effect, as discussed in the previous section. The introduction of inorganic nanoparticles into a membrane not only improves the membrane's hydrophilicity but also enhances other properties, such as membrane pore size, which reduces the permeation resistance of the membrane (Nasir et al., 2019).

There are three ways of incorporating inorganic nanoparticles into a membrane, as shown in Figure 2.6; (1) the nanoparticles are firstly dispersed in the solvent and stirred until a homogenous suspension is obtained, and the polymer material is then added and stirred to obtain the dope solution, (2) the polymer material is firstly dissolved in the solvent, followed by the addition of the nanoparticles into the dope solution, and (3) the nanoparticles are dispersed in the solvent, and the polymer material is dissolved in the solvent separately, then the nanoparticles suspension is added into the polymer solution and stirred to obtain the homogenous nanocomposite solution (Esfahani et al., 2019). Method (1) and (3) are the best approaches to incorporate the nanoparticles to ensure a well-dispersion of the nanoparticles and prevent their agglomeration, as agglomeration of the nanoparticles adversely affects the membrane property and performance (Esfahani et al., 2019). Agglomeration of nanoparticles is also promoted by introducing a high amount of the nanoparticles into the membrane (Yin & Deng, 2015), hence the optimum amount of the nanoparticles that give the best dispersion must be utilized for the membrane modification.

Over the years, various nanoparticles have been utilized to modify various polymeric membranes for application in the removal of organic contaminants from wastewater (Cosme et al., 2023; Oliveira et al., 2022; Loske et al., 2020). Matin et al. (2023) used ZnO nanoparticles to modify a polysulfone membrane for application to remove trace organic contaminants from wastewater. The modified membrane was reported to exhibit high removal efficiency toward the target contaminants (Matin et al., 2023). Polysulfone membrane was also modified by introducing TiO_2 nanoparticles, which resulted in improved membrane performance in removing organic contaminants from natural rubber wastewater (Kusworo, Susanto, et al., 2021). Another polymeric membrane, PVDF, was modified using Fe_3O_4 nanoparticles for application in the treatment of methylene blue-contaminated water (Huang et al., 2020). Improved hydrophilicity, Flux, and antifouling properties were reported as a result of the modification (Huang et al., 2020). Reduction of fouling was also reported when a PVDF

membrane was modified with TiO2 nanoparticles which prevented decline in the membrane performance over time (Maryam Tavakolmoghadam, 2022). TiO2 nanoparticles were also incorporated into a polyethersulfone membrane to mitigate fouling during the treatment of BSA and HA-contaminated water (X. Li et al., 2014). Unuigbe et al., (2020) improved the performance of a PES membrane using iron nanoparticles for the treatment of BTEX-contaminated water.

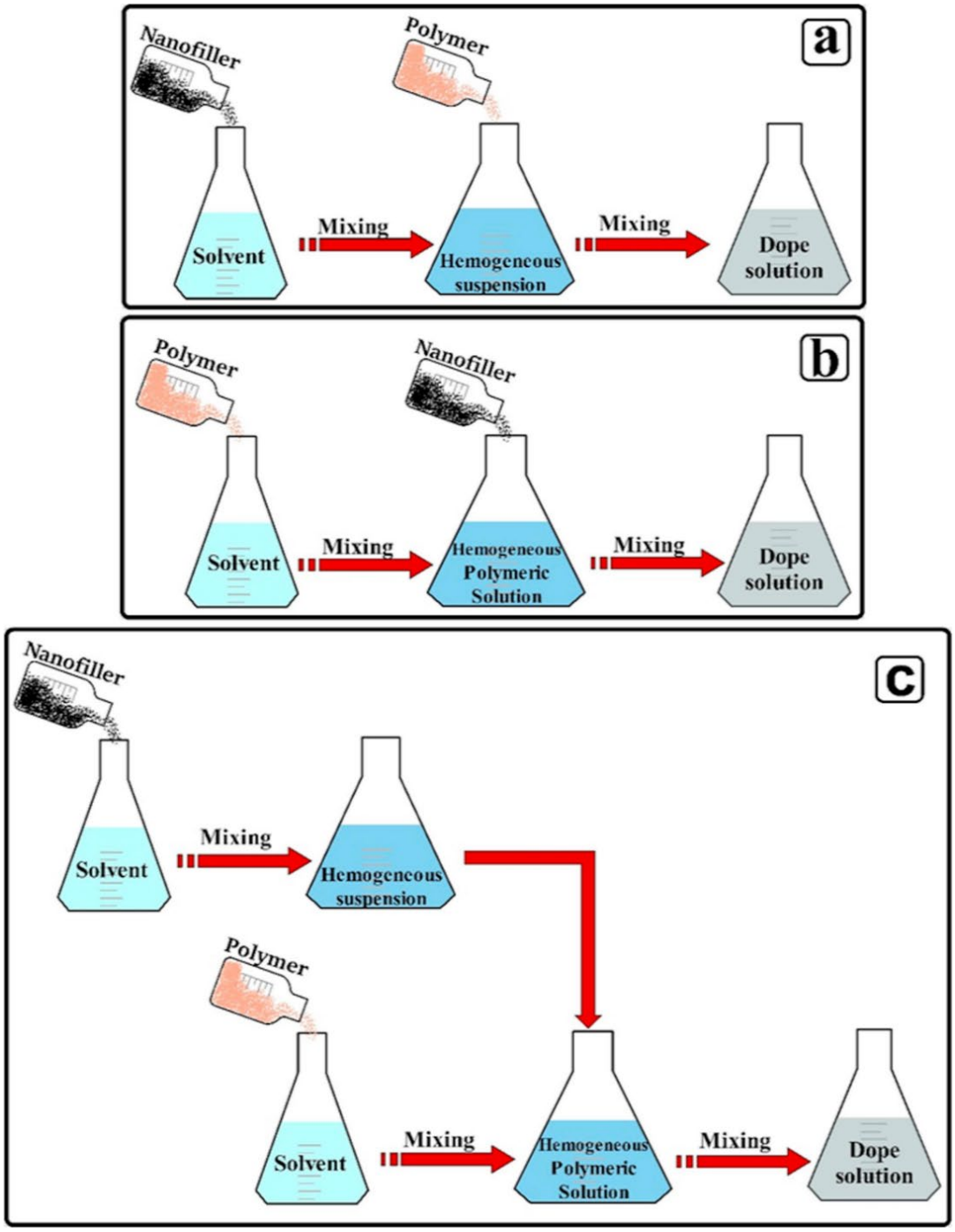


Figure 2. 6: Methods of incorporating inorganic nanoparticles into a membrane (Esfahani et al., 2019)

The increase in research interest in membrane modification using nanoparticles can be attributed to the feasibility of the process in terms of the easy availability of the nanoparticles and the ease of the modification process (Van der Bruggen, 2009). However, as briefly mentioned previously, agglomeration of the nanoparticles in the polymer matrix limits their use as a modification option (Balta et al., 2012). In addition, there is a tendency for the incorporated nanoparticles to leach from the membrane, which results in the deterioration of the membrane performance over time (Kajau et al., 2021).

2.3.1.1 Biogenic-synthesized nanoparticles for hydrophilic modification of membranes

Biogenic-synthesized nanoparticles are typically prepared by using biological components to reduce the metal precursors instead of the conventional use of chemicals in reducing the precursors (Heinemann et al., 2021; Soni et al., 2021; Jadoun et al., 2021). Biological components often used for bio-reduction in NPs synthesis include fungi, algae, and plant extracts (Gupta et al., 2023). The use of these biological substrates offers a more sustainable means to prepare hydrophilic NPs as opposed to the chemical method that utilizes toxic solvents and also generates toxic residues. NPs synthesized through biogenic means are also stabilized by some of the active phytochemicals in the biological substrate, which minimizes the agglomeration of the NPs (Martínez-Cabanas et al., 2016a). This is particularly beneficial in the use of the biogenic-synthesized NPs as hydrophilic modifiers in membrane modification because the NPs are more well-dispersed in the membrane matrix (Arif et al., 2023). In addition, some hydrophilic functional groups from plant extracts used in the synthesis are deposited on the NPs, thereby contributing to enhancing the hydrophilicity of the NPs (Dadari et al., 2022a) This is also important in the application of NPs in the hydrophilic modification of membranes. Figure 2.7 depicts a typical biosynthetic route for preparing NPs.

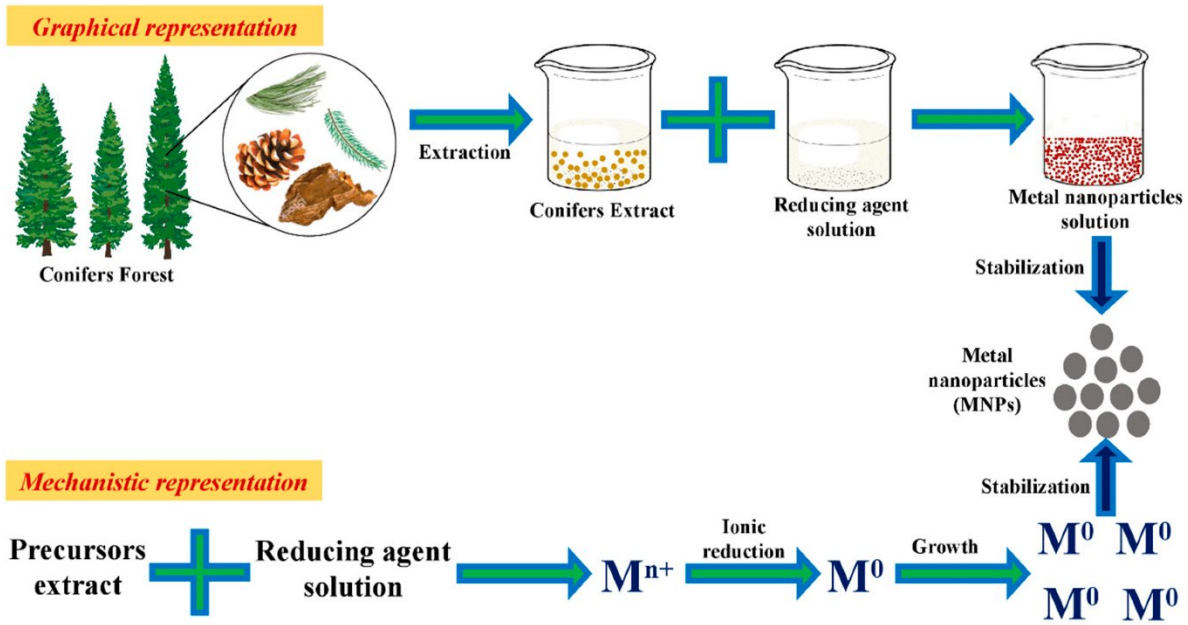


Figure 2. 7: Typical biosynthesis of NPs (Bhardwaj et al., 2020). This Figure is openly licensed via https://creativecommons.org/licenses/by/4.0/

2.3.2 Hydrophilic modification of membranes using hydrophilic polymers

Hydrophilic polymers are a class of polymers that exhibit a good affinity for water (Schmidt, 2019). The strong interaction of hydrophilic polymers with water arises from the presence of hydrophilic functional groups such as hydroxyl, carboxyl, and carbonyl in the polymer structure, as shown in Fig. 2.8 (Bayliss & Schmidt, 2023). On the introduction of the hydrophilic polymers into the membrane, the hydrophilicity of the membrane improves and their antifouling ability is enhanced. The improvement in the antifouling characteristics of the membrane is mainly achieved through the formation of a hydration layer on the membrane surface, thereby preventing hydrophobic interaction between the membrane and contaminants (R. Zhang et al., 2016a). Through hydrogen bonding with the water molecules, the hydrophilic polymer-modified membrane creates the hydration layer on the membrane surface (Ismail et al., 2020).

The most common examples of hydrophilic polymers for membrane modification include polyethylene glycol (PEG), polyacrylic acid (PAA), and polyvinyl alcohol (PVA). These polymers have been widely utilized for the modification of various hydrophobic membranes and applied for the removal of various organic contaminants. Their presence in the membrane helps maintain good performance of the membrane during the removal of the organic contaminants from the wastewater. Yunos et al. (2014) used PEG as a hydrophilic modifier to

improve the PSF membrane, and the membrane antifouling characteristics towards natural organic matter were improved. Similarly, PEG was used to enhance a PVDF membrane for the treatment of winery wastewater, and improved membrane performance was reported (Sonawane & Murthy, 2022). The hydrophilic polymer, PAA, was also introduced into a PVDF membrane and applied for the removal of BSA (Chiao et al., 2020). Improved antifouling and removal efficiency was reported, which was attributed to the PAA in the membrane (Chiao et al., 2020). Li et al., (2021) also used PAA as a modifier in a polyacrylonitrile membrane and improved membrane performance in an oil-water separation was obtained. PVA was employed as a hydrophilic modifier to enhance a PVDF membrane, which was applied to remove phenolphthalein and ß-naphthol from wastewater (Lu, Zhang, et al., 2022).Compared with the unmodified PVDF membrane, the modified membrane achieved high removal of the aromatic contaminants and better antifouling tendency (Lu, Zhang, et al., 2022). The antifouling and removal efficiency of a PVA/PVDF membrane in the treatment of protein and humic acid-contaminated wastewater was also significantly improved due to the presence of the PVA in the membrane (Lu & Li, 2021).]

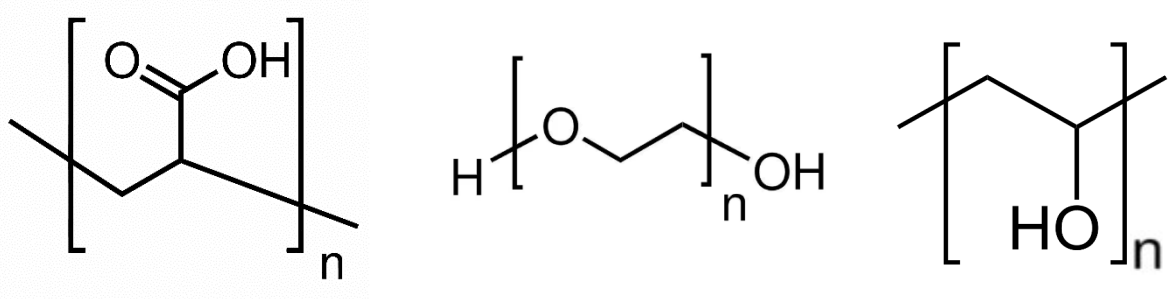


Figure 2. 8: Structure of some hydrophilic polymers showing their hydrophilic functional groups.

2.3.3 Hydrophilic modification using inorganic nanoparticles and hydrophilic polymers

Most recent hydrophilic membrane modifications focused on combining the hydrophilic properties of two or more modifiers to maximize the impact of the modifiers on the properties and performance of the membrane (Isawi, 2019; Shi et al., 2023; Haghighat et al., 2020). By harnessing the hydrophilic properties of more than one modifier, the integrity of the modified membrane becomes more reinforced. A feasible strategy is to harness the synergistic impact of two modifiers by the integration of both inorganic nanoparticles and hydrophilic polymers into a membrane. This approach of hydrophilic modification enables the use of easily available modifiers to maximize the performance of membranes.

Several inorganic nanoparticles and hydrophilic polymers have been combined to fabricate robust and high-performance membranes for the removal of organic contaminants from wastewater. Table 2.3 depicts some of the hydrophilic modifications that utilized both inorganic nanoparticles and hydrophilic polymers to improve membrane performance in the treatment of organic-contaminated wastewater.

Table 2. 3: Studies on hydrophilic membrane modification using inorganic nanoparticles and hydrophilic polymers

Support membrane	Hydrophilic modifiers	Target contaminant/s or foulant/s	Modified membrane property/performance	References
PVDF	PEGMA SiO_2	HA, BSA, oil.	Water contact angle reduced from 68.7° to 50.7°. Water flux improved from 39.2 L/m^{2}h to 114.5 L/m^{2}h. FRR improved from 0.53 to 0.84 for oil/water emulsion filtration.	(Saini et al., 2019)
PVDF	PEG TiO_2	HA	Water contact angle was reduced from 63.3° to 19.4°. Water flux improved from 210 L/m^{2}h to 375 L/m^{2}h. FRR improved from 57% to 70%.	(Younas et al., 2017)
PES	PDA TiO_2	SA Oil	Water contact angle reduced from ~69.0° to ~49.0°. Water flux improved from ~165 L/m^{2}h to ~460 L/m^{2}h. FRR improved from ~86% to ~96%.	(Kallem et al., 2022)
PSF	PVA ZnO	COD, TDS in petroleum refinery wastewater.	Water contact angle reduced from 76.3° to 27.0°. FRR improved from 70.0% to 94.6%.	(Kusworo, Kumoro, et al., 2021)

2.3.4 Biogenic-synthesized Fe_3O_4 NPs and PVA as potential hydrophilic modifiers for the removal of the organic contaminant, BTEX, from wastewater

Fe_3O_4 nanoparticles are among the frequently used nanoparticles applied in various treatment processes for organic-contaminated water (Wang et al., 2016; Saharan et al., 2014; Rouhani et al., 2022). Their wide preference as material for the removal of organic contaminants is due to their easy availability, low cost, and facile preparation process (Gutierrez et al., 2017). As inorganic nanoparticles, they exhibit good hydrophilicity, which has attracted their use for hydrophilic modification of membranes (Koulivand et al., 2019; Huang et al., 2020). Hence, the introduction of the Fe_3O_4 nanoparticles into a membrane improves its antifouling behaviour and helps to maintain good membrane performance during the treatment process (Daraei et al., 2013). The Fe_3O_4 nanoparticles not only improve the membrane performance but also reinforce its physical features, such as mechanical and thermal stability (Simeonidis et al., 2016). Moreover, their small surface area enables the effective transfer of their beneficial properties to the membrane upon being introduced into the membrane (Homayoonfal et al., 2013).

The main constraint in the use of Fe_3O_4 nanoparticles is their possible agglomeration in the matrix of the modified membrane. This can have an adverse effect on the performance of the modified membrane, such as blockage of the membrane pores and a decline in membrane flux (Wei et al., 2022a). However, biogenic synthesis of the NPs using plant extracts offers an approach to obtain fairly good dispersed NPs as molecules such as phenols in the plant extracts act as capping agents during the synthesis. In addition, by establishing the optimum amount of the nanoparticles that give their good dispersion in the membrane, the possible concern of the negative effects of agglomerated nanoparticles on the membrane performance can be eliminated.

PVA possesses abundant hydroxyl functional groups, which make the polymer very hydrophilic. By introducing PVA into a membrane, the hydrophilicity of the PVA is infused into the membrane resulting in a modified membrane with improved hydrophilicity. Another attribute that necessitates the wide adoption of PVA as a hydrophilic modifier is its low cost and easy availability (Aslam et al., 2018). Membranes modified with PVA have been applied to remove various organic contaminants/foulants such as oils (Liu et al., 2019), BSA (Hu et al., 2016; T. Liu et al., 2021), and methylene blue and malachite green (Wu et al., 2022). In all the aforementioned studies, membrane antifouling tendency was promoted as a result of the PVA in the membrane.

Utilizing the hydrophilic properties of both biogenic-synthesized Fe_3O_4 NPs and PVA is a feasible approach to the hydrophilic modification of membranes. Thus, offering an innovative strategy through harnessing the synergistic effects of the two modifiers in fabricating an antifouling and long-term operationally stable membrane for application in the treatment of BTEX-contaminated water. The two modifiers are also inexpensive and easily available or easily prepared; hence, they present a cost-efficient alternative for maintaining a high membrane separation performance in the treatment of BTEX-contaminated wastewater.

2.4 Performance assessment of membranes

A membrane's performance assessment is a crucial criterion that employs different parameters to determine the efficiency and effectiveness of the membrane in the wastewater treatment process. In other words, the membrane is subjected to various performance tests to ascertain its potential as a medium to remove, degrade, or recover targeted contaminants from wastewater. Parameters such as membrane flux, selectivity, and anti-fouling are tested, and the results of the tests are used to establish the performance of the membrane in the treatment process. For membrane treatment applications involving the filtration process, the performance parameters are obtained by measuring the related filtration or separation values and calculating the parameters from the obtained values according to their various equations. The test can be conducted in a dead-end filtration system or in a cross-flow filtration system, as depicted in Figure 2.9. The definitions of some of the performance parameters and the equations for calculating them are discussed below.

2.4.1 Membrane Flux

In a membrane filtration process, the flux of a membrane is defined as the flow rate of solvent through the membrane per unit membrane surface area (Nayak et al., 2022). This is governed by the membrane's properties, such as pore size, porosity, thickness, and hydrophilicity/hydrophobicity (Singh, 2006). The membrane flux also depends on the operation conditions, such as the applied pressure (Singh, 2006). Measuring the membrane flux involves subjecting the membrane to a filtration process in which the permeate solution passes through a membrane under an applied force, such as pressure. The volume of the permeate is collected after a specified filtration time, and the membrane flux is calculated using the equation:

$$J_w = \frac{V}{A \times t} \quad (1)$$

where V is the volume of the permeate (L), A is the effective membrane area (m^2), and t is the permeation time (min).

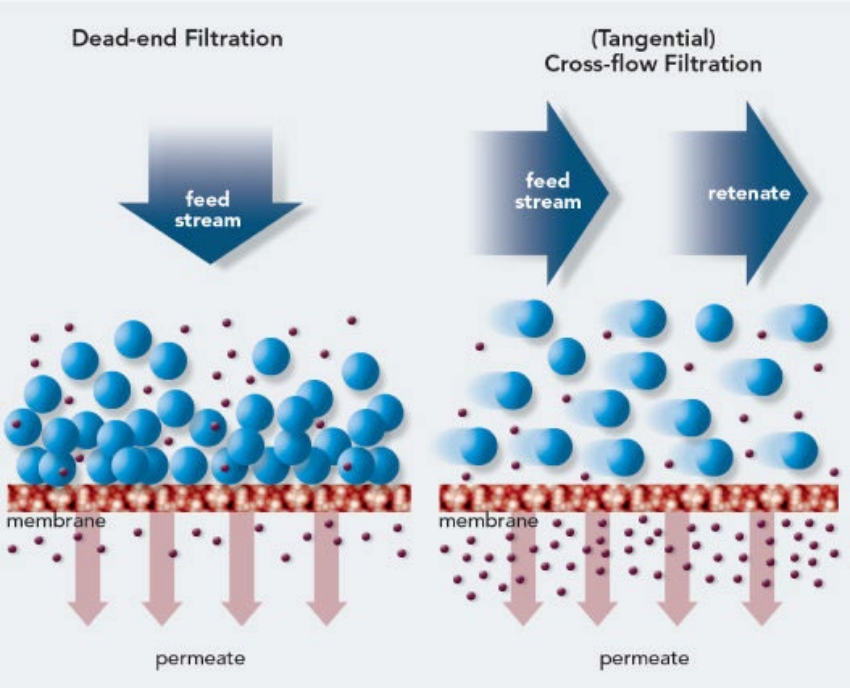


Figure 2. 9: Schematic depiction of dead-end and cross-flow filtration process (Paipuri, 2014).

2.4.2 Membrane selectivity

The selectivity of a membrane is another useful parameter for assessing its performance by determining the membrane separation tendency toward the target contaminant (Hillis, 2000). Factors such as the chemical and physical composition of the membrane govern the ability of the membrane to separate or remove the contaminants from the wastewater (Singh, 2006). Hence, depending on the membrane's chemical or physical characteristics, the mechanism of the separation could be through size exclusion (Couto et al., 2020), electrostatic repulsion (Srimuk et al., 2020), adsorption (Khulbe & Matsuura, 2018), or hydration layer barrier (Xiong et al., 2022)The selectivity of the membrane is determined by measuring the rejection coefficient or percentage, which gives a good indication of the membrane's separation ability towards the target contaminant. Eq. (2) is used to calculate the membrane's rejection ability after subjecting it to the separation test. Some of the membrane separation mechanism is shown in Fig. 2.10.

$$R\ (\%) = \frac{C_f - C_p}{C_f} \times 100 \qquad (2)$$

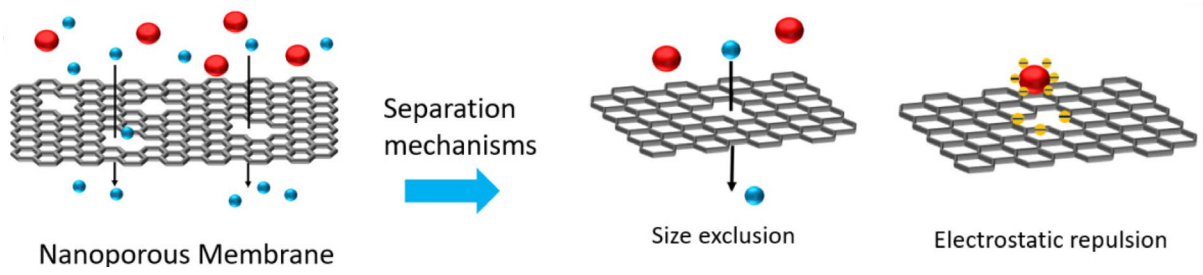


Figure 2. 10: Schematic depiction of some of the membrane separation mechanisms (Zhang et al., 2022). This Figure is openly licensed via https://creativecommons.org/licenses/by/4.0/

2.4.3 Membrane anti-fouling tendency

Membrane fouling is a major obstacle to achieving improved membrane performance during wastewater treatment. The fouling of a membrane arises from the undesirable adsorption or settlement of the contaminants on the membrane surface, thereby blocking the membrane pores and active sites (Zhao et al., 2018). This results in a decline in membrane performance, such as a decline in membrane flux. Flux decline in a pressure-driven filtration process can be due to membrane fouling caused by membrane hydraulic resistance, concentration polarization resistance, cake layer resistance, and adsorption resistance (Li et al., 2020). Membrane fouling can be reversible and irreversible fouling depending on the interaction between the foulant and membrane, and the ease of removal of the foulants from the membrane (Jhaveri & Murthy, 2016). While reversible fouling can be removed by physical cleaning, irreversible fouling requires chemical cleaning (Zhao et al., 2018). Fig. 2.11 shows a typical example of fouled and cleaned membranes.

Due to the adverse effects of fouling on membrane performance, the ability of membranes to resist fouling is evaluated during the treatment process to determine their anti-fouling capability. This is done by measuring the membrane's antifouling performance during the first filtration and after subsequent application of the cleaned membrane. Antifouling parameters such as reversible fouling ratio (R_r), irreversible fouling ratio (R_{ir}), flux recovery ratio (FRR), and total fouling ratio (R_t) are calculated to determine membrane antifouling tendency. The equations for calculating these parameters are:

$$R_r(\%) = \left(\frac{J_C - J_{w1}}{J_w}\right) \times 100 \quad (3)$$

$$R_{ir}(\%) = \left(\frac{J_w - J_c}{J_w}\right) \times 100 \quad (4)$$

$$\text{FRR}\ (\%) = \left(\frac{J_c}{J_w}\right) \times 100 \quad (5)$$

$$R_t = \left(\frac{J_w - J_{w1}}{J_w}\right) \times 100 \quad (6)$$

Where J_w is the pure water flux, J_{w1} is the flux of the feed solution, and J_c is the flux of the cleaned membranes.

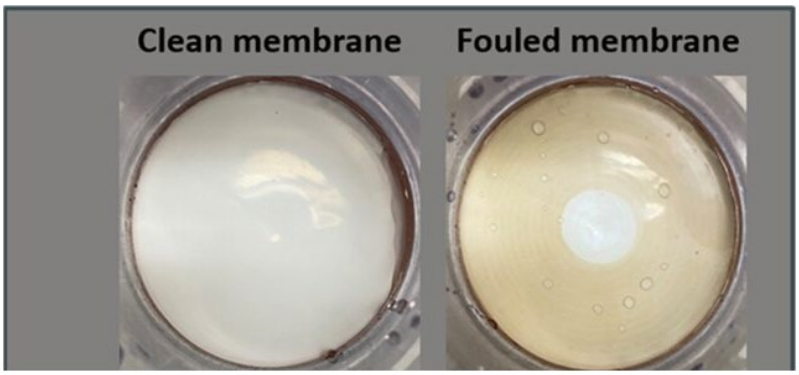


Figure 2. 11: Images of cleaned and fouled membrane (Dardor et al., 2021). This Figure is openly licensed via https://creativecommons.org/licenses/by-nc-nd/4.0/

References

Ahmed, S. F., Mehejabin, F., Momtahin, A., Tasannum, N., Faria, N. T., Mofijur, M., Hoang, A. T., Vo, D.-V. N., & Mahlia, T. M. I. (2022). Strategies to improve membrane performance in wastewater treatment. *Chemosphere*, *306*, 135527. https://doi.org/10.1016/j.chemosphere.2022.135527

Akram, S., Naddeo, V., Rehan, Z., Zahid, M., Rashid, A., & Razzaq, W. (2018). A Comprehensive Review on Polymeric Nano-Composite Membranes for Water Treatment. *Journal of Membrane Science & Technology*, *08*. https://doi.org/10.4172/2155-9589.1000179

Al Aani, S., Wright, C. J., Atieh, M. A., & Hilal, N. (2017). Engineering nanocomposite membranes: Addressing current challenges and future opportunities. *Desalination*, *401*, 1–15. https://doi.org/10.1016/j.desal.2016.08.001

Alberici, R. M., Zampronio, C. G., Poppi, R. J., & Eberlin, M. N. (2002). Water solubilization of ethanol and BTEX from gasoline: on-line monitoring by membrane introduction mass spectrometry. Analyst, 127(2), 230-234.

Anjum, H., Johari, K., Gnanasundaram, N., Ganesapillai, M., Arunagiri, A., Regupathi, I., & Thanabalan, M. (2019). A review on adsorptive removal of oil pollutants (BTEX) from wastewater using carbon nanotubes. *Journal of Molecular Liquids*, *277*, 1005–1025. https://doi.org/10.1016/j.molliq.2018.10.105

Arif, Z., Singh, B., & Sastry, S. V. A. R. (2023). Biogenic synthesis of TiO2 NPs for assessment of antifouling property PVDF/TiO2 composite membrane by surface energetics: XDLVO theory. *Biomass Conversion and Biorefinery*. https://doi.org/10.1007/s13399-023-04715-7

Aslam, M., Kalyar, M. A., & Raza, Z. A. (2018). Polyvinyl alcohol: A review of research status and use of polyvinyl alcohol based nanocomposites. *Polymer Engineering & Science*, *58*(12), 2119–2132. https://doi.org/10.1002/pen.24855

Atamaleki, A., Motesaddi Zarandi, S., Massoudinejad, M., Samimi, K., Fakhri, Y., Ghorbanian, M., & Mousavi Khaneghah, A. (2021). The effect of frying process on the emission of the volatile organic compounds and monocyclic aromatic group (BTEX). *International Journal of Environmental Analytical Chemistry*, *0*(0), 1–14. https://doi.org/10.1080/03067319.2021.1950148

Bahmani, M., Bitarafhaghighi, V., Badr, K., Keshavarz, P., & Mowla, D. (2014). The photocatalytic degradation and kinetic analysis of BTEX components in polluted wastewater by UV/H2O2-based advanced oxidation. *Desalination and Water Treatment*, *52*(16–18), 3054–3062. https://doi.org/10.1080/19443994.2013.797369

Balta, S., Sotto, A., Luis, P., Benea, L., Van der Bruggen, B., & Kim, J. (2012). A new outlook on membrane enhancement with nanoparticles: The alternative of ZnO. *Journal of Membrane Science*, *389*, 155–161. https://doi.org/10.1016/j.memsci.2011.10.025

Basile, A., Cassano, A., & Rastogi, N. K. (2015). *Advances in Membrane Technologies for Water Treatment: Materials, Processes and Applications*. Elsevier.

Bayliss, N., & Schmidt, B. (2023). *Hydrophilic Polymers: Current Trends and Visions for the Future*. https://doi.org/10.1016/j.progpolymsci.2023.101753

Bhardwaj, K., Dhanjal, D. S., Sharma, A., Nepovimova, E., Kalia, A., Thakur, S., Bhardwaj, S., Chopra, C., Singh, R., Verma, R., Kumar, D., Bhardwaj, P., & Kuča, K. (2020). Conifer-Derived Metallic Nanoparticles: Green Synthesis and Biological Applications. *International Journal of Molecular Sciences*, *21*(23), Article 23. https://doi.org/10.3390/ijms21239028

Bina, B., Amin, M. M., Rashidi, A., & Pourzamani, H. (2014). Water and wastewater treatment from BTEX by carbon nanotubes and Nano-Fe. *Water Resources*, *41*(6), 719–727. https://doi.org/10.1134/S0097807814060037

Bishnoi, H. L. S., Sarita Khaturia, Mamta Chahar, Anjali. (2023). Membrane and Membrane-Based Processes for Wastewater Treatment. In *Membrane and Membrane-Based Processes for Wastewater Treatment*. CRC Press.

Bustillo-Lecompte, C. F., Kakar, D., & Mehrvar, M. (2018). Photochemical treatment of benzene, toluene, ethylbenzene, and xylenes (BTEX) in aqueous solutions using advanced oxidation processes: Towards a cleaner production in the petroleum refining and petrochemical industries. *Journal of Cleaner Production*, *186*, 609–617. https://doi.org/10.1016/j.jclepro.2018.03.135

Chiao, Y.-H., Chen, S.-T., Yap Ang, M. B. M., Patra, T., Castilla-Casadiego, D. A., Fan, R., Almodovar, J., Hung, W.-S., & Wickramasinghe, S. R. (2020). High-Performance Polyacrylic Acid-Grafted PVDF Nanofiltration Membrane with Good Antifouling Property for the Textile Industry. *Polymers*, *12*(11), Article 11. https://doi.org/10.3390/polym12112443

Cosme, J. R. A., Castro-Muñoz, R., & Vatanpour, V. (2023). Recent Advances in Nanocomposite Membranes for Organic Compound Remediation from Potable Waters. *ChemBioEng Reviews*, *10*(2), 112–132. https://doi.org/10.1002/cben.202200017

Couto, C. F., Santos, A. V., Amaral, M. C. S., Lange, L. C., de Andrade, L. H., Foureaux, A. F. S., & Fernandes, B. S. (2020). Assessing potential of nanofiltration, reverse osmosis and membrane distillation drinking water treatment for pharmaceutically active compounds (PhACs) removal. *Journal of Water Process Engineering*, *33*, 101029. https://doi.org/10.1016/j.jwpe.2019.101029

Dadari, S., Rahimi, M., & Zinadini, S. (2022). Novel antibacterial and antifouling PES nanofiltration membrane incorporated with green synthesized nickel-bentonite nanoparticles for heavy metal ions removal. *Chemical Engineering Journal*, *431*, 134116. https://doi.org/10.1016/j.cej.2021.134116

Daraei, P., Madaeni, S. S., Ghaemi, N., Khadivi, M. A., Astinchap, B., & Moradian, R. (2013). Fouling resistant mixed matrix polyethersulfone membranes blended with magnetic nanoparticles: Study of magnetic field induced casting. *Separation and Purification Technology*, *109*, 111–121. https://doi.org/10.1016/j.seppur.2013.02.035

Dardor, D., Al-Maas, M., Minier-Matar, J., Janson, A., Sharma, R., Hassan, M. K., Al-Maadeed, M. A. A., & Adham, S. (2021). Protocol for Preparing Synthetic Solutions Mimicking Produced Water from Oil and Gas Operations. *ACS Omega*, *6*(10), 6881–6892. https://doi.org/10.1021/acsomega.0c06065

Davidson, C. J., Hannigan, J. H., & Bowen, S. E. (2021). Effects of inhaled combined Benzene, Toluene, Ethylbenzene, and Xylenes (BTEX): Toward an environmental exposure model. *Environmental Toxicology and Pharmacology*, *81*, 103518. https://doi.org/10.1016/j.etap.2020.103518

Delzer, G. C. (1996). *Occurrence of the Gasoline Oxygenate MTBE and BTEX Compounds in Urban Stormwater in the United States, 1991-95*. U.S. Geological Survey.

Duan, X., & Li, Y. (2017). Sources and fates of BTEX in the general environment and its distribution in coastal cities of China. Journal of Environmental Science and Public Health, 1(2), 86-106.

Eldos, H. I., Khan, M., Zouari, N., Saeed, S., & Al-Ghouti, M. A. (2022). Characterization and assessment of process water from oil and gas production: A case study of process wastewater in Qatar. *Case Studies in Chemical and Environmental Engineering*, *6*, 100210. https://doi.org/10.1016/j.cscee.2022.100210

EPA. (2018). *NSW Environment Protection Authority (EPA)*. https://www.epa.nsw.gov.au/

Esfahani, M. R., Aktij, S. A., Dabaghian, Z., Firouzjaei, M. D., Rahimpour, A., Eke, J., Escobar, I. C., Abolhassani, M., Greenlee, L. F., Esfahani, A. R., Sadmani, A., & Koutahzadeh, N. (2019). Nanocomposite membranes for water separation and purification: Fabrication, modification, and applications. *Separation and Purification Technology*, *213*, 465–499. https://doi.org/10.1016/j.seppur.2018.12.050

Fernandes, A., Makoś, P., Khan, J. A., & Boczkaj, G. (2019). Pilot scale degradation study of 16 selected volatile organic compounds by hydroxyl and sulfate radical based advanced oxidation processes. *Journal of Cleaner Production*, *208*, 54–64. https://doi.org/10.1016/j.jclepro.2018.10.081

Goh, P. S., Wong, T. W., Lim, J. W., Ismail, A. F., & Hilal, N. (2020). Chapter 9—Innovative and sustainable membrane technology for wastewater treatment and desalination application.

In C. M. Galanakis (Ed.), *Innovation Strategies in Environmental Science* (pp. 291–319). Elsevier. https://doi.org/10.1016/B978-0-12-817382-4.00009-5

Gupta, D., Boora, A., Thakur, A., & Gupta, T. K. (2023). Green and sustainable synthesis of nanomaterials: Recent advancements and limitations. *Environmental Research*, *231*, 116316. https://doi.org/10.1016/j.envres.2023.116316

Gusain, R., Gupta, K., Joshi, P., & Khatri, O. P. (2019). Adsorptive removal and photocatalytic degradation of organic pollutants using metal oxides and their composites: A comprehensive review. *Advances in Colloid and Interface Science*, *272*, 102009. https://doi.org/10.1016/j.cis.2019.102009

Gutierrez, A. M., Dziubla, T. D., & Hilt, J. Z. (2017). Recent advances on iron oxide magnetic nanoparticles as sorbents of organic pollutants in water and wastewater treatment. *Reviews on Environmental Health*, *32*(1–2), 111–117. https://doi.org/10.1515/reveh-2016-0063

Haghighat, N., Vatanpour, V., Sheydaei, M., & Nikjavan, Z. (2020). Preparation of a novel polyvinyl chloride (PVC) ultrafiltration membrane modified with Ag/TiO2 nanoparticle with enhanced hydrophilicity and antibacterial activities. *Separation and Purification Technology*, *237*, 116374. https://doi.org/10.1016/j.seppur.2019.116374

Heinemann, M. G., Rosa, C. H., Rosa, G. R., & Dias, D. (2021). Biogenic synthesis of gold and silver nanoparticles used in environmental applications: A review. *Trends in Environmental Analytical Chemistry*, *30*, e00129. https://doi.org/10.1016/j.teac.2021.e00129

Hillis, P. (2000). *Membrane Technology in Water and Wastewater Treatment*. Royal Society of Chemistry.

Homayoonfal, M., Mehrnia, M. R., Mojtahedi, Y. M., & Ismail, A. F. (2013). Effect of metal and metal oxide nanoparticle impregnation route on structure and liquid filtration performance of polymeric nanocomposite membranes: A comprehensive review. *Desalination and Water Treatment*, *51*(16–18), 3295–3316. https://doi.org/10.1080/19443994.2012.749055

Hu, N., Xiao, T., Cai, X., Ding, L., Fu, Y., & Yang, X. (2016). Preparation and Characterization of Hydrophilically Modified PVDF Membranes by a Novel Nonsolvent Thermally Induced Phase Separation Method. *Membranes*, *6*(4), Article 4. https://doi.org/10.3390/membranes6040047

Huang, Z.-H., Zhang, X., Wang, Y.-X., Sun, J.-Y., Zhang, H., Liu, W.-L., Li, M.-P., Ma, X.-H., & Xu, Z.-L. (2020). Fe3O4/PVDF catalytic membrane treatment organic wastewater with simultaneously improved permeability, catalytic property and anti-fouling. *Environmental Research*, *187*, 109617. https://doi.org/10.1016/j.envres.2020.109617

Ibiebele, D. D. (1986). Point-source inputs of petroleum wastewater into the Niger Delta, Nigeria. *Science of The Total Environment*, *52*(3), 233–238. https://doi.org/10.1016/0048-9697(86)90123-3

Isawi, H. (2019). Evaluating the performance of different nano-enhanced ultrafiltration membranes for the removal of organic pollutants from wastewater. *Journal of Water Process Engineering*, *31*, 100833. https://doi.org/10.1016/j.jwpe.2019.100833

Ismail, N. H., Salleh, W. N. W., Ismail, A. F., Hasbullah, H., Yusof, N., Aziz, F., & Jaafar, J. (2020). Hydrophilic polymer-based membrane for oily wastewater treatment: A review. *Separation and Purification Technology*, *233*, 116007. https://doi.org/10.1016/j.seppur.2019.116007

Jadoun, S., Arif, R., Jangid, N. K., & Meena, R. K. (2021). Green synthesis of nanoparticles using plant extracts: A review. *Environmental Chemistry Letters*, *19*(1), 355–374. https://doi.org/10.1007/s10311-020-01074-x

Jhaveri, J. H., & Murthy, Z. V. P. (2016). A comprehensive review on anti-fouling nanocomposite membranes for pressure driven membrane separation processes. *Desalination*, *379*, 137–154. https://doi.org/10.1016/j.desal.2015.11.009

Kajau, A., Motsa, M., Mamba, B. B., & Mahlangu, O. (2021). Leaching of CuO Nanoparticles from PES Ultrafiltration Membranes. *ACS Omega*, *6*(47), 31797–31809. https://doi.org/10.1021/acsomega.1c04431

Kallem, P., Pandey, R. P., Hegab, H. M., Gaur, R., Hasan, S. W., & Banat, F. (2022). High-performance thin-film composite forward osmosis membranes with hydrophilic PDA@TiO2 nanocomposite substrate for the treatment of oily wastewater under PRO mode. *Journal of Environmental Chemical Engineering*, *10*(3), 107454. https://doi.org/10.1016/j.jece.2022.107454

Kang, G., & Cao, Y. (2014). Application and modification of poly(vinylidene fluoride) (PVDF) membranes – A review. *Journal of Membrane Science*, *463*, 145–165. https://doi.org/10.1016/j.memsci.2014.03.055

Khanzada, N. K., Farid, M. U., Kharraz, J. A., Choi, J., Tang, C. Y., Nghiem, L. D., Jang, A., & An, A. K. (2020). Removal of organic micropollutants using advanced membrane-based water and wastewater treatment: A review. *Journal of Membrane Science*, *598*, 117672. https://doi.org/10.1016/j.memsci.2019.117672

Khulbe, K. C., & Matsuura, T. (2018). Removal of heavy metals and pollutants by membrane adsorption techniques. *Applied Water Science*, *8*(1), 19. https://doi.org/10.1007/s13201-018-0661-6

Kim, S., Chu, K. H., Al-Hamadani, Y. A. J., Park, C. M., Jang, M., Kim, D.-H., Yu, M., Heo, J., & Yoon, Y. (2018). Removal of contaminants of emerging concern by membranes in water and wastewater: A review. *Chemical Engineering Journal*, *335*, 896–914. https://doi.org/10.1016/j.cej.2017.11.044

Kochkodan, V., & Hilal, N. (2015). A comprehensive review on surface modified polymer membranes for biofouling mitigation. *Desalination*, *356*, 187–207. https://doi.org/10.1016/j.desal.2014.09.015

Koulivand, H., Shahbazi, A., & Vatanpour, V. (2019). Fabrication and characterization of a high-flux and antifouling polyethersulfone membrane for dye removal by embedding Fe3O4-MDA nanoparticles. *Chemical Engineering Research and Design*, *145*, 64–75. https://doi.org/10.1016/j.cherd.2019.03.003

Kusworo, T. D., Kumoro, A. C., Aryanti, N., Utomo, D. P., Qoyyimah, Hasbullah, H., & Alexandro, S. R. (2021). Effects of crosslinking and thermal annealing modifications on the performance of nanohybrid PSf-ZnO membranes for the treatment of raw and ozonated petroleum refinery wastewater. *Journal of Environmental Chemical Engineering*, *9*(5), 106200. https://doi.org/10.1016/j.jece.2021.106200

Kusworo, T. D., Susanto, H., Aryanti, N., Rokhati, N., Widiasa, I. N., Al-Aziz, H., Utomo, D. P., Masithoh, D., & Kumoro, A. C. (2021). Preparation and characterization of photocatalytic PSf-TiO2/GO nanohybrid membrane for the degradation of organic contaminants in natural rubber wastewater. *Journal of Environmental Chemical Engineering*, *9*(2), 105066. https://doi.org/10.1016/j.jece.2021.105066

Lee, S.-T., Vu, C. T., Lin, C., & Chen, K.-S. (2018). High occurrence of BTEX around major industrial plants in Kaohsiung, Taiwan. *Environmental Forensics*, *19*(3), 206–216. https://doi.org/10.1080/15275922.2018.1475432

Li, C., Sun, W., Lu, Z., Ao, X., & Li, S. (2020). Ceramic nanocomposite membranes and membrane fouling: A review. *Water Research*, *175*, 115674. https://doi.org/10.1016/j.watres.2020.115674

Li, H., Zhang, J., Zhu, L., Liu, H., Yu, S., Xue, J., Zhu, X., & Xue, Q. (2021). Reusable membrane with multifunctional skin layer for effective removal of insoluble emulsified oils and soluble dyes. *Journal of Hazardous Materials*, *415*, 125677. https://doi.org/10.1016/j.jhazmat.2021.125677

Li, L., Feng, Y., Chen, X., He, Z., Wang, H., & Xia, Y. (2023). Impacts of suspended sediment on oil spill in macro-tidal turbid waters: An example in Zhoushan Archipelago. *Journal of Marine Systems*, *240*, 103879. https://doi.org/10.1016/j.jmarsys.2023.103879

Li, X., Fang, X., Pang, R., Li, J., Sun, X., Shen, J., Han, W., & Wang, L. (2014). Self-assembly of TiO2 nanoparticles around the pores of PES ultrafiltration membrane for mitigating organic fouling. *Journal of Membrane Science*, *467*, 226–235. https://doi.org/10.1016/j.memsci.2014.05.036

Liden, T., Santos, I. C., Hildenbrand, Z. L., & Schug, K. A. (2018). Treatment modalities for the reuse of produced waste from oil and gas development. *Science of The Total Environment*, *643*, 107–118. https://doi.org/10.1016/j.scitotenv.2018.05.386

Lin, C., Mao, W.-M., & Nadim, F. (2007). Forensic investigation of BTEX contamination in the Houjing River in southern Taiwan. *J. Environ. Eng. Manage*, *17*, 395–402.

Liu, A., Hong, N., Zhu, P., & Guan, Y. (2018). Understanding benzene series (BTEX) pollutant load characteristics in the urban environment. *Science of The Total Environment*, *619–620*, 938–945. https://doi.org/10.1016/j.scitotenv.2017.11.184

Liu, F., Hashim, N. A., Liu, Y., Abed, M. R. M., & Li, K. (2011). Progress in the production and modification of PVDF membranes. *Journal of Membrane Science*, *375*(1), 1–27. https://doi.org/10.1016/j.memsci.2011.03.014

Liu, H., Yu, H., Yuan, X., Ding, W., Li, Y., & Wang, J. (2019). Amino-functionalized mesoporous PVA/SiO2 hybrids coated membrane for simultaneous removal of oils and water-

soluble contaminants from emulsion. *Chemical Engineering Journal*, *374*, 1394–1402. https://doi.org/10.1016/j.cej.2019.05.161

Liu, T., Chen, D., Cao, Y., Yang, F., Chen, J., Kang, J., Xu, R., & Xiang, M. (2021). Construction of a composite microporous polyethylene membrane with enhanced fouling resistance for water treatment. *Journal of Membrane Science*, *618*, 118679. https://doi.org/10.1016/j.memsci.2020.118679

Loske, L., Nakagawa, K., Yoshioka, T., & Matsuyama, H. (2020). 2D Nanocomposite Membranes: Water Purification and Fouling Mitigation. *Membranes*, *10*(10), Article 10. https://doi.org/10.3390/membranes10100295

Lu, Q., & Li, N. (2021). Preparation of hydrophilic polyvinylidene fluoride/polyvinyl alcohol ultrafiltration membrane via polymer/non-solvent co-induced phase separation method towards enhance anti-fouling performance. *Journal of Environmental Chemical Engineering*, *9*(6), 106431. https://doi.org/10.1016/j.jece.2021.106431

Lu, Q., Zhang, X., Hing Wong, N., Sunarso, J., & Li, N. (2022). Anti-biofouling polyvinylidene fluoride/quaternized polyvinyl alcohol ultrafiltration membrane selectively separates aromatic contaminants from wastewater by host–guest interactions. *Separation and Purification Technology*, *296*, 121387. https://doi.org/10.1016/j.seppur.2022.121387

Martínez-Cabanas, M., López-García, M., Barriada, J. L., Herrero, R., & Sastre de Vicente, M. E. (2016). Green synthesis of iron oxide nanoparticles. Development of magnetic hybrid materials for efficient As(V) removal. *Chemical Engineering Journal*, *301*, 83–91. https://doi.org/10.1016/j.cej.2016.04.149

Maryam Tavakolmoghadam. (2022). TiO2 Nanoparticles Effect on PVDF Membrane Filterability in Membrane Bioreactors: Fouling Reduction and Critical Flux Enhancement. *Journal of Water Chemistry and Technology*, *44*(1), 40–47. https://doi.org/10.3103/S1063455X2201009X

Matin, A., Baig, N., Anand, D., Ahmad, I., Sajid, M., & Nawaz, M. S. (2023). Thin-film nanocomposite membranes for efficient removal of emerging pharmaceutical organic contaminants from water. *Environmental Research*, *237*, 116905. https://doi.org/10.1016/j.envres.2023.116905

Megías-Sayago, C., Lara-Ibeas, I., Wang, Q., Le Calvé, S., & Louis, B. (2020). Volatile organic compounds (VOCs) removal capacity of ZSM-5 zeolite adsorbents for near real-time BTEX detection. *Journal of Environmental Chemical Engineering*, *8*(2), 103724. https://doi.org/10.1016/j.jece.2020.103724

Melaphi, K., Sadare, O. O., Simate, G. S., Wagenaar, S., & Moothi, K. (2023). Adsorptive removal of BTEX compounds from wastewater using activated carbon derived from macadamia nut shells. *Water SA*, *49*(1), Article 1.

Mohammadi, L., Rahdar, A., Bazrafshan, E., Dahmardeh, H., Susan, M. A. B. H., & Kyzas, G. Z. (2020). Petroleum Hydrocarbon Removal from Wastewaters: A Review. *Processes*, *8*(4), Article 4. https://doi.org/10.3390/pr8040447

Nasir, A. M., Goh, P. S., Abdullah, M. S., Ng, B. C., & Ismail, A. F. (2019). Adsorptive nanocomposite membranes for heavy metal remediation: Recent progresses and challenges. *Chemosphere*, *232*, 96–112. https://doi.org/10.1016/j.chemosphere.2019.05.174

Nayak, S. K., Dutta, K., & Gohil, J. M. (2022). *Advancement in Polymer-Based Membranes for Water Remediation*. Elsevier.

Oliveira, C. P. M. de, Fernandes Farah, I., Koch, K., Drewes, J. E., Viana, M. M., & Amaral, M. C. S. (2022). TiO2-Graphene oxide nanocomposite membranes: A review. *Separation and Purification Technology*, *280*, 119836. https://doi.org/10.1016/j.seppur.2021.119836

Overton, E. B., Wade, T. L., Radović, J. R., Meyer, B. M., Miles, M. S., & Larter, S. R. (2016). Chemical Composition of Macondo and Other Crude Oils and Compositional Alterations During Oil Spills. *Oceanography*, *29*(3), 50–63.

Paipuri, M. (2014). *Numerical Modelling of Membrane filtration using Lattice Boltzmann and Finite Volume Methods*. https://doi.org/10.13140/RG.2.2.26191.79524

Rasheed, T., Hassan, A. A., Bilal, M., Hussain, T., & Rizwan, K. (2020). Metal-organic frameworks based adsorbents: A review from removal perspective of various environmental contaminants from wastewater. *Chemosphere*, *259*, 127369. https://doi.org/10.1016/j.chemosphere.2020.127369

Rayaroth, M. P., Marchel, M., & Boczkaj, G. (2023). Advanced oxidation processes for the removal of mono and polycyclic aromatic hydrocarbons – A review. *Science of The Total Environment*, *857*, 159043. https://doi.org/10.1016/j.scitotenv.2022.159043

Rouhani, M., Ashrafi, S. D., Taghavi, K., Joubani, M. N., & Jaafari, J. (2022). Evaluation of tetracycline removal by adsorption method using magnetic iron oxide nanoparticles (Fe3O4) and clinoptilolite from aqueous solutions. *Journal of Molecular Liquids*, *356*, 119040. https://doi.org/10.1016/j.molliq.2022.119040

Rozell, D. J., & Reaven, S. J. (2012). Water Pollution Risk Associated with Natural Gas Extraction from the Marcellus Shale. *Risk Analysis*, *32*(8), 1382–1393. https://doi.org/10.1111/j.1539-6924.2011.01757.x

Saharan, P., Chaudhary, G. R., Mehta, S. K., & Umar, A. (2014). Removal of Water Contaminants by Iron Oxide Nanomaterials. *Journal of Nanoscience and Nanotechnology*, *14*(1), 627–643. https://doi.org/10.1166/jnn.2014.9053

Saini, B., Sinha, M. K., & Dash, S. K. (2019). Mitigation of HA, BSA and oil/water emulsion fouling of PVDF Ultrafiltration Membranes by SiO2-g-PEGMA nanoparticles. *Journal of Water Process Engineering*, *30*, 100603. https://doi.org/10.1016/j.jwpe.2018.03.018

Schmid, G. (2011). *Nanoparticles: From Theory to Application*. John Wiley & Sons.

Schmidt, B. V. K. J. (2019). Hydrophilic Polymers. *Polymers*, *11*(4), Article 4. https://doi.org/10.3390/polym11040693

Shi, Y., Chen, X., Wu, Q., Zhen, H., Wang, S., Dong, H., Wang, J., & Li, Y. (2023). Enhance organic pollutants removal of wastewater by a PVDF/PDA-TiO2 composite membrane with photocatalytic property. *Journal of Environmental Chemical Engineering*, *11*(5), 110389. https://doi.org/10.1016/j.jece.2023.110389

Simeonidis, K., Mourdikoudis, S., Kaprara, E., Mitrakas, M., & Polavarapu, L. (2016). Inorganic engineered nanoparticles in drinking water treatment: A critical review. *Environmental Science: Water Research & Technology*, *2*(1), 43–70. https://doi.org/10.1039/C5EW00152H

Singh, R. (2006). *Hybrid Membrane Systems for Water Purification: Technology, Systems Design and Operations*. Elsevier.

Singh, R., & Hankins, N. (2016). *Emerging Membrane Technology for Sustainable Water Treatment*. Elsevier.

Sirotkin, A. V., & Harrath, A. H. (2017). Influence of oil-related environmental pollutants on female reproduction. *Reproductive Toxicology*, *71*, 142–145. https://doi.org/10.1016/j.reprotox.2017.05.007

Sonawane, A. V., & Murthy, Z. V. P. (2022). Treatment of winery wastewater with PEG-600/PVDF mixed matrix membranes using submerged membrane bioreactor and process optimization by box–Behnken design. *International Journal of Environmental Research*, *16*(5), 92. https://doi.org/10.1007/s41742-022-00476-9

Soni, V., Raizada, P., Singh, P., Cuong, H. N., S, R., Saini, A., Saini, R. V., Le, Q. V., Nadda, A. K., Le, T.-T., & Nguyen, V.-H. (2021). Sustainable and green trends in using plant extracts for the synthesis of biogenic metal nanoparticles toward environmental and pharmaceutical advances: A review. *Environmental Research*, *202*, 111622. https://doi.org/10.1016/j.envres.2021.111622

Srimuk, P., Su, X., Yoon, J., Aurbach, D., & Presser, V. (2020). Charge-transfer materials for electrochemical water desalination, ion separation and the recovery of elements. *Nature Reviews Materials*, *5*(7), 517–538. https://doi.org/10.1038/s41578-020-0193-1

Su, F., Lu, C., Johnston, K. R., & Hu, S. (2010). CHAPTER 5—Kinetics, Thermodynamics, and Regeneration of BTEX Adsorption in Aqueous Solutions via NaOCl-Oxidized Carbon Nanotubes. In M. Fan, C.-P. Huang, A. E. Bland, Z. Wang, R. Slimane, & I. Wright (Eds.), *Environanotechnology* (pp. 71–97). Elsevier. https://doi.org/10.1016/B978-0-08-054820-3.00005-8

Subasi, Y., & Cicek, B. (2017). Recent advances in hydrophilic modification of PVDF ultrafiltration membranes – a review: Part II. *Membrane Technology*, *2017*(11), 5–11. https://doi.org/10.1016/S0958-2118(17)30233-1

Uddin, M. J., Ampiaw, R. E., & Lee, W. (2021). Adsorptive removal of dyes from wastewater using a metal-organic framework: A review. *Chemosphere*, *284*, 131314. https://doi.org/10.1016/j.chemosphere.2021.131314

Unuigbe, C. F., Fayemiwo, O. M., & Daramola, M. O. (2020). Performance evaluation of iron nanoparticles infused polyethersulphone (Fe-NPs/PES) membrane during treatment of BTEX-contaminated wastewater. *Water and Environment Journal*, *34*(S1), 74–86. https://doi.org/10.1111/wej.12506

US EPA, (2014). *Persistent Organic Pollutants: A Global Issue, A Global Response* [Overviews and Factsheets]. https://www.epa.gov/international-cooperation/persistent-organic-pollutants-global-issue-global-response

USGS. (2006). *Open-File Report* (Open-File Report) [Open-File Report].

Van der Bruggen, B. (2009). Chemical modification of polyethersulfone nanofiltration membranes: A review. *Journal of Applied Polymer Science*, *114*(1), 630–642. https://doi.org/10.1002/app.30578

Vanloocke, R., De Borger, R., Voets, J. P., & Verstraete, W. (1975). Soil and groundwater contamination by oil spills; problems and remedies. *International Journal of Environmental Studies*, *8*(1–4), 99–111. https://doi.org/10.1080/00207237508709721

Varjani, S. J., Gnansounou, E., & Pandey, A. (2017). Comprehensive review on toxicity of persistent organic pollutants from petroleum refinery waste and their degradation by microorganisms. *Chemosphere*, *188*, 280–291. https://doi.org/10.1016/j.chemosphere.2017.09.005

Wang, P., Wang, X., Yu, S., Zou, Y., Wang, J., Chen, Z., Alharbi, N. S., Alsaedi, A., Hayat, T., Chen, Y., & Wang, X. (2016). Silica coated Fe3O4 magnetic nanospheres for high removal of organic pollutants from wastewater. *Chemical Engineering Journal*, *306*, 280–288. https://doi.org/10.1016/j.cej.2016.07.068

Warsinger, D. M., Chakraborty, S., Tow, E. W., Plumlee, M. H., Bellona, C., Loutatidou, S., Karimi, L., Mikelonis, A. M., Achilli, A., Ghassemi, A., Padhye, L. P., Snyder, S. A., Curcio, S., Vecitis, C. D., Arafat, H. A., & Lienhard, J. H. (2018). A review of polymeric membranes and processes for potable water reuse. *Progress in Polymer Science*, *81*, 209–237. https://doi.org/10.1016/j.progpolymsci.2018.01.004

Wei, X., Liu, Y., Zheng, J., Wang, X., Xia, S., & Van der Bruggen, B. (2022). A critical review on thin-film nanocomposite membranes enabled by nanomaterials incorporated in different positions and with diverse dimensions: Performance comparison and mechanisms. *Journal of Membrane Science*, *661*, 120952. https://doi.org/10.1016/j.memsci.2022.120952

Wiesenthal, A., Hunter, L., Wang, S., Wickliffe, J., & Wilkerson, M. (2011). Nanoparticles: Small and mighty. *International Journal of Dermatology*, *50*(3), 247–254. https://doi.org/10.1111/j.1365-4632.2010.04815.x

Wu, S., Li, K., Shi, W., & Cai, J. (2022). Preparation and performance evaluation of chitosan/polyvinylpyrrolidone/polyvinyl alcohol electrospun nanofiber membrane for heavy metal ions and organic pollutants removal. *International Journal of Biological Macromolecules*, *210*, 76–84. https://doi.org/10.1016/j.ijbiomac.2022.05.017

Xiong, Z., Liu, J., Yang, Y., Lai, Q., Wu, X., Yang, J., Zeng, Q., Zhang, G., & Zhao, S. (2022). Reinforcing hydration layer on membrane surface via nano-capturing and hydrothermal crosslinking for fouling reduction. *Journal of Membrane Science*, *644*, 120076. https://doi.org/10.1016/j.memsci.2021.120076

Yin, J., & Deng, B. (2015). Polymer-matrix nanocomposite membranes for water treatment. *Journal of Membrane Science*, *479*, 256–275. https://doi.org/10.1016/j.memsci.2014.11.019

Younas, H., Bai, H., Shao, J., Han, Q., Ling, Y., & He, Y. (2017). Super-hydrophilic and fouling resistant PVDF ultrafiltration membranes based on a facile prefabricated surface. *Journal of Membrane Science*, *541*, 529–540. https://doi.org/10.1016/j.memsci.2017.07.035

Yu, B., Yuan, Z., Yu, Z., & Xue-song, F. (2022). BTEX in the environment: An update on sources, fate, distribution, pretreatment, analysis, and removal techniques. *Chemical Engineering Journal*, *435*, 134825. https://doi.org/10.1016/j.cej.2022.134825

Yunos, M. Z., Harun, Z., Basri, H., & Ismail, A. F. (2014). Studies on fouling by natural organic matter (NOM) on polysulfone membranes: Effect of polyethylene glycol (PEG). *Desalination*, *333*(1), 36–44. https://doi.org/10.1016/j.desal.2013.11.019

Zambianchi, M., Durso, M., Liscio, A., Treossi, E., Bettini, C., Capobianco, M. L., Aluigi, A., Kovtun, A., Ruani, G., Corticelli, F., Brucale, M., Palermo, V., Navacchia, M. L., & Melucci, M. (2017). Graphene oxide doped polysulfone membrane adsorbers for the removal of organic contaminants from water. *Chemical Engineering Journal*, *326*, 130–140. https://doi.org/10.1016/j.cej.2017.05.143

Zhang, H., Zheng, Y., Yu, S., Chen, W., & Yang, J. (2022). A Review of Advancing Two-Dimensional Material Membranes for Ultrafast and Highly Selective Liquid Separation. *Nanomaterials*, *12*(12), Article 12. https://doi.org/10.3390/nano12122103

Zhang, R., Liu, Y., He, M., Su, Y., Zhao, X., Elimelech, M., & Jiang, Z. (2016). Antifouling membranes for sustainable water purification: Strategies and mechanisms. *Chemical Society Reviews*, *45*(21), 5888–5924. https://doi.org/10.1039/C5CS00579E

Zhao, X., Zhang, R., Liu, Y., He, M., Su, Y., Gao, C., & Jiang, Z. (2018). Antifouling membrane surface construction: Chemistry plays a critical role. *Journal of Membrane Science*, *551*, 145–171. https://doi.org/10.1016/j.memsci.2018.01.039

CHAPTER 3: Materials and Experimental Procedures

This chapter briefly discusses the materials and experimental procedures used to achieve the goals of this study. The study focused on developing a new treatment strategy for BTEX removal through the use of biogenic-synthesized iron oxide NPs and PVA to develop an antifouling membrane that can maintain its performance in both short-term and long-term applications. The procedure for the biosynthesis of the iron oxide NPs and the fabrication of the membranes are briefly discussed. Some of the characterization techniques used in the study are also discussed.

3.1 Biosynthesis of iron oxide NPs

Three different parts of the pomegranate were used to prepare extracts for the bio-reduction of the iron precursor to the iron oxide NPs. The properties and BTEX removal capacities of the biogenic-synthesized iron oxide NPs were compared. A detailed description of the biosynthesis of the NPs is presented in Paper 1 in the next chapter.

3.2 Fabrication of the Fe_3O_4 NPs and Fe_3O_4 NPs/PVA-modified membranes

The control and modified membranes were fabricated through non-solvent-induced phase inversion using DI water as the coagulation bath. A detailed description of the fabrication process is presented in the respective Papers in chapter 5 and 6..

3.3 Iron oxide NPs and membrane characterization

The properties of the biogenic-synthesized iron oxide NPs and the membranes were obtained using characterization techniques such as powder X-ray diffraction (PXRD), Fourier transform infrared spectroscopy (FTIR), scanning electron microscopy (SEM), transmission electron microscopy (TEM), and Brunauer-Emmett-Teller (BET).

3.3.1 PXRD

PXRD is a common characterization technique for the determination of a sample's crystal structure or composition. The analysis of a sample using PXRD involves the constructive interference of monochromatic X-rays and the samples (Bunaciu et al., 2015). The X-rays are produced in a cathode ray tube by heating a filament to generate electrons, and the samples are bombarded with the generated electrons by applying a voltage. Characteristic X-ray spectra of the sample are obtained when the bombarding electrons have sufficient energy to dislodge the

inner shell electrons of the sample. Figure 3.1 shows a depiction of a typical X-ray diffraction mechanism.

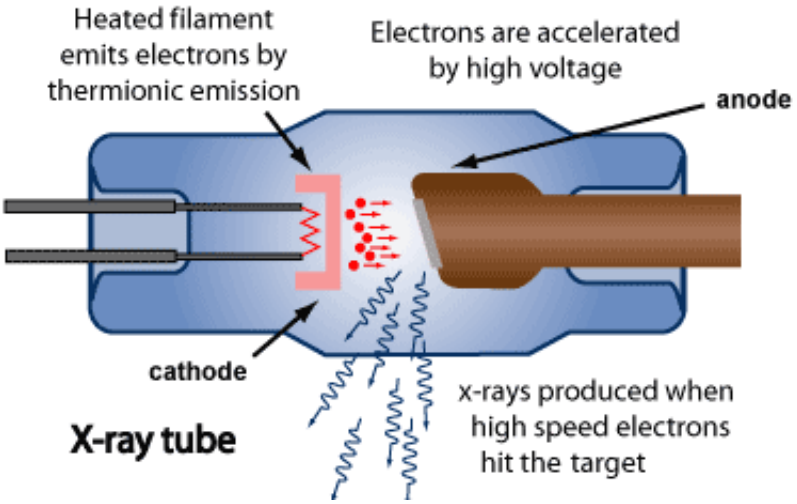


Figure 3. 1: Schematic representation of X-ray mechanism (ARPANSA, 2015).

3.3.2 FTIR

FTIR is a common technique for analyzing the functional groups in a sample and thus provides information on the sample's composition. It is performed by passing a beam of infrared (IR) radiation through the sample, resulting in the sample adsorbing some of the IR radiation while transmitting some (Qu et al., 2017). This generates a unique spectrum for the sample, which represents its molecular fingerprint and identifies the sample's composition (Jaggi & Vij, 2006). The size of the peaks in the spectrum also gives an indication of the amount of the components present in the sample (Qu et al., 2017). A simple schematic depiction of the FTIR principle is shown in Figure 3.2.

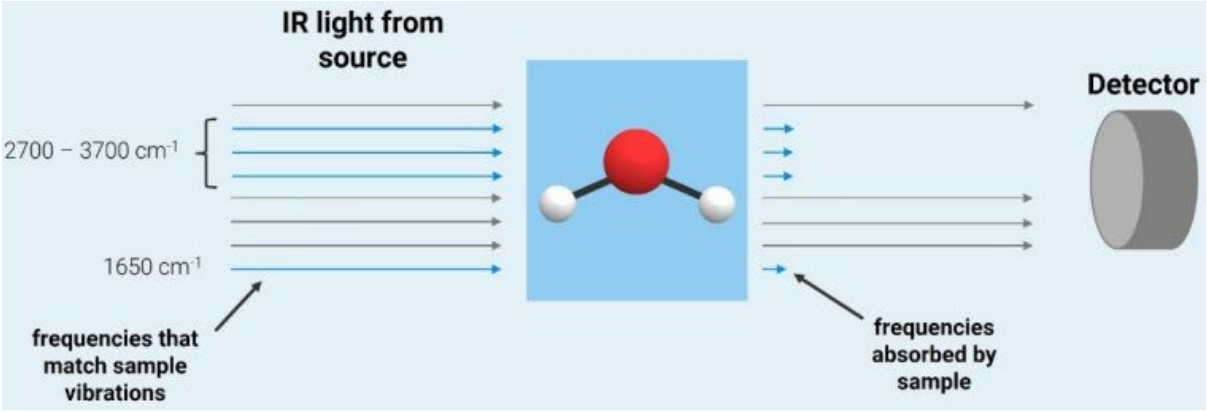


Figure 3. 2: Schematic representation of FTIR mechanism (Bruker, 2019).

3.3.3 SEM

SEM is a versatile characterization technique used to analyze the morphology or topography of the surface of a sample. The analysis of a sample using SEM involves scanning the sample's surface with electron beams in a raster scan pattern, and the interaction of the electrons with the sample atoms produces signals that have information on the morphology or topography of the sample (Liu et al., 2010). By detecting the signal emanating from the emitted secondary electrons of the sample, a detailed visual image of the surface of the sample is obtained (Zhou et al., 2007). A schematic depiction of the principle of SEM is shown in Figure 3.3.

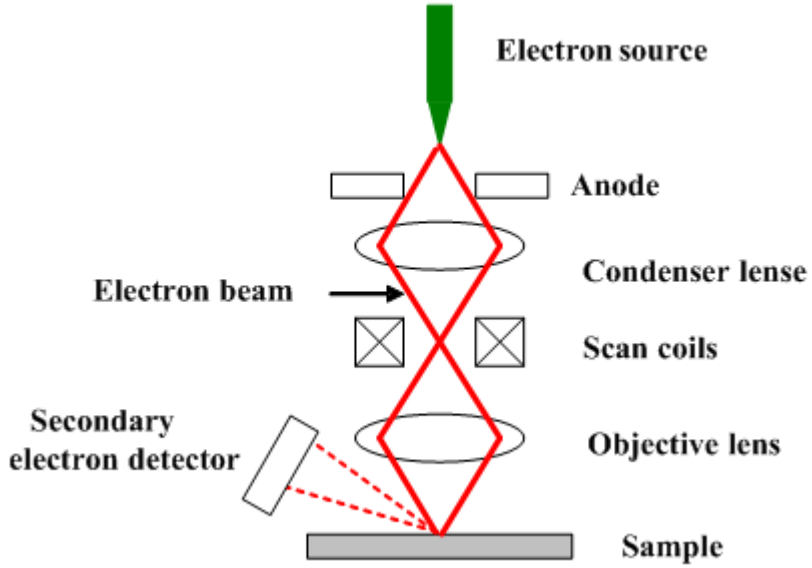


Figure 3. 3: Schematic depiction of the principle of SEM (SubsTech, 2015).

3.3.4 TEM

Unlike SEM, the electron beams pass through the sample; hence TEM is used to analyze the internal morphology of a sample. The principles of SEM and TEM are similar; however, in contrast to SEM, TEM measures how the focused beams of electrons change as they are scattered in the sample (Liu et al., 2010). TEM images of the sample are then obtained from the transmitted electrons, which are focused on the objective lens and appear on the imaging screen (Asadi Asadabad & Jafari Eskandari, 2015). A typical schematic depiction of TEM principle is shown in Figure 3.4.

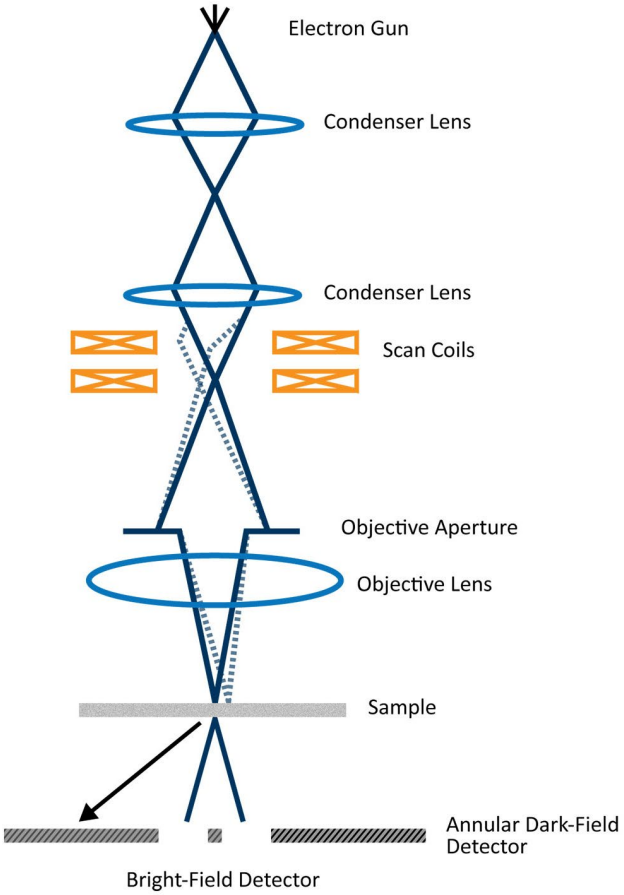


Figure 3. 4: Schematic depiction of the TEM principle (Nanoscience Instruments, 2020)

.

3.4 Membrane performance assessment

The performance assessment of the various membranes fabricated in this study is extensively detailed in the respective papers as presented in chapters 5 and 6 of this thesis. Key performance parameters such as membrane flux, selectivity, and antifouling assessments were calculated to determine the modified membranes' performance in BTEX wastewater treatment. The formula for calculating the various performance parameters is outlined in Chapter 2 of this thesis.

References

ARPANSA. (2015). *X-ray*. https://www.arpansa.gov.au/understanding-radiation/what-is-radiation/ionising-radiation/x-ray

Asadi Asadabad, M., & Jafari Eskandari, M. (2015). Transmission Electron Microscopy as best technique for characterization in nanotechnology. *Synthesis and Reactivity in Inorganic, Metal-Organic, and Nano-Metal Chemistry*, *45*(3), 323–326. https://doi.org/10.1080/15533174.2013.831901

Bruker. (2019). *Guide to FT-IR Spectroscopy*. https://www.bruker.com/en/products-and-solutions/infrared-and-raman/ft-ir-routine-spectrometer/what-is-ft-ir-spectroscopy.html

Bunaciu, A. A., Udriştioiu, E. gabriela, & Aboul-Enein, H. Y. (2015). X-Ray Diffraction: Instrumentation and Applications. *Critical Reviews in Analytical Chemistry*, *45*(4), 289–299. https://doi.org/10.1080/10408347.2014.949616

Jaggi, N., & Vij, D. R. (2006). Fourier Transform Infrared Spectroscopy. In D. R. Vij (Ed.), *Handbook of Applied Solid State Spectroscopy* (pp. 411–450). Springer US. https://doi.org/10.1007/0-387-37590-2_9

Liu, F., Wu, J., Chen, K., & Xue, D. (2010). Morphology study by using Scanning Electron Microscopy. *Microscopy: Science, Technology, Applications and Education*.

Qu, S., Fang, J., Zang, D., Xing, H., Wang, L., & Wu, H. (2017). Dielectric and Magnetic Loss Behavior of Nanooxides. In *Spectroscopic Methods for Nanomaterials Characterization* (pp. 301–319). https://doi.org/10.1016/B978-0-323-46140-5.00011-X

SubsTech. (2015). *Scanning Electron Microscope*. https://www.substech.com/dokuwiki/doku.php?id=scanning_electron_microscope

Zhou, W., Apkarian, R., Wang, Z. L., & Joy, D. (2007). Fundamentals of Scanning Electron Microscopy (SEM). In W. Zhou & Z. L. Wang (Eds.), *Scanning Microscopy for Nanotechnology: Techniques and Applications* (pp. 1–40). Springer. https://doi.org/10.1007/978-0-387-39620-0_1

CHAPTER 4: Comparative study of biogenic iron oxide nanoparticles from various extracts of pomegranate and their efficient application for removal of BTEX

This chapter is composed of the initial investigation of the potential of biogenic-synthesized iron oxide nanoparticles in BTEX removal from wastewater, as reported in the first manuscript of this study, **Paper 1**. The manuscript has been submitted to the **Journal of Cleaner Production** for evaluation and publication.

The manuscript explored the biosynthesis of iron oxide NPs using the extracts of pomegranate leaves, peels, and seeds. A comparison of the ability of the different biogenic-synthesized iron oxide NPs to remove BTEX from wastewater was studied. Hence, this section of the study provides information on the potential of the biogenic-synthesized iron oxide NPs in treating BTEX-contaminated water and, thus, establishes the potential contribution of the NPs when used in BTEX wastewater treatment.

Abstract

This study explored the effectiveness of biogenic-synthesized iron oxide nanoparticles (FeNPs) in the adsorptive removal of benzene, toluene, ethylbenzene, and xylene (BTEX) from wastewater. The FeNPs were prepared using the leaves, peels, and seeds extracts of pomegranate to reduce the iron precursor. The features of the FeNPs were analyzed using XRD, FTIR, SEM, TEM, BET, and zeta potential measurement. According to the XRD results, reducing the iron precursor with the pomegranate leaves extract yielded magnetite, while the peels and seeds extract produced maghemite. All three FeNPs, that is, the FeNPs-leaves, FeNPs-peels, and FeNPs-seeds are mesoporous materials as determined from their BET results. The adsorption study shows that pH 5 was the ideal pH to achieve the highest adsorption capacity for BTEX using the FeNPs adsorbents. At the equilibrium time of 40 min, the BTEX removal efficiency, R (%), of the FeNPs is as follows: FeNPs-leaves (B; 78.60, T; 75.72, E; 75.30; X; 69.84), FeNPs-peels (B; 91.54, T; 91.02, E; 90.7, X; 86.96) and FeNPs-seeds (B; 87.72, T; 89.30, E; 88.38, X; 86.76). Kinetic and isotherm fitting of the adsorption data revealed that the adsorption process conformed with pseudo-second-order and Langmuir isotherm, respectively. The FeNPs maintained high BTEX removal efficiency after four cycles of adsorption-desorption experiments, thus confirming their regenerability. Overall, the study

presented biogenic-synthesized FeNPs as potential adsorbents for BTEX removal from wastewater.

4.1 Introduction

Pollution of water bodies remains a significant obstacle to water accessibility and sustainable management (United Nations, 2015). The water pollution mainly occurs through anthropogenic activities, such as the industrial release of inorganic and organic contaminants into the water system (Mokarram et al., 2020; Bielen et al., 2017). The presence of these contaminants in the water system constitutes both health and environmental threats, which could be mild or severe depending on the level of exposure to the contaminants (Bielen et al., 2017). Such contaminants include benzene, toluene, ethylbenzene, and xylene, collectively known as BTEX, which are organic contaminants mainly discharged into the water system from untreated or poorly treated industrial wastewater (Yu et al., 2022; Fayemiwo et al., 2017). High levels of BTEX have been reported in water bodies across the globe, thereby highlighting the issue of BTEX water contamination as a global challenge (Lee et al., 2018; Asejeje et al., 2021; Nambi et al., 2017; Gross et al., 2013; Chittick & Srebotnjak, 2017; Rodrigo-Ilarri et al., 2023; Astrahan et al., 2023). The human exposure to BTEX could lead to health complications such as chronic lymphocytic leukemia, kidney and liver dysfunction, premature births, and mutagenic diseases (Davidson et al., 2021; Yu et al., 2022; Bulatović et al., 2022; Partha et al., 2022). In addition, aquatic organisms exposed to BTEX-contaminated water could experience growth, development, and reproductive complications (Xu et al., 2020; Eom et al., 2023). The atmospheric environment could also be adversely affected as the volatilization of BTEX from the contaminated water body into the atmosphere could result in poor air quality, which could also be detrimental to human health (Moridzadeh et al., 2020; Dantas et al., 2022).

Several techniques have been devised to remove BTEX from wastewater to address the issue of BTEX water contamination. These techniques include advanced oxidation processes (Bustillo-Lecompte et al., 2018; Jiménez et al., 2019), biofiltration (Leili et al., 2017), membrane technology (Enemuo et al., 2024; Zhang et al., 2019), and adsorption (Bartilotti et al., 2021; Varela et al., 2021). The adsorptive removal of BTEX from wastewater has been a prime research focus due to the ease, low cost, and high effectiveness of the process and the easy preparation of the adsorbent materials (Anjum et al., 2019; Medeiros et al., 2022). Among the adsorbent materials used for the adsorptive removal of BTEX are nanoparticles, which have shown high effectiveness in BTEX removal from wastewater (Yu et al., 2022; Kim et al., 2013;

Azizi et al., 2016). The effectiveness of nanoparticles as good adsorbent for most contaminants is due to their high surface area, which provides more sites for the adsorption of the contaminants (Kumari et al., 2019; Prathna. et al., 2018). Liu et al., 2015 used highly crosslinked polymer (HCP) nanoparticles for BTEX adsorption from aqueous solutions, and high BTEX adsorption affinities of the HCP nanoparticles were reported (S. Liu et al., 2015). Modified graphene oxide nanoparticles were employed by Azizi et al., 2016 to remove toluene, ethylbenzene, and xylene from aqueous solution, and high removal efficiency was obtained (Azizi et al., 2016). High benzene uptake was reported when oleic acid-modified iron oxide nanoparticles were used for benzene adsorption from synthetic wastewater (Masuku et al., 2021). The BTEX removal efficiency of zero-valent iron nanoparticles was reported to be high when the nanoparticles were applied for BTEX adsorption from aqueous solutions (Mahmoud et al., 2017).

For the application of iron oxide/ iron nanoparticles in BTEX adsorptive removal, the above research results identified the nanoparticles as good potential adsorbent for BTEX. Despite the promising attribute of iron oxide nanoparticles in the adsorptive removal of BTEX from wastewater, very few research has been conducted utilizing the nanoparticles for BTEX adsorption from wastewater. To the best of our knowledge, only two research have utilized iron oxide or iron nanoparticles as a single adsorbent for the adsorptive removal of all four components of BTEX from wastewater (Eldos et al., 2023; Mahmoud et al., 2017). In both studies, the nanoparticles were prepared using chemical methods involving the use of hazardous chemicals to reduce the iron precursors to the iron oxide/iron nanoparticles (Eldos et al., 2023; Mahmoud et al., 2017). Other studies that utilized iron oxide nanoparticles in BTEX adsorptive removal from wastewater used the nanoparticles not as a single adsorbent but as a composite with another adsorbent to further improve the adsorbents' capacity for BTEX removal (Fernández et al., 2016; Bartilotti et al., 2021). The synthesis of the composite also involved the use of hazardous chemicals to reduce the iron precursor.

In response to the idea of a sustainable approach to synthesis, it is important that the iron oxide adsorbents used for BTEX adsorption are prepared in a more eco-friendly approach. This includes replacing the hazardous chemicals used to reduce the iron precursor to more eco-friendly alternatives such as plant extracts. Most extracts contain phytochemicals such as polyphenols that act as reducing agents for iron oxide nanoparticle synthesis (Gupta et al., 2023). However, different plant extracts could contain distinct types or amounts of active phytochemicals, which could result in different forms of bio-synthesized nanoparticles (Jadoun

et al., 2021). In addition, some of the active functional groups of the phytochemicals are deposited on the surface of the biogenic synthesized nanoparticles (Soni et al., 2021), thereby introducing some functional groups that can enhance the BTEX adsorption tendency of the nanoparticles. This improves the effectiveness of the biogenic synthesized nanoparticle as a single adsorbent in the treatment of BTEX wastewater.

To the best of our knowledge, this study provides, for the first time, a comparative study on the biogenic synthesis of iron oxide nanoparticles from the extracts of the leaves, peels, and seeds of the pomegranate for application in BTEX adsorptive removal from wastewater. Thus, hazardous reducing agents are replaced with these plant extracts in the synthesis of the nanoparticles for application in BTEX adsorption. The use of the three parts of the pomegranate is considered sustainable in terms of food conservation, as the pomegranate fruit peels and seeds are food waste, and the leaves are not edible food. The properties of the bio-synthesized nanoparticles were compared using techniques such as X-ray diffraction (XRD), Fourier transform infrared (FTIR), scanning electron microscopy (SEM), transmission electron microscopy (TEM), and Brunauer-Emmett-Teller (BET). The characterization showed that three distinct iron oxide nanoparticles were obtained from the three different pomegranate extracts. The nanoparticles were applied for BTEX adsorptive removal from wastewater, and their performance was compared through batch adsorption study.

4.2 Experimental

4.2.1 Materials

The pomegranates' leaves, peels, and seeds were collected from the pomegranate tree at the School of Chemical Engineering, University of the Witwatersrand, Johannesburg. Folin-ciocalteu reagent, gallic acid, sodium carbonate, Iron (III) chloride, benzene (99.8%), toluene (99.9%), ethylbenzene (>99.9%), and xylene (≥99%) were purchased from Sigma Aldrich. Deionized water (DI water, 18.2 MΩcm @25^{o}C) supplied from the Direct-Q UV millipore system was used throughout this study. The chemicals were used as received without any further purification.

4.2.2 Preparation of the extracts of the pomegranate

The peels and seeds were obtained from the pomegranate fruits by separating these parts from the fruit, while the leaves were directly plucked from the tree. All the parts (leaves, seeds, and peels) were thoroughly washed with tap water to remove dust or impurities and then left to dry

in a clean, open space. Afterward, the parts were further dried in an oven at 50°C for 3 days to obtain well-dried pomegranate leaves, peels, and seeds. The dried parts were separately ground into fine powders using a clean grinder. The aqueous extracts of the parts were then obtained by mixing 20g of each powder separately with 200 mL of DI water and shaking the mixture for 8 hours at 150 rpm, followed by sonicating for 30 mins. The mixtures were then first filtered using a sieve, followed by vacuum filtration with a Whatman filter no. 1. The obtained separate extract of the leaves, peels, and seeds of the pomegranate were stored at 4°C and used for the synthesis of the Iron oxide nanoparticles (FeNPs).

4.2.3 Synthesis of the Iron oxide NPs

The iron oxide NPs were biogenically synthesized using the various prepared pomegranate extracts to reduce the iron precursor, $FeCl_3$. Three iron oxide NPs were obtained by using either the leaves, peels, and seeds extracts to reduce the precursor according to the procedure described below:

$FeCl_3$ solution was first obtained by dissolving 1.2g of $FeCl_3$ in 70 mL of DI water with continuous stirring. 140 mL of the pomegranate extract was added to the $FeCl_3$ solution and stirred continuously for 3 hrs at 80°C. At this stage, the colour of the reaction mixtures containing the peels and leaves extract changed from yellow to black, while the colour of the reaction mixture containing the seeds extract changed to yellowish-brown, as shown in Figure 4. 1. This indicates the complete reduction of the iron precursor to the iron oxide NPs. The reaction mixture was left to cool and then centrifuged to recover the NPs. The NPs were washed three times with ethanol and water by shaking the NPs suspension for 15 min and sonicating for 10 min to remove impurities. The sonication of the NPs also ensures the breakdown of the clusters of the NPs into individual NPs. Lastly, the resulting NPs were dried in an oven at 50°C for 3 hours to obtain the NPs in dry form, which was crushed with mortar and pestle into fine NP powder. The NPs were then stored in an airtight container and used for the related characterizations and performance analysis in this study.

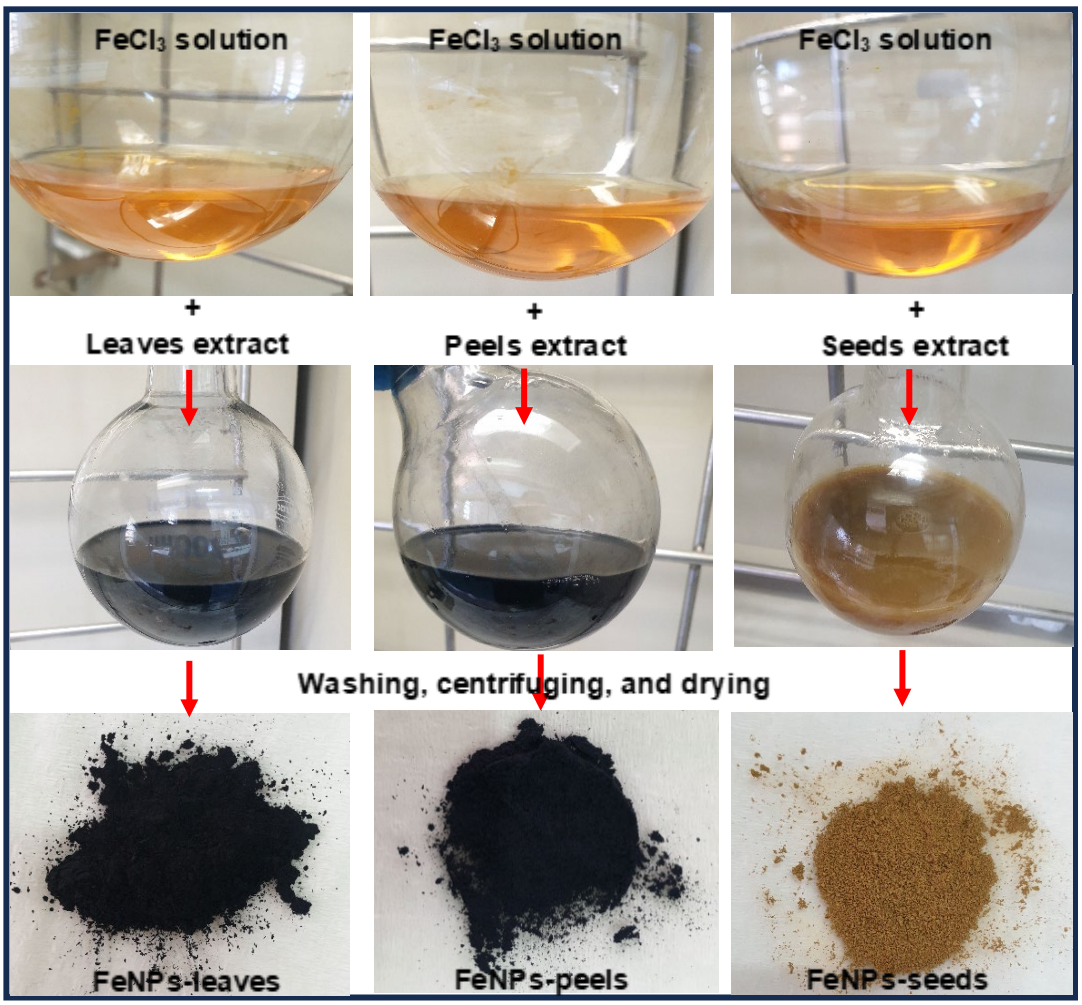


Figure 4. 1: The experimental procedure for the synthesis of the iron oxide NPs.

4.3 Characterization of the pomegranate extracts and iron oxide NPs

The total phenolic content of the extracts was measured according to the Folin-Ciocalteu assay (Singleton & Rossi, 1965), with few modifications such as the volume of the Folin-Ciocalteu reagent used, the volume of the extract used, and the Na_2CO_3 concentration. I mL of the Folin-Ciocalteu reagent was diluted with 9 mL of DI water. Na_2CO_3 solution was prepared by dissolving 7.5 g of Na_2CO_3 in 100 mL of DI water to obtain 7.5% (w/v) Na_2CO_3 solution. Then, 200 µL of each prepared extract (10 mg/mL) was well mixed with 1.0 mL of the diluted Folin-Ciocalteu reagent, and the mixture was left to stand in darkness for 5 mins. Afterward, 0.8 mL of the 7.5%(w/v) Na_2CO_3 was added to the mixture, thoroughly mixed for 1 min using a velp scientifica vortex mixer, and left to stand in the dark for 2 h. Gallic acid was used as the standard compound, and a stock solution of the gallic acid was prepared by thoroughly dissolving 0.5g of gallic acid in 100 mL of DI water to obtain a 5 mg/mL stock solution. The standard amounts

(0.05, 0.1, 0.15, 0.25, and 0.5 mg/mL) were prepared by taking aliquots of the stock solution and diluting accordingly, and 1 mL of the diluted Folin-Ciocalteu reagent and 0.8 mL of 7.5% (w/v) OF Na_2CO_3 were added to each of the standards. The standards were left to stand in the dark for 2 h. The absorbance of the standards and pomegranate extracts at 765nm was measured against a blank using an Agilent Cary Series UV-Vis Spectrophotometer. All the measurements were done in triplicates, and the total phenolic content was expressed as mg gallic acid equivalents (GAE) per g of either the dry leaves, peels, or seeds, which was calculated using Eq. (7).

$$C = cV/M \tag{7}$$

Where C is the total phenolic content (mg GAE/g of dry plant). c, V, and M are the concentration of gallic acid obtained from the calibration curve (mg/mL), volume of the extract (mL), and mass of the dry plant (g), respectively. The prepared standards and samples for total phenolic content measurement are shown in Fig. 4.2.

The phytochemicals in the pomegranate extracts were determined using an Agilent GC 7890B, with a 30m × 0.25mm ID × 0.25µm Rxi-5Sil MS capillary column, equipped with a Gerstel multipurpose sampler and a Pegasus 4D GC×GC-TOFMS. The pomegranate extracts were filtered using a 0.45 µm PTFE filter before the analysis. The injection volume was 1 µL in a splitless mode, with helium as the carrier gas. The oven temperature gradient was programmed as follows: 50ºC for 30 sec, then 300ºC for 2 min at a rate of 15ºC/min. The National Institute Standard and Technology (NIST) database was used to interpret the GC-MS spectra and match the phytochemicals found in the extracts.

Some of the pomegranate extracts were lyophilized using a Christ Alpha 1-2 LD plus freeze-dryer, and the functional groups in the lyophilized extracts were studied by Fourier transform infrared spectroscopy (FTIR) done on a Bruker Tensor 27.

The NPs were identified by X-ray diffraction (XRD) performed on a Bruker D2 phaser. Scanning electron microscopy (SEM) and transmission electron microscopy (TEM) were employed to determine the shape and size of the NPs using a high-resolution Carl Zeiss SEM and JEOL JEM-2100F TEM, respectively. Brunauer-Emmett-Teller (BET) Micrometrics Tristar Plus 3.03 was utilized to determine the textural property of the NPs via N_2 physio-sorption at 77k. The surface charge of the NPs was determined by measuring their zeta potential, which was done on a Zetasizer Nano ZS system, Malvern Instruments.

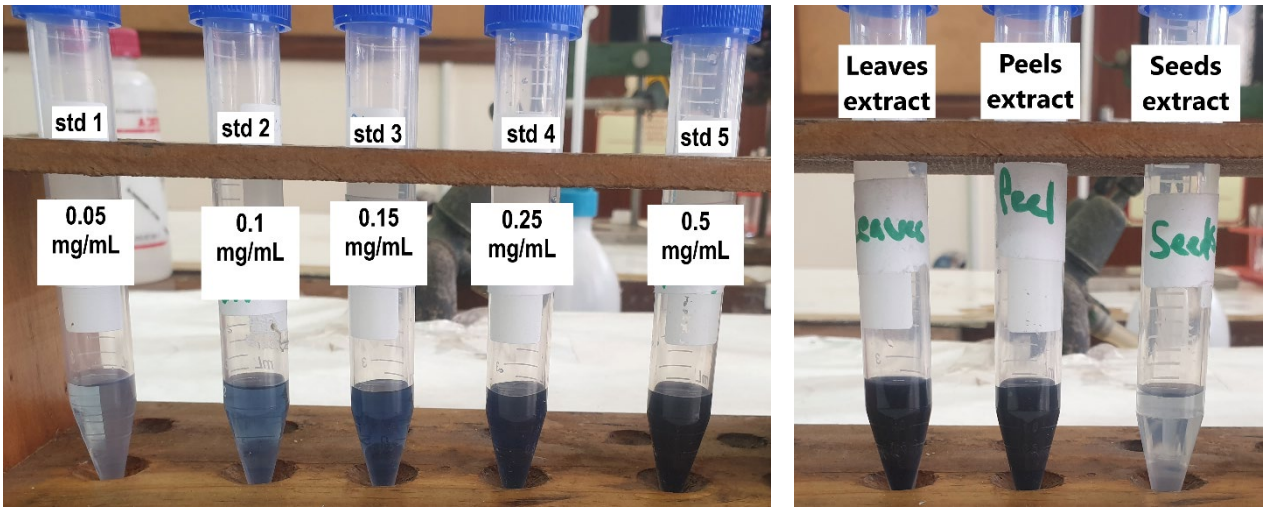


Figure 4. 2: The prepared standards and pomegranate extracts for total phenolic content measurements.

4.4 Batch adsorption experiments

Batch adsorption experiments were performed to investigate the adsorptive behaviour of the biogenic synthesized iron oxide NPs towards BTEX removal. Lab-prepared BTEX wastewater was used in the study because of the difficulty in obtaining real BTEX wastewater from the industries. The effects of parameters such as pH (2-12), NPs dosage (0.2-1.0 g/L), contact time (2-80 mins), and concentration (20-180 mg/L) on the BTEX adsorption tendency of the iron oxide NPs were investigated.

The adsorption experiments were performed by placing 50 mL of the prepared BTEX solutions in glass bottles, then adding the required dose of the iron oxide NPs to the BTEX solutions, and shaking the suspension at 150 rpm for the specified period of time. The required parameters, such as the pH, NPs dosage, contact time, and BTEX concentration employed in the various adsorption experiments, were stated in the result section. At the end of each specific test, the NPs were separated from the BTEX solutions through centrifugation. An aliquot of the BTEX solutions was taken, and the final concentration was measured using an Agilent 7890A gas chromatograph GC with a 30m × 0.25mm ID BP5MS × 0.25µm column, equipped with an Agilent 7693A automatic liquid sampler and a flame ionization detector FID. The injection volume was 0.2 µL in a splitless mode, and nitrogen was the carrier gas, which was set at a constant flow rate of 2.64 mL/min. The oven initial temperature was set at 40°C and held for 2 min, then ramped to 90°C at 10°C/min, held for 3 min, and finally to 200°C at a rate of 20°C/min and held for 2 min.

The adsorption tendency of the NPs was then determined by calculating their adsorption capacity and percentage of BTEX removal according to Eqs. (8) and (9), respectively.

$$q_t = \frac{(C_o - C_t)V}{m} \quad (8)$$

$$Removal\ (\%) = \frac{C_o - C_t}{C_o} \times 100 \quad (9)$$

Where q_t (mg/g) is the adsorption capacity, V (L) is the volume of the BTEX solution, and m (g) is the weight of the NPs adsorbents. C_o (mg/L) and C_t (mg/L) are the initial and final BTEX concentrations, respectively.

4.5 Results and discussion

4.5.1 Characterization of the pomegranate extracts

The phenolic compounds are important phytochemicals in the pomegranate extracts responsible for reducing the iron precursor to iron oxide NPs. Their concentration in the plant extract can affect the kinetics of the reaction and the characteristics of the produced nanoparticles (Kumar et al., 2019). The total phenolic content of the aqueous extracts, reported as the gallic acid equivalents (GAE) per g of dry weight of the pomegranate parts, showed that the leaves and peels extracts have similar amounts of phenolic content. The leaves extract has a total phenolic content of 47.44 ± 0.58 mg GAE/g dry wt of leaves, and that of the peels extract was 47.16 ± 0.72 mg GAE/g dry wt of peels. A total phenolic content of 0.60 ± 0.02 mg GAE/g of dry wt of seeds was obtained for the seeds extract, thus indicating that the seeds extract has the lowest phenolic content among the three pomegranate parts.

The phytochemicals in the pomegranate extracts were further determined using GC-MS, and the chromatograms are shown in Figure 4. 3. Active phytochemicals such as furfural, 2-isopropoxyphenol, 5-hydroxymethylfurfural, rhamnose, salicylic acid, maltol, and dodecanoic acid were found in the extracts. These phytochemicals are capable of the bio-reduction of the iron precursor to the iron oxide nanoparticles and also stabilizing the nanoparticles.

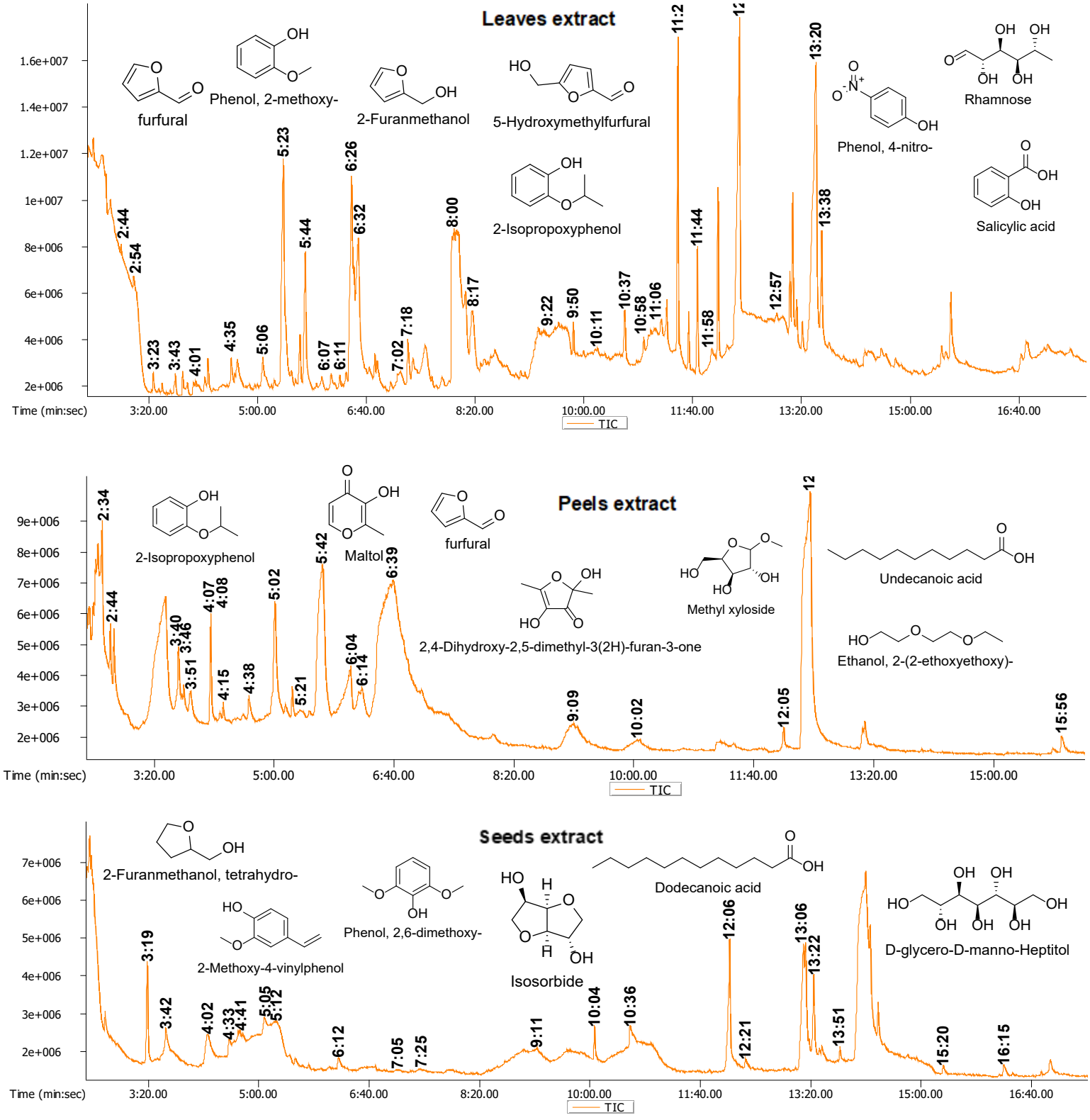


Figure 4. 3: GC-MS chromatograms of the pomegranate leaves, peels, and seeds extract.

4.5.2 Characterization of the various iron oxide NPs

4.5.2.1 Powder X-ray Diffraction (PXRD) results

The phase identification of the iron oxide NPs (FeNPs) obtained using powder X-ray Diffraction (PXRD) is shown in Figure 4. 4 (a,b,c). In the XRD pattern of the FeNPs-leaves, diffraction peaks were observed at 30.29º, 35.68º, 43.36º, 53.81º, 57.36º, and 62.99º, which are respectively indexed to (200), (311), (400), (422), (511), and (440) planes cubic phase of magnetite (Fe_3O_4) (ICSD collection code 29129). The FeNPs- peels and FeNPs-seeds displayed similar diffraction peaks at 26.16º, 30.30º, 33.97º, 35.69º, 43.38º, 44.78º, 50.10º, 53.83º, 57.38º, 63.02º, and 74.59º which respectively corresponds to miller indices of (211), (220), (310), (311), (400), (410), (421), (422), (511), (440), and (533) planes of cubic phase of maghemite (Fe_2O_3) (ICSD collection code 250541). While the peels and seeds extract of the pomegranate both produced maghemite, the colour of the maghemite differs. Maghemite exists in various colours, including brown, bluish-black, yellow, and yellowish-brown (Cornell & Schwertmann, 2003). The FeNPs-peels are bluish-black maghemite, while the FeNPs-seeds are yellowish-brown maghemite, as depicted in Figure 4. 1. Hence, the XRD results show that different forms of iron oxide were obtained by using the different extracts of the pomegranate to reduce $FeCl_3$.

4.5.2.2 Chemical composition analysis

FTIR was performed to compare the functional groups in the pomegranate extracts and the subsequent FeNPs and establish the capping ability of the extracts on the FeNPs. The FTIR spectra of the pomegranate extracts and their subsequent FeNPs in the region 400 – 4000 cm^{-1} are presented in Figure 4. 4 (d,e,f) and show that the leaves extract has a broad band around 3253 cm-1, which was due to the O—H stretching vibration in the phenols and alcohols present in the extract (Jin et al., 2018; Nandiyanto et al., 2019). The band at 1716 cm^{-1} could be attributed to the C=O stretching vibration of the carboxylic acid-containing compounds in the extract (Saha & Dutta Gupta, 2017; Nandiyanto et al., 2019). Bands at 1206 and 1022 cm^{-1} could be due to the C—O stretching vibration of the phenols and alcohols, respectively (Nandiyanto et al., 2019; Shen et al., 2017). The other bands at 2931, 1602, and 1338 cm^{-1} could be attributed to the asymmetric and symmetric stretching vibrations of the C—H, stretching vibration of C=C, and the stretching vibration of C—N respectively (Stan et al., 2017; Luo et al., 2016; Nandiyanto et al., 2019). Comparing the spectra of the leaves extract, and the FeNPs-leaves, the FeNPs-leaves exhibit bands at 3253, 1716, 1602, 1338, 1206, and

1054 cm^{-1}, which were all similar to the bands seen in the spectra of the leaves extract. This confirms the deposition of some of the active phytochemicals from the leaves extract onto the surface of the biogenic synthesized FeNPs, thereby capping and stabilizing the FeNPs. The presence of functional groups such as the O—H and the C—N on the FeNPs-leaves can also provide more active sites for the removal of organic contaminants such as BTEX from wastewater (X. Liang et al., 2021). Additional bands at 522 and 430 cm^{-1} of the FeNPs-leaves spectra correspond to the stretching of Fe-O of the Fe_3O_4.

The spectra of the peels extract show bands at 3280, 2937, 1718, 1603, 1331, and 1024 cm^{-1}, which are, respectively, attributed to the O—H, C—H, C=O, C=C, C—N, and C—O functional groups in the phytochemicals of the extract as previously discussed. Similar bands were observed in the spectra of the FeNPs-peels at 3280, 1724, 1657, 1344, and 958 cm^{-1}, which also corresponds to O—H, C—H, C=O, C=C, C—N, and C—O functional groups respectively. The seeds extract exhibit bands at 3313, 2928, 1721, 1604, 1343, and 1022 cm^{-1} which are attributed to O—H, C—H, C=O, C=C, C—N, and C—O respectively, and the FeNPs-seeds shows bands at 3313, 1716, 1605, 1325, 1201, and 1011 cm^{-1} also corresponding to O—H, C—H, C=O, C=C, C—N, and C—O respectively. This indicates that there is deposition of some active phytochemicals from the peels or seeds extract onto their respective FeNPs, which can cap and stabilize the FeNPs. Some of the functional groups, such as O—H and the C—N on the FeNPs, could provide active sites for the removal of organic contaminants such as BTEX (X. Liang et al., 2021). The spectra of the FeNPs-peels show additional bands at 837 and 414 $cm^{-1,}$ while additional bands were observed for the FeNPs-seeds at 665 and 489 cm^{-1}, which are due to the Fe—O of the Fe_2O_3 phase (Patiño-Ruiz et al., 2020).

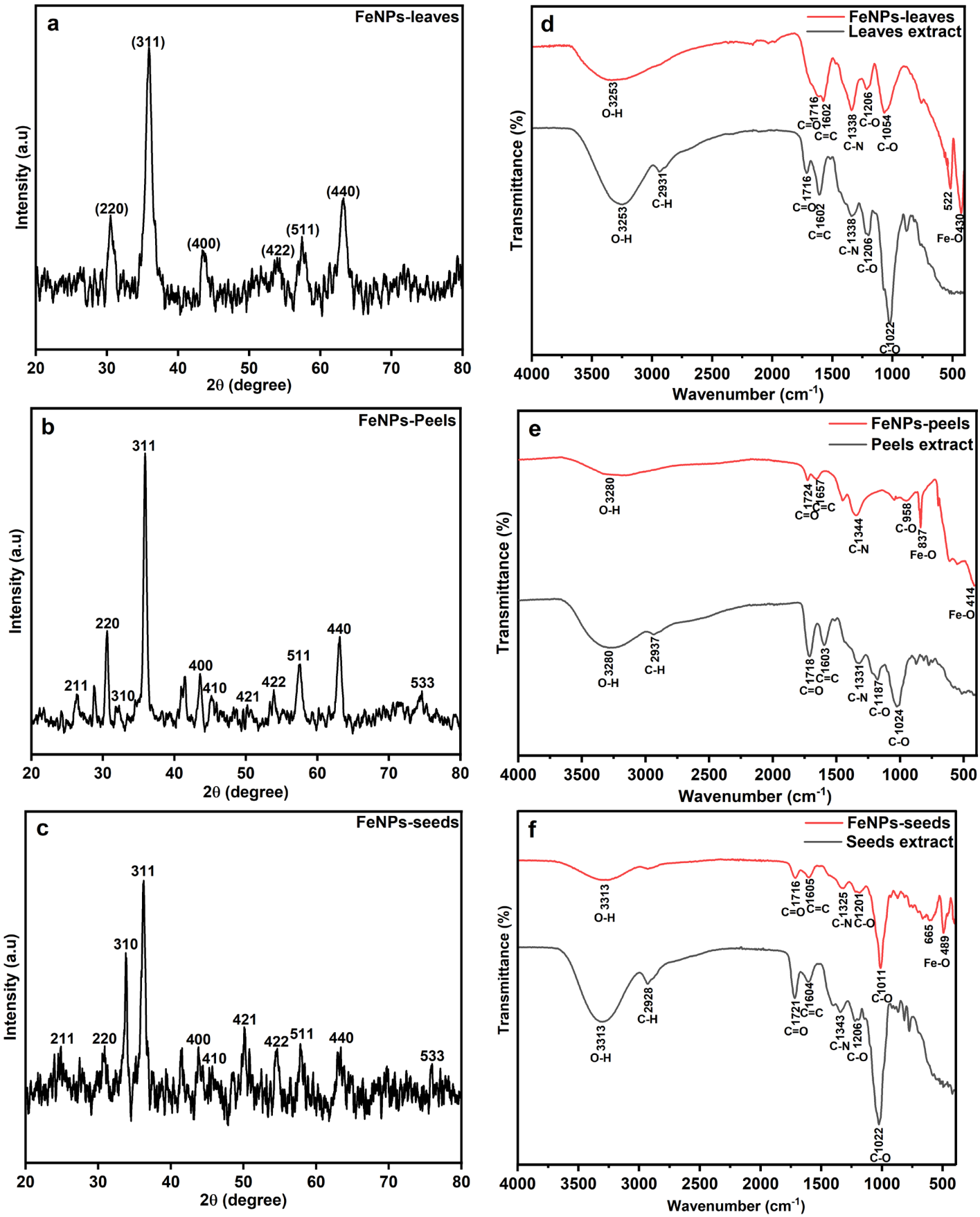


Figure 4. 4: (a,b,c) XRD patterns of the FeNPs, and (d,e,f) FTIR spectra of the FeNPs and the pomegranate extracts.

4.5.2.3 Morphological characterization

SEM and TEM were used to determine the morphology of the FeNPs, and the images are shown in Figure 4. 5. The SEM images show that all the FeNPs are mostly spherical in shape, with fairly good dispersion, as seen in their respective TEM images. All the FeNPs have rough surfaces, as shown in their TEM images. The average particle sizes of the FeNPs were measured and summarized from their TEM images using ImageJ software. FeNPs-leaves have an average particle size of 73.35 ± 8.7 nm, while FeNPs-peels and FeNPs-seeds have average particle sizes of 39.51 ± 6.6 nm and 37.20 ± 7.6 nm, respectively.

4.5.2.4 Textural properties of the FeNPs

BET analysis was performed to determine the textural properties of the FeNPs in terms of their porous nature and specific surface area, and the nitrogen adsorption/desorption isotherm curves obtained using the BET technique are presented in Figure 4. 6. According to the IUPAC classification of isotherm curves, all the FeNPs had type IV isotherms, which indicates their mesoporous nature. Mesoporous materials are known to be good adsorbents for removing many organic contaminants from wastewater (Wu & Zhao, 2011); hence, the FeNPs could be potential adsorbents for target organic contaminants such as BTEX. Among all the FeNPs, the FeNPs-peels have the highest BET specific surface area of 48.45 m^2/g, and the FeNPs-seeds have a specific surface area of 35.40 m^2/g, while FeNPs-leaves have the lowest specific surface area of 8.61 m^2/g.

The FeNPs pore sizes were determined using the Barrett-Joyner-Halenda (BJH) method using the desorption branch. The insets of Figure 4. 6 show the respective pore sizes of the FeNPs, which further establishes mesopores in the FeNPs. Mesoporous materials typically have pore diameters between 2 - 50 nm (Wang et al., 2018), and most of the pores of the FeNPs are within this range, as shown in the insets of Figure 4.6. The pore sizes with the highest pore volumes are 2.48 nm, 15.82 nm, and 22.79 nm for FeNPs-leaves, FeNPs-peels, and FeNPs-seeds, respectively. The BET results of the FeNPs indicate their effective porous nature and potential application as adsorbents for organic contaminants such as BTEX.

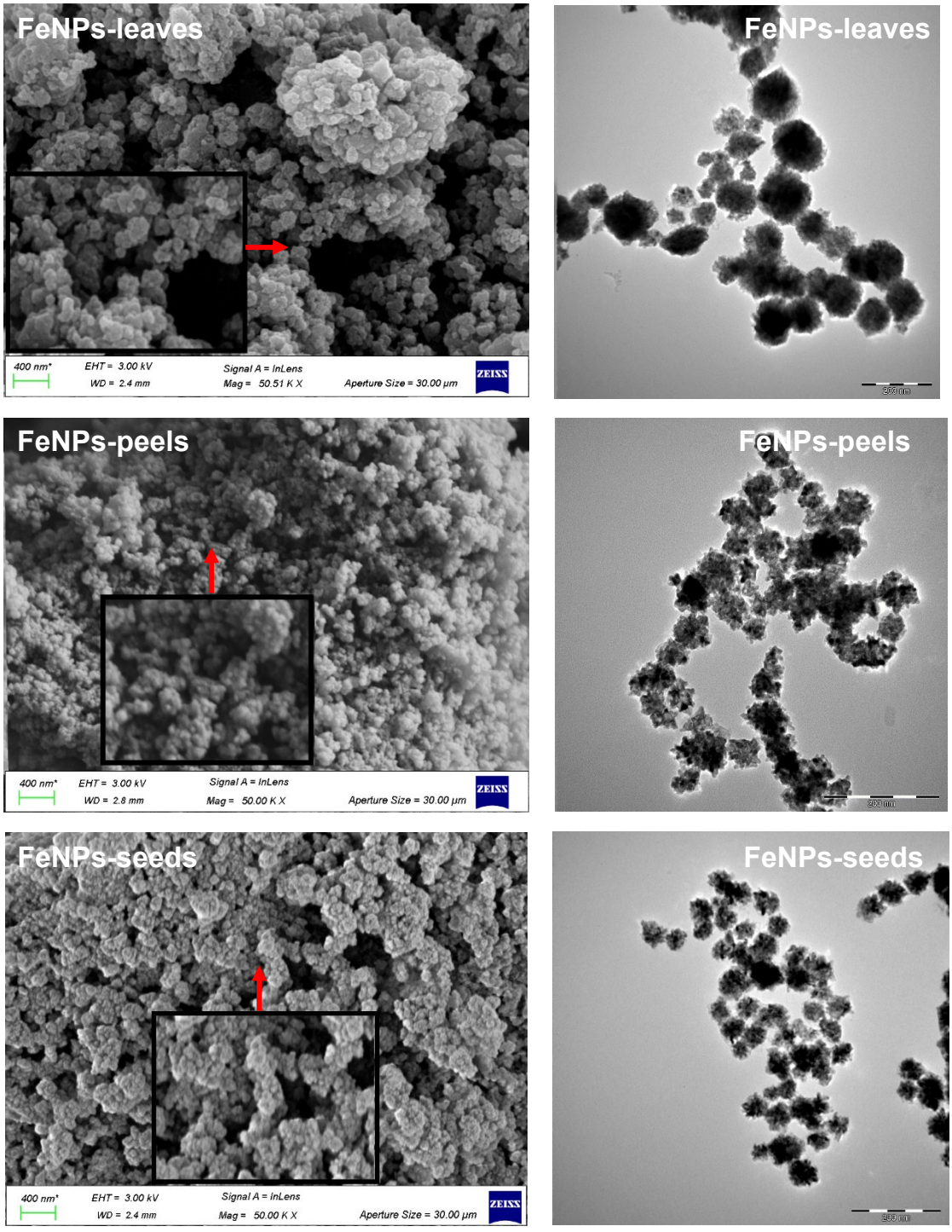


Figure 4. 5: SEM and TEM image of the FeNPs.

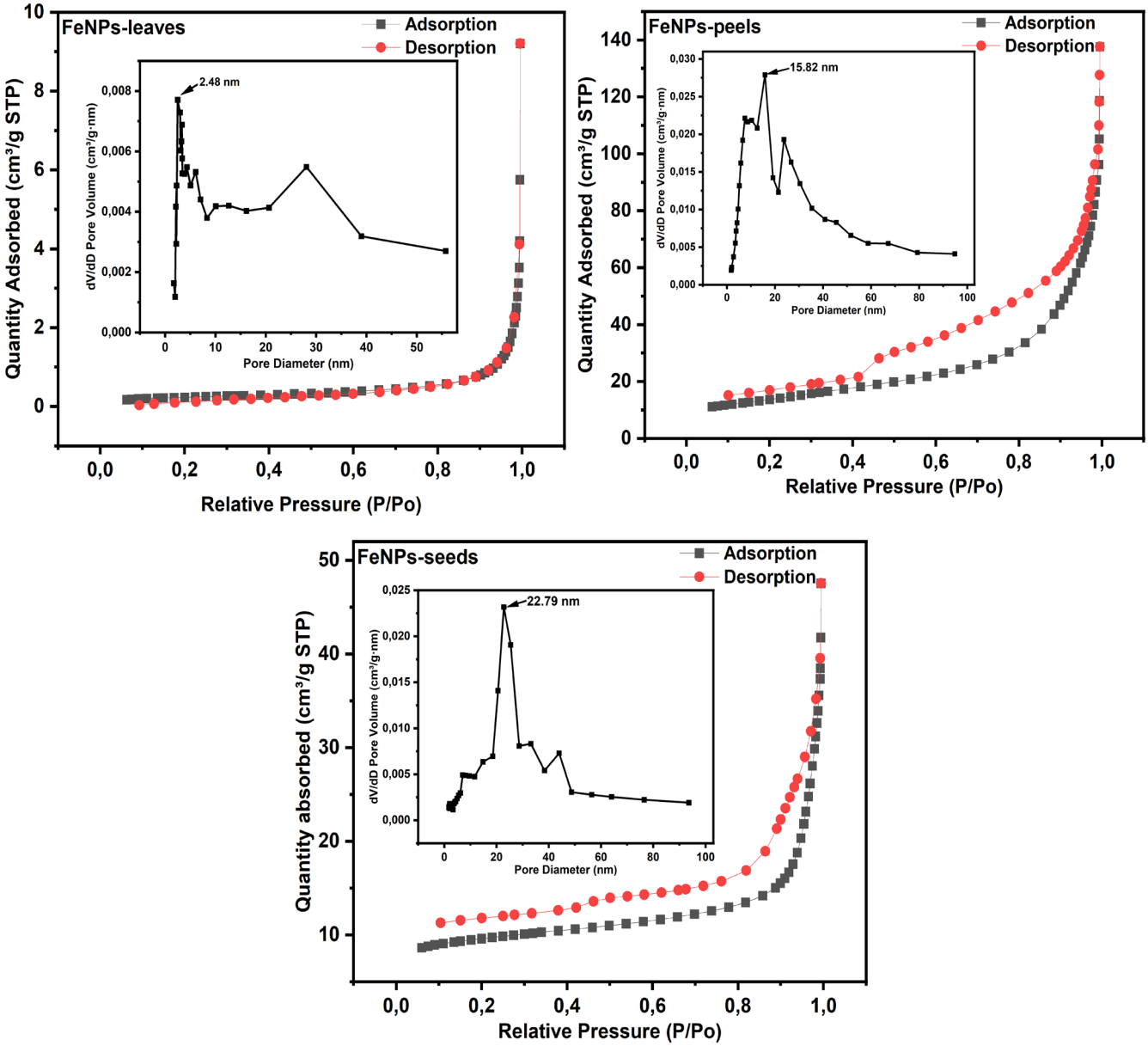


Figure 4. 6: The N_2 adsorption-desorption isotherms and pore size distributions (inset) of the FeNPs.

4.5.2.5 Zeta potential results

The zeta potential measurements were performed to determine the surface charge of the FeNPs at the measured pH range between 2 to 12, as shown in Figure 4. 7. At lower pHs, all three FeNPs have high zeta potential and are positively charged. This behaviour of the FeNPs at lower pHs could be due to the protonation of their surface groups at the lower pH ranges. As shown in their FTIR, the surface of the FeNPs has functional groups, such as the hydroxyl and amine groups, which can be protonated at low pH. Moreover, metal oxide has the tendency to hydrate in an aqueous solution, thereby having its surfaces covered with hydroxyl group, which

could be protonated at low pH (Wang et al., 2013; Yeap et al., 2018). The protonation of these surface groups on the FeNPs resulted in positively charged NPs at the low pHs. At a pH of 4.92, the FeNPs-peels established its point of zero charge, while the point of zero charge (pH_{pzc}) of the FeNPs-leaves and the FeNPs-seeds was 5.18. Above the pH_{pzc}, the surface charge of the FeNPs becomes negative, which could be attributed to the deprotonation of the aforementioned functional groups on their surfaces at higher pHs (Wang et al., 2013). As the pHs were increased, the zeta potentials of all the FeNPs became more negative, reaching -39.9, -38.7, and -39.5 at pH 12 for the FeNPs-leaves, FeNPs-peels, and FeNPs-seeds, respectively. The results of the zeta potential of the FeNPs could provide an understanding of their behaviour towards BTEX adsorption at various pHs.

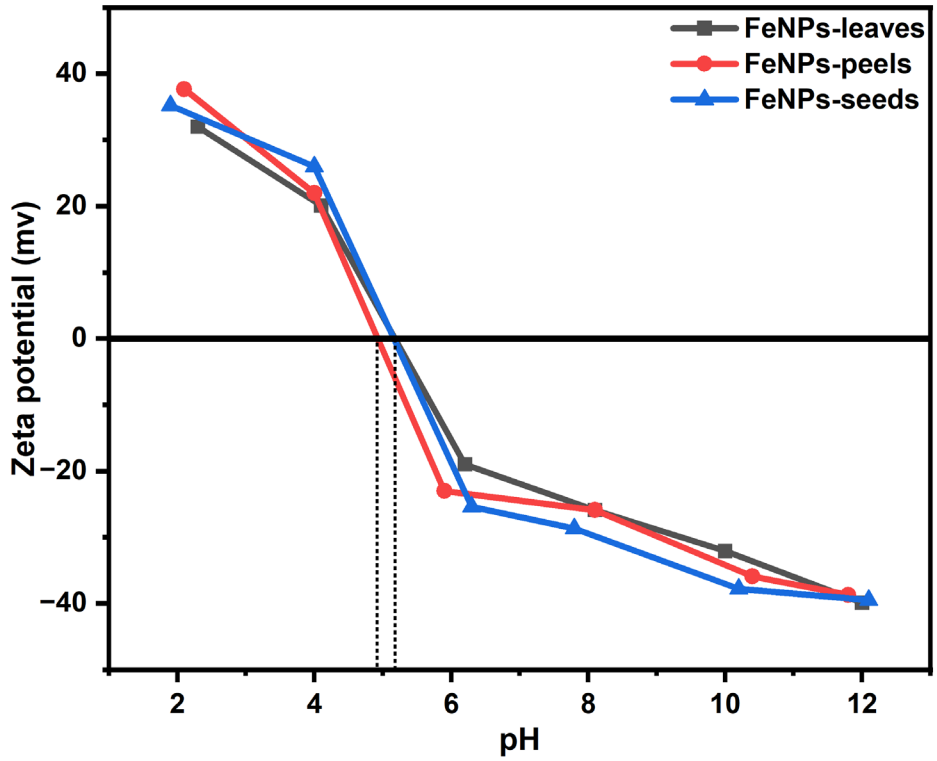


Figure 4. 7: Zeta potential of the FeNPs.

4.5.3 BTEX adsorption study

4.5.3.1 Effect of solution pH on BTEX adsorption

The initial pH of the solution is an important parameter that can affect the behaviour of the FeNPs adsorbents towards the adsorption of the BTEX (D. C. C. da S. Medeiros et al., 2022). According to the zeta potential results in Figure 4. 7, the FeNPs exhibit varying surface charges

at different pHs, and the surface charges of the FeNPs affect the interaction between the FeNPs adsorbents and the BTEX adsorbate (D. C. C. da S. Medeiros et al., 2022). Hence, the effect of the solution pH on the adsorption of the BTEX using the FeNPs was determined at different pHs (2 – 12) for 40 min. 10mg of FeNPs and 20 mg/L (50 mL) of the BTEX solution were used for the test. As depicted in Figure 4. 8, the adsorption capacity of the FeNPs towards all the components of BTEX (that is, benzene, toluene, ethylbenzene, and xylene) increased as the pH increased and reached its maximum at pH 5. This behaviour at lower pH can be explained by the ability of iron oxide to accept protons under acidic conditions to form positively charged species (Masuku et al., 2021). Thus, the positive charge favours electrostatic interaction between the FeNPs and the π-electrons of the BTEX. However, the π-electrons interaction depends on the available active sites on the FeNPs (Ye & Ariya, 2015) . With the FeNPs interacting with the H^+ at low pH, the available active sites for it to interact with the π-electrons of the BTEX decrease. As the pH increases, the amount of H^+ reduces, thus reducing the amount of H^+ interacting with the FeNPs, thereby providing more active sites for the π-electrons interaction with the FeNPs. Above pH 5, the adsorption capacity started to decrease. As shown in Figure 4. 7, the surface charges of the FeNPs were negative above pH 5. In addition, there was the presence of OH^- at higher pHs. The negative surface charge of the FeNPs above pH 5 and the OH^- in the solution repelled the π-electrons of the BTEX, thereby diminishing the interaction between the FeNPs and the BTEX; hence, the decrease in adsorption capacity obtained at higher pHs.

The FeNPs-leaves exhibited the lowest BTEX adsorption across all the tested pHs, while the FeNPs-peels and FeNPs-seeds showed fairly the same BTEX adsorption performance. The lower BTEX adsorption of the FeNPs-leaves could be due to its lower specific surface area, as previously reported in its BET results.

Since it has been established that the pH has a considerable effect on the adsorption performance of the FeNPs, the subsequent adsorption experiments were maintained at a specific pH, and the optimum pH 5 was chosen.

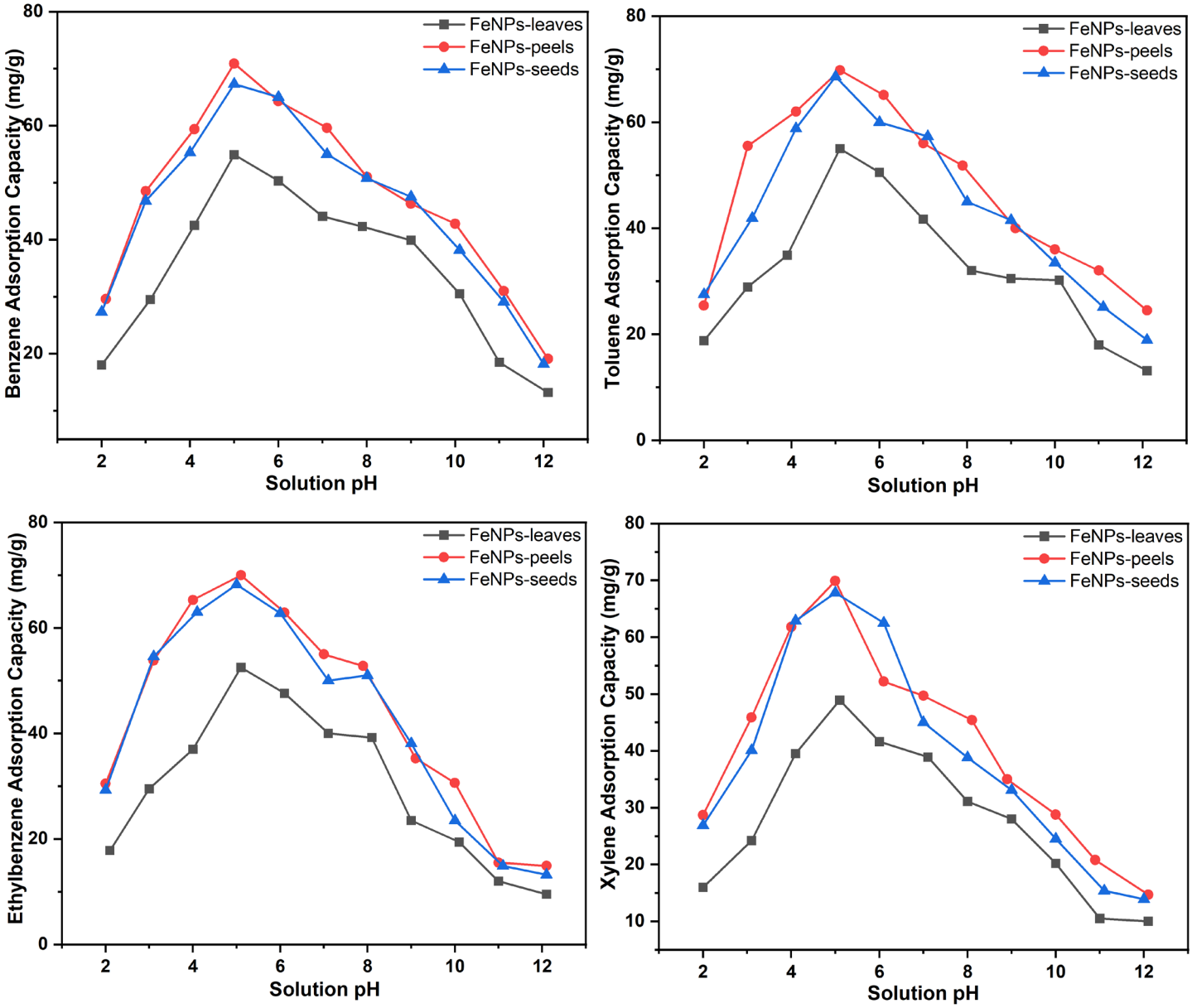


Figure 4. 8: Effect of solution pH on BTEX adsorption onto the FeNPs.

4.5.3.2 Effect of adsorbent dosage

This test was performed to determine the effect of the FeNPs dosages on the adsorption and removal efficiency of BTEX at pH 5 using 50 mL (20mg/L) of BTEX solution for a duration of 40 min while varying the NPs dosage from 0.2g/L to 1.0g/L. As shown in Figure 4. 9 and Table 4. 1, the BTEX adsorption capacity decreased as the FeNPs dosage increased, while their corresponding BTEX percentage removal increased. This decline in the adsorption capacity could be attributed to the increased number of the FeNPs adsorbent with constant BTEX concentration. On the other hand, the increment in the BTEX percentage removal was due to increased availability of the adsorption sites and surfaces as more adsorbents were introduced at constant BTEX concentration, thereby increasing the removal efficiency. Thus, this test

established that there is a considerable effect on the adsorption performance of the FeNPs as their dosages are varied.

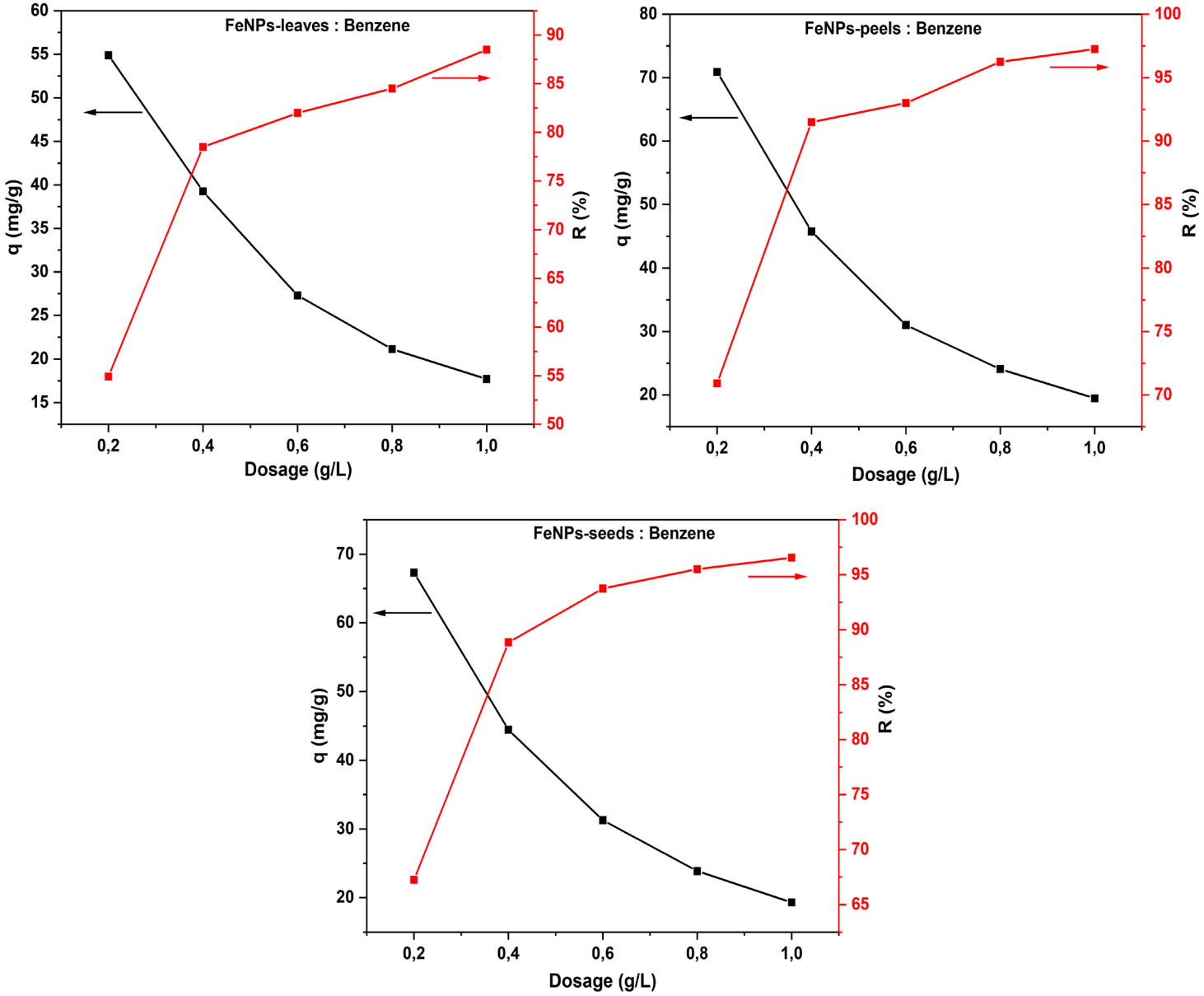


Figure 4. 9: Effect of FeNPs dosage on benzene adsorption.

Table 4. 1: Effect of FeNPs dosage on toluene, ethylbenzene, and xylene adsorption.

Pollutant	Dosage (g/L)	FeNPs-leaves		FeNPs-peels		FeNPs-seeds	
		q (mg/g)	R (%)	q (mg/g)	R (%)	q (mg/g)	R (%)
Toluene	0.2	55.10	55.10	69.80	69.80	68.60	68.60
	0.4	37.75	75.50	45.30	90.60	45.90	91.80
	0.6	28.17	84.50	31.50	94.50	30.97	92.90
	0.8	21.56	86.25	24.09	96.35	24.05	96.20
	1.0	17.61	88.05	19.55	97.75	19.45	97.25
Ethylbenzene	0.2	52.50	52.50	70.45	70.45	68.20	68.20
	0.4	37.96	75.90	43.92	87.85	44.50	89.00
	0.6	25.82	77.45	31.63	94.90	31.04	93.10
	0.8	20.50	82.00	24.05	96.20	23.95	95.80
	1.0	17.52	87.60	19.63	98.15	19.24	96.20
Xylene	0.2	48.95	48.95	69.90	69.90	67.85	67.85
	0.4	35.65	71.30	43.82	87.65	44.25	88.50
	0.6	25.80	77.40	30.97	92.90	30.02	90.05
	0.8	21.93	87.70	24.18	96.70	23.50	94.00
	1.0	17.64	88.20	19.48	97.40	19.02	95.10

4.5.3.3 Effect of contact time and adsorption kinetics

The effect of contact time on the BTEX adsorption performance of the FeNPs adsorbents was studied at pH 5 using 20mg of FeNPs and 20 mg/L (50 mL) of BTEX solution while the contact time varied from 2 min to 80 min. The result, as depicted in Figure 4. 10 (a, b, c, d), shows that all three FeNPs adsorbents exhibited similar adsorption trends when the contact time was varied. From the result, the adsorption of the BTEX onto the different NPs initially occurred

quickly until 15 min; then, the adsorption rate gradually became slower until equilibrium was attained at 40 mins. This behaviour can be attributed to the high availability of active sites on the adsorbents at the initial stages of the adsorption, thus accelerating the adsorption of BTEX at the early stages. As the adsorption process proceeded, the available active sites gradually decreased, which resulted in a slower adsorption rate until all the sites were saturated at the equilibrium stage.

To understand the adsorption kinetic process, pseudo-first-order (PFO) and pseudo-second-order (PSO) models were used to fit the adsorption data and calculate the kinetic parameters. The linearized form of the models used to determine the adsorption kinetic parameters are expressed as follows:

Pseudo-first-order model:

$$\log\ (q_e - q_t) = \log\ q_e - \frac{k_1 t}{2.303} \tag{10}$$

Pseudo-second-order model:

$$\frac{t}{q_t} = \frac{1}{k_2 {q_e}^2} + \frac{t}{q_e} \tag{11}$$

where q_e (mg/g) and q_t (mg/g) are the adsorption capacity at equilibrium time and time t (min), respectively; t (min) is the adsorption time; k_1 (min^{-1}) and k_2 ($gmg^{-1}min^{-1}$) are the rate constants of the pseudo-first-order and pseudo-second-order models, respectively.

Figure 4.11 depicts the fitting curves for the pseudo-first-order, while those for the pseudo-second-order are shown in Figure 4. 10 (e, f, g, h). Their corresponding kinetic parameters are presented in Table 4. 2. From the fitting curves, it is evident that the pseudo-second-order model has a better correlation with the adsorption process than the pseudo-first-order, as inferred from the higher correlation coefficient (R^2) of the pseudo-second-order model. In addition, the calculated q_e values ($q_{e,\ cal}$) obtained from the pseudo-second-order were closer to the experimentally determined values ($q_{e,\ exp}$), as shown in Table 4. 2. For instance, the calculated q_e values (q_e, $_{cal}$) for FeNPs-leaves adsorption of benzene were 19.11 mg/g and 41.49 mg/g for the pseudo-first-order and the pseudo-second-order models, respectively, while the experimentally obtained value was 39.52 mg/g. Thus, indicating that the pseudo-second-order model gave a more accurate description of the BTEX adsorption process on the FeNP adsorbents. Pseudo-second-order model typically represents chemisorption processes (Guo &

Wang, 2019); hence chemisorption was the rate-controlling step in the BTEX adsorption process using the biogenic-synthesized FeNPs.

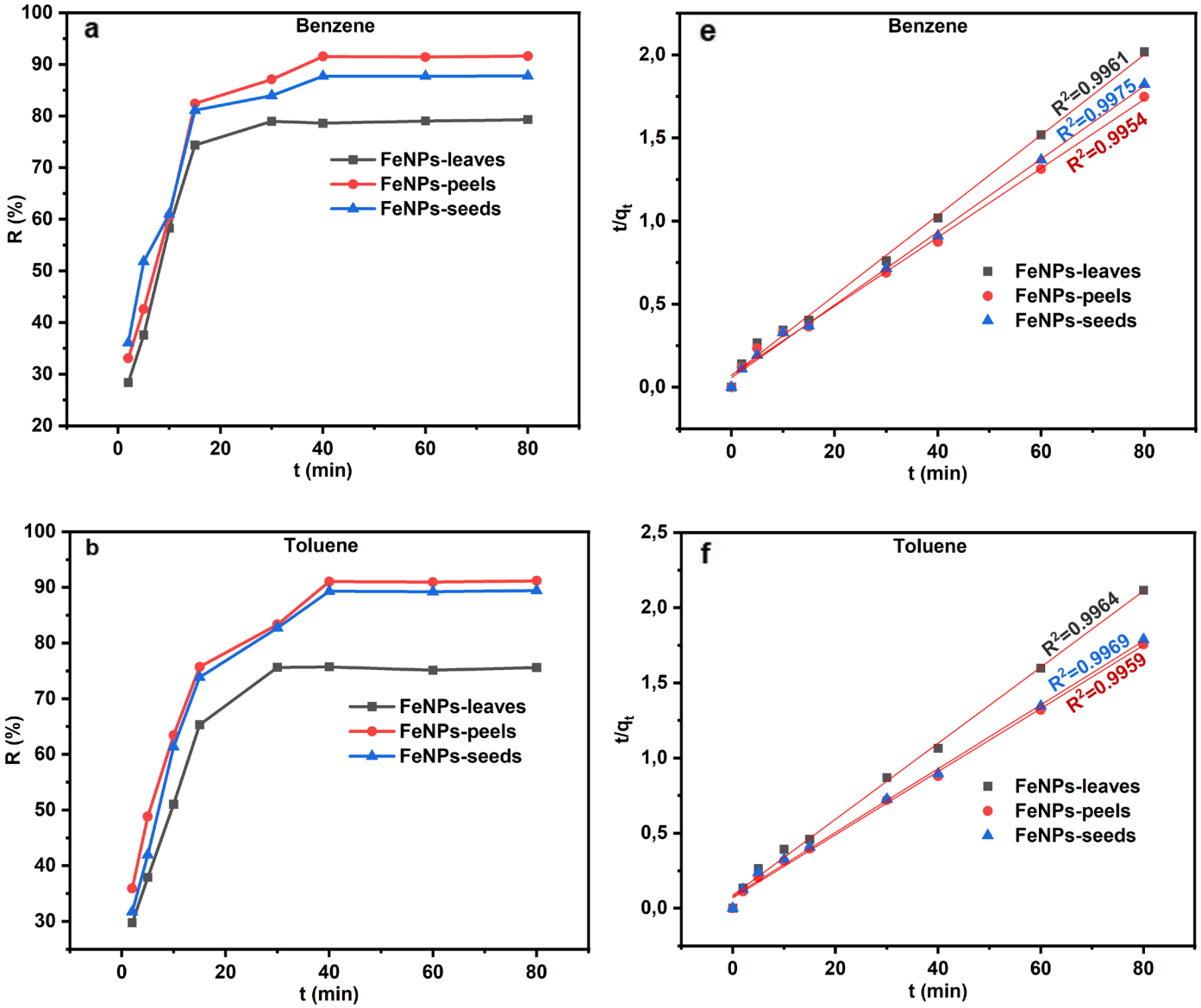


Figure 4. 10: (a, b, c, d) Effect of contact time on BTEX adsorption on the FeNPs

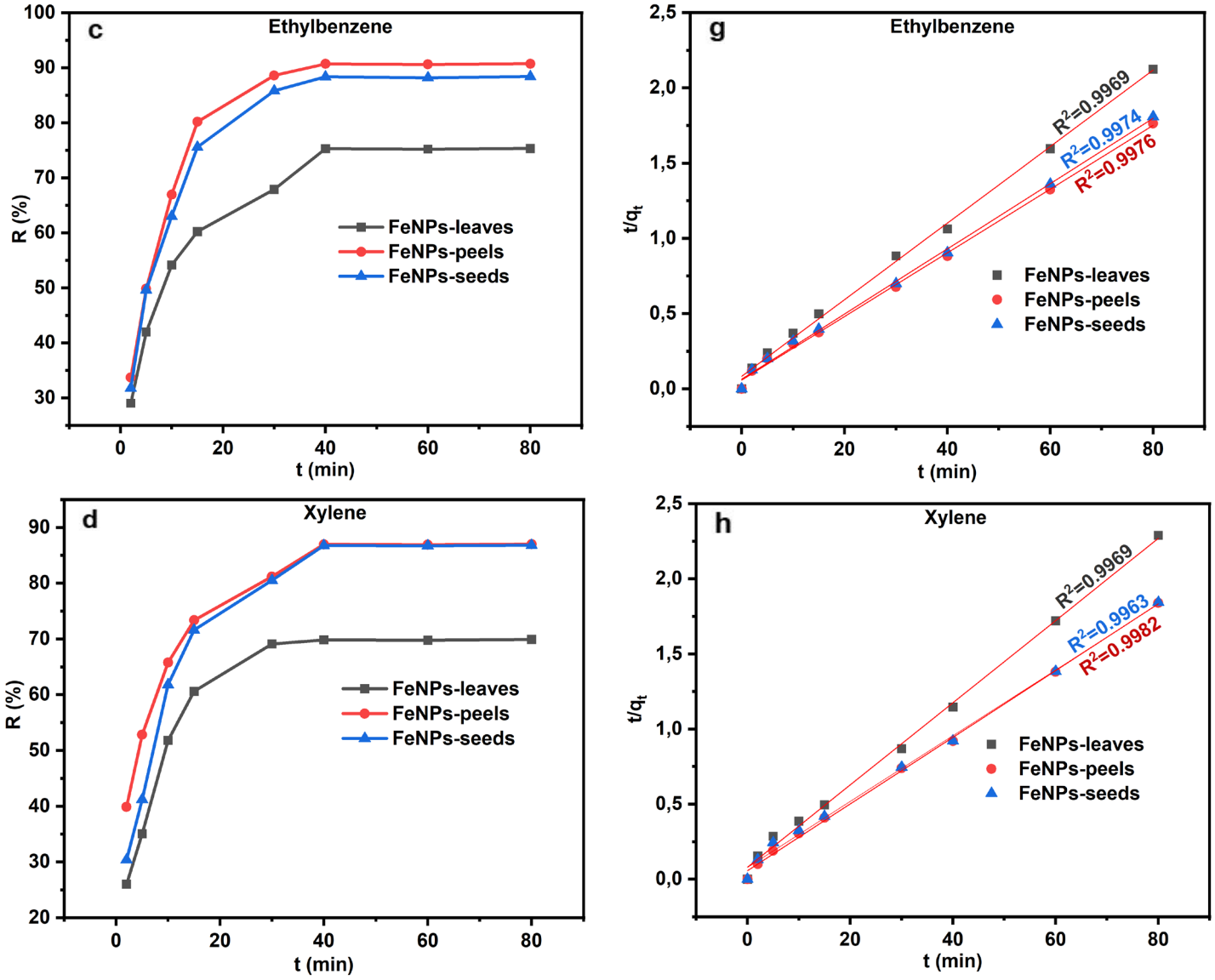


Figure 4. 10: (e, f, g, h) their respective linear fit for pseudo-second-order kinetic model.

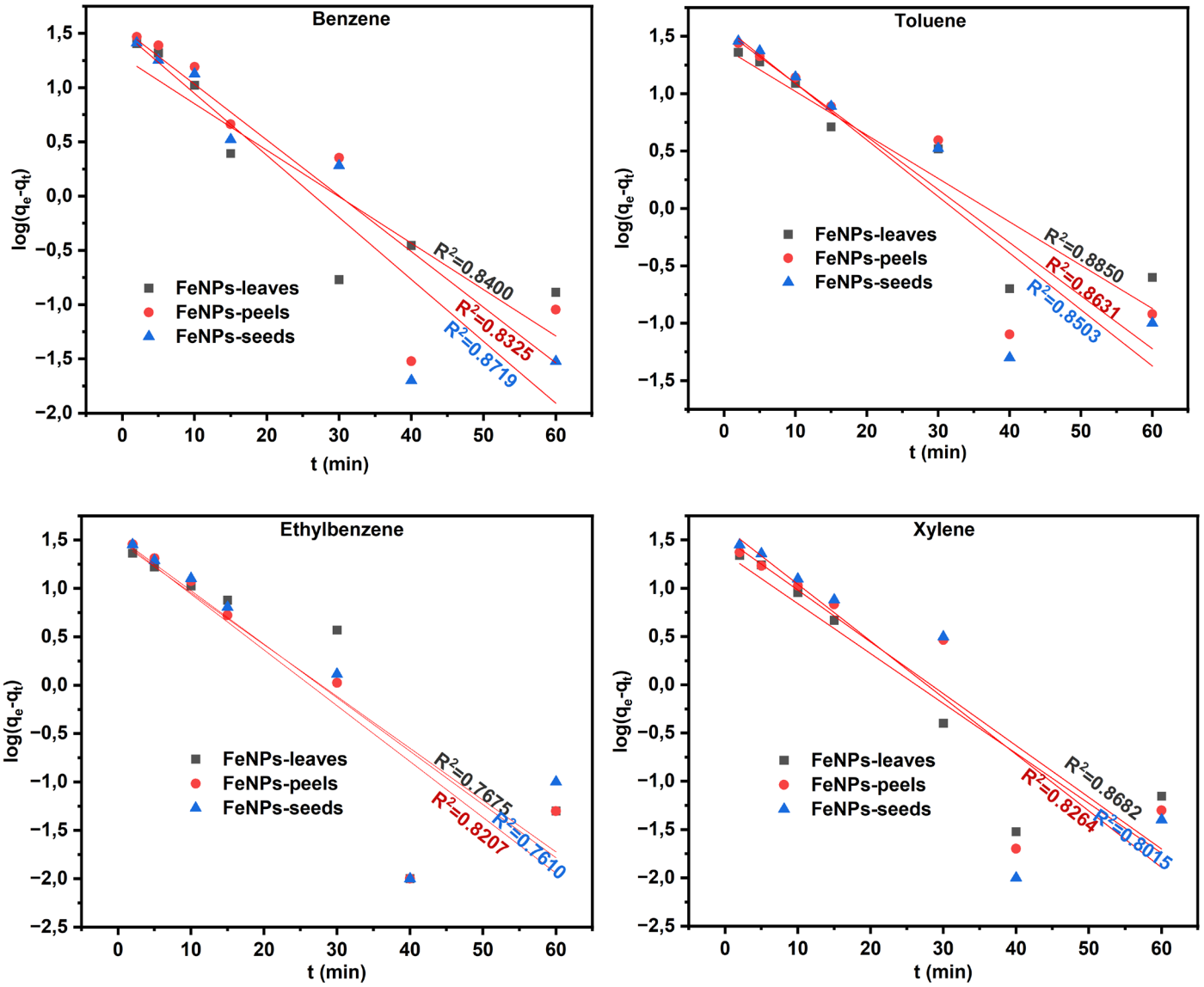


Figure 4. 101: Linear fit for the pseudo-first-order kinetic model for BTEX adsorption on FeNPs

Table 4. 2: Kinetic pseudo-first and pseudo-second-order parameters of BTEX adsorption by the FeNPs.

Adsorbent	Pollutant	$q_{e,\ exp}$ (mg/g)	PFO		PSO	
			$q_{e,\ cal}$ (mg/g)	k_1 (min^{-1})	$q_{e,\ cal}$ (mg/g)	k_2 (g/mg/min)
FeNPs-leaves	Benzene	39.52	19.11	0.0986	41.49	0.0084
	Toluene	37.80	25.01	0.0873	39.53	0.0075
	Ethylbenzene	37.61	33.83	0.1271	39.37	0.0077
	Xylene	34.95	22.81	0.1191	36.49	0.0094
FeNPs-peels	Benzene	45.75	35.11	0.1183	48.08	0.0060
	Toluene	45.47	35.69	0.1066	47.62	0.0064
	Ethylbenzene	45.31	33.02	0.1329	47.17	0.0078
	Xylene	43.50	32.85	0.1234	45.04	0.0089
FeNPs-seeds	Benzene	43.88	32.99	0.1315	45.45	0.0086
	Toluene	44.70	38.29	0.1135	46,.95	0.0058
	Ethylbenzene	44.20	31.04	0.1234	46.08	0.0074
	Xylene	43.39	32.36	0.1351	45.66	0.0061

4.5.3.4 Effect of initial concentration and adsorption isotherms

The adsorption performance of the FeNPs adsorbents was studied at different initial concentrations ranging from 20 mg/L to 180 mg/L of the BTEX solution (50 mL) at pH 5 using 20 mg of the FeNPs for a duration of 40 min. The results, as presented in Figure 4. 12, show that the percentage removal, R (%), of BTEX using the FeNPs decreased as the concentrations increased. This could be due to the decline in the number of available sites on the FeNPs adsorbents as the BTEX concentration increased, thereby reducing the removal efficiency of the FeNPs adsorbents towards BTEX. Thus, the use of the biogenic-synthesized FeNPs in the adsorptive removal of BTEX is more effective at low BTEX concentrations.

To gain insights into the nature of the adsorption process, the experimental adsorption data was fitted with two isotherm models; Langmuir and Freundlich models. Langmuir model describes monolayer adsorption processes and homogenous interactions at the surface of the adsorbent, with all sites on the adsorbent having equal affinity towards the adsorbate (Al-Ghouti & Da'ana, 2020). On the other hand, the Freundlich model mainly describes multilayer adsorption processes on heterogeneous adsorbent surfaces, and the affinity of the adsorbent's active sites towards the adsorbate does not need to be uniform (Al-Ghouti & Da'ana, 2020). The fitting of the experimental adsorption data using these models was performed using the linear form of the models according to the below expressions:

Langmuir isotherm model:

$$\frac{C_e}{q_e} = \frac{1}{K_L q_m} + \frac{C_e}{q_m} \tag{12}$$

Freundlich isotherm model:

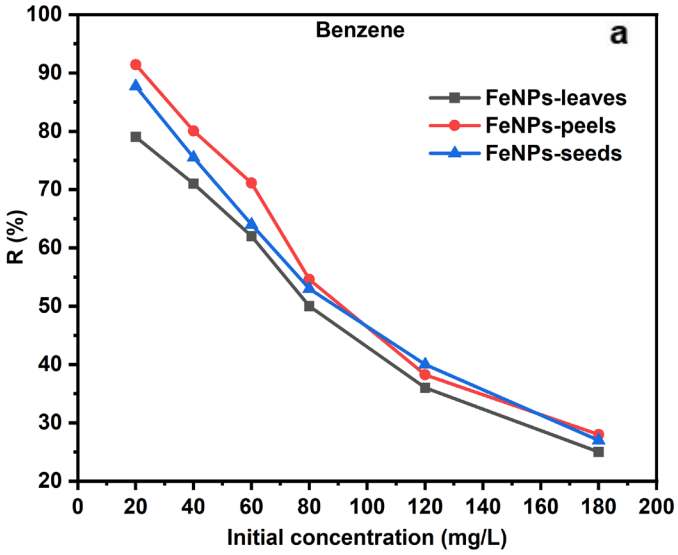
$$In\ q_e = In\ K_F + \frac{1}{n}\ In\ C_e \tag{13}$$

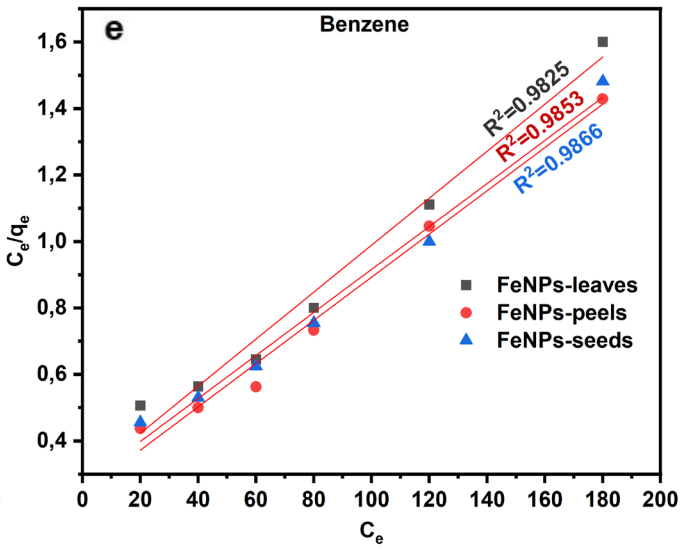
where q_e (mg/g) and q_m (mg/g) is the equilibrium adsorption capacity and the maximum adsorption capacity, respectively. C_e (mg/L) is the equilibrium concentration of the BTEX solution, K_L (L/mg) is the Langmuir constant, K_F (mg/g) is the Freundlich constant, and n corresponds to the adsorption density related to the feasibility of the adsorption process. Due to the high volatility of BTEX, the adsorption isotherm study was performed only at room temperature.

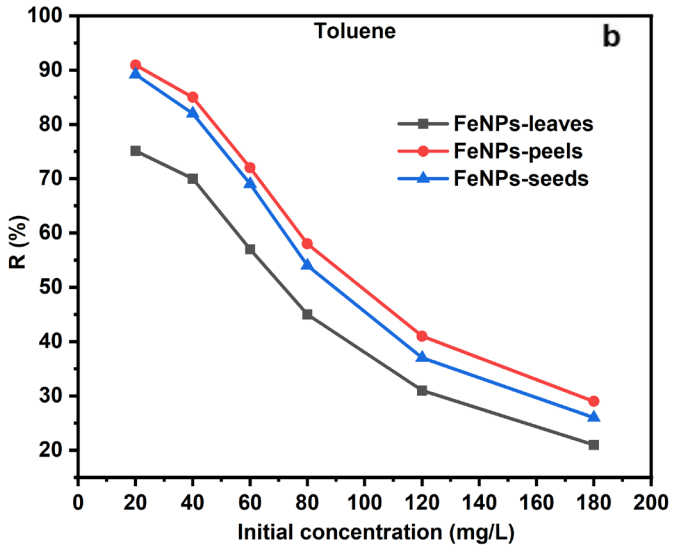
The plots of $\frac{C_e}{q_e}$ vs C_e (for Langmuir isotherm) and $In\ q_e$ vs $In\ C_e$ (for Freundlich isotherm) are presented in Figure 4. 12 and Figure 4.13 respectively. The subsequent isotherm parameters, as presented in Table 4. 3, were calculated from the related isotherm plot, that is; q_m and K_L were calculated from the $\frac{C_e}{q_e}$ vs C_e Langmuir isotherm plot while K_F and n were calculated from the $In\ q_e$ vs $In\ C_e$ Freundlich isotherm plot.

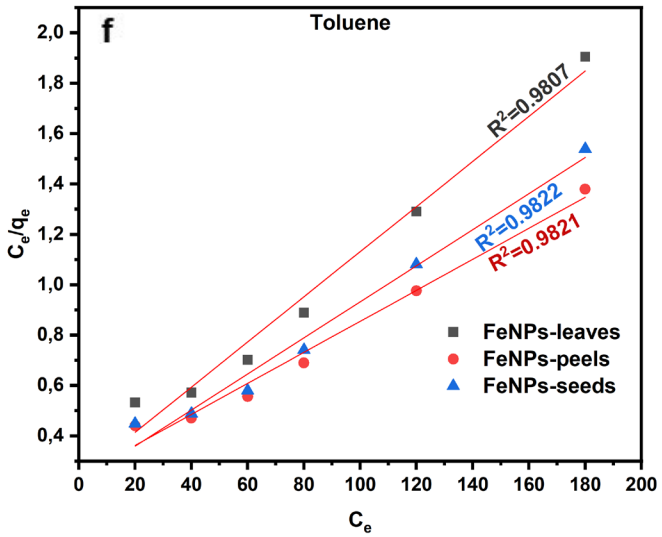
The R^2 obtained from fitting the adsorption data with the Langmuir isotherm model was higher than the R^2 obtained from the Freundlich isotherm model, as shown in their respective plots. This suggests that the BTEX adsorption onto the FeNPs adsorbents occurred through monolayer adsorption with homogenous interaction of the BTEX at the FeNPs surfaces.

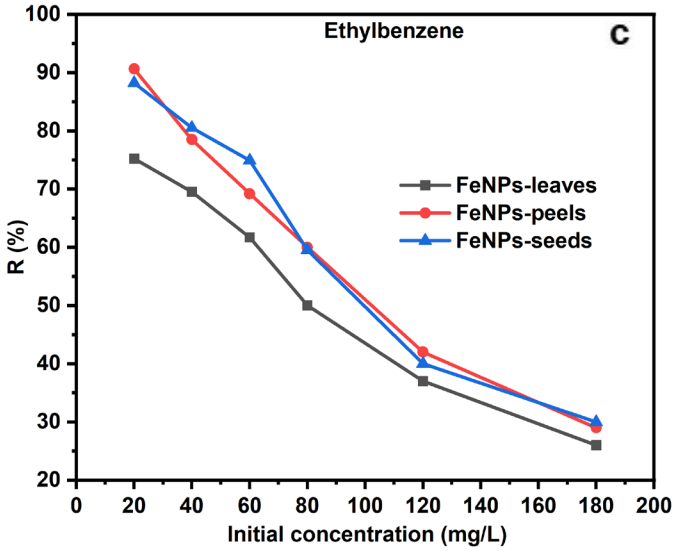
The comparison of the performance of the FeNPs and other adsorbents is shown in Table 4. 4 and indicates that the calculated maximum adsorption capacity (q_m) obtained in this study was relatively high compared to other similar studies that utilized iron oxide nanoparticles as a single adsorbent for BTEX removal. Note that the parameters, such as the adsorbent dosage, temperature, and BTEX solution concentrations, used in the different adsorption studies differ; hence, the comparison may not directly relate and compare the performance of the iron oxide used in the various studies.

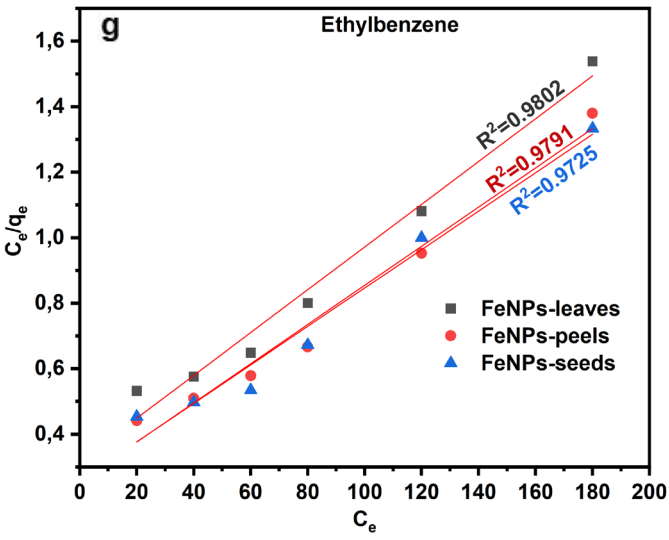

Benzene
a
FeNPs-leaves
FeNPs-peels
FeNPs-seeds
R (%)
Initial concentration (mg/L)


e
Benzene
R²=0.9825
R²=0.9853
R²=0.9866
FeNPs-leaves
FeNPs-peels
FeNPs-seeds
Ce/qe
Ce


Toluene
b
FeNPs-leaves
FeNPs-peels
FeNPs-seeds
R (%)
Initial concentration (mg/L)


f
Toluene
R²=0.9807
R²=0.9822
R²=0.9821
FeNPs-leaves
FeNPs-peels
FeNPs-seeds
Ce/qe
Ce


Ethylbenzene
c
FeNPs-leaves
FeNPs-peels
FeNPs-seeds
R (%)
Initial concentration (mg/L)


g
Ethylbenzene
R²=0.9802
R²=0.9791
R²=0.9725
FeNPs-leaves
FeNPs-peels
FeNPs-seeds
Ce/qe
Ce

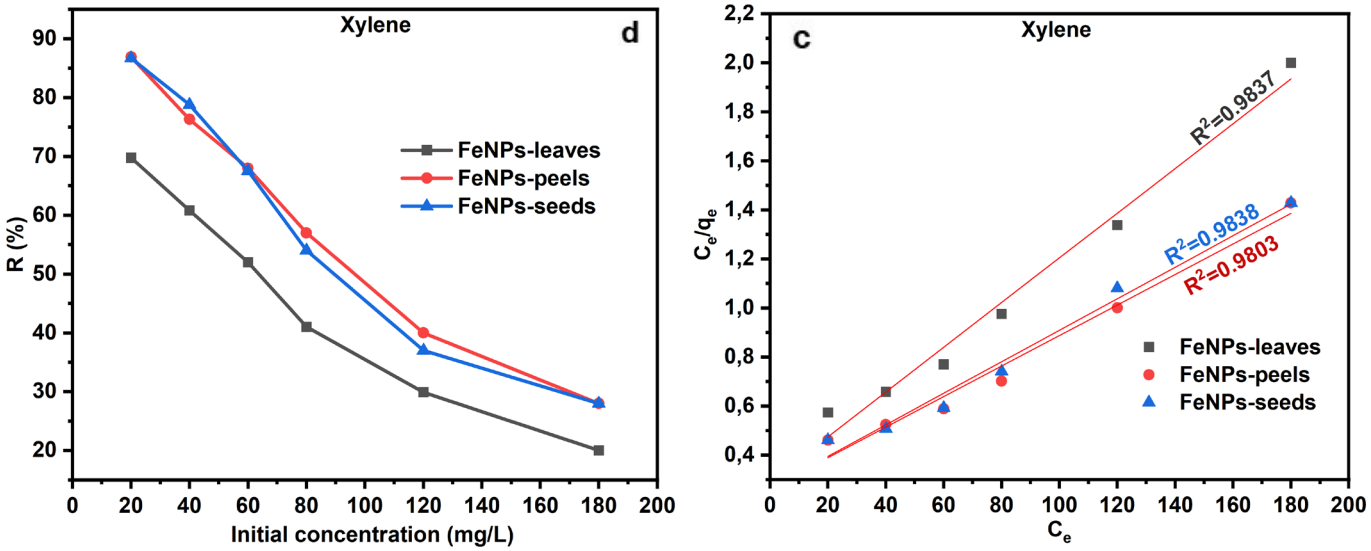


Figure 4. 11: (a, b, c, d) Effect of BTEX initial concentration on their adsorption on the FeNPs, and (e, f, g, h) their subsequent linear fit for Langmuir isotherm model.

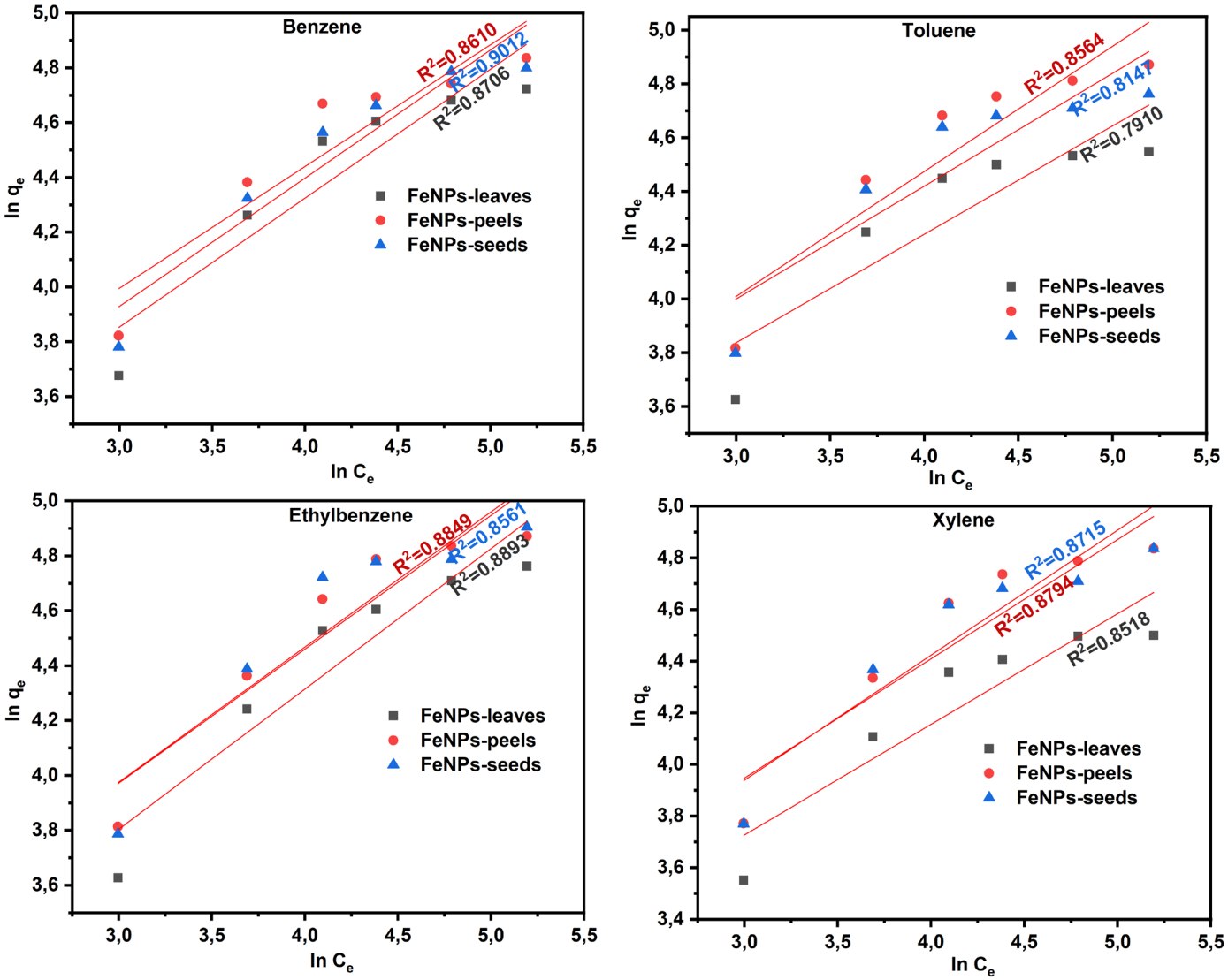


Figure 4. 12: The linear fit of Freundlich isotherm model for BTEX adsorption on FeNPs.

Table 4. 3: Langmuir and Freundlich isotherm parameters of BTEX adsorption by the FeNPs.

Adsorbent	Pollutant	Langmuir		Freundlich	
		q_m (mg/g)	K_L (L/mg)	K_F (mg/g)	n
FeNPs-leaves	Benzene	140.85	0.025	11.51	2.44
	Toluene	111.11	0.038	13.86	2.63
	Ethylbenzene	153.85	0.020	9,.69	2.01
	Xylene	109.89	0.031	11.48	2.33
FeNPs-peels	Benzene	153.60	0.027	14.34	2.25
	Toluene	161.29	0.026	13.67	2.15
	Ethylbenzene	166.67	0.023	12.32	2.05
	Xylene	161.29	0.024	12.00	2.06
FeNPs-seeds	Benzene	154.56	0.027	12.49	2.14
	Toluene	138.89	0.033	15.51	2.38
	Ethylbenzene	169.49	0.023	12.18	2.03
	Xylene	156.25	0.024	12.96	2.16

Table 4. 4: Comparison of the adsorption capacities of various iron/iron oxide nanoparticles adsorbents in BTEX adsorption.

Adsorbent and their synthetic route	Adsorbent dosage (g/L)	Temp. (°C)	q_m (mg/g)				Reference
			B	T	E	X	
Nano zero-valent iron (chemical method)	0.22	40	6.3	66,.75	81.44	53.62	(Mahmoud et al., 2017)
Iron oxide nanoparticles (chemical method)	1.00	25	0.09[a]				(Eldos et al., 2023)
Iron oxide nanoparticles[b] (biosynthetic method)	0.4	25	153.60	161.29	166.67	161.29	This study

[a] Reported as cumulative q_m value (Eldos et al., 2023).

[b] q_m value for FeNPs-peels (This study).

4.5.4 Possible adsorption mechanism

A series of interactions could be responsible for the adsorptive removal of BTEX using the biogenic-synthesized iron oxide NPs, which depends on the properties of the iron oxide NPs and the BTEX. Based on the NPs characterization and adsorption results, three of the possible mechanisms are depicted in Figure 4.14. Mechanism A, as shown in Figure 4.14, involves electrostatic interaction between the charged iron oxide nanoparticles and the π electrons of the BTEX. Metal oxide NPs hydrate in an aqueous solution, resulting in an M-OH hydrated form (Wang et al., 2013). Under acidic or basic conditions, the M-OH can either be protonated or deprotonated, leading to the formation of $M\text{-}OH_2^+$ (acidic) or $M\text{-}O^-$ (basic). At low pH, there is electrostatic attraction between positively charged NPs and the π electrons of the BTEX

(Dzade et al., 2014); thus necessitating the adsorption of the BTEX to the NPs. In mechanism B, the presence of functional groups such as the carboxylic acid and hydroxyl group on the surface of the iron oxide nanoparticles, as shown in their FTIR results, initiate an OH- π interaction between the NPs and the BTEX. Such OH- π interaction is often responsible for the adsorption of aromatic compounds such as BTEX on hydroxylated NPs (Nakamura et al., 2020; Di Mino et al., 2023). Adsorption could also occur according to mechanism C, that is, through pore filling by diffusion. This is inferred from BET analysis of the NPs, which showed that the NPs are mesoporous materials with porous structures ideal for the adsorption of organic contaminants such as BTEX. Hence, BTEX could be absorbed into the NPs' pore cavities through pore filling.

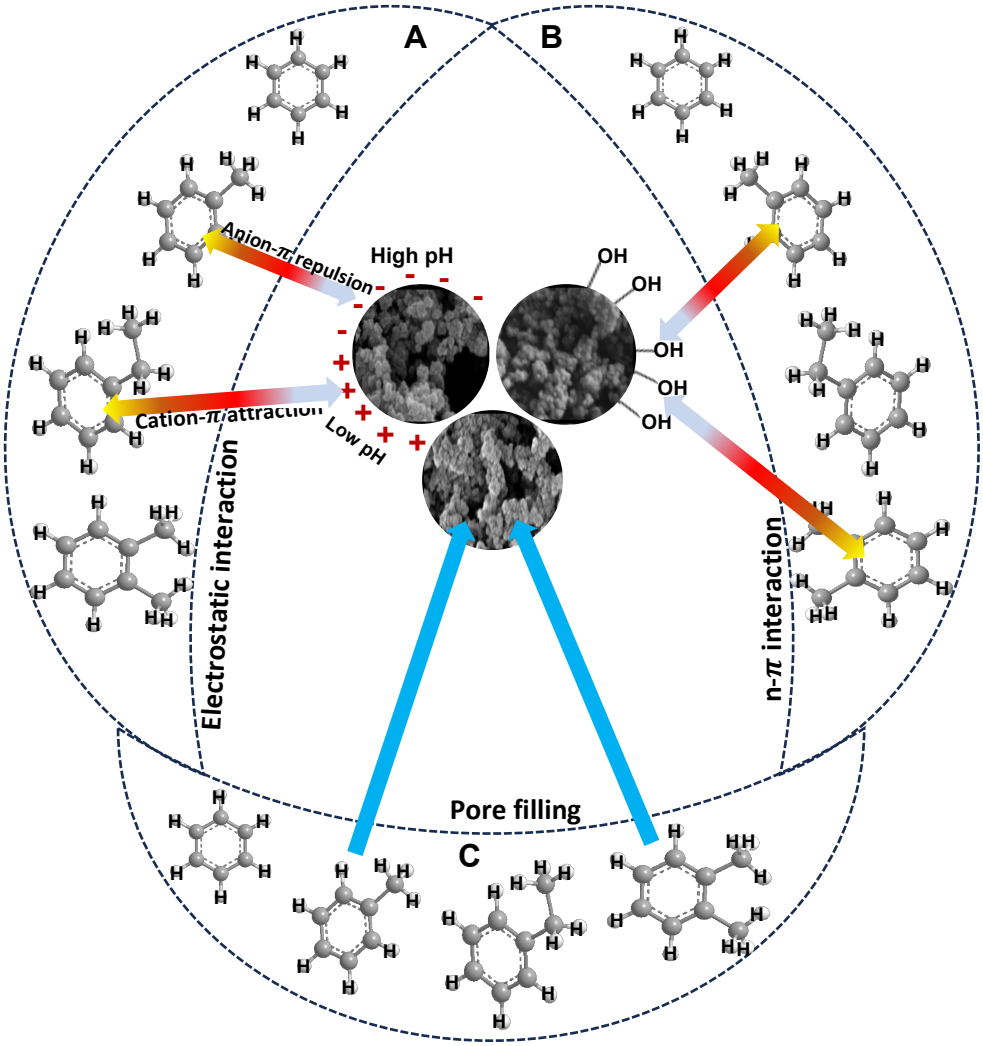


Figure 4. 13: Schematic diagram of the possible adsorption mechanism of BTEX on the FeNPs.

4.5.5 Regeneration of the biogenic-synthesized FeNPs

The regeneration study was performed to determine the plausibility of reusing the biogenic-synthesized FeNPs after applying them for BTEX adsorption. This was done through adsorption-desorption experiments using methanol to desorb the BTEX after each adsorption application. The used FeNPs were put in methanol and stirred for 1 hr, and then filtered and reapplied for further BTEX adsorption. The process was repeated four times, and the % rejection (%R) was measured after each cycle. Figure 4.15 depicts the results of the regeneration study, which shows that there was a decline in the BTEX removal efficiency of the FeNPs after the first adsorption-desorption experiment. The decline could be due to the washing off of some of the active functional groups on the FeNPs during the first desorption process, thereby reducing the active sites on the FeNPs. However, there were slight changes in the %R of the FeNPs after the subsequent adsorption-desorption cycles. This indicates that there may still be some stable active functional sites on the FeNPs after the first desorption. Combined with the diffusion of the BTEX into the pores of the FeNPs, high removal of BTEX was still obtained after each cycle, thus, the FeNPs can be reused to perform multiple BTEX adsorption. This established the biogenic-synthesized FeNPs as a potential adsorbent for multiple uses in the removal of BTEX from contaminated wastewater.

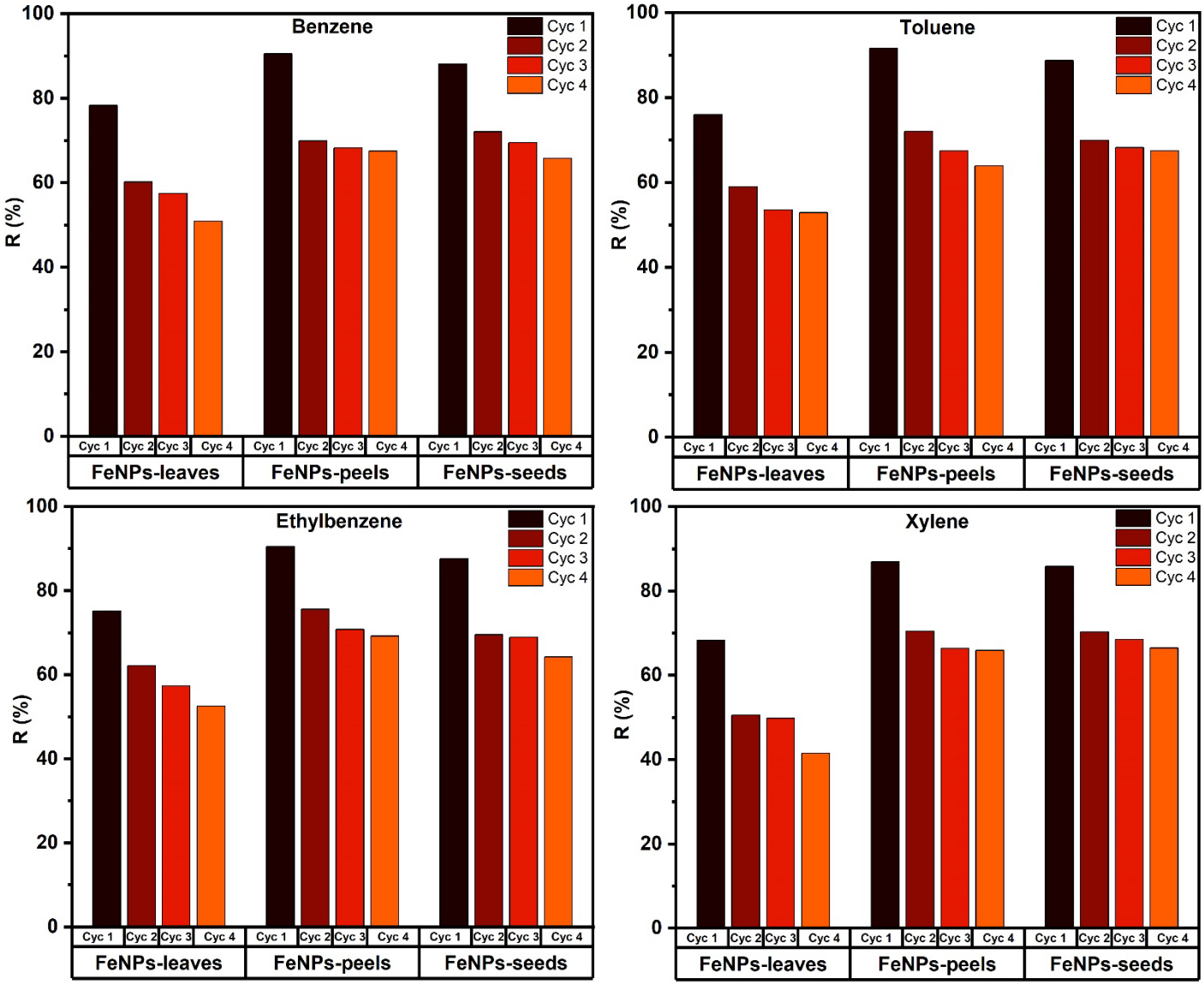


Figure 4. 14: Regeneration of the various FeNPs in BTEX adsorption.

4.6 Conclusion

This work identified the potential of biogenic-synthesized FeNPs as an adsorbent for the removal of BTEX from contaminated wastewater. Pomegranate extracts were used for the biogenic synthesis of the FeNPs, thereby replacing the use of toxic chemicals in the reduction of the iron precursor to the iron oxide nanoparticles. According to the XRD results, different forms of iron oxide were obtained from using the leaves, peels, and seeds extracts of the pomegranate in reducing iron (III) chloride to iron oxide nanoparticles. All three biogenic-synthesized FeNPs exhibited similar trends in their performance in the adsorptive removal of BTEX. However, the FeNPs-peels and FeNPs-seeds showed slightly better performance than the FeNPs-leaves. The optimum BTEX adsorption of the FeNPs was achieved at pH 5, and

their adsorption equilibrium was attained at 40 min. The adsorption process conformed to a pseudo-second-order model and a Langmuir isotherm model, thereby establishing that the adsorption occurred mainly through chemisorption in a monolayer adsorption process and having homogenous interaction of the BTEX with the FeNPs surfaces. Regeneration of the FeNPs was also established from the regeneration studies, which showed that there was a decline in the %R of the FeNPs in the first adsorption-desorption experiment. However, only a slight loss in the performance of FeNPs was observed in the subsequent adsorption-desorption cycles. The findings of this study identified biogenic-synthesized FeNPs as a promising adsorbent for the adsorptive removal of BTEX from contaminated wastewater.

References

Al-Ghouti, M. A., & Da'ana, D. A. (2020). Guidelines for the use and interpretation of adsorption isotherm models: A review. *Journal of Hazardous Materials*, *393*, 122383. https://doi.org/10.1016/j.jhazmat.2020.122383

Anjum, H., Johari, K., Gnanasundaram, N., Ganesapillai, M., Arunagiri, A., Regupathi, I., & Thanabalan, M. (2019). A review on adsorptive removal of oil pollutants (BTEX) from wastewater using carbon nanotubes. *Journal of Molecular Liquids*, *277*, 1005–1025. https://doi.org/10.1016/j.molliq.2018.10.105

Asejeje, G. I., Ipeaiyeda, A. R., & Onianwa, P. C. (2021). Occurrence of BTEX from petroleum hydrocarbons in surface water, sediment, and biota from Ubeji Creek of Delta State, Nigeria. *Environmental Science and Pollution Research*, *28*(12), 15361–15379. https://doi.org/10.1007/s11356-020-11196-y

Astrahan, P., Lupu, A., Leibovici, E., & Ninio, S. (2023). BTEX and PAH contributions to Lake Kinneret water: A seasonal-based study of volatile and semi-volatile anthropogenic pollutants in freshwater sources. *Environmental Science and Pollution Research*, *30*(21), 61145–61159. https://doi.org/10.1007/s11356-023-26724-9

Azizi, A., Torabian, A., Moniri, E., Hassani, A. H., & Ahmad Panahi, H. (2016). Adsorption performance of modified graphene oxide nanoparticles for the removal of toluene, ethylbenzene, and xylenes from aqueous solution. *Desalination and Water Treatment*, *57*(59), 28806–28821. https://doi.org/10.1080/19443994.2016.1193769

Bartilotti, M., Viana, T. S., de Oliveira, D. P., Santos, E. V., Rojas-Mantilla, H. D., Santos, M. C., & Zanoni, M. V. B. (2021). Assessment of the improved performance of magnetite-

modified vermiculite in the reduction of BTEX and metals, as well as toxicity in petroleum-produced water. *Journal of Water Process Engineering*, *39*, 101749. https://doi.org/10.1016/j.jwpe.2020.101749

Bielen, A., Šimatović, A., Kosić-Vukšić, J., Senta, I., Ahel, M., Babić, S., Jurina, T., González Plaza, J. J., Milaković, M., & Udiković-Kolić, N. (2017). Negative environmental impacts of antibiotic-contaminated effluents from pharmaceutical industries. *Water Research*, *126*, 79–87. https://doi.org/10.1016/j.watres.2017.09.019

Bulatović, S., Ilić, M., Šolević Knudsen, T., Milić, J., Pucarević, M., Jovančićević, B., & Vrvić, M. M. (2022). Evaluation of potential human health risks from exposure to volatile organic compounds in contaminated urban groundwater in the Sava river aquifer, Belgrade, Serbia. *Environmental Geochemistry and Health*, *44*(10), 3451–3472. https://doi.org/10.1007/s10653-021-01119-2

Bustillo-Lecompte, C. F., Kakar, D., & Mehrvar, M. (2018). Photochemical treatment of benzene, toluene, ethylbenzene, and xylenes (BTEX) in aqueous solutions using advanced oxidation processes: Towards a cleaner production in the petroleum refining and petrochemical industries. *Journal of Cleaner Production*, *186*, 609–617. https://doi.org/10.1016/j.jclepro.2018.03.135

Chittick, E. A., & Srebotnjak, T. (2017). An analysis of chemicals and other constituents found in produced water from hydraulically fractured wells in California and the challenges for wastewater management. *Journal of Environmental Management*, *204*, 502–509. https://doi.org/10.1016/j.jenvman.2017.09.002

Cornell, R. M., & Schwertmann, U. (2003). *The Iron Oxides: Structure, Properties, Reactions, Occurrences and Uses*. John Wiley & Sons.

Dantas, G., Gorne, I., da Silva, C. M., & Arbilla, G. (2022). Benzene, Toluene, Ethylbenzene and Xylene (BTEX) concentrations in urban areas impacted by chemical and petrochemical industrial emissions. *Bulletin of Environmental Contamination and Toxicology*, *108*(2), 204–211. https://doi.org/10.1007/s00128-021-03336-y

Davidson, C. J., Hannigan, J. H., & Bowen, S. E. (2021). Effects of inhaled combined Benzene, Toluene, Ethylbenzene, and Xylenes (BTEX): Toward an environmental exposure model. *Environmental Toxicology and Pharmacology*, *81*, 103518. https://doi.org/10.1016/j.etap.2020.103518

Di Mino, C., Seel, A. G., Clancy, A. J., Headen, T. F., Földes, T., Rosta, E., Sella, A., & Skipper, N. T. (2023). Strong structuring arising from weak cooperative O-H···π and C-H···O hydrogen bonding in benzene-methanol solution. *Nature Communications*, *14*(1), Article 1. https://doi.org/10.1038/s41467-023-41451-y

Dzade, N. Y., Roldan, A., & De Leeuw, N. H. (2014). A Density Functional Theory study of the adsorption of benzene on hematite (α-Fe_2O_3) surfaces. *Minerals*, *4*(1), Article 1. https://doi.org/10.3390/min4010089

Eldos, H. I., Khan, M., Zouari, N., Saeed, S., & Al-Ghouti, M. A. (2023). Adsorptive removal of volatile petroleum hydrocarbons from aqueous solution by zeolite imidazole framework (ZIF-8) and iron oxide (Fe_3O_4) nanoparticles. *Environmental Technology & Innovation*, *32*, 103382. https://doi.org/10.1016/j.eti.2023.103382

Enemuo, N., Richards, H., & Daramola, M. O. (2024). Evaluation of the performance of Fe_3O_4-NPs/PVDF nanocomposite membrane for removal of BTEX from contaminated water. *Journal of Water Process Engineering*, *60*, 105185. https://doi.org/10.1016/j.jwpe.2024.105185

Eom, H., Kim, S., & Oh, S.-E. (2023). Evaluation of joint toxicity of BTEX mixtures using sulfur-oxidizing bacteria. *Journal of Environmental Management*, *325*, 116435. https://doi.org/10.1016/j.jenvman.2022.116435

Fayemiwo, O., Moothi, K., & Daramola, M. (2017). BTEX compounds in water – future trends and directions for water treatment. *Water SA*, *43*(4), 602–613. https://doi.org/10.4314/wsa.v43i4.08

Fernández, E., Vidal, L., & Canals, A. (2016). Zeolite/iron oxide composite as sorbent for magnetic solid-phase extraction of benzene, toluene, ethylbenzene and xylenes from water samples prior to gas chromatography□mass spectrometry. *Journal of Chromatography A*, *1458*, 18–24. https://doi.org/10.1016/j.chroma.2016.06.049

Gross, S. A., Avens, H. J., Banducci, A. M., Sahmel, J., Panko, J. M., & Tvermoes, B. E. (2013). Analysis of BTEX groundwater concentrations from surface spills associated with hydraulic fracturing operations. *Journal of the Air & Waste Management Association*, *63*(4), 424–432. https://doi.org/10.1080/10962247.2012.759166

Guo, X., & Wang, J. (2019). A general kinetic model for adsorption: Theoretical analysis and modeling. *Journal of Molecular Liquids*, *288*, 111100. https://doi.org/10.1016/j.molliq.2019.111100

Gupta, D., Boora, A., Thakur, A., & Gupta, T. K. (2023). Green and sustainable synthesis of nanomaterials: Recent advancements and limitations. *Environmental Research*, *231*, 116316. https://doi.org/10.1016/j.envres.2023.116316

Jadoun, S., Arif, R., Jangid, N. K., & Meena, R. K. (2021). Green synthesis of nanoparticles using plant extracts: A review. *Environmental Chemistry Letters*, *19*(1), 355–374. https://doi.org/10.1007/s10311-020-01074-x

Jiménez, S., Andreozzi, M., Micó, M. M., Álvarez, M. G., & Contreras, S. (2019). Produced water treatment by advanced oxidation processes. *Science of The Total Environment*, *666*, 12–21. https://doi.org/10.1016/j.scitotenv.2019.02.128

Jin, X., Liu, Y., Tan, J., Owens, G., & Chen, Z. (2018). Removal of Cr(VI) from aqueous solutions via reduction and absorption by green synthesized iron nanoparticles. *Journal of Cleaner Production*, *176*, 929–936. https://doi.org/10.1016/j.jclepro.2017.12.026

Kim, S.-H., Park, J.-H., & Lee, C.-Y. (2013). Surface-functionalized mesoporous silica nanoparticles as sorbents for BTEX. *Journal of Porous Materials*, *20*(5), 1087–1093. https://doi.org/10.1007/s10934-013-9690-6

Kumar, V., Singh, S., Srivastava, B., Bhadouria, R., & Singh, R. (2019). Green synthesis of silver nanoparticles using leaf extract of Holoptelea integrifolia and preliminary investigation of its antioxidant, anti-inflammatory, antidiabetic and antibacterial activities. *Journal of Environmental Chemical Engineering*, *7*(3), 103094. https://doi.org/10.1016/j.jece.2019.103094

Kumari, P., Alam, M., & Siddiqi, W. A. (2019). Usage of nanoparticles as adsorbents for waste water treatment: An emerging trend. *Sustainable Materials and Technologies*, *22*, e00128. https://doi.org/10.1016/j.susmat.2019.e00128

Lee, S.-T., Vu, C. T., Lin, C., & Chen, K.-S. (2018). High occurrence of BTEX around major industrial plants in Kaohsiung, Taiwan. *Environmental Forensics*, *19*(3), 206–216. https://doi.org/10.1080/15275922.2018.1475432

Leili, M., Farjadfard, S., Sorial, G. A., & Ramavandi, B. (2017). Simultaneous biofiltration of BTEX and Hg° from a petrochemical waste stream. *Journal of Environmental Management*, *204*, 531–539. https://doi.org/10.1016/j.jenvman.2017.09.033

Liang, X., Feng, W., Liang, D., Xu, Y., & Qiu, X. (2021). Hydroxyl/amino and Fe(III) co-grafted graphite carbon nitride for photocatalytic removal of volatile organic compounds. *Environmental Research*, *197*, 111044. https://doi.org/10.1016/j.envres.2021.111044

Liu, S., Chen, D., Zheng, J., Zeng, L., Jiang, J., Jiang, R., Zhu, F., Shen, Y., Wu, D., & Ouyang, G. (2015). The sensitive and selective adsorption of aromatic compounds with highly crosslinked polymer nanoparticles. *Nanoscale*, *7*(40), 16943–16951. https://doi.org/10.1039/C5NR04624F

Luo, F., Yang, D., Chen, Z., Megharaj, M., & Naidu, R. (2016). One-step green synthesis of bimetallic Fe/Pd nanoparticles used to degrade Orange II. *Journal of Hazardous Materials*, *303*, 145–153. https://doi.org/10.1016/j.jhazmat.2015.10.034

Mahmoud, A. S., Mostafa, M. K., & Abdel-Gawad, S. A. (2017). Artificial intelligence for the removal of benzene, toluene, ethyl benzene and xylene (BTEX) from aqueous solutions using iron nanoparticles. *Water Supply*, *18*(5), 1650–1663. https://doi.org/10.2166/ws.2017.225

Masuku, M., Ouma, L., & Pholosi, A. (2021). Microwave assisted synthesis of oleic acid modified magnetite nanoparticles for benzene adsorption. *Environmental Nanotechnology, Monitoring & Management*, *15*, 100429. https://doi.org/10.1016/j.enmm.2021.100429

Medeiros, D. C. C. da S., Chelme-Ayala, P., Benally, C., Al-Anzi, B. S., & Gamal El-Din, M. (2022). Review on carbon-based adsorbents from organic feedstocks for removal of organic contaminants from oil and gas industry process water: Production, adsorption performance and research gaps. *Journal of Environmental Management*, *320*, 115739. https://doi.org/10.1016/j.jenvman.2022.115739

Mokarram, M., Saber, A., & Sheykhi, V. (2020). Effects of heavy metal contamination on river water quality due to release of industrial effluents. *Journal of Cleaner Production*, *277*, 123380. https://doi.org/10.1016/j.jclepro.2020.123380

Moridzadeh, M., Dehghani, S., Rafiee, A., Hassanvand, M. S., Dehghani, M., & Hoseini, M. (2020). Assessing BTEX exposure among workers of the second largest natural gas reserve in

the world: A biomonitoring approach. *Environmental Science and Pollution Research*, *27*(35), 44519–44527. https://doi.org/10.1007/s11356-020-10379-x

Nakamura, S., Tsuji, Y., & Yoshizawa, K. (2020). Role of hydrogen-bonding and OH−π interactions in the adhesion of epoxy resin on hydrophilic surfaces. *ACS Omega*, *5*(40), 26211–26219. https://doi.org/10.1021/acsomega.0c03798

Nambi, I. M., Rajasekhar, B., Loganathan, V., & RaviKrishna, R. (2017). An assessment of subsurface contamination of an urban coastal aquifer due to oil spill. *Environmental Monitoring and Assessment*, *189*(4), 148. https://doi.org/10.1007/s10661-017-5833-6

Nandiyanto, A. B. D., Oktiani, R., & Ragadhita, R. (2019). How to read and interpret FTIR spectroscope of organic material. *Indonesian Journal of Science and Technology*, *4*(1), Article 1.

Partha, D. B., Cassidy-Bushrow, A. E., & Huang, Y. (2022). Global preterm births attributable to BTEX (benzene, toluene, ethylbenzene, and xylene) exposure. *Science of The Total Environment*, *838*, 156390. https://doi.org/10.1016/j.scitotenv.2022.156390

Patiño-Ruiz, D., Sánchez-Botero, L., Tejeda-Benitez, L., Hinestroza, J., & Herrera, A. (2020). Green synthesis of iron oxide nanoparticles using *Cymbopogon citratus* extract and sodium carbonate salt: Nanotoxicological considerations for potential environmental applications. *Environmental Nanotechnology, Monitoring & Management*, *14*, 100377. https://doi.org/10.1016/j.enmm.2020.100377

Prathna, T. C., Sharma, S. K., & Kennedy, M. (2018). Nanoparticles in household level water treatment: an overview. Separation and Purification Technology, 199, 260-270.

Rodrigo-Ilarri, J., Rodrigo-Clavero, M.-E., Capilla, J. E., & Romero-Ballesteros, L. (2023). Environmental assessment of soil and groundwater pollution by BTEX leaching in valencia region (Spain). *Water*, *15*(18), Article 18. https://doi.org/10.3390/w15183279

Saha, N., & Dutta Gupta, S. (2017). Low-dose toxicity of biogenic silver nanoparticles fabricated by *Swertia chirata* on root tips and flower buds of *Allium cepa*. *Journal of Hazardous Materials*, *330*, 18–28. https://doi.org/10.1016/j.jhazmat.2017.01.021

Shen, W., Qu, Y., Pei, X., Li, S., You, S., Wang, J., Zhang, Z., & Zhou, J. (2017). Catalytic reduction of 4-nitrophenol using gold nanoparticles biosynthesized by cell-free extracts of

Aspergillus sp. WL-Au. *Journal of Hazardous Materials*, *321*, 299–306. https://doi.org/10.1016/j.jhazmat.2016.07.051

Singleton, V. L., & Rossi, J. A. (1965). Colorimetry of total phenolics with phosphomolybdic-phosphotungstic acid reagents. *American Journal of Enology and Viticulture*, *16*(3), 144–158. https://doi.org/10.5344/ajev.1965.16.3.144

Soni, V., Raizada, P., Singh, P., Cuong, H. N., S, R., Saini, A., Saini, R. V., Le, Q. V., Nadda, A. K., Le, T.-T., & Nguyen, V.-H. (2021). Sustainable and green trends in using plant extracts for the synthesis of biogenic metal nanoparticles toward environmental and pharmaceutical advances: A review. *Environmental Research*, *202*, 111622. https://doi.org/10.1016/j.envres.2021.111622

Stan, M., Lung, I., Soran, M.-L., Leostean, C., Popa, A., Stefan, M., Lazar, M. D., Opris, O., Silipas, T.-D., & Porav, A. S. (2017). Removal of antibiotics from aqueous solutions by green synthesized magnetite nanoparticles with selected agro-waste extracts. *Process Safety and Environmental Protection*, *107*, 357–372. https://doi.org/10.1016/j.psep.2017.03.003

United Nations. (2015). *The 17 Goals | Sustainable Development*. https://sdgs.un.org/goals

Varela, C. F., Pazos, M. C., & Alba, M. D. (2021). Organophilization of acid and thermal treated sepiolite for its application in BTEX adsorption from aqueous solutions. *Journal of Water Process Engineering*, *40*, 101949. https://doi.org/10.1016/j.jwpe.2021.101949

Wang, J., Ma, Q., Wang, Y., Li, Z., Li, Z., & Yuan, Q. (2018). New insights into the structure–performance relationships of mesoporous materials in analytical science. *Chemical Society Reviews*, *47*(23), 8766–8803. https://doi.org/10.1039/C8CS00658J

Wang, N., Hsu, C., Zhu, L., Tseng, S., & Hsu, J.-P. (2013). Influence of metal oxide nanoparticles concentration on their zeta potential. *Journal of Colloid and Interface Science*, *407*, 22–28. https://doi.org/10.1016/j.jcis.2013.05.058

Wu, Z., & Zhao, D. (2011). Ordered mesoporous materials as adsorbents. *Chemical Communications*, *47*(12), 3332–3338. https://doi.org/10.1039/C0CC04909C

Xu, J., Zheng, L., Yan, Z., Huang, Y., Feng, C., Li, L., & Ling, J. (2020). Effective extrapolation models for ecotoxicity of benzene, toluene, ethylbenzene, and xylene (BTEX). *Chemosphere*, *240*, 124906. https://doi.org/10.1016/j.chemosphere.2019.124906

Ye, C. Z., & Ariya, P. A. (2015). Co-adsorption of gaseous benzene, toluene, ethylbenzene, m-xylene (BTEX) and SO2 on recyclable Fe3O4 nanoparticles at 0–101% relative humidities. *Journal of Environmental Sciences*, *31*, 164–174. https://doi.org/10.1016/j.jes.2014.10.019

Yeap, S. P., Lim, J., Ooi, B. S., & Ahmad, A. L. (2018). Feasibility of electrostatic-mediated *post*-functionalization to induce long term colloidal stability and stability after freeze drying of amphoteric nanoparticles. *Colloid and Interface Science Communications*, *23*, 14–20. https://doi.org/10.1016/j.colcom.2018.02.003

Yu, B., Yuan, Z., Yu, Z., & Xue-song, F. (2022). BTEX in the environment: An update on sources, fate, distribution, pretreatment, analysis, and removal techniques. *Chemical Engineering Journal*, *435*, 134825. https://doi.org/10.1016/j.cej.2022.134825

Zhang, Z., Du, X., Carlson, K. H., Robbins, C. A., & Tong, T. (2019). Effective treatment of shale oil and gas produced water by membrane distillation coupled with precipitative softening and walnut shell filtration. *Desalination*, *454*, 82–90. https://doi.org/10.1016/j.desal.2018.12.011

Chapter 5: Evaluation of the performance of Fe_3O_4-NPs/PVDF nanocomposite membrane for removal of BTEX from contaminated water

This chapter consists of a study on the application of the biogenic synthesized iron oxide nanoparticles to enhance the performance of a PVDF membrane in the treatment of BTEX-contaminated wastewater. The content of this chapter is reported in **Paper 2** and has been published in the **Journal of Water Process Engineering** (Enemuo, N., Richards, H., & Daramola, M. O. (2024). Evaluation of the performance of Fe_3O_4-NPs/PVDF nanocomposite membrane for removal of BTEX from contaminated water. *Journal of Water Process Engineering*, *60*, 105185. https://doi.org/10.1016/j.jwpe.2024.105185)

The paper evaluated the performance of PVDF membranes modified with various amounts of biogenic-synthesized Fe_3O_4-NPs in treating BTEX-contaminated water. Thus, this chapter presents the optimum conditions for fabricating an ideal nanocomposite membrane using biogenic-synthesized Fe_3O_4-NPs and applying it to BTEX wastewater treatment.

Abstract

With the increase in reported cases of toxic organic contaminants such as benzene, toluene, ethylbenzene, and xylene (BTEX) in the aquatic environment, membrane technology offers a viable option for removing BTEX from wastewater. However, hydrophilic modification of the membranes is vital to reduce the rapid accumulation of the BTEX organic contaminants and maintain improved membrane performance in BTEX removal. In this study, biogenically-synthesized Fe_3O_4-NPs were embedded into a PVDF membrane to endow the membrane with hydrophilicity, which necessitates the reduction in BTEX accumulation on the membrane, consequently maintaining improved membrane performance towards BTEX removal. Different Fe_3O_4-NPs loadings (0 wt% to 5 wt%) were used for the PVDF modification to establish the optimum blending amount of the Fe_3O_4-NPs required to achieve the most effective membrane. The water contact angle was reduced from 84.2° (pristine PVDF) to 52° for the membrane modified with 1 wt% of the Fe_3O_4-NPs. Other membrane features such as porosity, surface roughness, and mechanical strength were also enhanced. Performance evaluation of the membranes revealed that the flux and BTEX rejection of the Fe_3O_4-NPs/PVDF membrane were improved. The antifouling test results showed a reduction in the total fouling from 52.1% (pristine membrane) to 36.3% for the membrane modified with 1 wt% of the Fe_3O_4-NPs. Our

findings provide a strategy utilizing biogenically synthesized Fe_3O_4-NPs to enhance PVDF membranes' performance for removing BTEX from wastewater.

5.1 Introduction

Discharging untreated or poorly treated wastewater into water bodies is a global challenge that has highlighted the need for continuous development of better means of wastewater treatment before discharge (Wang et al., 2019; Nazir, 2018; Freeman et al., 1992). One of the implications of discharging poorly treated wastewater into the water sources is the release of harmful contaminants into our aquatic system (Butkovskyi et al., 2017; Yusta-García et al., 2017). Among the top contaminants reported to be released into the water bodies from industrial discharge are benzene, toluene, ethylbenzene, and xylene, collectively known as BTEX (Yu et al., 2022; Davidson et al., 2021; Lee et al., 2018). According to the United States Environmental Protection Agency (2007), the health implications of exposure to BTEX-contaminated water include cancer, reproductive complications, and neurological problems, among others. BTEX also poses environmental issues such as the pollution of aquatic systems, and its volatilization from the contaminated water body into the atmosphere causes poor air quality (Bolden et al., 2015; Lueders, 2017).

In response to the adverse health and environmental consequences of BTEX-contaminated water bodies, several treatment techniques have been developed to ensure the removal of BTEX from wastewater before discharge. Such treatment methods include hydrocyclones, flotation, API separators, and membrane technology (Ekins et al., 2007; Zha et al., 2016; Mikhak et al., 2019). Among these treatment techniques, membrane technology is the most efficient and effective. In contrast, the other techniques are either not very effective in removing BTEX, are cost and energy-intensive, or lead to secondary pollution.(Amakiri et al., 2022; Igunnu & Chen, 2014). Although most membranes, such as polyvinylidene fluoride (PVDF), possess the ideal physical properties required for BTEX wastewater treatment, they are limited by their hydrophobic nature (Khanzada et al., 2020b). This limitation springs from the strong hydrophobic interaction between the membrane and the BTEX organic contaminants, which results in rapid accumulation of the BTEX on the membrane and subsequent membrane fouling (Subasi & Cicek, 2017). Membrane fouling results in deterioration of the membrane performance, such as flux decline, poor rejection, and reduced membrane lifespan (Van der Bruggen, 2009; Miller et al., 2013; Tummons et al., 2020). To minimize membrane fouling and maintain good membrane performance during the treatment of organic contaminated

wastewater, the membrane is made hydrophilic by incorporating hydrophilic components such as hydrophilic polymers and nanoparticles (NPs) into the membrane (Kang & Cao, 2014; Yin & Deng, 2015; Miller et al., 2017). The incorporated hydrophilic components not only improve the membrane's performance but also reinforce the membrane's physical properties, such as morphology and mechanical stability (Al Aani et al., 2017; C. Wang et al., 2022).

Over the years, nanoparticles such as TiO_2 (Vatanpour et al., 2022), Ag (Zou et al., 2020), Al_2O_3 (Lin et al., 2017), and Fe_3O_4 (Zhu et al., 2020) have successfully been utilized in enhancing the hydrophilicity of membranes to reduce fouling and achieve good membrane performance in the removal of organic contaminants from wastewater. Matindi et al. (2021) incorporated TiO_2 NPs into a polyethersulfone/polysulfone (PES/PS) composite membrane to improve the membrane performance in oil-in-water emulsion separation. They reported that the embedded TiO_2 significantly improved the hydrophilicity of the membrane; as a consequence, the membrane performance, such as flux and separation efficiency, was enhanced. In another modification strategy, Fe_3O_4@MoS_2 NPs were anchored in a PES membrane, and its performance integrity in treating bovine serum albumin (BSA) and humic acid (HA) contaminated water was assessed (Kong et al., 2022). The Fe_3O_4@MoS_2 NPs modified membrane improved its permeability and rejection due to the enhanced hydrophilicity introduced in the membrane by the Fe_3O_4@MoS_2 NPs (Kong et al., 2022). The removal efficiency of another organic contaminant, methylene blue, was improved by modifying the PVDF membrane used for the removal of the dye with Fe_3O_4 NPs (Huang et al., 2020).

Very little research has been reported on treating BTEX-contaminated wastewater using Fe_3O_4 NPs-modified membrane. In fact, to the best of our knowledge, only two research studies have been conducted on iron or iron oxide-modified membranes for the treatment of BTEX-contaminated wastewater. The first research incorporated Fe-NPs into a polyethersulfone (PES) membrane for the treatment of BTEX-contaminated water and reported an improvement in the performance of the modified membrane compared to the pristine PES (Unuigbe et al., 2020b). However, the Fe-NPs used in the fabrication were reported to be agglomerated, and the cumulative BTEX rejection of the modified membrane was 64.55% (Unuigbe et al., 2020b). The second research used a tannin iron complex (TA-Fe^{III}), not iron nanoparticles, to modify a PES membrane to treat BTEX wastewater, and enhanced performance of the modified membrane was reported (Makhani et al., 2022).

Considering the studies mentioned above on the use of iron-modified membranes for the treatment of BTEX-contaminated wastewater, there is a need to improve the dispersion of the iron nanoparticles during their synthesis. This is because the incorporation of agglomerated nanoparticles in a membrane often adversely affects the physical and performance characteristics of the membrane (Oliveira et al., 2022; Wei et al., 2022; Ursino et al., 2018). To establish the optimum conditions for treating the BTEX-contaminated wastewater, there is also a need to explore the influence of the operational conditions on the performance of the modified membrane. In addition, an antifouling test on the iron-modified membrane is needed to establish the effect of the incorporated NPs on fouling mitigation. Furthermore, PVDF is known to be more chemically resistant to all four components of BTEX: benzene, toluene, ethylbenzene, and xylene (Wypych, 2022). Hence, using a more BTEX-resistant base polymer to treat the wastewater would ensure that there would be no or minimal deterioration of the membrane performance due to chemical degradation of the polymer by the BTEX contaminants.

Therefore, in this study, biogenic synthesis of Fe_3O_4-NPs was performed using the extract of pomegranate leaf to reduce iron precursor to the Fe_3O_4-NPs, and the leaf extract also stabilized the synthesized Fe_3O_4-NPs; thus, a dispersed NPs was obtained. Subsequently, the PVDF membrane was modified with the biogenically synthesized Fe_3O_4-NPs, and the effect of the NPs on the physical features and performance of the membrane was investigated. Furthermore, the effect of pressure and BTEX feed concentration on the flux and rejection of the Fe_3O_4-NPs/PVDF membrane was also investigated. In addition, the influence of the Fe_3O_4-NPs on the antifouling tendency of the modified membrane was further assessed.

5.2 Experimental

5.2.1 Materials

PVDF pellets (M_w ~ 180,000gmol^{-1}), PSF pellets (M_w ~ 35,000gmol^{-1}), 1-methyl-2-pyrrolidinone (NMP, ≥99.0%), iron (III) chloride ($FeCl_3$), benzene (99.8%), toluene (99.9%), ethylbenzene (>99.9%), and xylene (≥99%) were purchased from Sigma Aldrich. The Direct-Q UV millipore system supplied deionized water (DI water, 18.2 MΩcm @25oC). All the reagents were used as received without any further purification. The pomegranate leaves were collected from the tree at the School of Chemical Engineering, University of the Witwatersrand, Johannesburg.

5.2.2 Synthesis of Fe_3O_4-NPs

The Fe_3O_4-NPs were biogenically synthesized using the extract of the pomegranate leaves. To obtain the leaves extract, pomegranate leaves were thoroughly washed with water to remove dust particles, dried, and then ground with a grinder. 20 g of the dried leaves powder was mixed with 200 mL of DI water and shaken for 8 hours at 150 rpm, followed by sonication for 30 minutes. The mixture was first filtered with a sieve and then with Whatman grade 1 filter paper. The obtained filtrate was stored at 4°C for the synthesis of the Fe_3O_4-NPs.

To synthesize the Fe_3O_4-NPs, $FeCl_3$ was biogenically reduced by the leaves extract following a method by Xu et al. (2020) with some modifications, which include changing the reaction duration and temperature. Plant extracts are known to exhibit an inherent ability to act as reducing, size-control, and stabilizing agents in the synthesis of nanoparticles (S. Ying et al., 2022a). For this synthesis, 1.2g of $FeCl_3$ was thoroughly dissolved in 70 mL of DI water, and 140 mL of leaf extract was added to the $FeCl_3$ solution under rigorous stirring. The reaction mixture was continuously stirred for 3 hours at 80°C, and during this time, the colour of the reaction solution changed from yellow ($FeCl_3$ solution) to black, indicating the formation of the Fe_3O_4-NPs. The resulting mixture was centrifuged, and the product was washed three times with ethanol and water to remove impurities and then dried in an oven for 3 hours at 50°C to obtain the Fe_3O_4-NPs in dry form for the enhancement of the features of PVDF membranes for BTEX wastewater treatment.

5.2.3 Fabrication of Fe_3O_4-NPs/PVDF membranes

The base membrane ideal for the BTEX wastewater treatment was selected based on the ability of the membrane to exhibit high tolerance to BTEX water with no or minimal membrane damage. Two fabricated membranes (PSF and PVDF) were tested for their tolerance towards BTEX water by immersing the membranes in different concentrations (500 ppm, 1000 ppm, and 2000 ppm) of BTEX solutions at room temperature for 30 days. The exposed membranes were removed from the BTEX solutions after 30 days, rinsed with DI water, and oven-dried at 40°C for 2 hours. Physical observation and SEM were used to determine the BTEX tolerance of the two membranes. The membrane with the best tolerance to BTEX was subsequently chosen as the base membrane for treating the BTEX wastewater.

PVDF was selected as the base membrane based on its high tolerance to BTEX water, as shown in the results session in Figures 5.4 and 5.5. Various amounts of the Fe_3O_4-NPs, ranging from 0.0 to 5.0 wt.% loadings, as depicted in Table 5.2, were embedded in the PVDF membrane.

The Fe_3O_4-NPs/PVDF membranes were prepared by thoroughly dispersing the appropriate amount of the Fe_3O_4-NPs in NMP and dissolving the PVDF pellets in a separate NMP solvent. Well-dispersion of the Fe_3O_4-NPs was achieved by stirring the Fe_3O_4-NPs suspension for 2 hours, followed by sonication for 30 mins. The Fe_3O_4-NPs suspension was then slowly poured into the PVDF solution under constant stirring, and the mixture was stirred for 8 hours at 50 ^oC. Then, the obtained dope solution was left to degas for 1 hour to remove air bubbles and cast on an elcometer film applicator. The cast membranes were fabricated using the non-solvent induced phase inversion method with DI water as the coagulation bath. The fabricated membranes were washed with DI water to remove any remaining solvent and dried in the oven at 40^oC for 6 hours.

5.3 Characterization of the leaves extract, Fe_3O_4-NPs, and the membranes

The leaves extract was analyzed to determine its constituent phytochemicals using an Agilent GC 7890B, with a 30m × 0.25mm ID × 0.25µm Rxi-5Sil MS capillary column, equipped with a Gerstel multipurpose sampler and a Pegasus 4D GC×GC-TOFMS. Before the analysis, the leaves extract was filtered using a 0.45 µm PTFE filter. The injection volume was 1 µL in a splitless mode, and helium was the carrier gas. The oven temperature gradient was programmed as follows: 50^oC for 30 sec, then 300^oC for 2 min at a rate of 15^oC/min.

The Fe_3O_4-NPs were identified by X-ray diffraction (XRD) using Bruker D2 phaser, and the functional groups were evaluated using Fourier transform infrared spectroscopy (FTIR) performed on a Bruker Tensor 27. The textural property of the Fe_3O_4-NPs was determined via N_2 physisorption at 77k using Brunauer-Emmett-Teller (BET) Micrometrics Tristar Plus 3.03. The morphology of the Fe_3O_4-NPs was studied using a high-resolution Carl Zeiss scanning electron microscopy (SEM) and FEI Tecnai T12 transmission electron microscopy (TEM). Energy-dispersive X-ray spectroscopy (EDX) was done using the same Carl Zeiss SEM. For X-ray photoelectron spectroscopy (XPS) measurements, X-rays were generated from a monochromatic Al K_a X-ray source. A hemispherical electron energy analyzer, SPECS Phoibos 150, determined the energies of the emitted electrons. The total energy resolution was approximately 0.7 eV.

The morphology of the fabricated membranes was obtained using the same high-resolution Carl Zeiss SEM and WITec alpha 300 atomic force microscope (AFM). The contact angle was measured by the sessile drop method using a KRUSS G10 goniometer. Seven measurements were done for each membrane, and the average was calculated. The thickness of the prepared

membranes (excluding the membranes used for the BTEX tolerance test) was measured using a digital micrometer. The thickness of each of the membranes was measured at five different positions, and the average thickness was calculated. ImageJ open-source software was used to measure the pore sizes of the membrane from the SEM images, and the mean pore size was calculated. The porosity (ε) and equilibrium water content (EWC) of the membranes were measured using the gravimetric method according to Eqs. 14 and 15, respectively.

$$\varepsilon\,(\%) = \frac{(W_{wet} - W_{dry})}{\rho \times A \times l} \times 100 \tag{14}$$

$$EWC\ (\%) = \left(\frac{W_{wet} - W_{dry}}{W_{wet}}\right) \times 100 \tag{15}$$

where W_{dry} and W_{wet} represent the masses of the dry membrane and the wet membrane respectively. ρ, A, and l are the density of water (g/cm^3), the effective area of the tested membrane (m^2), and the thickness of the membrane (m), respectively. The wet membrane was obtained by immersing the membrane in DI water for 48 hours. After 48 hours, the membrane was removed from the DI water, thoroughly wiped to remove excess water on the membrane, and subsequently weighed to obtain its weight.

The surface charge properties of the membranes were obtained using the Zetasizer Nano ZS system, Malvern Instruments. Each membrane was soaked in KOH (0.01M, 300 mL) electrolyte solution for 48 h, and measurements were conducted at pH ranging from 1.8 to 12.1 at 25°C. The membrane was cut and then fitted with the active side facing upward into the custom dip-cell immersed in the background electrolyte solution. The pH was adjusted using a dilute HCl and NaOH solution. A thermogravimetric analyzer, TA SDT Q600, was used to measure the thermal stability of the membranes between 25ºC and 700ºC at a heating rate of 10ºC/min under nitrogen. The mechanical properties were determined using a Tesla analyzer, XT plus TA.

5.4 Membrane performance evaluation

For the performance evaluation, a dead-end stirred cell (HP4750; Sterlitech Corp., USA) was utilized for the filtration of DI water and synthetic BTEX water. Synthetic BTEX water was used because of the difficulty in accessing BTEX-contaminated wastewater from the industries. The pressure at which filtration is performed has an impact on the membrane flux and rejection (Emadzadeh et al., 2019). Hence, the investigation of the effect of pressure on the membrane flux and rejection gives an indication of the ideal pressure required to achieve good flux and

rejection. To measure the effect of pressure on the pure water flux of the membranes, each membrane was mounted on the filtration cell, and the cell was filled with DI water. The DI water was filtered through the membrane for 1 hour at pressures of 100 kPa, 300 kPa, and 500 kPa, and the permeate was collected and measured. Each membrane was compacted using DI water to achieve a steady permeation before filtration. The pure water flux J_w (L m^{-2} h^{-1}) was calculated using Eq. 16, where V is the volume of the permeate (L), A is the effective membrane area (m^2), and t is the permeation time (min) (Chen et al., 2019).

$$J_w = \frac{V}{A \times t} \tag{16}$$

The effect of pressure on the BTEX flux and rejection of the membranes was measured by filtering synthetic BTEX water containing 100 ppm each of benzene, toluene, ethylbenzene, and xylene through the individual membranes under continuous stirring at a pressure of 100 kPa, 300 kPa, and 500 kPa using the same procedure described above. The BTEX flux was also calculated using Eq. 16, while the BTEX rejection was calculated according to Eq. 17.

$$R\ (\%) = \frac{C_f - C_p}{C_f} \tag{17}$$

where C_f is the BTEX concentration in the prepared feed water (ppm), and C_p is the BTEX concentration in the permeate (ppm). C_p was measured using an Agilent 7890A gas chromatograph GC, with a 30m × 0.25mm ID BP5MS × 0.25µm column, and equipped with an Agilent 7693A automatic liquid sampler and a flame ionization detector FID. The injection volume was 0.2 µL in splitless mode, and the carrier gas was nitrogen set at a constant flow rate of 2.64 mL/min. The oven initial temperature was set at 40ºC and held for 2 min, then ramped to 90ºC at 10ºC/min, held for 3 min, and finally to 200ºC at a rate of 20ºC/min and held for 2 min.

The concentration of feed solutions also affects the rejection capacity of membranes (Nikbakht Fini et al., 2019); hence, the BTEX rejection percentage of the membranes was evaluated at feed concentrations of 50, 100, 150, and 200 ppm to establish the feed concentrations that are ideal for effective BTEX rejection using the fabricated membranes.

The fouling resistance of the membranes towards BTEX was assessed by measuring four parameters: reversible fouling ratio (R_r), irreversible fouling ratio (R_{ir}), flux recovery ratio (FRR), and total fouling ratio (R_t). Antifouling test was done by first performing pure water filtration for 1 hour, followed by BTEX filtration (500 mL of 100 ppm) under continuous

stirring, then cleaning the membranes with water through backwashing followed by mild sonication in water. The backwashing of the membrane was performed by placing the bottom side of the membrane in an upward position in the dead-end cell and filtering 200 mL of DI water through the membrane. This is followed by another filtration of 100 mL of DI water through the top side of the membrane and subsequent mild sonication of the membrane in DI water for 15 mins. The cleaned membrane was again used for water filtration. The equations for calculating the R_r, R_{ir}, FRR, and R_t are shown in Eqs. (18), (19), (20), and (21) respectively.

$$R_r(\%) = \left(\frac{J_C - J_{BTEX}}{J_w}\right) \times 100 \quad (18)$$

$$R_{ir}(\%) = \left(\frac{J_w - J_c}{J_w}\right) \times 100 \quad (19)$$

$$FRR\ (\%) = \left(\frac{J_c}{J_w}\right) \times 100 \quad (20)$$

$$R_t = \left(\frac{J_w - J_{BTEX}}{J_w}\right) \times 100 \quad (21)$$

Where J_w is the pure water flux, J_{BTEX} is the flux of the BTEX solution, and J_c is the flux of the cleaned membranes.

5.5 Results and discussion

5.5.1 Phytochemical composition of the pomegranate leaf extract and characterization of the biosynthesized Fe_3O_4-NPs

The phytochemical composition of the leaf extract of the pomegranate was determined using GC-MS, and the chromatogram is shown in Figure 5.1. The GC-MS chromatogram indicates the presence of many active phytochemicals such as 2,3-Dihydroxy-2-methylpentanoic acid, 2-Propenoic acid, 3-(2-furanyl)-, Phenol, 4-nitro-, and 2-Methoxy-4-vinylphenol in the leaf extract. These phytochemicals are the active compounds capable of bio-reducing metal precursors and subsequently stabilizing the biogenically produced nanoparticles (Bandeira et al., 2020); hence, they are responsible for the bio-reduction of the iron precursor to the Fe_3O_4-NPs and stabilizing the NPs. Table 5.1 presents some of the active compounds with their retention time (R_T), molecular weight, and structural formula.

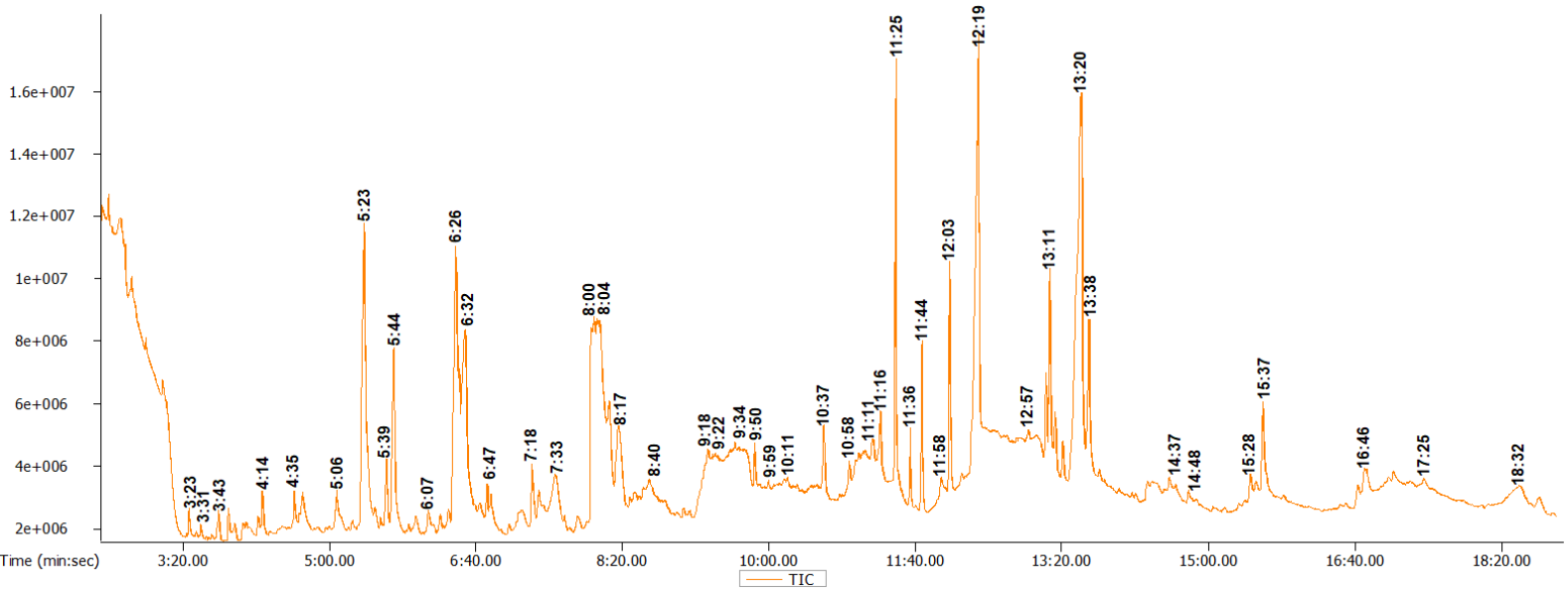
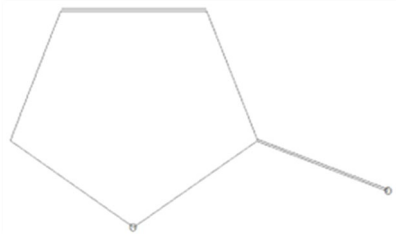
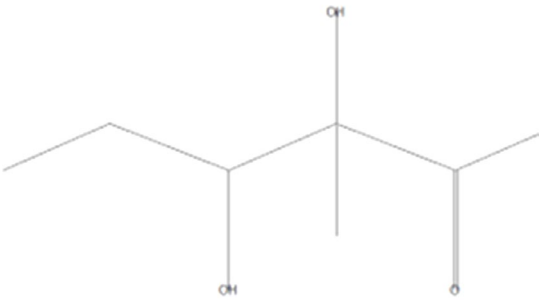
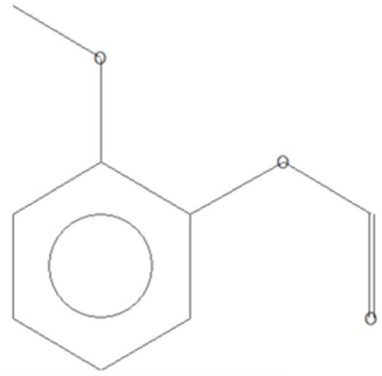
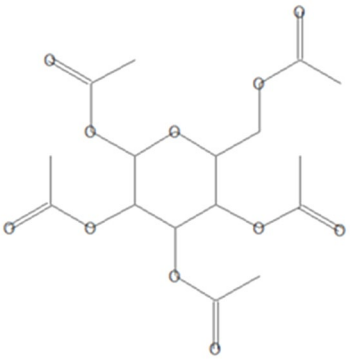
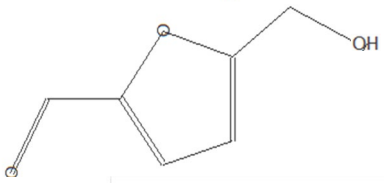
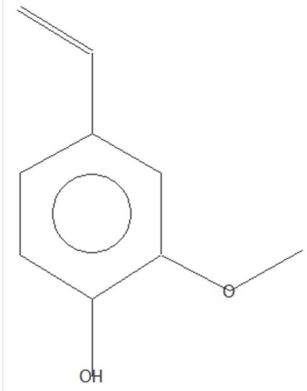
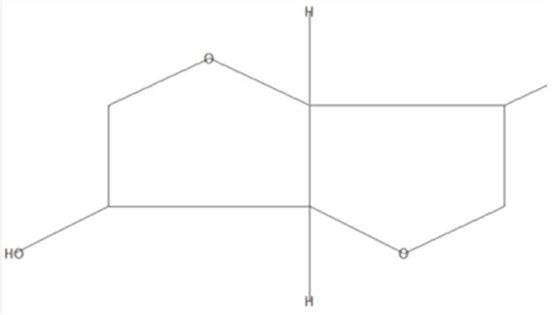
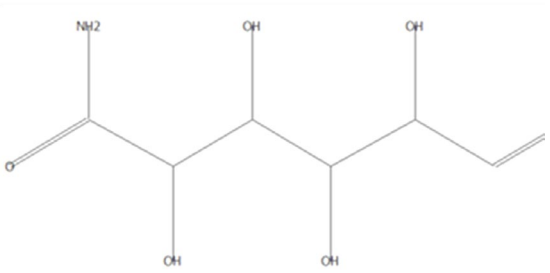
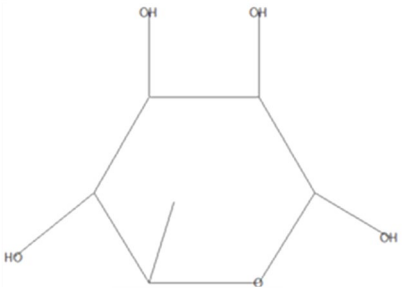
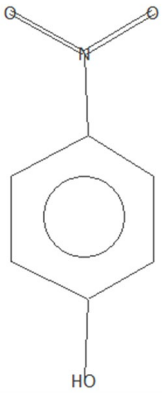
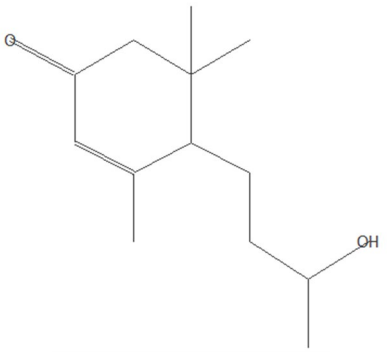
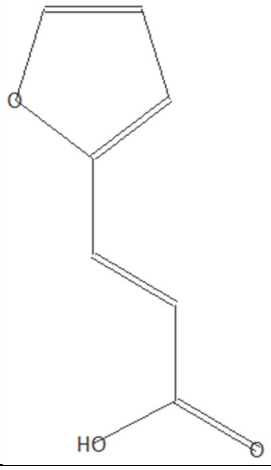


Figure 5. 1: GC-MS chromatogram of the pomegranate leaves extract.

Table 5. 1: Some of the active phytochemicals in the pomegranate leaves extract with their compound name, retention time (R_T), and structure.

Name of compound	R_T (min)	Molecular weight	Structural formula
2(5H)-Furanone	3:23	84	
2,3-Dihydroxy-2-methylpentanoic acid	3:43	148	

Formic acid, 2-methoxyphenyl ester	5:06	152	
á-D-Glucopyranose pentaacetate	5:39	390	
5-Hydroxymethylfurfural	6:32	126	
2-Methoxy-4-vinylphenol	7:18	150	
Isosorbide	8:00	146	

Glucuronamide	8:04	193	
Rhamnose	8:17	164	
Phenol, 4-nitro-	9:22	134	
2-Cyclohexen-1-one, 4-(3-hydroxybutyl)-3,5,5-trimethyl-	10:37	210	
2-Propenoic acid, 3-(2-furanyl)-	12:11	138	

The XRD pattern of the Fe_3O_4-NPs shown in Figure 5.2 (a) reveals the characteristic peaks at 2q = 30.1°, 35.5°, 43.1°, 53.4°, 57.0°, and 62.6° corresponding to diffraction planes of (220), (311), (400), (422), (511), and (440) respectively which indicates that the synthesized NPs are Fe_3O_4 (Radoń et al., 2017). The observed sharp peaks confirm the ability of the leaves extract of the pomegranate to completely reduce the iron (III) chloride precursor to crystalline Fe_3O_4-NPs.

FTIR study was performed to identify and compare the functional groups present in the leaves extract, and the Fe_3O_4-NPs to establish the capping ability of the leaves extract on the Fe_3O_4-NPs. As shown in the FTIR spectra depicted in Figure 5.2(b), a broad peak at about 3320 cm^{-1} is seen for both the leaves extract and the Fe_3O_4-NPs and this peak corresponds to the O-H of hydroxyl-containing groups such as carboxylic acid, phenolic acids, alcohols, and phenols (Kumar et al., 2019). The pomegranate leaves are rich in such hydroxyl-containing compounds, which are deposited on the Fe_3O_4-NPs during the biogenic reduction of the iron precursor by the leaf extracts (Swilam & Nematallah, 2020). Other peaks at 1712 cm^{-1}, 1605 cm^{-1}, 1340 cm^{-1}, and 1069 cm^{-1}, which correspond to the C=O, C=C, O-H, and C-O groups, are seen in the spectra of the leaves extract and Fe_3O_4-NPs with a relative shift in the peak positions and intensity. This indicates the involvement of the various functional groups in the formation and capping of the Fe_3O_4-NPs (Saratale et al., 2018).

The SEM and TEM images of the Fe_3O_4-NPs are depicted in Figure 5.2(c) and 5.2(d), respectively, and describe the morphology of the NPs. As seen in the SEM image, the NPs were spherically shaped with nanoscale dimensions, with the smallest NPs being about 15 nm, as shown in the TEM image. Strong EDX signals (depicted in the inset of the SEM image) of elemental iron and oxygen confirm the presence of Fe_3O_4-NPs.

The textural property of the Fe_3O_4-NPs is presented in Figure 5.2(e). The nitrogen adsorption/desorption isotherm curves obtained for the Fe_3O_4-NPs using the BET technique show a type IV adsorption-desorption isotherm, a characteristic feature of mesoporous materials (Wickramaratne et al., 2013). Thus, the mesoporous nature of the Fe_3O_4-NPs could contribute to improving the flux of the membrane due to their characteristic uniform array of nanochannels that could facilitate the permeability of water through the membrane. In addition, the NPs have a high specific surface area of 81.95 m^2/g, which could necessitate the availability of the hydrophilic sites of the NPs, resulting in an enhanced contribution of the NPs to improve the membrane properties and performance. The desorption branch of the Barrett-Joyner-

Halenda (BJH) method was used to determine the pore size distribution of the Fe_3O_4-NPs, and it shows that the Fe_3O_4-NPs have broad pore size distribution with an average pore size of 12.08 nm, as depicted in the inset in Figure 5.2(e). However, most Fe_3O_4-NPs have small pore sizes within 1.73 nm and 20.64 nm.

The XPS spectrum of the Fe 2p core level is shown in Figure 5.3. As is usual for fitting when Fe(III) components are involved, only the Fe $2p_{3/2}$ component was fitted (Biesinger et al., 2011). A Shirley background was used. As can be seen, a good fit is obtained using the multiplets of Fe^{3+} and Fe^{2+} as calculated for Fe_3O_4 (Biesinger et al., 2011). The differences in energies between the various peaks of the multiplets and their relative intensities were kept constant for the fit. This confirms that the iron present in the sample is Fe_3O_4. This can also be seen qualitatively from the line shape by comparison with the literature (McIntyre & Zetaruk, 1977; Grosvenor et al., 2004).

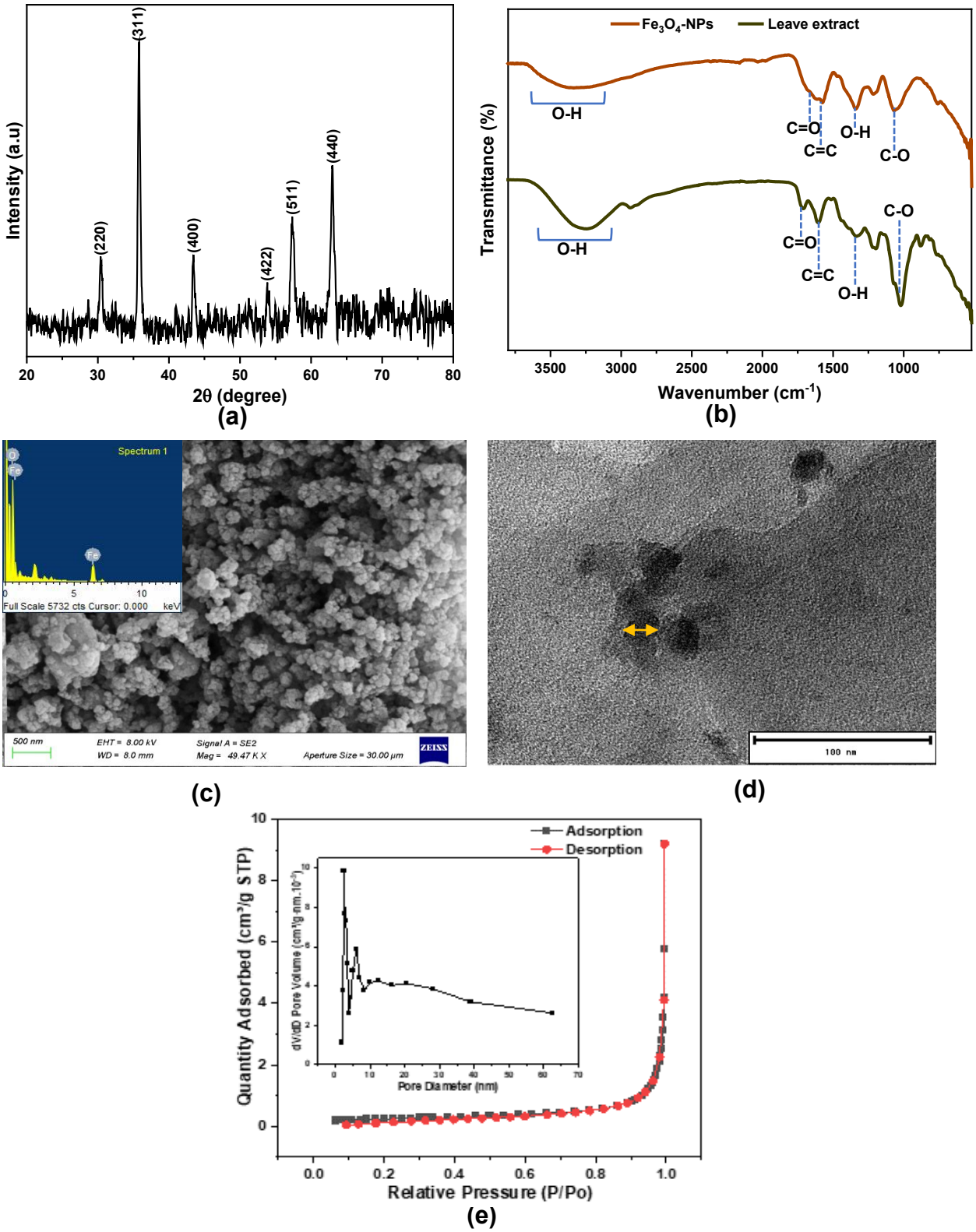


Figure 5. 2: (a) XRD pattern, (b) FTIR spectra, (c) SEM image, (d) TEM image, and (e) N_2 adsorption-desorption isotherm and pore size distribution (inset) of the Fe_3O_4-NPs.

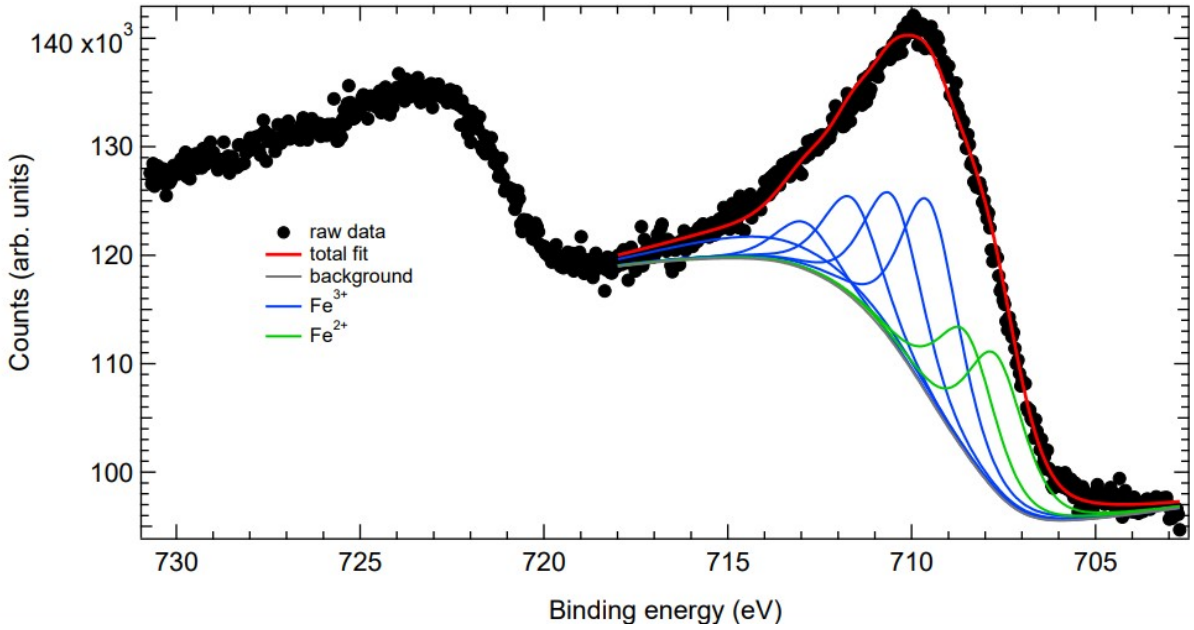


Figure 5. 3: XPS spectra of the Fe 2p core level.

5.5.2 Characterization of Fe_3O_4-NPs/PVDF membrane

The outcome of the exposure of two polymeric membrane materials, PSF and PVDF, to different concentrations of synthetic BTEX is shown in Figures 5. 4 and 5. 5. Figure 5. 4 shows the membranes after exposure to the BTEX solution. The images show that the PSF was very prone to severe damage when exposed to BTEX. Hence, using PSF as a base membrane for BTEX wastewater treatment will result in rapid membrane damage by the BTEX contaminant, eventually leading to loss of membrane property and performance. In contrast, the PVDF membrane exhibited high tolerance to the BTEX solution under all the tested BTEX concentrations. The same observation was seen in the SEM images of the PSF and PVDF membranes depicted in Figure 5. 5. The SEM image shows that the morphology of the PSF membrane was severely affected as its finger-like pores were shrunk and damaged. In contrast, the morphology of the PVDF membrane was not affected by the BTEX exposure. Because of the excellent tolerance of the PVDF membrane to the target contaminant, it was selected as the base membrane in this study.

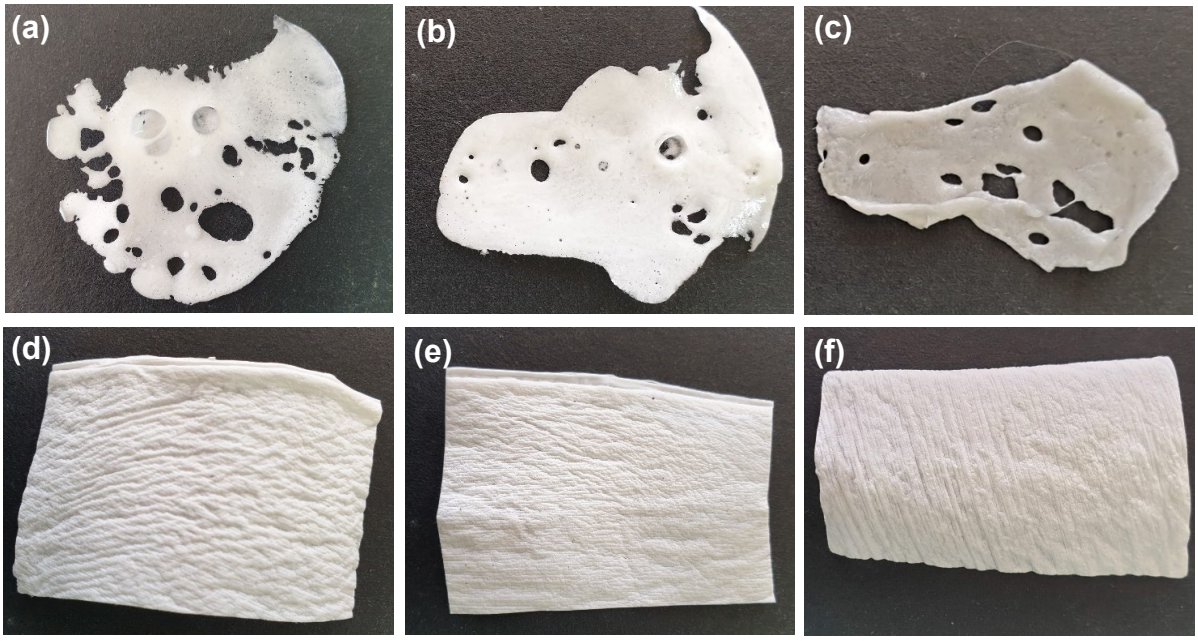


Figure 5. 4: The images of the PSF and PVDF membranes after exposure to BTEX solutions. PSF exposed to BTEX concentration of (a) 500 ppm, (b) 1000 ppm, and (c) 2000 ppm. PVDF exposed to BTEX concentration of (d) 500 ppm, (e) 1000 ppm, and (f) 2000 ppm.

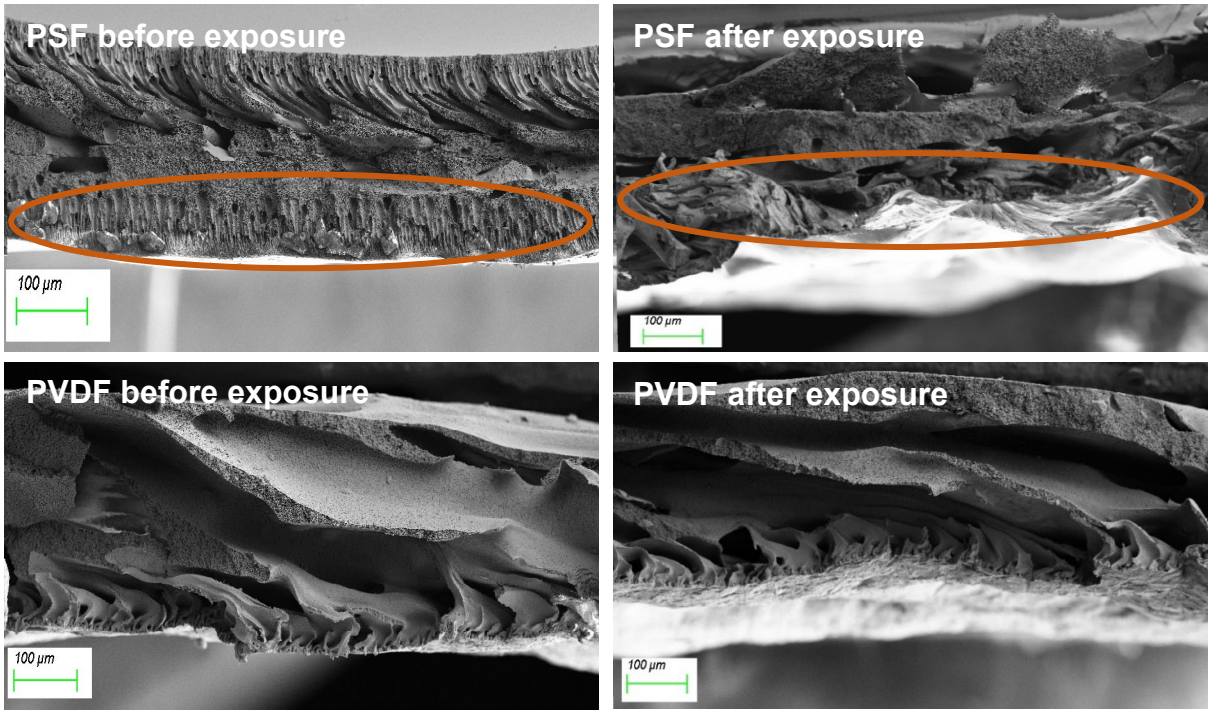


Figure 5. 5: SEM images of the before and after-exposure of PSF and PVDF membrane to BTEX solution.

The results of the tests on four of the prepared membranes, PVDF 0, PVDF 0.2, PVDF 1.0, and PVDF 3.0, are mainly discussed for a comprehensible presentation of the findings of this study.

Table 5. 2: Composition of the fabricated membranes.

Membrane ID	PVDF (wt.%)	NMP (wt.%)	Fe_3O_4-NPs (wt.%)
PVDF 0	15	85.00	0.00
PVDF 0.05	15	84.95	0.05
PVDF 0.1	15	84.90	0.10
PVDF 0.2	15	84.80	0.20
PVDF 0.5	15	84.50	0.50
PVDF 1.0	15	84.00	1.00
PVDF 2.0	15	83.00	2.00
PVDF 3.0	15	82.00	3.00
PVDF 5.0	15	80.00	5.00

The chemical composition of the membranes was evaluated using FTIR, and the spectra are presented in Figure 5. 6. From the region of 600 cm^{-1} to 1500cm^{-1}, no notable peak change was observed for both the pristine membrane and the modified membranes, and the peaks appearing in those regions are characteristic peaks for PVDF (C. Ma et al., 2020). Two distinct peaks at 1650 cm^{-1} and 3400 cm^{-1} for C=O and OH stretching vibrations were observed for PVDF 1.0 and PVDF 3.0 membranes. These two peaks revealed the presence of carboxylic acid and hydroxyl groups in the embedded Fe_3O_4-NPs, which could be from chemical groups such as phenolic acid and phenol in the leaves extract of the pomegranate. The lack of notable presence of these two peaks in PVDF 0.2 could be due to the small amount of the Fe_3O_4-NPs incorporated into the membrane.

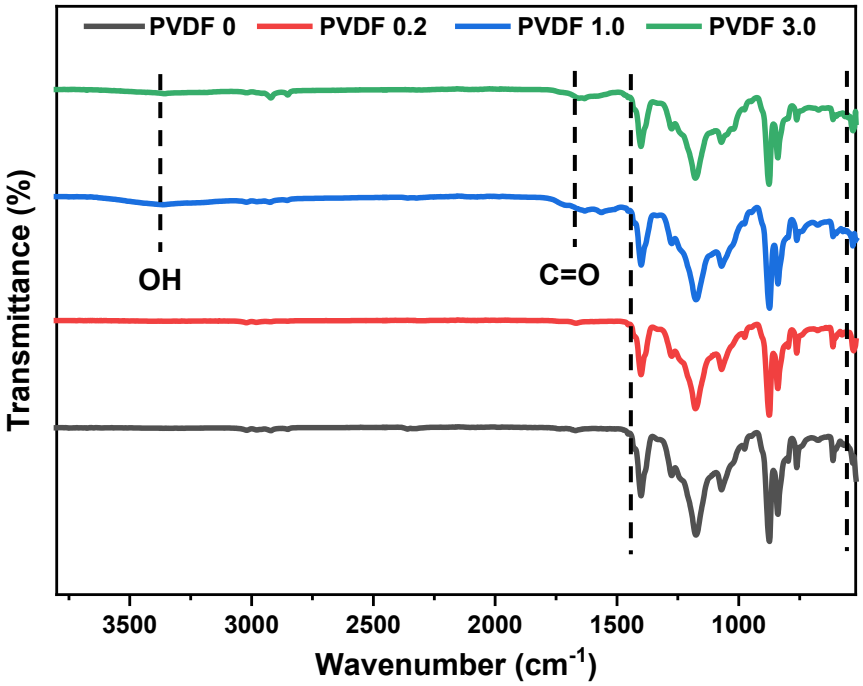


Figure 5. 6: FTIR spectra of the fabricated membranes

The SEM images of the membranes depicting their morphology are shown in Figure 5. 7. All the membranes have finger-like pore structures, which is indicative of membranes fabricated through nonsolvent-induced phase inversion (Khan et al., 2018; Alkhouzaam & Qiblawey, 2021). The finger-like structures of the Fe_3O_4-NPs/PVDF membranes are broader and longer than that of the pristine membrane due to the hydrophilicity of the Fe_3O_4-NPs, which induces fast solvent and nonsolvent exchange during the phase inversion process (Wang et al., 2021; Du et al., 2022). Such well-formed finger-like macrovoids in the modified membranes are beneficial in improving the permeability of the membranes (Sherazi et al., 2022). The dispersion of the Fe_3O_4-NPs on the surface and inner structure of the membranes are shown in the EDX mapping and higher magnification cross-section images, respectively. The EDX mapping shows fairly good dispersion of the Fe_3O_4-NPs in PVDF 0.2 and PVDF 1.0 membranes, while the Fe_3O_4-NPs in PVDF 3.0 seem more agglomerated. This correlates with the dispersion of the Fe_3O_4-NPs in the membranes' inner structure, which shows the agglomerated Fe_3O_4-NPs in the PVDF 3.0 membrane clogging its inner pores. Such NPs agglomeration often adversely affects the membrane property and performance (Baig et al., 2019).

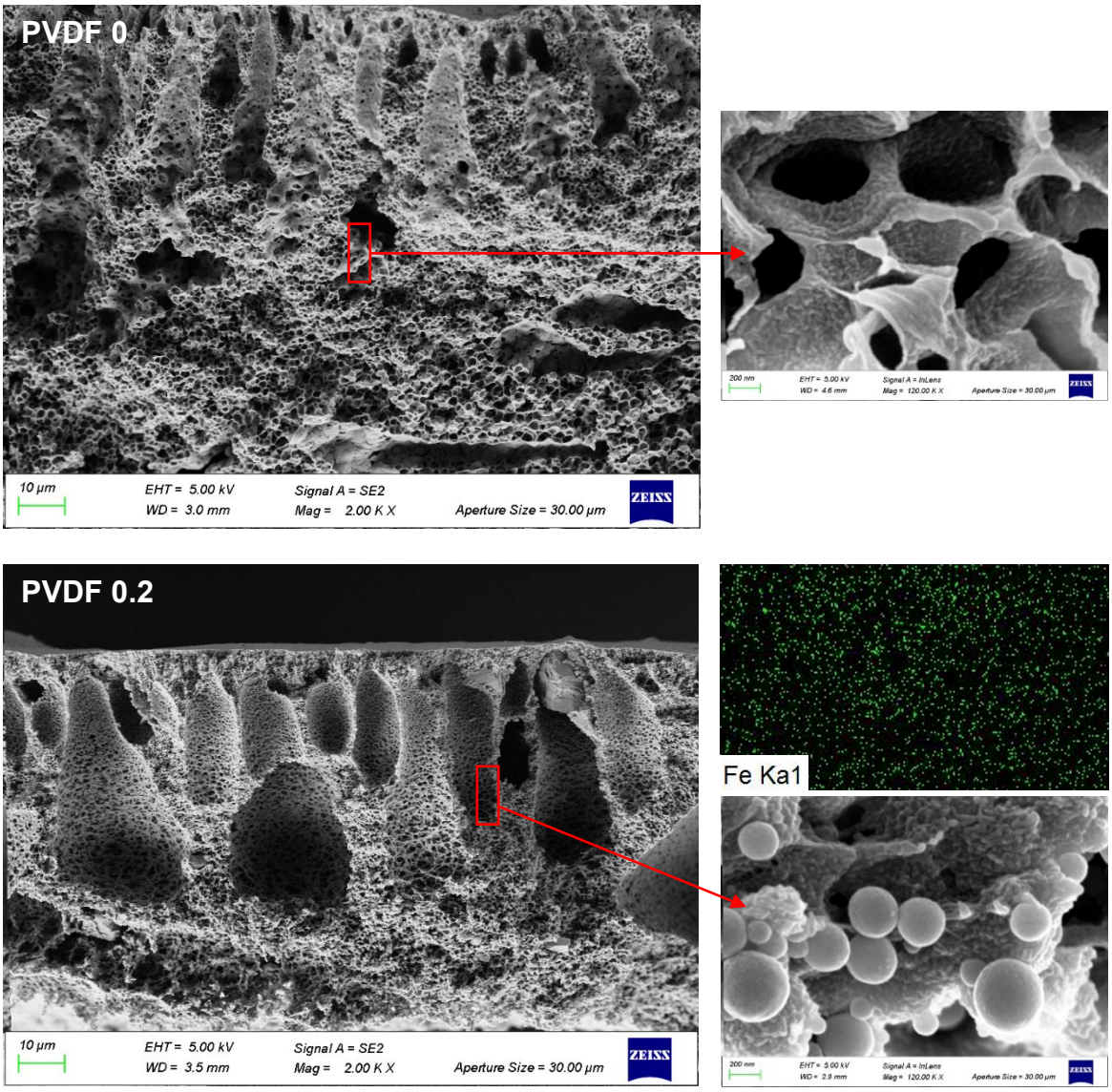


Figure 5. 7a: Cross-section SEM images of fabricated membranes with their respective EDX mapping images

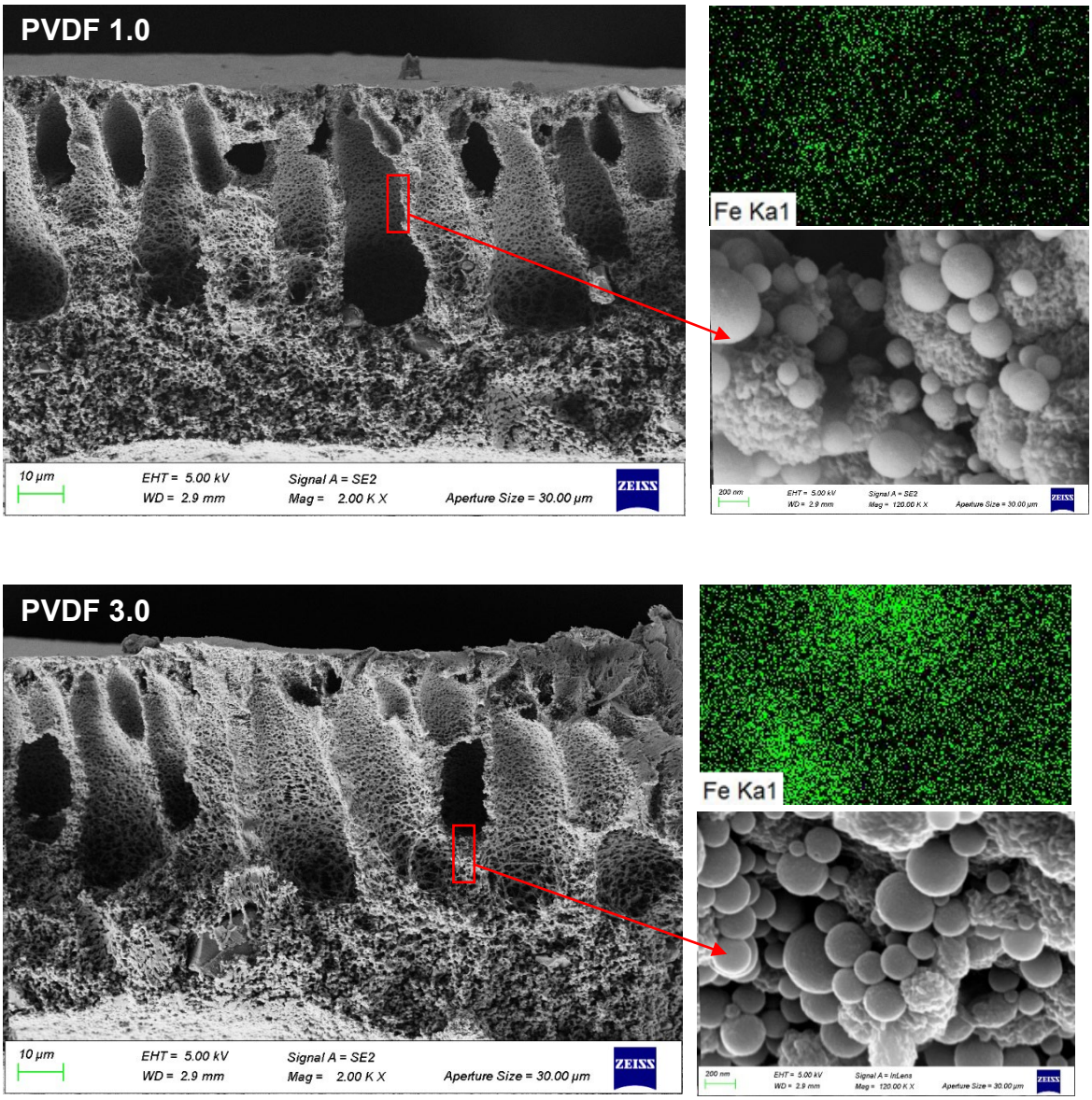


Figure 5. 8b: Cross-section SEM images of fabricated membranes with their respective EDX mapping images.

The morphology of the membranes in terms of their surface roughness is presented in the AFM images in Figure 5. 8. An increment in the membranes' roughness was observed as the amount of the Fe_3O_4-NPs in the membrane increased, with the pristine PVDF membrane having the lowest surface roughness. The roughness parameter was obtained by measuring the membrane's average roughness (Sa) and root mean square (Sq). PVDF 0 has Sa and Sq values of 44.2 nm and 48.6 nm, respectively. The Sa and Sq values increased to 47.5 nm and 49.2 nm for PVDF 0.2, while the Sa and Sq values for PVDF 1.0 were 55.6 nm and 60.4 nm, respectively. However, the Sa and Sq values of PVDF 3.0, which were 45.8 nm and 48.9 nm, were lower than that of PVDF 0.2 and PVDF 1.0 but slightly higher than the roughness

parameters of the pristine membrane. This deviation from the incremental trend observed in the modified membranes could be due to a decline in the porosity of PVDF 3.0 as well as the increased viscosity of the dope solution of PVDF 3.0, which led to the formation of a dense and smoother top layer (Tan et al., 2017). A similar trend was obtained by Rowley and Abu-Zahra (2019).

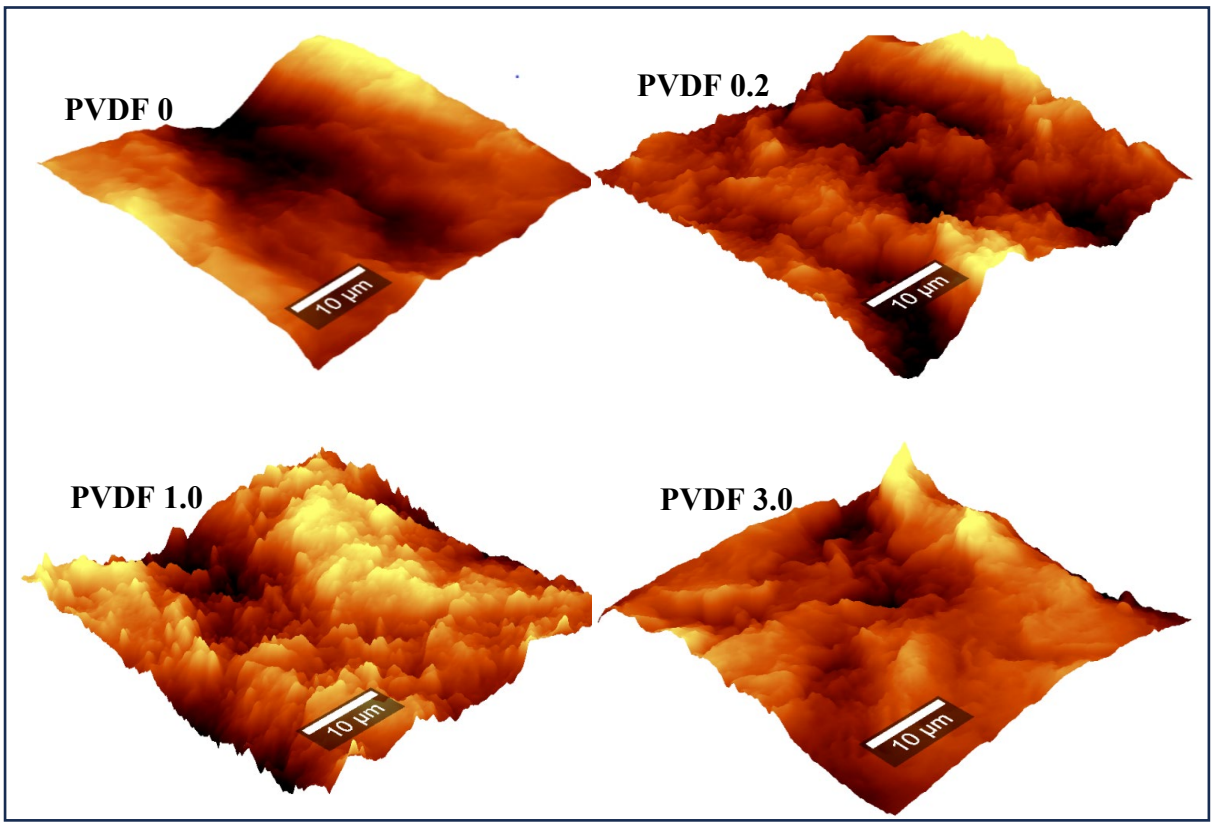


Figure 5. 9: Surface roughness images of the membranes.

Figure 5. 9 (a) depicts the water contact angle of the membranes, which is a measure of their hydrophilicity. Hydrophilicity is a significant factor that determines the permeability and antifouling ability of membranes (Yin & Deng, 2015), and contact angle (CA) measurement offers a precise determination of hydrophilicity, with a lower contact angle signifying a hydrophilic membrane and vice versa (Akram et al., 2018). As shown in Figure 5. 9(a), the pristine PVDF has a high CA of 84.2°, and a significant reduction in the CA of the membranes was seen with loading of the Fe_3O_4-NPs up to 1.0 wt.%. Two fundamental properties of the NPs facilitate the improvement in hydrophilicity. First, the presence of the hydrophilic O-H functional group on the surface of the Fe_3O_4-NPs, as confirmed by the FTIR result, provided polar sites that can form hydrogen bonding with water, thereby enhancing the hydrophilicity of the membranes. Secondly, the inorganic nanoparticles, Fe_3O_4-NPs, are intrinsically hydrophilic, providing hydration sites on the membranes and thus contributing to their

improved hydrophilicity (Wei et al., 2022b; Liu et al., 2020). At Fe_3O_4-NPs loadings above 1.0 wt.%, agglomeration, a characteristic of high concentrations of NPs, takes effect. The agglomeration of the NPs reduces their effective surface area, thus reducing the hydrophilic sites in the membrane and the subsequent higher CA observed in PVDF 2.0 and PVDF 3.0 membranes. Agglomeration of the embedded nanoparticles also decreases the porosity of the membranes, which increases their CA, resulting in reduced hydrophilicity. A similar trend was observed by Vatanpour et al. (2021) and Liang et al. (2021). Therefore, the Fe_3O_4-NPs loading of 1.0 wt.% and below can be denoted as the viable amount to achieve improved hydrophilicity, and the PVDF 1.0 membrane exhibited the optimum hydrophilicity. In addition, the membranes' contact angle and their surface roughness are correlated according to the Wenzel model. The Wenzel model stipulated that the wettability of a surface is amplified by increasing its surface roughness (Wenzel, 1936). Relating the surface roughness of the membranes with their CA, a trend of reduced CA is observed as the surface roughness increases. This confirms that their surface roughness might influence the membranes' hydrophilicity. Therefore, the hydrophilic nature of the Fe_3O_4-NPs and the membranes' surface roughness contribute to improving their hydrophilicity.

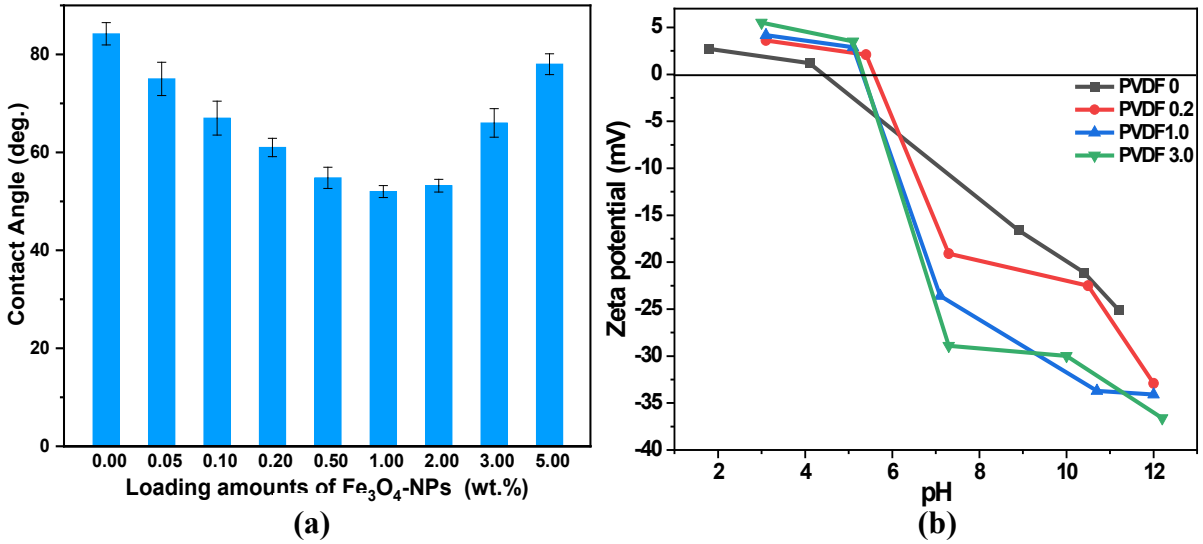


Figure 5. 10: (a) Contact angle values as a function of the Fe_3O_4-NPs loadings and (b) zeta potential of the tested membranes

The hydrophilicity results correlate with the results of the porosity measurements shown in Table 5. 3, which revealed that the porosity of the membranes increases with an increase in the Fe_3O_4-NPs loading of up to 1.0 wt.%. The observed increase in porosity can also be attributed to the high hydrophilicity of the Fe_3O_4-NPs, which induces fast solvent and non-solvent

exchange during the phase inversion, resulting in the formation of more pores in the membranes (Lin et al., 2016). At Fe_3O_4-NPs loadings higher than 1 wt.%, the opposite effect was seen due to the increase in the viscosity of the dope solutions at high NP concentration, leading to the reduction in the rate of the solvent and non-solvent exchange during the phase inversion, resulting to less porous membranes (Yuliwati & Ismail, 2011). The decrease in porosity at high Fe_3O_4-NPs loadings was also facilitated by the blockage of the membrane's pores due to the agglomeration of the NPs at higher concentrations resulting in a less porous membrane.

The equilibrium water content (EWC) of the various membranes, also presented in Table 5. 3, was consistent with their calculated porosity. An increase in EWC was obtained as the concentration of the Fe_3O_4-NPs in the membranes increased, indicating that the hydrophilicity of the Fe_3O_4-NPs plays a significant role in improving the EWC of membranes. The EWC of the pristine PVDF was 53.5%, which increased to 75.5% for the membrane modified with 1.0 wt.% of Fe_3O_4-NPs. Above 1.0 wt.% of Fe_3O_4-NPs loading, the EWC of the membrane decreases, which could also be explained by the agglomeration of the highly concentrated Fe_3O_4-NPs leading to the blockage of membrane pores and the eventual decrease in the EWC of the membranes.

Table 5. 3: The thickness, porosity, EWC, and mean pore size of all the fabricated membranes.

Membrane ID	Thickness (μm)	Porosity (%)	EWC (%)	Mean pore size (nm)
PVDF 0	112 ± 4	60.5 ± 0.7	53.5 ± 0.7	40.3 ± 1.5
PVDF 0.05	110 ± 2	64.0 ± 0.8	60.5 ± 0.5	41.0 ± 1.7
PVDF 0.1	114 ± 2	67.0 ± 1.4	66.5 ± 0.7	44.0 ± 3.8
PVDF 0.2	109 ± 3	73.0 ± 1.4	70.5 ± 0.7	44.6 ± 3.2
PVDF 0.5	112 ± 3	75.0 ± 1.4	73.0 ± 1.4	48.3 ± 2.5
PVDF 1.0	109 ± 1	77.5 ± 0.7	75.5 ± 0.7	55.2 ± 0.9
PVDF 2.0	113 ± 3	73.5 ± 0.7	69.0 ± 1.4	54.6 ± 2.4
PVDF 3.0	112 ± 3	66.5 ± 1.1	65.5 ± 1.4	49.3 ± 1.5
PVDF 5.0	115 ± 1	62.0 ± 1.4	60.0 ± 0.8	42.3 ± 2.3

The zeta potentials of the membranes at various pH are shown in Figure 5. 9(b), and it describes the nature of the charges of the membranes at the measured pH of the solution; hence, it plays a vital role in predicting the performance of membranes at varying pH (Zhu et al., 2020). The

isoelectric point (IEP) of the pristine membrane was observed at pH 4.3. The Fe_3O_4-NPs/PVDF membranes have positive zeta potentials at low pH, which becomes negative at higher pH. This observed trend can be attributed to the tendency of metal oxide nanoparticles to hydrate in aqueous solution, and the surface functional groups of the hydrated metal oxide can be protonated or deprotonated depending on the pH of the solution (Wang et al., 2013). Thus, the hydrated Fe_3O_4-NPs in the membrane were either protonated or deprotonated at low or high pH, resulting in the positive or negative charge observed for the modified membrane at the various pH ranges.

The mechanical property of the membranes is an essential factor that can determine their practical application in terms of their ability to withstand various operational conditions that the membranes will be subjected to during their usage in the treatment of wastewater (Al Aani et al., 2017b). Thus, the mechanical properties of the fabricated membranes with different loadings of the Fe_3O_4-NPs were investigated using a Tesla analyzer and are shown in the stress-strain curves in Figure 5. 10(a). Significant improvement in the tensile strength of the membranes was seen as the Fe_3O_4-NPs were incorporated into the membranes. The ultimate tensile strength of the pristine PVDF was 3.17 MPa, while the PVDF 0.2 and PVDF 1.0 had a tensile strength of 4.46 MPa and 4.24 MPa, respectively. The observed improvement in the tensile strength of the membranes is due to the inherent rigidity of the nanoparticles, which enhanced their stiffness. As the FTIR spectra of the NPs in Figure 5. 2 (b) show the presence of the -OH group in the NPs, there may be dipole-dipole bonding of the -OH group in the Fe_3O_4-NPs and the polar -CF group in the matrix of the modified membranes which could contribute to enhancing the mechanical stability of the membrane, hence the observed increase in tensile strength. A further increase in the Fe_3O_4-NPs loadings led to a decline in the tensile strength of the membrane, as seen in the lower tensile strength of PVDF 3.0, which could be due to agglomeration of the NPs at higher loading. The agglomeration reduces the interfacial area between the NPs and the PVDF matrix (Wu et al., 2018). Thus, the effective fraction of the Fe_3O_4-NPs in the membrane matrix was reduced, resulting in the NPs' lesser ability to provide stiffness to the membranes.

A decrease in the strain at break was observed for all the membranes incorporated with the Fe_3O_4-NPs. This is expected as the Fe_3O_4-NPs introduce rigidity to the membranes, which minimizes their stretching capacity, resulting in the lower strain at break observed for the modified membranes.

The effect of the different Fe_3O_4-NPs loading on the thermal stability of the membranes, measured using thermogravimetric analysis (TGA), is shown in Figure 5. 10(b). All the membranes exhibited a single-step degradation between 440°C and 500°C. The degradation temperature of the pristine membrane was 440°C, which increased slightly to 456°C as 0.2 wt.% and 1 wt.% of the Fe_3O_4-NPs were embedded into the PVDF membrane. This indicates a moderate improvement in the thermal stability of the membranes as the loading amount of the Fe_3O_4-NPs was increased. The significant weight loss between the region 440°C and 500°C is due to the decomposition of the PVDF polymers. At 800°C, the mass of the residuals remaining after the decomposition of the PVDF is 6.94 %, 16.25 %, 21.95 %, and 22.7 % for PVDF 0, PVDF 0.2, PVDF 1.0, and PVDF 3.0 respectively. The incremental order of the residuals, which consist of carbon and the embedded Fe_3O_4-NPs, correlates with the increasing amount of the NPs across PVDF 0 to PVDF 3.0.

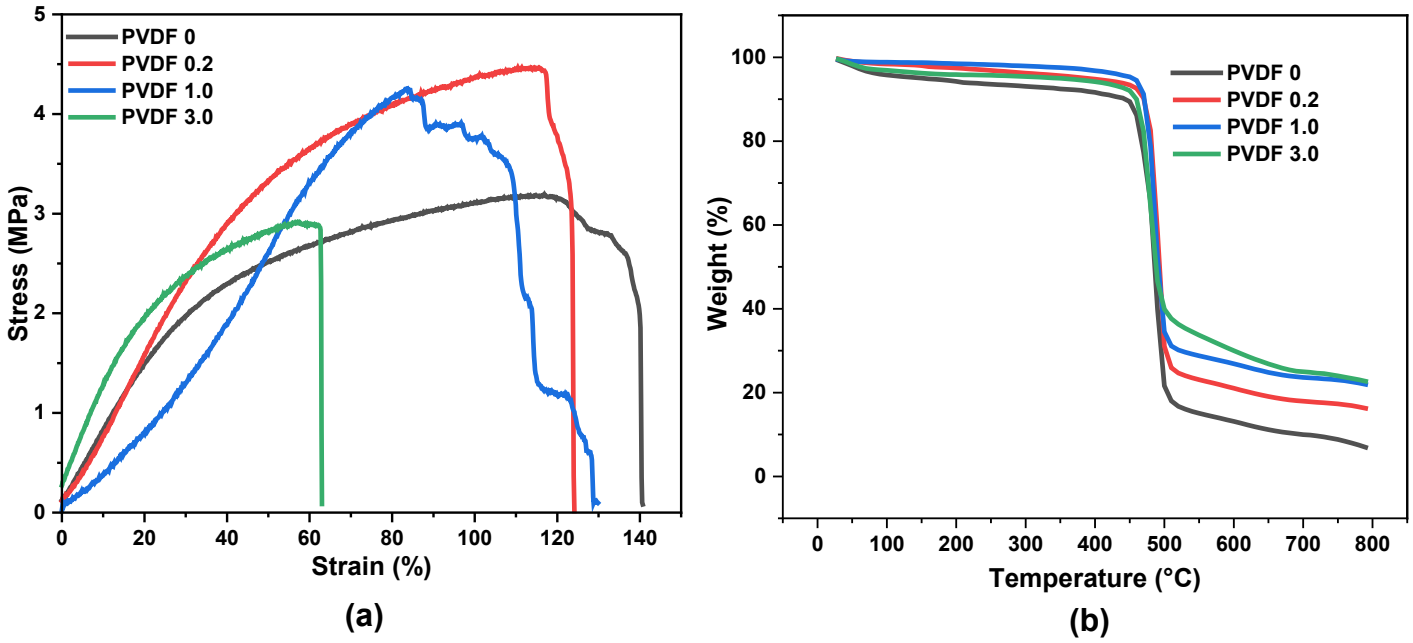


Figure 5. 11: (a) Stress-strain curves, and (b) TGA curves of the tested membranes.

5.5.3 Membrane performance evaluation

5.5.3.1 Pure water and BTEX permeation performance

The effect of the Fe_3O_4-NPs loadings on the membrane flux was investigated by measuring the pure water flux (PWF) and BTEX flux of the membranes at different transmembrane pressures (TMP). Figure 5. 11(a) depicts the PWF of the PVDF 0, PVDF 0.2, PVDF 1.0, and PVDF 3.0

membranes, and their respective BTEX flux is shown in Figure 5. 11(b). 100 ppm (of each component) of BTEX solution was used to evaluate the BTEX flux. The result shows that the PWF and the BTEX flux of all the membranes increased linearly as the TMP was increased, and all the Fe_3O_4-NPs/PVDF membranes exhibited higher PWF and BTEX flux than the pristine membrane. The observed improvement in the flux of the Fe_3O_4-NPs/PVDF membranes is due to the improved porosity of the membranes and the intrinsic hydrophilic nature of the Fe_3O_4-NPs, which reduced the water permeation resistance of the membranes. The porous nature of the Fe_3O_4-NPs, previously depicted in Figure 5. 2(e), also provided more hydrophilic nanochannels for improved water permeation through the membranes. While the increase in the PWF and BTEX flux of PVDF 0.2 and PVDF 1.0 is consistent with their Fe_3O_4-NPs loadings, the PWF and BTEX flux of PVDF 3.0 did not correlate with the amount of its Fe_3O_4-NPs loading because both fluxes of PVDF 3.0 were lower than that of the PVDF 0.2 and PVDF 1.0 across all the applied TMP. This dramatic decline in the fluxes of PVDF 3.0 could be attributed to the agglomeration of the Fe_3O_4-NPs as seen in its SEM image, which reduced the effective hydrophilic surface area of the embedded nanoparticles in the polymer matrix (Hosseini et al., 2019; T.-Y. Liu et al., 2015). The agglomerated Fe_3O_4-NPs also blocked the membrane's pores, thereby intensifying the membrane's water permeation resistance. A similar trend was observed by Dadari et al. (2022) in which a nickel-bentonite nanoparticles loading of 1.0 wt.% led to the agglomeration of the nanoparticles in the membrane matrix, resulting in reduced PWF.

The BTEX flux of all the tested membranes was lower than their respective PWF across all the TMP, with the pristine membrane having the highest flux reduction. Among all the Fe_3O_4-NPs modified membranes, the PVDF 1.0 exhibited the lowest flux reduction across all the applied TMP. For instance, at a TMP of 300kPa, the flux reduction of PVDF 1.0 was 35%, while that of PVDF 0.2 and PVDF 3.0 were 38% and 42%, respectively. This could be explained by the better dispersion of the embedded nanoparticles in PVDF 1.0, which resulted in less pore tightening due to agglomerated nanoparticles. Hence, pore blockage of the PVDF 1.0 membrane by BTEX during the filtration is minimized, resulting in less permeation resistance. Hence, from the result of the evaluation of the PWF and BTEX flux of the membranes at the different Fe_3O_4-NPs loadings, the PVDF 1.0 membrane has the optimal flux among all the fabricated membranes; thus, 1.0 wt.% of the NPs can be established as the optimum amount of the NPs that should be blended into a PVDF membrane to achieve an improvement in its flux.

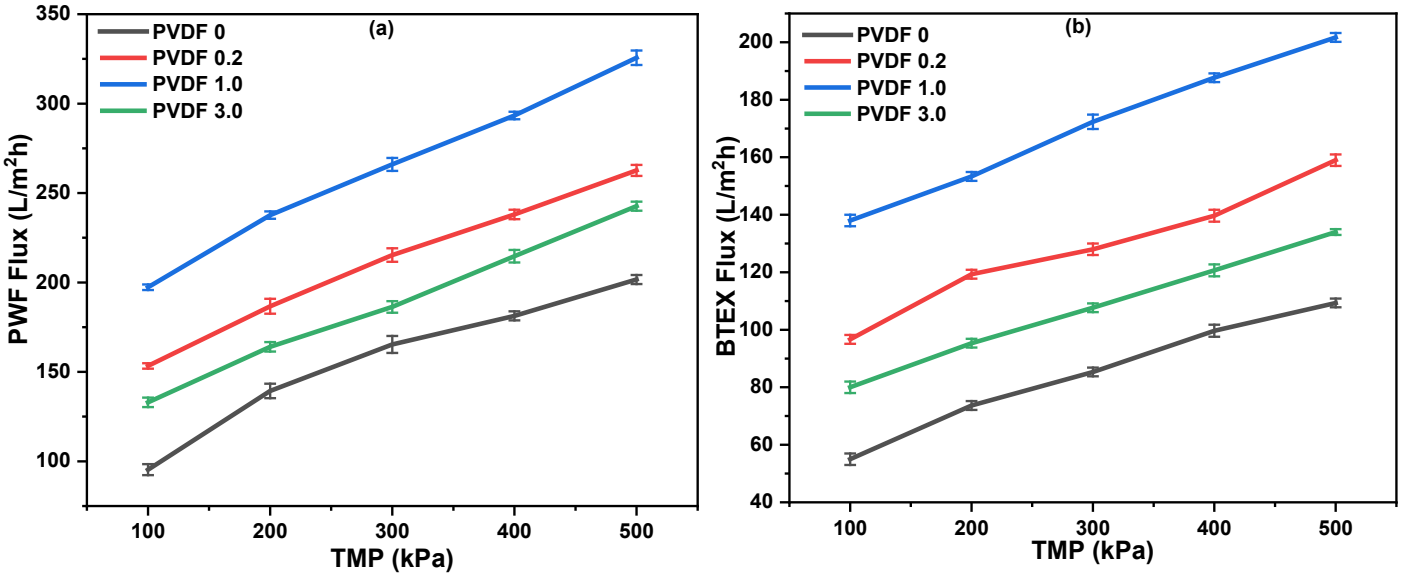


Figure 5. 12: (a) Pure water flux and (b) BTEX flux of the tested membranes.

5.5.3.2 BTEX removal from synthetic BTEX water

The effect of the Fe_3O_4-NPs loadings on the membranes' separation performance was ascertained by measuring the %R of BTEX by the different fabricated membranes. Since the separation performance of membranes is influenced by operational conditions such as TMP and concentrations (Medhat & Pakizeh, 2018; Zhang et al., 2016), the BTEX rejection tests were performed at varying TMP and BTEX concentrations.

As presented in Figure 5. 12, all the Fe_3O_4-NPs/PVDF membranes exhibited higher BTEX rejection than the pristine membrane across all the applied TMP, with an increase in the membranes' BTEX rejection capacity as the Fe_3O_4-NPs amount increases. This establishes the role of the Fe_3O_4-NPs in acting as both hydrophilic modifiers and nanofillers in the membrane matrix. With the surface of the membrane being hydrophilic, a hydration layer was formed on the membrane, which acted as an extra separation barrier. In addition, the BTEX rejection was in the order B < T < E ≤ X, which suggests that the BTEX contaminants that might have penetrated through the hydration layer were removed through size exclusion. This is because the rejection pattern seems to correlate with the molecular diameters of B, T, E, and X, which are 0.58, 0.60, 0.63, and 0.63nm, respectively (Su et al., 2016); hence, the NPs nanofillers might have contributed to the pore tightening of the membrane, as a consequence, the BTEX rejection was increased as the NPs loadings increase. Although the flux of PVDF 3.0, depicted in Figure 5. 11, was the lowest, the performance of PVDF 3.0 in terms of its BTEX rejection capacity improved, as seen in its higher BTEX rejection across all the TMP. Since

agglomeration of NPs significantly reduces the membranes' free volume and creates extra barriers in their matrix (Sardarabadi et al., 2022), the higher BTEX rejection seen in PVDF 3.0 could be attributed to the agglomerated Fe_3O_4-NPs presented previously in the SEM image of the membrane. The agglomerated Fe_3O_4-NPs further tighten the membrane pores, resulting in the enhanced separation barrier of the PVDF 3.0 membrane.

Increasing the TMP led to a reduction in the BTEX rejection capacity of all the membranes as seen in Figure 5. 12. For instance, the %R of the PVDF 1.0 membrane for B are 73.2%, 70.2%, and 61.4% at 100kPa, 300kPa, and 500kPa respectively; for T are 75.5%, 72.5%, and 66.1% at 100kPa, 300kPa, and 500kPa respectively; for E are 80.0%, 79.1%, and 70.6% at 100kPa, 300kPa, and 500kPa respectively; for X are 80.5%, 79.2%, and 71.0% at 100kPa, 300kPa, and 500kPa respectively. Thus, under higher pressure, there was a higher chance of the contaminants penetrating through the hydration layer and the membrane due to the increased applied force, resulting in the observed decline in rejection as pressure increased. A similar observation was made by Wu et al. (2016) when the rejection of bisphenol A and norfloxacin through an ultrafiltration membrane was tested under various TMPs.

To achieve good BTEX rejection using the membranes fabricated in this study, low TMP should be used during the filtration process. Considering both the membranes' BTEX flux and their BTEX rejection, 300 kPa can be designated as an ideal TMP where a reasonable tradeoff between flux and selectivity is achieved. Hence, 300 kPa is selected as the optimum TMP for the fabricated membranes.

The effect of the BTEX concentration on the rejection capacity of the membranes was studied at 300 kPa by filtering 200 mL of 50 ppm, 100 ppm, 150 ppm, and 200 ppm of BTEX solutions through the membranes under constant stirring. As shown in Figure 5. 13, the BTEX rejection capacity of all the Fe_3O_4-NPs/PVDF membranes increased as the BTEX concentration increased from 50ppm to 100ppm and remained relatively constant on further increase of the BTEX concentration. The constant rejection exhibited at higher BTEX concentrations can be explained by the accumulation of the BTEX on the membranes, which intensifies at the higher BTEX concentrations, thereby acting as an extra separation layer, resulting in the subsequent deposition of the BTEX on this layer. A similar trend was observed by Wu et al. (2016) on the effect of feed concentration on the rejection of other organic contaminants, bisphenol A and norfloxacin, using ultrafiltration membranes.

Hence, the fabricated membranes can maintain stable BTEX separation without a decline in membrane rejection efficiency at the studied BTEX concentrations and feed volume.

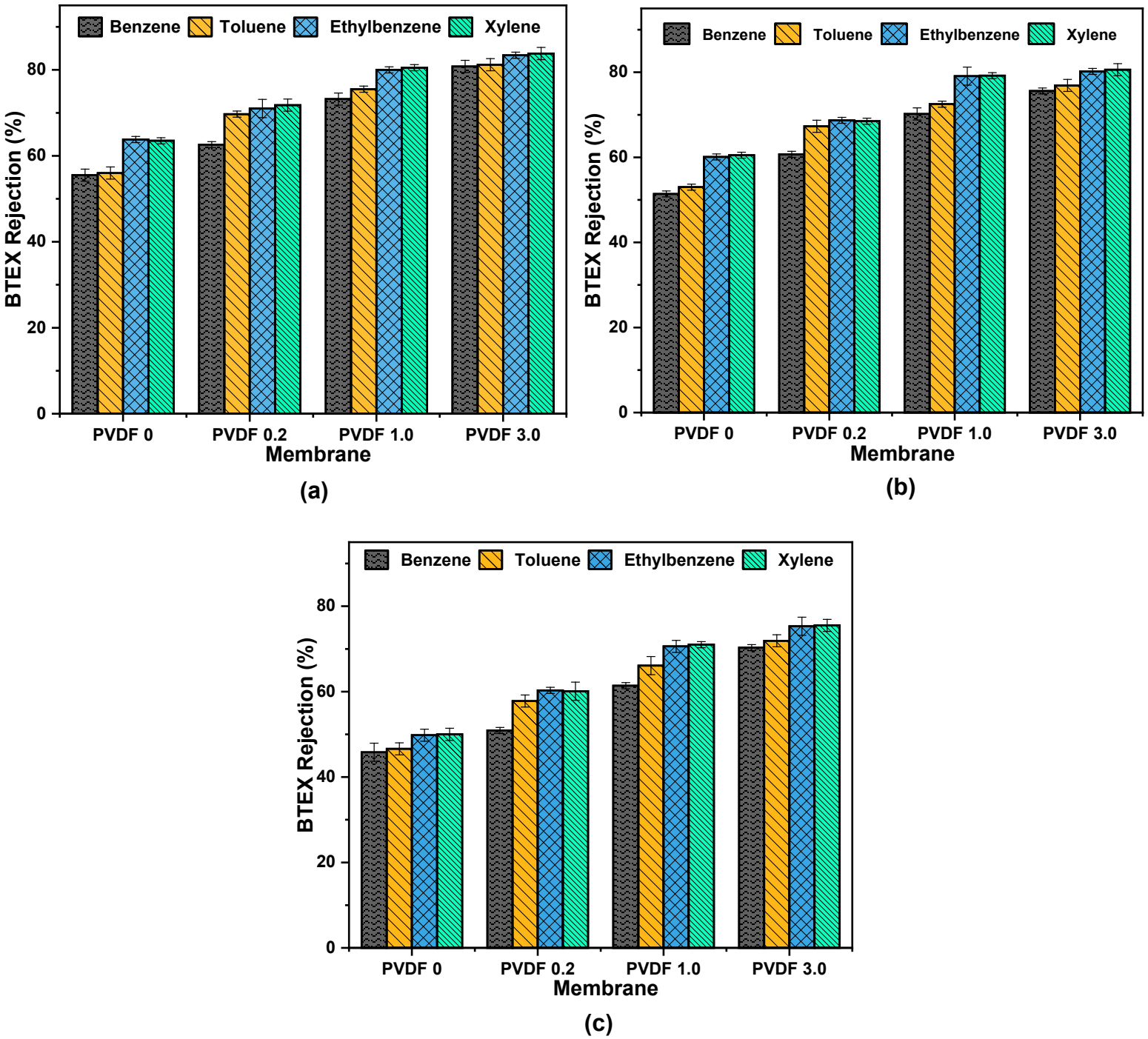


Figure 5. 13: Effect of TMP on the BTEX rejection of the membranes at (a) 100 kPa, (b) 300 kPa, and (c) 500 kPa.

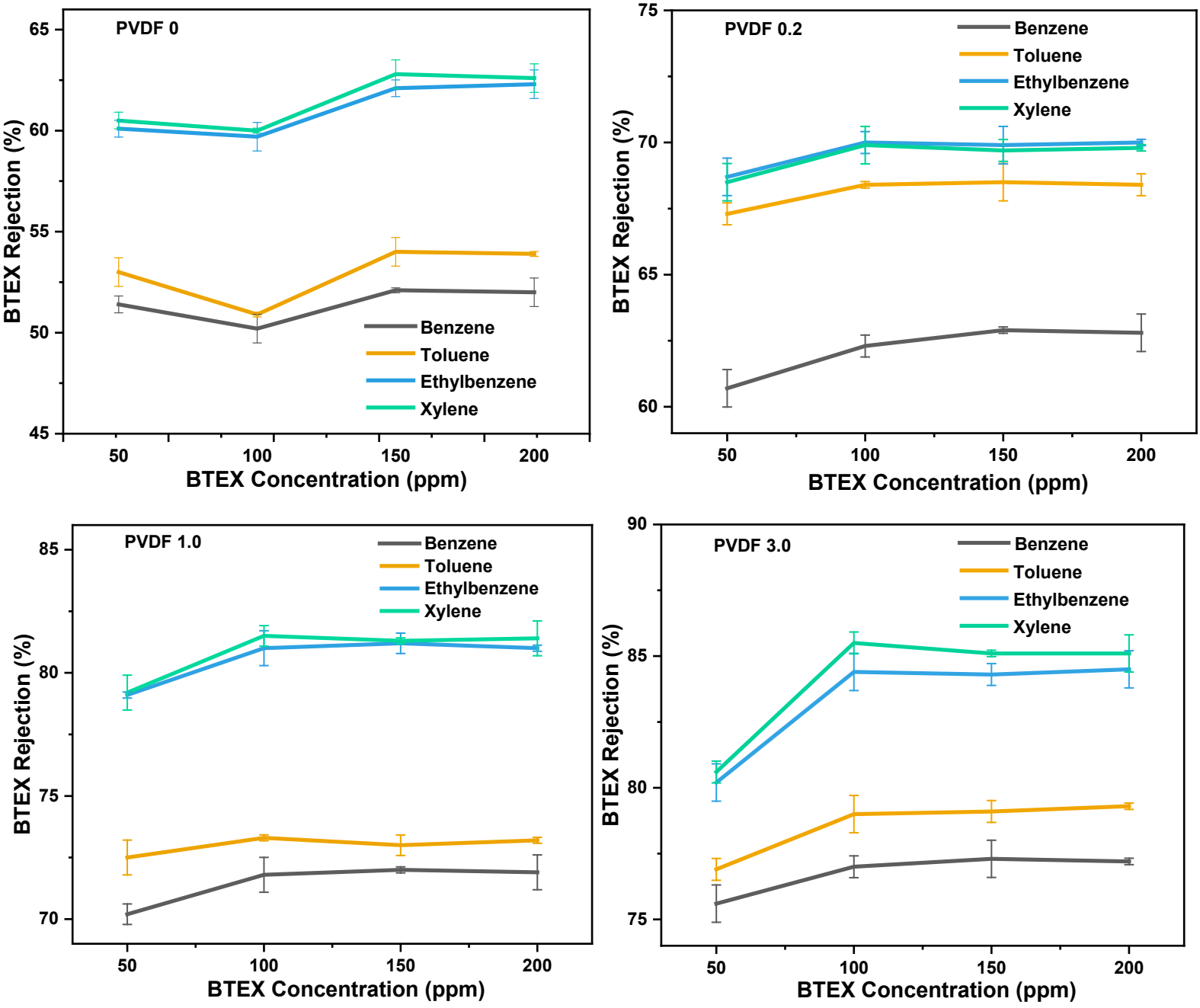


Figure 5. 14: Effect of BTEX concentrations on membranes' rejection capacity.

5.5.3.3 Antifouling and reusability study

The effect of the various Fe_3O_4-NPs loadings on the antifouling ability of the tested membranes is shown in Figure 5. 14(a). The total fouling ratios of the modified membranes are lower than that of the pristine membrane, with the PVDF 1.0 having the lowest total fouling ratio of 36.3%, which indicates about 30% improvement in fouling reduction compared to the pristine membrane. The improvement in the antifouling tendency of the modified membranes could be attributed to the reduction in the hydrophobic nature of the membranes by introducing the

hydrophilic Fe_3O_4-NPs into the membrane. Hydrophobic membranes are known to exacerbate fouling during the treatment of organic contaminated wastewater, while hydrophilic membranes reduce fouling by forming a hydration layer on the membranes, thereby minimizing the non-specific interaction of the foulants on the membranes (Zhang et al., 2016).

The antifouling results also show that most of the fouling occurring during the BTEX filtration is irreversible, which could be a result of the penetration and trapping of the BTEX on the inner pores of the membranes, leading to less success in its removal through physical cleaning. The irreversibility of the fouling decreases as the Fe_3O_4 loading increases up to 1.0 wt.%, which signifies that the incorporated nanoparticles significantly reduce the non-specific adsorption of BTEX on the membranes. PVDF 1.0 membrane was the only membrane whose reversible fouling was higher than its irreversible fouling. Hence, the membrane can be assigned an optimum performance based on its better ease of physical cleaning. The FRR of the PVDF 1.0 membrane was 81%, which is the highest among all the membranes, which further shows its better performance in the recovery of its flux after fouling through physical cleaning.

The reusability of the membranes was evaluated by performing two cycles of BTEX filtration. Each cycle was followed by cleaning using backwashing with water, mild sonication in water, and then pure water filtration. Despite thoroughly cleaning the membranes, all the membranes exhibited a slight decline in PWF after each BTEX filtration and cleaning, as shown in Figure 5. 14(b). This could be due to the irreversible fouling that was established to be present in all the membranes during the antifouling test (Figure 5. 14a). The irreversible fouling is a result of stronger interactions between the BTEX and the membranes, which could not be easily removed by physical cleaning (Sherazi et al., 2022). The penetration of the BTEX in the pores of the embedded Fe_3O_4-NPs in the modified membranes might also reduce the effectiveness of using physical cleaning to regenerate the modified membranes because of the small pore sizes of the Fe_3O_4-NPs which would make it difficult to remove the BTEX through physical cleaning. With the gradual decline of flux, the membranes may eventually lose their performance and require chemical cleaning to re-establish their performance.

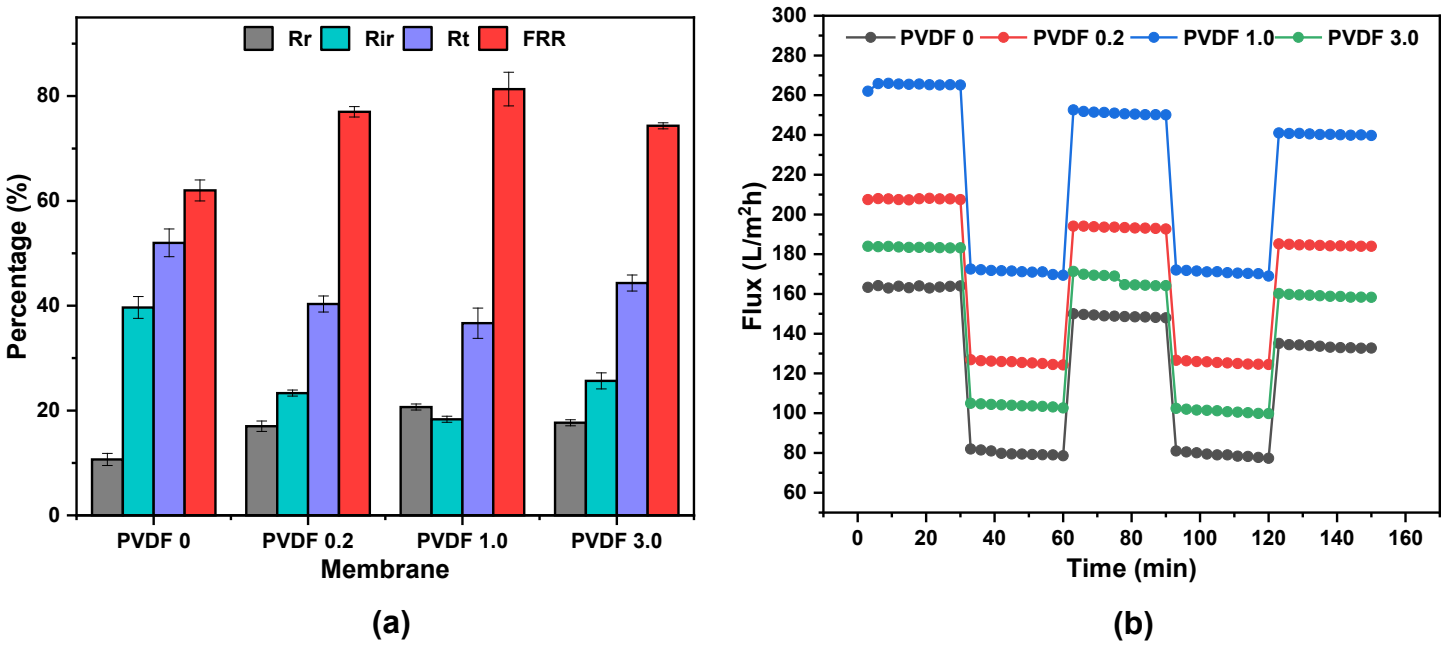


Figure 5. 15: (a) fouling resistance of the membranes, (b) Fluctuation of the flux of pure water and BTEX water over time.

5.6 Comparison with literature

Table 5. 4 presents the comparison of this work with other studies that used modified membranes for the treatment of BTEX wastewater. It is important to note that this may not totally reflect the direct comparison of the performance of the various membranes due to the different filtration conditions used in the studies. However, the Fe_3O_4-NPs/PVDF membrane exhibited a better pure water flux than the other studies. The %R in Table 5. 4 depicts the highest reported rejection of any of the components of BTEX, i.e., benzene, toluene, ethylbenzene, and xylene. The Fe_3O_4-NPs/PVDF membrane showed a high %R and FRR. Overall, the comparison of this study with other similar studies revealed the Fe_3O_4-NPs/PVDF membrane as a potential membrane for removing BTEX from wastewater.

Table 5. 4: Comparison of the performance of the Fe_3O_4-NPs/PVDF membrane with other studies in the literature

Membrane composition	PWF (L/m^2h)	%R	FRR	Ref.
TA-Fe^{III}/PES	150.0	≈ 90%	-	(Makhani et al., 2022)
Fe-NPs/ PES	84.73	≈ 60%	-	(Unuigbe et al., 2020b)
Carbon nanotube/PVDF	7.1	≈ 90%	-	(Su et al., 2016)
Fe_3O_4-NPs/PVDF	266.0	≈ 80%	≈ 80%	This study

5.7 Conclusion

Hydrophilic and porous Fe_3O_4-NPs, synthesized using the aqueous extract of pomegranate leaves, were used to modify PVDF membranes to improve the membrane's performance towards BTEX removal. The SEM and AFM results show that the Fe_3O_4-NPs/PVDF membranes exhibited longer finger-like pores and rougher surfaces. The water contact angle decreased from 84.2° (pristine PVDF membrane) to 52.0° for the membrane modified with 1 wt% of the Fe_3O_4-NPs. Above 1 wt%, the water contact angle increased, thus suggesting that 1 wt% of the Fe_3O_4-NPs is optimal for improving the membrane hydrophilicity. The PWF and BTEX flux also improved, with the PVDF 1.0 exhibiting the optimum performance in this regard. The fluxes also increased as the TMP increased. PVDF 3.0 showed the highest BTEX rejection among all the fabricated membranes, and the rejection decreased as the TMP was increased. The Fe_3O_4-NPs/PVDF membranes also showed good antifouling propensity, with PVDF 1.0 having the highest FRR of 81%. Overall, the Fe_3O_4-NPs/PVDF membranes presented improved filtration, separation, and antifouling performance, identifying them as potential membranes for BTEX removal from wastewater.

References

Akram, S., Naddeo, V., Rehan, Z., Zahid, M., Rashid, A., & Razzaq, W. (2018). A Comprehensive Review on Polymeric Nano-Composite Membranes for Water Treatment. *Journal of Membrane Science & Technology*, *08*. https://doi.org/10.4172/2155-9589.1000179

Al Aani, S., Wright, C. J., Atieh, M. A., & Hilal, N. (2017a). Engineering nanocomposite membranes: Addressing current challenges and future opportunities. *Desalination*, *401*, 1–15. https://doi.org/10.1016/j.desal.2016.08.001

Al Aani, S., Wright, C. J., Atieh, M. A., & Hilal, N. (2017b). Engineering nanocomposite membranes: Addressing current challenges and future opportunities. *Desalination*, *401*, 1–15. https://doi.org/10.1016/j.desal.2016.08.001

Alkhouzaam, A., & Qiblawey, H. (2021). Novel polysulfone ultrafiltration membranes incorporating polydopamine functionalized graphene oxide with enhanced flux and fouling resistance. *Journal of Membrane Science*, *620*, 118900. https://doi.org/10.1016/j.memsci.2020.118900

Amakiri, K. T., Canon, A. R., Molinari, M., & Angelis-Dimakis, A. (2022). Review of oilfield produced water treatment technologies. *Chemosphere*, *298*, 134064. https://doi.org/10.1016/j.chemosphere.2022.134064

Baig, M. I., Ingole, P. G., Jeon, J., Hong, S. U., Choi, W. K., & Lee, H. K. (2019). Water vapor transport properties of interfacially polymerized thin film nanocomposite membranes modified with graphene oxide and GO-TiO2 nanofillers. *Chemical Engineering Journal*, *373*, 1190–1202. https://doi.org/10.1016/j.cej.2019.05.122

Bandeira, M., Giovanela, M., Roesch-Ely, M., Devine, D. M., & da Silva Crespo, J. (2020). Green synthesis of zinc oxide nanoparticles: A review of the synthesis methodology and mechanism of formation. *Sustainable Chemistry and Pharmacy*, *15*, 100223. https://doi.org/10.1016/j.scp.2020.100223

Biesinger, M. C., Payne, B. P., Grosvenor, A. P., Lau, L. W. M., Gerson, A. R., & Smart, R. St. C. (2011). Resolving surface chemical states in XPS analysis of first row transition metals, oxides and hydroxides: Cr, Mn, Fe, Co and Ni. *Applied Surface Science*, *257*(7), 2717–2730. https://doi.org/10.1016/j.apsusc.2010.10.051

Bolden, A. L., Kwiatkowski, C. F., & Colborn, T. (2015). New Look at BTEX: Are Ambient Levels a Problem? *Environmental Science & Technology*, *49*(9), 5261–5276. https://doi.org/10.1021/es505316f

Butkovskyi, A., Bruning, H., Kools, S. A. E., Rijnaarts, H. H. M., & Van Wezel, A. P. (2017). Organic Pollutants in Shale Gas Flowback and Produced Waters: Identification, Potential Ecological Impact, and Implications for Treatment Strategies. *Environmental Science & Technology*, *51*(9), 4740–4754. https://doi.org/10.1021/acs.est.6b05640

Chen, X., Huang, G., An, C., Feng, R., Wu, Y., & Huang, C. (2019). Plasma-induced PAA-ZnO coated PVDF membrane for oily wastewater treatment: Preparation, optimization, and characterization through Taguchi OA design and synchrotron-based X-ray analysis. *Journal of Membrane Science*, *582*, 70–82. https://doi.org/10.1016/j.memsci.2019.03.091

Dadari, S., Rahimi, M., & Zinadini, S. (2022). Novel antibacterial and antifouling PES nanofiltration membrane incorporated with green synthesized nickel-bentonite nanoparticles for heavy metal ions removal. *Chemical Engineering Journal*, *431*, 134116. https://doi.org/10.1016/j.cej.2021.134116

Davidson, C. J., Hannigan, J. H., & Bowen, S. E. (2021). Effects of inhaled combined Benzene, Toluene, Ethylbenzene, and Xylenes (BTEX): Toward an environmental exposure model. *Environmental Toxicology and Pharmacology*, *81*, 103518. https://doi.org/10.1016/j.etap.2020.103518

Du, Y., Pramanik, B. K., Zhang, Y., & Jegatheesan, V. (2022). Influence of molecular weight cut-off (MWCO) of commercial ultrafiltration substrate on the performance of thin film composite nanofiltration membrane. *Desalination*, *541*, 116020. https://doi.org/10.1016/j.desal.2022.116020

Ekins, P., Vanner, R., & Firebrace, J. (2007). Zero emissions of oil in water from offshore oil and gas installations: Economic and environmental implications. *Journal of Cleaner Production*, *15*(13), 1302–1315. https://doi.org/10.1016/j.jclepro.2006.07.014

Freeman, H., Harten, T., Springer, J., Randall, P., Curran, M. A., & Stone, K. (1992). Industrial Pollution Prevention! A Critical Review. *Journal of the Air & Waste Management Association*, *42*(5), 618–656. https://doi.org/10.1080/10473289.1992.10467016

Grosvenor, A. P., Kobe, B. A., Biesinger, M. C., & McIntyre, N. S. (2004). Investigation of multiplet splitting of Fe 2p XPS spectra and bonding in iron compounds. *Surface and Interface Analysis*, *36*(12), 1564–1574. https://doi.org/10.1002/sia.1984

Hosseini, S. M., Sohrabnejad, S., Nabiyouni, G., Jashni, E., Van der Bruggen, B., & Ahmadi, A. (2019). Magnetic cation exchange membrane incorporated with cobalt ferrite nanoparticles for chromium ions removal via electrodialysis. *Journal of Membrane Science*, *583*, 292–300. https://doi.org/10.1016/j.memsci.2019.04.069

Huang, Z.-H., Zhang, X., Wang, Y.-X., Sun, J.-Y., Zhang, H., Liu, W.-L., Li, M.-P., Ma, X.-H., & Xu, Z.-L. (2020). Fe3O4/PVDF catalytic membrane treatment organic wastewater with simultaneously improved permeability, catalytic property and anti-fouling. *Environmental Research*, *187*, 109617. https://doi.org/10.1016/j.envres.2020.109617

Igunnu, E. T., & Chen, G. Z. (2014). Produced water treatment technologies. *International Journal of Low-Carbon Technologies*, *9*(3), 157–177. https://doi.org/10.1093/ijlct/cts049

Kang, G., & Cao, Y. (2014). Application and modification of poly(vinylidene fluoride) (PVDF) membranes – A review. *Journal of Membrane Science*, *463*, 145–165. https://doi.org/10.1016/j.memsci.2014.03.055

Khan, A., Sherazi, T. A., Khan, Y., Li, S., Naqvi, S. A. R., & Cui, Z. (2018). Fabrication and characterization of polysulfone/modified nanocarbon black composite antifouling ultrafiltration membranes. *Journal of Membrane Science*, *554*, 71–82. https://doi.org/10.1016/j.memsci.2018.02.063

Khanzada, N. K., Farid, M. U., Kharraz, J. A., Choi, J., Tang, C. Y., Nghiem, L. D., Jang, A., & An, A. K. (2020). Removal of organic micropollutants using advanced membrane-based water and wastewater treatment: A review. *Journal of Membrane Science*, *598*, 117672. https://doi.org/10.1016/j.memsci.2019.117672

Kong, N., Chen, C., Zeng, Q., Li, B., Shen, L., & Lin, H. (2022). Enriching Fe3O4@MoS2 composites in surface layer to fabricate polyethersulfone (PES) composite membrane: The improved performance and mechanisms. *Separation and Purification Technology*, *302*, 122178. https://doi.org/10.1016/j.seppur.2022.122178

Kumar, V., Singh, S., Srivastava, B., Bhadouria, R., & Singh, R. (2019). Green synthesis of silver nanoparticles using leaf extract of Holoptelea integrifolia and preliminary investigation of its antioxidant, anti-inflammatory, antidiabetic and antibacterial activities. *Journal of Environmental Chemical Engineering*, *7*(3), 103094. https://doi.org/10.1016/j.jece.2019.103094

Lee, S.-T., Vu, C. T., Lin, C., & Chen, K.-S. (2018). High occurrence of BTEX around major industrial plants in Kaohsiung, Taiwan. *Environmental Forensics*, *19*(3), 206–216. https://doi.org/10.1080/15275922.2018.1475432

Liang, Z., Wang, J., Zhang, Q., Zhuang, T., Zhao, C., Fu, Y., Zhang, Y., & Yang, F. (2021). Composite PVDF ultrafiltration membrane tailored by sandwich-like GO@UiO-66 nanoparticles for breaking the trade-off between permeability and selectivity. *Separation and Purification Technology*, *276*, 119308. https://doi.org/10.1016/j.seppur.2021.119308

Liao, Z., Zhu, J., Li, X., & Van der Bruggen, B. (2021). Regulating composition and structure of nanofillers in thin film nanocomposite (TFN) membranes for enhanced separation performance: A critical review. *Separation and Purification Technology*, *266*, 118567. https://doi.org/10.1016/j.seppur.2021.118567

Lin, J., Ye, W., Zhong, K., Shen, J., Jullok, N., Sotto, A., & Van der Bruggen, B. (2016). Enhancement of polyethersulfone (PES) membrane doped by monodisperse Stöber silica for water treatment. *Chemical Engineering and Processing - Process Intensification*, *107*, 194–205. https://doi.org/10.1016/j.cep.2015.03.011

Lin, Y., Loh, C. H., Shi, L., Fan, Y., & Wang, R. (2017). Preparation of high-performance Al2O3/PES composite hollow fiber UF membranes via facile in-situ vapor induced hydrolyzation. *Journal of Membrane Science*, *539*, 65–75. https://doi.org/10.1016/j.memsci.2017.05.069

Liu, T.-Y., Liu, Z.-H., Zhang, R.-X., Wang, Y., Bruggen, B. V. der, & Wang, X.-L. (2015). Fabrication of a thin film nanocomposite hollow fiber nanofiltration membrane for wastewater treatment. *Journal of Membrane Science*, *488*, 92–102. https://doi.org/10.1016/j.memsci.2015.04.020

Liu, Y., Wang, X., Gao, X., Zheng, J., Wang, J., Volodin, A., Xie, Y. F., Huang, X., Van der Bruggen, B., & Zhu, J. (2020). High-performance thin film nanocomposite membranes enabled by nanomaterials with different dimensions for nanofiltration. *Journal of Membrane Science*, *596*, 117717. https://doi.org/10.1016/j.memsci.2019.117717

Lueders, T. (2017). The ecology of anaerobic degraders of BTEX hydrocarbons in aquifers. *FEMS Microbiology Ecology*, *93*(1), fiw220. https://doi.org/10.1093/femsec/fiw220

Ma, C., Hu, J., Sun, W., Ma, Z., Yang, W., Wang, L., Ran, Z., Zhao, B., Zhang, Z., & Zhang, H. (2020). Graphene oxide-polyethylene glycol incorporated PVDF nanocomposite ultrafiltration membrane with enhanced hydrophilicity, permeability, and antifouling performance. *Chemosphere*, *253*, 126649. https://doi.org/10.1016/j.chemosphere.2020.126649

Makhani, T., Sadare, O. O., Wagenaar, S., Moothi, K., Moutloali, R. M., & Daramola, M. O. (2022). Fabrication and performance evaluation of tannin iron complex (TA-FeIII/PES) UF membrane in treatment of BTEX wastewater. *Water SA*, *48*(4), Article 4.

Matindi, C. N., Hu, M., Kadanyo, S., Ly, Q. V., Gumbi, N. N., Dlamini, D. S., Li, J., Hu, Y., Cui, Z., & Li, J. (2021). Tailoring the morphology of polyethersulfone/sulfonated polysulfone ultrafiltration membranes for highly efficient separation of oil-in-water emulsions using TiO2 nanoparticles. *Journal of Membrane Science*, *620*, 118868. https://doi.org/10.1016/j.memsci.2020.118868

McIntyre, N. S., & Zetaruk, D. G. (1977). X-ray photoelectron spectroscopic studies of iron oxides. *Analytical Chemistry*, *49*(11), 1521–1529. https://doi.org/10.1021/ac50019a016

Medhat Bojnourd, F., & Pakizeh, M. (2018). Preparation and characterization of a PVA/PSf thin film composite membrane after incorporation of PSSMA into a selective layer and its application for pharmaceutical removal. *Separation and Purification Technology*, *192*, 5–14. https://doi.org/10.1016/j.seppur.2017.09.054

Mikhak, Y., Torabi, M. M. A., & Fouladitajar, A. (2019). Chapter 3—Refinery and petrochemical wastewater treatment. In C. M. Galanakis & E. Agrafioti (Eds.), *Sustainable Water and Wastewater Processing* (pp. 55–91). Elsevier. https://doi.org/10.1016/B978-0-12-816170-8.00003-X

Miller, D. J., Dreyer, D. R., Bielawski, C. W., Paul, D. R., & Freeman, B. D. (2017). Surface Modification of Water Purification Membranes. *Angewandte Chemie International Edition*, *56*(17), 4662–4711. https://doi.org/10.1002/anie.201601509

Miller, D. J., Paul, D. R., & Freeman, B. D. (2013). A crossflow filtration system for constant permeate flux membrane fouling characterization. *Review of Scientific Instruments*, *84*(3), 035003. https://doi.org/10.1063/1.4794909

Nazir, F. (2018). *Factors Effecting Water Pollution*.

Nikbakht Fini, M., Madsen, H. T., & Muff, J. (2019). The effect of water matrix, feed concentration and recovery on the rejection of pesticides using NF/RO membranes in water treatment. *Separation and Purification Technology*, *215*, 521–527. https://doi.org/10.1016/j.seppur.2019.01.047

Oliveira, C. P. M. de, Fernandes Farah, I., Koch, K., Drewes, J. E., Viana, M. M., & Amaral, M. C. S. (2022). TiO2-Graphene oxide nanocomposite membranes: A review. *Separation and Purification Technology*, *280*, 119836. https://doi.org/10.1016/j.seppur.2021.119836

Radoń, A., Drygała, A., Hawełek, Ł., & Łukowiec, D. (2017). Structure and optical properties of Fe3O4 nanoparticles synthesized by co-precipitation method with different organic modifiers. *Materials Characterization*, *131*, 148–156. https://doi.org/10.1016/j.matchar.2017.06.034

Rowley, J., & Abu-Zahra, N. H. (2019). Synthesis and characterization of polyethersulfone membranes impregnated with (3-aminopropyltriethoxysilane) APTES-Fe3O4 nanoparticles for As(V) removal from water. *Journal of Environmental Chemical Engineering*, *7*(1), 102875. https://doi.org/10.1016/j.jece.2018.102875

Saratale, R. G., Shin, H. S., Kumar, G., Benelli, G., Kim, D.-S., & Saratale, G. D. (2018). Exploiting antidiabetic activity of silver nanoparticles synthesized using Punica granatum leaves and anticancer potential against human liver cancer cells (HepG2). *Artificial Cells, Nanomedicine, and Biotechnology*, *46*(1), 211–222. https://doi.org/10.1080/21691401.2017.1337031

Sardarabadi, H., Kiani, S., Karkhanechi, H., Mousavi, S. M., Saljoughi, E., & Matsuyama, H. (2022). Effect of Nanofillers on Properties and Pervaporation Performance of Nanocomposite Membranes: A Review. *Membranes*, *12*(12), Article 12. https://doi.org/10.3390/membranes12121232

Sherazi, T. A., Azam, S., Shah, S. H., Hussain, S., Naqvi, S. A. R., & Li, S. (2022). Zwitterionic analog structured ultrafiltration membranes for high permeate flux and improved anti-fouling performance. *Journal of Membrane Science*, *643*, 120060. https://doi.org/10.1016/j.memsci.2021.120060

Su, F., Lu, C., & Tai, J.-H. (2016). Separation of Benzene, Toluene, Ethylbenzene and P-Xylene from Aqueous Solutions by Carbon Nanotubes/Polyvinylidene Fluoride Nanocomposite Membrane. *Journal of Water Resource and Protection*, *8*(10), Article 10. https://doi.org/10.4236/jwarp.2016.810075

Subasi, Y., & Cicek, B. (2017). Recent advances in hydrophilic modification of PVDF ultrafiltration membranes – a review: Part II. *Membrane Technology*, *2017*(11), 5–11. https://doi.org/10.1016/S0958-2118(17)30233-1

Swilam, N., & Nematallah, K. A. (2020). Polyphenols profile of pomegranate leaves and their role in green synthesis of silver nanoparticles. *Scientific Reports*, *10*(1), Article 1. https://doi.org/10.1038/s41598-020-71847-5

Tan, Y. H., Goh, P. S., Ismail, A. F., Ng, B. C., & Lai, G. S. (2017). Decolourization of aerobically treated palm oil mill effluent (AT-POME) using polyvinylidene fluoride (PVDF) ultrafiltration membrane incorporated with coupled zinc-iron oxide nanoparticles. *Chemical Engineering Journal*, *308*, 359–369. https://doi.org/10.1016/j.cej.2016.09.092

Tummons, E., Han, Q., Tanudjaja, H. J., Hejase, C. A., Chew, J. W., & Tarabara, V. V. (2020). Membrane fouling by emulsified oil: A review. *Separation and Purification Technology*, *248*, 116919. https://doi.org/10.1016/j.seppur.2020.116919

Unuigbe, C. F., Fayemiwo, O. M., & Daramola, M. O. (2020). Performance evaluation of iron nanoparticles infused polyethersulphone (Fe-NPs/PES) membrane during treatment of BTEX-contaminated wastewater. *Water and Environment Journal*, *34*(S1), 74–86. https://doi.org/10.1111/wej.12506

Ursino, C., Castro-Muñoz, R., Drioli, E., Gzara, L., Albeirutty, M. H., & Figoli, A. (2018). Progress of Nanocomposite Membranes for Water Treatment. *Membranes*, *8*(2), Article 2. https://doi.org/10.3390/membranes8020018

USEPA. (2023, September 28). *U.S. Environmental Protection Agency | US EPA*. https://www.epa.gov/

Van der Bruggen, B. (2009). Chemical modification of polyethersulfone nanofiltration membranes: A review. *Journal of Applied Polymer Science*, *114*(1), 630–642. https://doi.org/10.1002/app.30578

Vatanpour, V., Esmaeili, M., Chahvari, S., & Masteri-Farahani, M. (2021). Evaluation of morphology, performance and fouling tendency of mixed matrix PVDF ultrafiltration membranes incorporated by different size-controlled SAPO-34 nanozeolites. *Journal of Environmental Chemical Engineering*, *9*(5), 105900. https://doi.org/10.1016/j.jece.2021.105900

Vatanpour, V., Hazrati, M., Sheydaei, M., & Dehqan, A. (2022). Investigation of using UV/H2O2 pre-treatment process on filterability and fouling reduction of PVDF/TiO2

nanocomposite ultrafiltration membrane. *Chemical Engineering and Processing - Process Intensification*, *170*, 108677. https://doi.org/10.1016/j.cep.2021.108677

Wang, C., Park, M. J., Yu, H., Matsuyama, H., Drioli, E., & Shon, H. K. (2022). Recent advances of nanocomposite membranes using layer-by-layer assembly. *Journal of Membrane Science*, *661*, 120926. https://doi.org/10.1016/j.memsci.2022.120926

Wang, N., Hsu, C., Zhu, L., Tseng, S., & Hsu, J.-P. (2013). Influence of metal oxide nanoparticles concentration on their zeta potential. *Journal of Colloid and Interface Science*, *407*, 22–28. https://doi.org/10.1016/j.jcis.2013.05.058

Wang, P., Yao, J., Wang, G., Hao, F., Shrestha, S., Xue, B., Xie, G., & Peng, Y. (2019). Exploring the application of artificial intelligence technology for identification of water pollution characteristics and tracing the source of water quality pollutants. *Science of The Total Environment*, *693*, 133440. https://doi.org/10.1016/j.scitotenv.2019.07.246

Wang, Y., Shen, H., Cui, C., Hou, L., Chen, W., Liu, Q., Xu, J., Wang, Z., & Hu, J. (2021). Towards to better permeability and antifouling sulfonated poly (aryl ether ketone sulfone) with carboxyl group ultrafiltration membrane blending with amine functionalization of SBA-15. *Separation and Purification Technology*, *265*, 118512. https://doi.org/10.1016/j.seppur.2021.118512

Wei, X., Liu, Y., Zheng, J., Wang, X., Xia, S., & Van der Bruggen, B. (2022a). A critical review on thin-film nanocomposite membranes enabled by nanomaterials incorporated in different positions and with diverse dimensions: Performance comparison and mechanisms. *Journal of Membrane Science*, *661*, 120952. https://doi.org/10.1016/j.memsci.2022.120952

Wei, X., Liu, Y., Zheng, J., Wang, X., Xia, S., & Van der Bruggen, B. (2022b). A critical review on thin-film nanocomposite membranes enabled by nanomaterials incorporated in different positions and with diverse dimensions: Performance comparison and mechanisms. *Journal of Membrane Science*, *661*, 120952. https://doi.org/10.1016/j.memsci.2022.120952

Wenzel, R. N. (1936). RESISTANCE OF SOLID SURFACES TO WETTING BY WATER. *Industrial & Engineering Chemistry*, *28*(8), 988–994. https://doi.org/10.1021/ie50320a024

Wickramaratne, N. P., Perera, V. S., Park, B.-W., Gao, M., McGimpsey, G. W., Huang, S. D., & Jaroniec, M. (2013). Graphitic Mesoporous Carbons with Embedded Prussian Blue-Derived Iron Oxide Nanoparticles Synthesized by Soft Templating and Low-Temperature

Graphitization. *Chemistry of Materials*, *25*(14), 2803–2811. https://doi.org/10.1021/cm401124d

Wu, H., Niu, X., Yang, J., Wang, C., & Lu, M. (2016). Retentions of bisphenol A and norfloxacin by three different ultrafiltration membranes in regard to drinking water treatment. *Chemical Engineering Journal*, *294*, 410–416. https://doi.org/10.1016/j.cej.2016.02.117

Wu, Y., Wang, F., & Huang, Y. (2018). Facile and simple fabrication of strong, transparent and flexible aramid nanofibers/bacterial cellulose nanocomposite membranes. *Composites Science and Technology*, *159*, 70–76. https://doi.org/10.1016/j.compscitech.2018.02.036

Wypych, G. (2022). *Handbook of Polymers*. Elsevier.

Xu, Q., Li, W., Ma, L., Cao, D., Owens, G., & Chen, Z. (2020). Simultaneous removal of ammonia and phosphate using green synthesized iron oxide nanoparticles dispersed onto zeolite. *Science of The Total Environment*, *703*, 135002. https://doi.org/10.1016/j.scitotenv.2019.135002

Yin, J., & Deng, B. (2015). Polymer-matrix nanocomposite membranes for water treatment. *Journal of Membrane Science*, *479*, 256–275. https://doi.org/10.1016/j.memsci.2014.11.019

Ying, S., Guan, Z., Ofoegbu, P. C., Clubb, P., Rico, C., He, F., & Hong, J. (2022). Green synthesis of nanoparticles: Current developments and limitations. *Environmental Technology & Innovation*, *26*, 102336. https://doi.org/10.1016/j.eti.2022.102336

Yu, B., Yuan, Z., Yu, Z., & Xue-song, F. (2022). BTEX in the environment: An update on sources, fate, distribution, pretreatment, analysis, and removal techniques. *Chemical Engineering Journal*, *435*, 134825. https://doi.org/10.1016/j.cej.2022.134825

Yuliwati, E., & Ismail, A. F. (2011). Effect of additives concentration on the surface properties and performance of PVDF ultrafiltration membranes for refinery produced wastewater treatment. *Desalination*, *273*(1), 226–234. https://doi.org/10.1016/j.desal.2010.11.023

Yusta-García, R., Orta-Martínez, M., Mayor, P., González-Crespo, C., & Rosell-Melé, A. (2017). Water contamination from oil extraction activities in Northern Peruvian Amazonian rivers. *Environmental Pollution*, *225*, 370–380. https://doi.org/10.1016/j.envpol.2017.02.063

Zha, S., Zhang, G., Dawson, N., Yu, J., Liu, N., & Lee, R. (2016). Study of PVDF/Si-R hybrid hollow fiber membranes for removal of dissolved organics from produced water by membrane

adsorption. *Separation and Purification Technology*, *163*, 290–299. https://doi.org/10.1016/j.seppur.2016.03.003

Zhang, R., Liu, Y., He, M., Su, Y., Zhao, X., Elimelech, M., & Jiang, Z. (2016). Antifouling membranes for sustainable water purification: Strategies and mechanisms. *Chemical Society Reviews*, *45*(21), 5888–5924. https://doi.org/10.1039/C5CS00579E

Zhang, W., Ding, L., Luo, J., Jaffrin, M. Y., & Tang, B. (2016). Membrane fouling in photocatalytic membrane reactors (PMRs) for water and wastewater treatment: A critical review. *Chemical Engineering Journal*, *302*, 446–458. https://doi.org/10.1016/j.cej.2016.05.071

Zhu, J., Zhou, S., Li, M., Xue, A., Zhao, Y., Peng, W., & Xing, W. (2020). PVDF mixed matrix ultrafiltration membrane incorporated with deformed rebar-like Fe3O4–palygorskite nanocomposites to enhance strength and antifouling properties. *Journal of Membrane Science*, *612*, 118467. https://doi.org/10.1016/j.memsci.2020.118467

Zou, D., Chen, X., Drioli, E., Ke, X., Qiu, M., & Fan, Y. (2020). Facile co-sintering process to fabricate sustainable antifouling silver nanoparticles (AgNPs)-enhanced tight ceramic ultrafiltration membranes for protein separation. *Journal of Membrane Science*, *593*, 117402. https://doi.org/10.1016/j.memsci.2019.117402

Chapter 6: Preparation of hydrophilic PVDF membrane via blending with Fe_3O_4 nanoparticles and PVA for improved membrane performance in BTEX removal from wastewater

This chapter contains a study into improving the antifouling and operational stability of a PVDF membrane using biogenic-synthesized Fe_3O_4-NPs and PVA. The content of this chapter is reported in the manuscript **Paper 3**, which has been submitted to **Journal of Environmental Chemical Engineering** for evaluation and publication.

The manuscript explored the use of biogenic-synthesized Fe_3O_4-NPs and PVA to enhance the performance of a PVDF membrane in the treatment of BTEX-contaminated water. Hence this section of the study was performed to assess the potential use of the two hydrophilic modifiers in modifying a PVDF membrane to obtain antifouling and operationally stable membrane.

Abstract

The recurring cases of the presence of organic contaminants such as benzene, toluene, ethylbenzene, and xylene (collectively known as BTEX) in our water bodies have reaffirmed the need for continuous development of new strategies for the proper treatment of BTEX-contaminated wastewater before discharge. The application of membrane technology in the treatment of organic-contaminated wastewater is often limited by the hydrophobic nature of most membranes; hence, hydrophilic membrane modification is important to maintain good membrane performance. In this study, biogenic-synthesized iron oxide nanoparticles (Fe_3O_4-NPs) and polyvinyl alcohol (PVA) were blended into a polyvinylidene fluoride (PVDF) membrane to mitigate the non-specific hydrophobic interaction of BTEX and the membrane and improve membrane performance. Fourier transform infrared spectroscopy (FTIR) was used for the chemical compositional analysis of the membrane, which confirmed that hydrophilic functional groups were introduced into the membrane due to blending the Fe_3O_4-NPs and PVA into the PVDF membrane. Compared with the pristine membrane, the modified membrane exhibited improved hydrophilicity as indicated by its water contact angle (WCA) of 40.5°. This improved hydrophilicity consequently enhanced the fouling resistance of the modified membrane during the treatment of the BTEX water, as indicated by the results of its anti-fouling performance test. For the short-term filtration test, the total fouling ratio (R_t) of the pristine PVDF was 0.48, of which 0.25 and 0.23 are irreversible (R_{ir}) and reversible (R_r) fouling, respectively. This was reduced to an R_t of 0.18 for the modified membrane, and the

irreversible fouling declined to 0.02, while 0.16 of the fouling is reversible. The porosity of the modified membrane was also enhanced, resulting in the pure water flux of the membrane improving from 165.3 $Lm^{-2}h^{-1}$ (pristine membrane) to 313.7 $Lm^{-2}h^{-1}$ (modified membrane). With the Fe_3O_4-NPs acting as nanofillers in the membrane matrix, the rejection efficiency of the membrane was not adversely affected by the enhanced membrane porosity. The test of the stability of the modified membrane under long-term filtration revealed that the membrane has good and improved operational stability compared to the pristine membrane.

6.1 Introduction

The release of harmful organic contaminants such as benzene, toluene, ethylbenzene, and xylene (BTEX) into the water bodies has constituted a significant environmental challenge that has intensified the need for the development of improved treatment strategies for effective treatment of the contaminated water before discharge (Yu et al., 2022; Liu et al., 2018; Lee et al., 2018). Human exposure to BTEX-contaminated water could result in mild or severe health complications depending on various factors such as the level of the BTEX in the water system, the method of exposure, and the duration of the exposure (Shores et al., 2017; Bulatović et al., 2022; Ma et al., 2024). The aquatic organisms are also adversely impacted by BTEX water contamination as the exposed organisms could experience growth impairment, degenerative organ damage, and embryonic deformation, amongst others (Gissi et al., 2021; Medeiros et al., 2017; Delunardo et al., 2020; Hansen et al., 2019). Moreover, the volatilization of the BTEX from the contaminated water body results in poor air quality in the surrounding atmosphere (Shores et al., 2017).

To address the health and environmental risks associated with BTEX water contamination, various approaches have been developed to remove the BTEX from the contaminated wastewater before discharge (Muneron Mello et al., 2019; Rene et al., 2007; Bustillo-Lecompte et al., 2018; Munirasu et al., 2016). Among the treatment approaches, membrane technology offers a more efficient means of treatment of BTEX-contaminated water (Padaki et al., 2015; Samuel et al., 2022). This is due to the ease of the membrane fabrication and application, low cost, minimal energy consumption, and low chances of generating secondary pollution during the treatment process (Alzahrani & Mohammad, 2014; Drioli et al., 2016; Padaki et al., 2015). Despite these remarkable attributes of membranes in organic wastewater treatment, their application is limited by the hydrophobic nature of most membrane materials (Zhang et al., 2020; Ismail et al., 2020). This is because of the hydrophobic interactions between the

membranes and the organic contaminants during the treatment process, which results in membrane fouling and subsequent deterioration of the performance of the membranes (Kim et al., 2018; Zhang et al., 2016).

To overcome this challenge, several strategies have been employed to suppress such hydrophobic interaction between the membranes and the organic contaminants to ensure long-term and sustainable membrane performance (Miller et al., 2017; Chew et al., 2017; Liu et al., 2021). Among the membrane modification strategies is the incorporation of hydrophilic additives such as nanomaterials and hydrophilic polymers into the membranes (Li et al., 2017; Kusworo et al., 2021; Subasi & Cicek, 2017). The role of these additives as hydrophilic modifiers to resist membrane fouling is achieved through two main mechanisms: the formation of a hydration layer and the steric repulsion effect (Zhang et al., 2019).

Nanomaterials such as silver (Zhang et al., 2020), titanium dioxide (Li et al., 2019), zinc oxide (Sun et al., 2022), and iron oxide (Barati et al., 2021) nanoparticles have been extensively used as modifiers for many hydrophobic membranes due to their intrinsic hydrophilic properties. Another vital feature of nanomaterials that is key to their use in membrane modification is their nano size, which provides a large surface-to-volume ratio, thereby ensuring more efficient interaction of the particles with the membranes (Savage & Diallo, 2005). However, agglomeration of the nanomaterials in the matrix of the membranes remains a significant drawback to their use as membrane modifiers (Ying et al., 2017). The agglomeration of the nanomaterials occurs due to their high surface energy, resulting in increased interaction between the nano-sized particles; hence, the amount of nanomaterials used in membrane modification is limited to low concentration to minimize such agglomeration (Kim & Van der Bruggen, 2010). Oftentimes, nanomaterials are biogenically synthesized to harness the capping ability of the biological extracts used in the synthesis and reduce their tendency to agglomerate (Li et al., 2020; Ying et al., 2022). Although such a method of nanomaterial preparation may not completely eliminate agglomeration, it greatly minimizes the agglomeration (Ying et al., 2022). In addition, some compounds in the biological extracts, such as polyphenols, are rich in hydrophilic functional groups, which further contributes to the nanomaterials' hydrophilicity (J. Qu et al., 2021).

Hydrophilic polymers are another class of modifiers notably employed in endowing hydrophobic membranes with improved hydrophilicity (Ismail et al., 2020). Some of the most common hydrophilic polymers used in membrane modifications are polyethylene glycol (PEG)

(Y.-C. Lin et al., 2021), polyacrylonitrile (PAN) (Yalcinkaya et al., 2017), and polyvinyl alcohol (PVA) (Li et al., 2022). These polymers are rich in hydrophilic functional groups; hence, these hydrophilic functional groups are introduced into a hydrophobic membrane during the modification process, thereby improving the hydrophilicity of the membrane. PVA, for instance, as a polyhydroxy, consists of many hydroxyl groups that are exploited to endow hydrophobic membranes with hydrophilic properties by coating or blending the PVA on the membrane (Zhang et al., 2014; Li et al., 2022).

To achieve optimal hydrophilic membranes, most research has focused on utilizing more than one hydrophilic modifier in the membrane modification (Sun et al., 2020; Liu et al., 2021; Du et al., 2021). Zuo et al., 2021 utilized two hydrophilic modifiers, pyrogallol, and polyethyleneimine, to enhance the hydrophilicity of a PVDF membrane, subsequently improving the membrane performance in the separation of oil/water emulsion. Similarly, Liu et al., 2019 harnessed the hydrophilic properties of SiO_2 and PVA to improve the hydrophilicity and performance of a PVDF membrane for oil-in-water emulsions separation. For hydrophilic membrane modification specifically for the separation of BTEX from wastewater, very few studies have been conducted. Saeedi-Jurkuyeh et al., 2021 used graphene oxide and PEG to modify a polysulfone (PSF) membrane for the removal of two of the constituents of BTEX, benzene and toluene. Improved separation performance of the modified PSF membrane was obtained under a short-term separation test (Saeedi-Jurkuyeh et al., 2021). Makhani et al., 2022 modified a PES membrane using a single hydrophilic modifier, tannin iron complex (TA-Fe^{III}), for BTEX separation. The membrane permeability and rejection were improved compared to the pristine membrane; however, the rejection of some of the BTEX constituents was as low as 60% due to the enlarged macro-voids of the membranes as a result of the agglomeration of the TA-Fe^{III} at high concentration (Makhani et al., 2022). Similarly, iron nanoparticles were utilized as a single modifier to improve the performance of a PES membrane in the treatment of BTEX-contaminated water (Unuigbe et al., 2020b). However, the nanoparticles were agglomerated in the membrane matrix, especially at high concentrations which reduced the expected impact of the Fe-Np on the membrane performance (Unuigbe et al., 2020b).

Owing to the very limited number of potential hydrophilic modifiers that have been studied for use in the hydrophilic modification of membranes for the removal of BTEX from wastewater, it is vital that more hydrophilic modifiers be explored for this purpose. Biogenic-synthesized iron oxide nanoparticles (Fe_3O_4-NPs) are one of the potential hydrophilic modifiers that can be

utilized for membrane modification. The incorporation of Fe_3O_4-NPs into the membrane is a low-cost and easy approach for membrane modification (Ghaemi et al., 2015), and the extract of the plant used for the biogenic synthesis caps the Fe_3O_4-NPs and reduces their agglomeration (Martínez-Cabanas et al., 2016b). Although the plant extract reduces the Fe_3O_4-NPs agglomeration, there is still a tendency for the NPs to agglomerate at very high concentrations (Martínez-Cabanas et al., 2016b). Hence, the use of low concentrations of the NPs is necessary to prevent the NPs agglomeration. However, the low amount of the NPs is often not sufficient to achieve a highly hydrophilic membrane. Thus, the incorporation of another hydrophilic modifier could be a viable means of further improving the hydrophilicity and separation performance of membranes. PVA is a low-cost hydrophilic polymer that can be used for hydrophilic modification of membranes. However, polymer incompatibility between the PVA and the membrane can occur at high concentrations of the PVA. Hence low concentration of PVA is ideal for achieving a stable polymer blend (Zhang et al., 2017). With the blending amounts of the two potential modifiers being limited, utilizing a hybrid of the ideal amounts of both modifiers could provide a cost-effective and easy approach to improve the hydrophilicity of membranes for the treatment of BTEX wastewater.

This study explored the synergistic effect of blending biogenic-synthesized iron oxide nanoparticles (Fe_3O_4-NPs) and PVA into a PVDF membrane to mitigate the fouling tendency of the membrane during the treatment of BTEX wastewater. Low concentrations of the Fe_3O_4-NPs and PVA were used for the membrane modification to prevent the agglomeration of the Fe_3O_4-NPs or polymer incompatibility between PVDF and PVA. However, the combined effect of the two modifiers compensates for the low amount of the individual modifiers used to enhance the membrane's performance. The fouling resistance of the PVA-Fe_3O_4-PVDF membrane was investigated by performing anti-fouling tests with synthetic BTEX wastewater. Other performance tests were also conducted by measuring parameters such as pure water flux, BTEX flux, and BTEX rejection capacity of the modified membrane. Operational stability of the membrane was also investigated. The physical features of the modified membrane were assessed using characterization techniques such as water contact angle, scanning electron microscopy (SEM), atomic force microscopy (AFM), and Fourier transform infrared spectroscopy (FTIR). The stability of the modifiers in the membrane matrix was also assessed by performing leaching studies of the membrane.

6.2 Experimental

6.2.1 Materials

PVDF pellets (M_w ~ 180,000), PVA (M_w ~ 23,000), 1-methyl-2-pyrrolidinone (NMP, ≥99.0%), maleic acid, benzene (99.8%), toluene (99.9%), ethylbenzene (>99.9%), and xylene (≥99%) were obtained from Sigma Aldrich. Deionized water (DI water, 18.2 MΩcm @25ºC) was used throughout this study and supplied from the Direct-Q UV millipore system. All the reagents were used as received without any further purification.

6.2.2 Preparation of the hydrophilic-modified membrane

The first step in the fabrication of the membrane was to select a base membrane ideal for the treatment of the BTEX-contaminated water. The suitability of the base membrane was assessed based on the membrane's tolerance to BTEX exposure. For this test, PES and PVDF membranes were immersed in 1000 ppm of BTEX water at room temperature. After 30 days, the membranes were removed from the BTEX water, rinsed with DI water, and dried in the oven at 40ºC for 2 hrs. The BTEX tolerance of the membranes was inferred from the physical observation of the immersed membranes and their SEM images. As depicted in Figure 6. 1 of the results section, PVDF exhibited the best BTEX tolerance; hence PVDF was selected as a base membrane for the fabrication of the modified membrane.

The Fe_3O_4-NPs used for the membrane modification were biogenically synthesized, and the synthetic procedure was discussed in our previous work (Enemuo et al., 2024). The composition of the casting solution for the modified membrane was 83.7 wt.%, 15 wt.%, 1 wt.%, 0.1 wt.%, 0.1 wt%, and 0.1 wt.% of NMP, PVDF, Fe_3O_4-NPs, PVA, maleic acid, and HCl respectively. The casting solution was prepared by first obtaining a homogenous Fe_3O_4-NPs suspension by dispersing the Fe_3O_4-NPs in 1 mL of NMP and sonicating for 1 hour. PVA was thoroughly dissolved in NMP, and the well-dispersed Fe_3O_4-NPs suspension was poured into the PVA solution. The mixture was stirred for 3 hours at 80ºC until a homogenous mixture of the Fe_3O_4-NPs and PVA was obtained, then maleic acid and HCl were poured into the mixture and stirred vigorously for 2 min. PVDF was thoroughly dissolved in NMP, added to the Fe_3O_4-NPs/PVA mixture, stirred for 3 hours, sonicated for 30 min, and then stirred again for 1 hour. The obtained casting solution was cooled and degassed to remove air bubbles and cast on a clean, smooth glass plate using the elcometer film applicator. After a short while, the cast film was immersed in deionized water (coagulation bath) for about 5 min to ensure the

complete exchange of the NMP from the formed membrane. The membrane was then thoroughly washed with deionized water and dried in an oven at 40ºC for about 2 hours.

For the pristine membrane, 15 wt.% of PVDF was dissolved in 85 wt.% of NMP at 80ºC for 8 hours under rigorous stirring. The pristine membrane was then cast and dried using the same procedure described above for the modified membrane. The pristine membrane was used as a control membrane to assess improvement in the properties and performance of the modified membrane.

6.3 Characterization of the membrane

The morphological properties of the modified and pristine membranes were analyzed using a high-resolution Carl Zeiss SEM and WITec alpha 300 atomic force microscope (AFM). The membranes for SEM cross-section analysis were frozen in liquid nitrogen and carefully fractured. Energy-dispersive X-ray spectroscopy (EDX), performed on the same high-resolution Carl Zeiss SEM, was used to confirm the incorporation of the Fe_3O_4-NPs into the membrane. Before the SEM analysis, all membranes were sputter-coated with Pd/Au and carbon using EmiTech K550X Sputtercoater for Pd/Au and EmiTech K950X Turboevaporator (Quorum Technologies, Lewes, England) for carbon.

The compositional analysis of the membranes was performed with an FTIR Bruker Tensor 27 to confirm the successful introduction of the hydrophilic functional groups into the membrane.

The hydrophilicity of the membranes was tested by measuring their water contact angle (WCA) using the sessile drop method done on a goniometer G10, KRUSS. Five measurements were done for each membrane, and the average was reported. Membrane's hydrophilicity can also be stipulated by measuring their equilibrium water content (EWC) (Ju et al., 2010). The EWC is also directly proportional to the porosity (ε) of membranes, and both parameters (EWC and porosity) can be measured using the gravimetric method according to Eq. (1) and (2). The W_{dry} and W_{wet} represent the masses of the dry membrane and wet membrane after immersing in DI water for 48 hours at room temperature, respectively. ρ, A, and l in Eq. (2) is the density of water (g/cm^3), the effective area of the tested membrane (m^2), and the thickness of the membrane (m), respectively. The immersed membrane was thoroughly wiped to remove excess water on its surface and weighed immediately.

$$EWC\ (\%) = \left(\frac{W_{wet} - W_{dry}}{W_{wet}}\right) \times 100 \quad (1)$$

$$\varepsilon(\%) = \frac{(W_{wet} - W_{dry})}{\rho \times A \times l} \times 100 \quad (2)$$

The surface charge of the membranes was measured using the Zetasizer Nano ZS system, Malvern Instruments. Each membrane was immersed in KOH (0.01M, 300 mL) electrolyte solution for 48 hours, and the measurements were done at different pH (1.8 to 12.1) at 25°C. The soaked membrane was cut and fitted into the custom dip-cell, which was immersed in the background electrolyte solution. The required solution pH was adjusted by dosing with a dilute HCl or NaOH.

The thermal stability of the membranes was determined at a heating rate of 10ºC/min under nitrogen between 25ºC and 800ºC using a thermogravimetric analyzer, TA SDT Q600. A Tesla analyzer, XT plus TA, was used to test the mechanical properties of the membranes.

6.4 Membrane performance evaluation

Synthetic BTEX water was used in the study because of the difficulty in accessing industrial wastewater containing BTEX contaminants. The short-term filtration and BTEX rejection tests were performed using a dead-end stirred cell, HP4750; Sterlitech Corp., USA. Before the tests, each membrane was compacted using DI water at a transmembrane pressure (TMP) of 350 kPa for 30 min to achieve a steady flux. The flux and separation tests were conducted at a TMP of 300 kPa using DI water and synthetic BTEX water. The pure water flux and BTEX flux were calculated using Eq.16.

$$J = \frac{V}{A \times \Delta t} \quad (16)$$

Where J is the pure water flux or BTEX flux (L/m^{2}h), V is the volume of the permeate (L), A is the effective filtration area of the tested membrane (m^2), and Δt is the permeation time (h).

The BTEX rejection capacity of the membranes was evaluated by filtering the BTEX water through the membrane under constant stirring of the feed solution at 300 kPa and room temperature. The concentration of each of the contaminants, that is, benzene, toluene, ethylbenzene, and xylene, in the feed solution, was 100 ppm, which is above their reported environmental level (Leusch & Bartkow, 2010; Mukherjee & De, 2016). The BTEX concentration in the permeate was measured using an Agilent 7890A gas chromatograph GC with a 30m × 0.25mm ID BP5MS × 0.25µm column, equipped with a flame ionization detector FID and Agilent 7693A automatic liquid sampler. Nitrogen was used as the carrier gas, which was set at a constant flow rate of 2.64 mL/min, and the injection volume was 0.2 µL in a

splitless mode. The oven initial temperature was set at 40ºC and held for 2 min, then ramped to 90ºC at 10ºC/min, held for 3 min, and finally to 200ºC at a rate of 20ºC/min and held for 2 min. The BTEX percentage rejection was calculated using Eq. (17).

$$R\ (\%) = \frac{C_f - C_p}{C_f} \tag{17}$$

Where C_f and C_p are the BTEX concentration (ppm) in the feed and permeate solution, respectively.

The effect of the hydrophilic modifiers on improving the fouling resistance of the membrane was evaluated by performing antifouling tests. For this test, the pure water flux (PWF) of the membrane was obtained for 3 h at 300 kPa, followed by the filtration of BTEX solution for 3 h under the same TMP. The membrane was subsequently cleaned by washing and backwashing with DI water for 1 h and ultrasonically for another 30 min. The PWF of the cleaned membrane was measured for 3 h filtration. The fouling resistance of the membrane was determined by calculating the reversible fouling ratio (R_r), irreversible fouling ratio (R_{ir}), total fouling ratio (R_t), and the flux recovery ratio (FRR) according to Eq. (18), (19), (20), and (21), respectively. The cleaning efficiency (η_c) of the membrane was also calculated using Eq. (22).

$$R_r = \frac{J_C - J_{BTEX}}{J_w} \tag{18}$$

$$R_{ir} = \frac{J_w - J_C}{J_w} \tag{19}$$

$$FRR = \frac{J_C}{J_w} \tag{20}$$

$$R_t = R_r + R_{ir} \tag{21}$$

$$\eta_c = \left(\frac{J_C - J_{BTEX}}{J_W - J_{BTEX}}\right) \tag{22}$$

Where J_w is the first PWF, J_{BTEX} is the flux of the BTEX solution and J_C is the flux obtained after cleaning the membrane.

The stability of the membrane in terms of its operational stability and the stability of the incorporated modifiers in the membrane matrix was investigated. For operational stability, the flux and BTEX rejection capacity of the membrane, under the same parameters described above, were studied for a longer period using a crossflow filtration system, Sterlitech

membrane test system. The procedure involves the filtration of the synthetic BTEX solution through the membrane for 120 hours, with filtrate samples collected every 6 hours. To determine the stability of the modifiers in the membrane matrix, the filtrates were analyzed using an inductively coupled plasma mass spectrometer, ICP-MS (PerkinElmer, USA), to obtain the concentration of the iron in the filtrate, which was utilized to infer the leaching tendency of the Fe_3O_4-NPs from the membrane. The morphology and chemical composition of the used membrane were also obtained using SEM and FTIR to determine any morphological or compositional changes due to the leaching of the incorporated modifiers.

6.5 Results and discussion

6.5.1 Fe_3O_4-NPs characterization

The identification, chemical composition, morphology, and textural properties of the biogenic-synthesized Fe_3O_4-NPs were extensively discussed in Paper 1 (Chapter 5).

Selection of the base membrane

Figure 6. 1 depicts the outcome of the exposure of PES and PVDF membrane materials to BTEX water. As seen in Figure 6. 1(a), there was some damage to the PES membrane after being exposed to the BTEX water, as the membrane became a little flaky. The damage is further confirmed by the crackiness on the membrane, as shown in the SEM image of the top surface of the membrane in Figure 6. 1(b). However, the inner structure of the PES membrane was not affected by the exposure to BTEX, as shown in Figure 6. 1(c). On the other hand, the PVDF membrane exhibited excellent tolerance to the BTEX water, as shown in all the images (Figure 6. 1(d, e, f) of the membrane after its exposure to the BTEX water. This high PVDF resistance to BTEX can be attributed to the presence of strong carbon-flouride bond in PVDF. Because of the excellent tolerance of PVDF to BTEX water, it was chosen as the base membrane for the fabrication of the modified membrane for use in the treatment of BTEX-contaminated water.

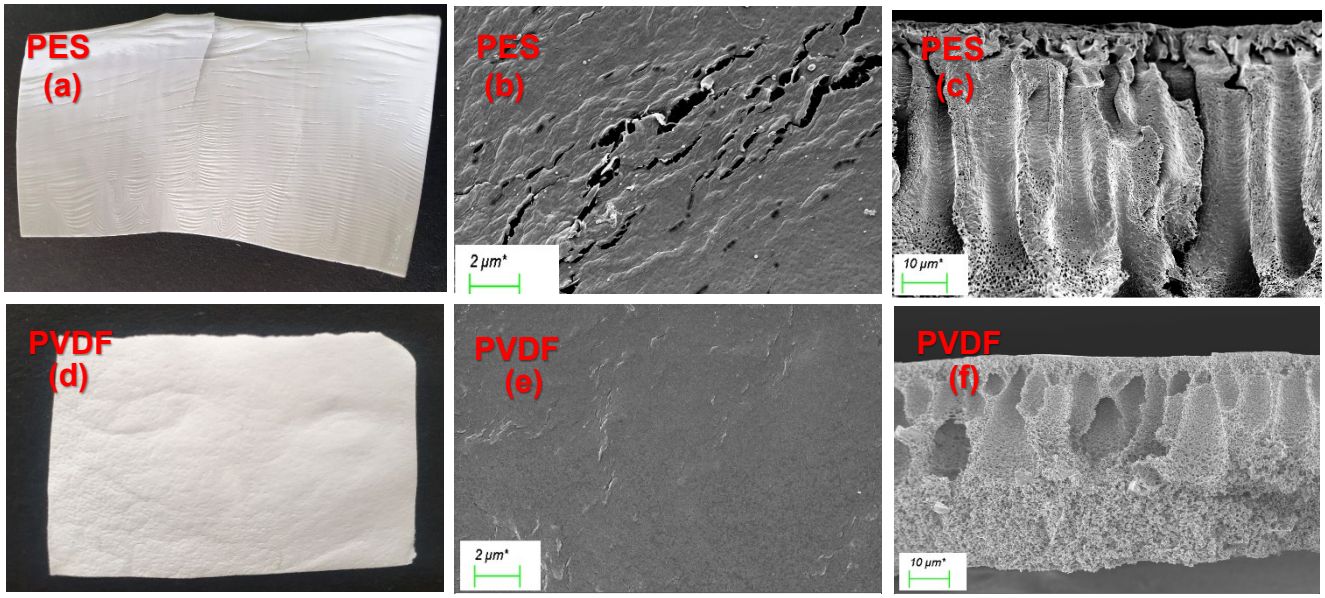


Figure 6. 1: The outcome of BTEX exposure of PES and PVDF membrane depicted by (a, d) photographs, (b, e) SEM image of membrane top surface, and (c, f) SEM image of membrane cross-section.

6.5.2 Membrane chemical composition

The blending of PVA into the PVDF membrane was confirmed by the FTIR spectra shown in Figure 6. 2. The pristine PVDF membrane shows peaks at 679 cm^{-1} and 762 cm^{-1} which is due to the functional group of CF_2 chemical bonds, and the peaks at 1180 cm^{-1} and 1072 cm^{-1} are assigned to the asymmetric and symmetric stretching of the -CF_2 (Kusworo et al., 2023; Sakarkar et al., 2020). The peak for CH deformation appeared at 1401 cm^{-1}, and other peaks at 873 cm^{-1} and 832 cm^{-1} are due to the C-C-C bonds of the PVDF membrane (Zhang, et al., 2022). For the PVA, the broad peak at 3288 cm^{-1} represents the O-H stretching. The other peaks at 2934, 2905, 1416, 1323, 1138, 1083, 916, and 829 cm^{-1} are due to asymmetric stretching of CH_2, symmetric stretching of CH_2, the bending of CH_2, OH rocking with CH wagging, shoulder stretching of C-O, stretching of C=O and bending of OH, rocking of CH_2, and C-C stretching respectively (Deleanu et al., 2012). Comparing the spectra of the pristine membrane and the modified membrane, there were obvious peak changes as a result of the modification. For instance, unlike the pristine PVDF, the PVA-Fe_3O_4-PVDF membrane exhibited a broad peak at 3288 $cm^{-1,}$ which was ascribed to O-H stretching, thus confirming the presence of the hydrophilic hydroxyl functional group in the modified membrane. In addition, there were peak changes in the region between 1272 cm^{-1} and 1033 cm^{-1} which is due to the entanglement of the molecular chains of PVDF and PVA, thus confirming the integration of the two polymers.

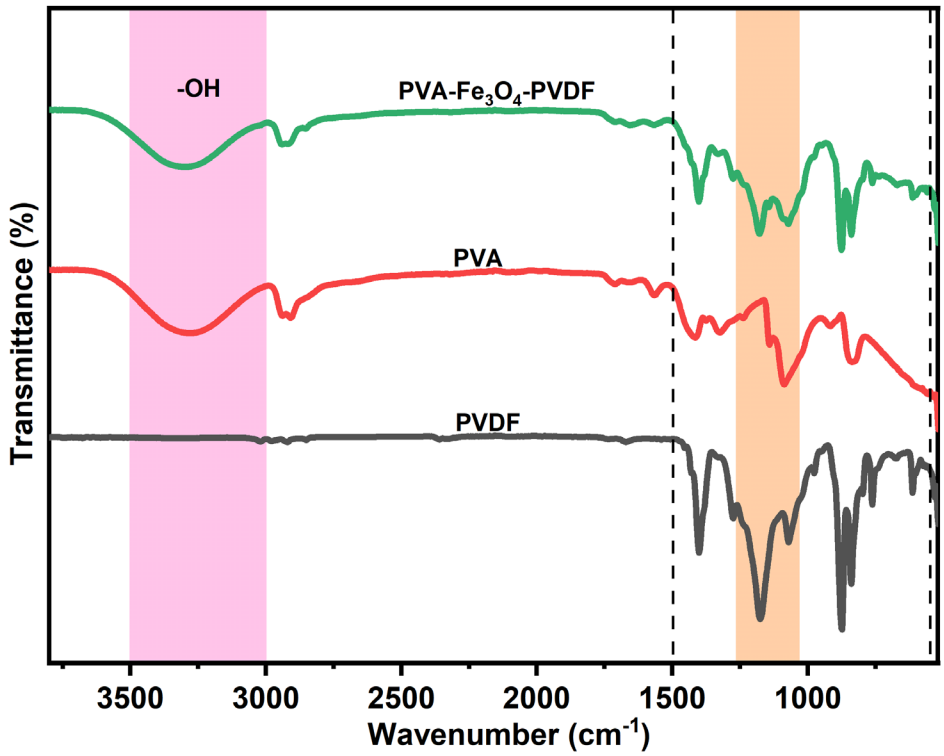


Figure 6. 2: FTIR spectra of PVDF, PVA, and PVA-Fe_3O_4-PVDF.

6.5.3 Membrane morphology

The SEM image of the modified and pristine membranes depicted in Figure 6. 3 shows the effect of the modifiers on the surface and inner morphology of the membrane. The surface of the pristine membrane was smooth and less porous, while the PVA-Fe_3O_4-PVDF membrane had a rougher and more porous surface, as shown in Figure 6. 3(a) and (c). This observed change on the surface of the modified membrane indicates that the incorporation of the modifiers accelerated the demixing process during the phase inversion due to the hydrophilic nature of the modifiers. Hence, the better hydrophilicity of the modified membrane cast solution necessitated a fast solvent-nonsolvent exchange which resulted in the formation of a more porous membrane structure.

Comparing the cross-section morphology of the two membranes also indicates that the addition of the modifiers increased the diffusion rate of the solvent and non-solvent during the phase inversion. This is established in the difference in the formation of the finger-like pores in the membranes. As depicted in Figure 6. 3(b), the finger-like pores of the pristine membrane were shorter, while the finger-like pores of the modified membrane, shown in Figure 6. 3(e), were longer. With the incorporated hydrophilic modifiers, the membrane solution had more affinity for water; hence, on immersing the casted membrane into the coagulation bath, the diffusion

of water into the membrane was faster. This results in the formation of longer finger-like pores in the modified membrane, which is expected to enhance the flux of the membrane but may negatively affect its BTEX rejection efficiency. The concern about the possible reduced rejection capacity of the modified membrane due to its enhanced pore structure was addressed by the presence of the Fe_3O_4 nanoparticles in its matrix, as shown in the higher magnification image of the membrane in Figure 6. 3(g) and Figure 6. 3(h). The role of the Fe_3O_4 nanoparticles as nanofillers is evident in the images, and it will be significant in ensuring that the membrane's rejection capacity is not notably compromised by the longer macropores of the modified membrane.

The Fe_3O_4-NPs in the modified membrane were not agglomerated but were well dispersed throughout the membrane, as shown in Figure 6. 3(g) and Figure 6. 3(h); thus, all the expected attributes of the Fe_3O_4-NPs would be maximized in improving the properties and performance of the membrane.

Morphological interpretation in terms of the surface roughness of the membrane was obtained using AFM analysis of the membrane, and the roughness images are presented in Figure 6. 4. The average roughness (Sa) and root mean square roughness (Sq) of the pristine membrane were 44.2 nm and 48.6 nm respectively. On adding the modifiers to the membrane, the Sa and Sq increased to 59.3 nm and 62.8 nm, respectively. This indicates that the modification of the PVDF membrane using the Fe_3O_4-NPs and PVA significantly enhanced the surface roughness of the membrane. According to Wenzel's model, the roughness of a surface influences its wettability, with a rougher surface exhibiting higher wettability and vice versa (Zheng et al., 2022). Thus, the improved surface roughness of the PVA-Fe_3O_4-PVDF membrane could be beneficial in enhancing the wettability of the membrane which consequently results in improved membrane permeability. In addition, the rougher membrane surface provides more membrane area, which also favours the membrane permeability.

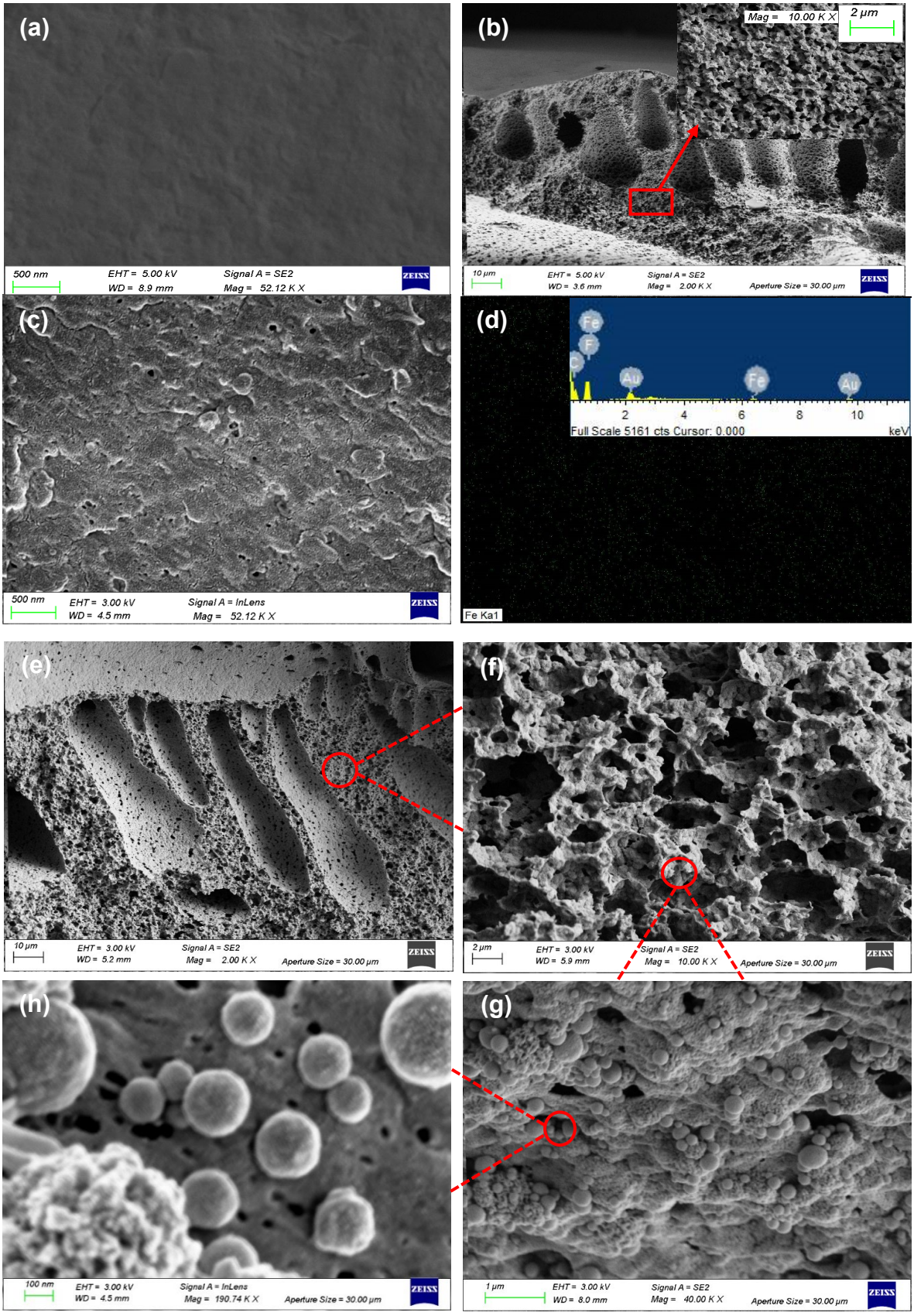


Figure 6. 3: SEM image of the (a) surface of pristine PVDF, (b) inner structure of pristine PVDF, (c) surface of PVA-Fe_3O_4-PVDF, (d) EDX mapping image of PVA-Fe_3O_4-PVDF, and the inner structure of PVA-Fe_3O_4-PVDF at magnification (e) 2.00 KX, (f) 10.00KX, (g) 40.00KX, and (h) 190.74KX.

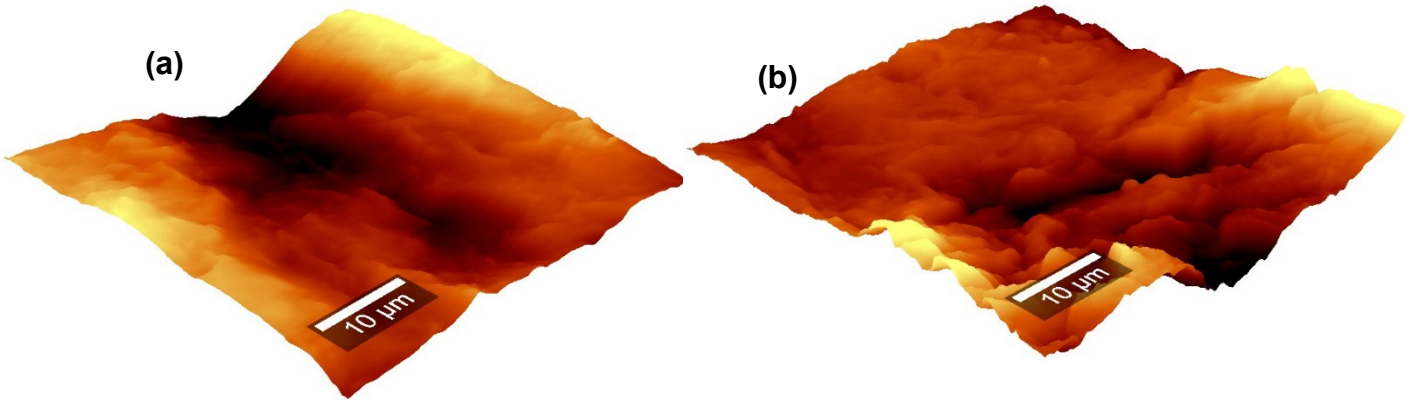


Figure 6. 4: AFM images of the (a) pristine PVDF membrane, and (b) PVA-Fe_3O_4-PVDF membrane.

6.5.4 Membrane hydrophilicity, equilibrium water content, and porosity.

The effect of the modifiers on the hydrophilicity of the membrane was investigated using the sessile drop water contact angle measurements, and the result is shown in Figure 6. 5(a). On incorporation of the modifiers into the PVDF, the WCA of the membrane decreases from 84.2° to 40.5°, which signifies an improvement in its hydrophilicity. This is due to the hydrophilic nature of the two modifiers which were embedded into the membrane. Iron oxide nanoparticles are intrinsically hydrophilic, and their high surface area to volume ratio ensures good transfer of the hydrophilic property to the membrane (Ng et al., 2013; J. Kim & Van der Bruggen, 2010).

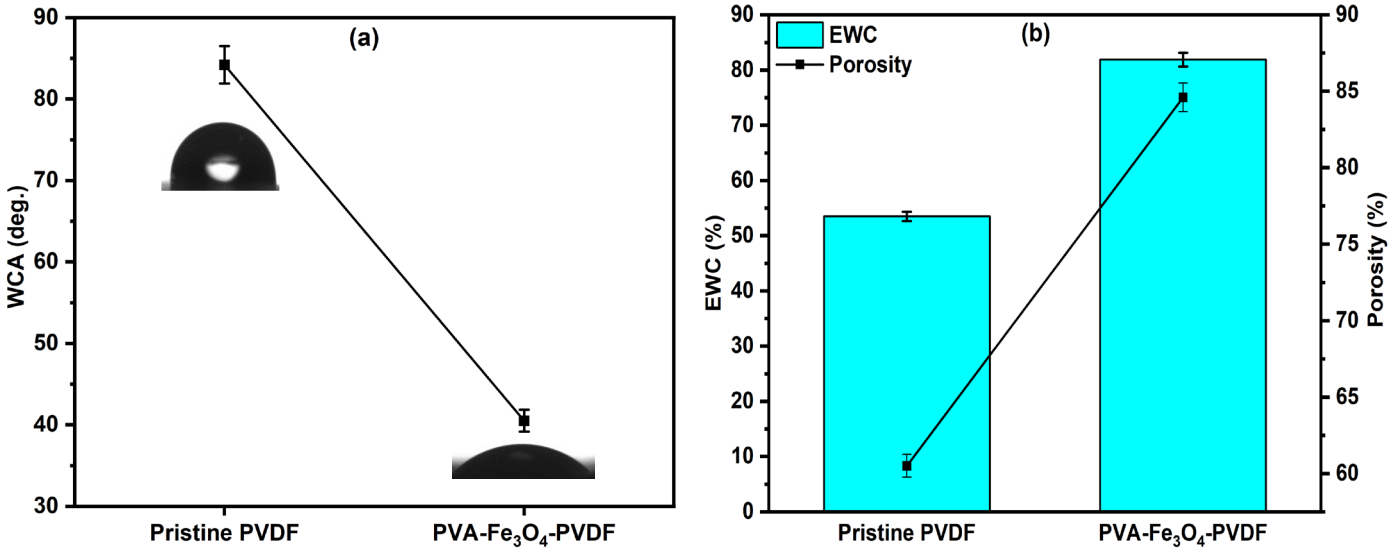


Figure 6. 5: (a) WCA, and (b) EWC and porosity of the pristine PVDF and PVA-Fe_3O_4-PVDF membrane.

The other modifier, PVA, is composed of hydroxyl groups which are highly hydrophilic functional groups (Liu et al., 2022). This hydrophilic feature of the PVA is incorporated into the PVDF membrane, thereby contributing to the improvement of the hydrophilicity of the modified membrane. Thus, the synergistic effect of the hydrophilic nature of the two modifiers bestowed the modified membrane with improved hydrophilicity. With such enhanced hydrophilicity, the membrane surface can form a hydration layer with the water molecules during the filtration process (Zarghami et al., 2019; Gu et al., 2021). This is beneficial in promoting the permeation of water through the membrane and also reducing the rapid deposition of the organic foulants on the membrane (Zhao et al., 2018).

The equilibrium water content (EWC) of the membranes is presented in Figure 6. 5(b), and it further establishes that the hydrophilicity of the modified membrane was enhanced by incorporating the modifiers into the membrane. Compared with the pristine membrane, the modified membrane has a 53% increase in its EWC, which indicates a significant improvement in the membrane's affinity for water. The EWC is also governed by the porosity of a membrane (Saini et al., 2020), and the result of the membrane's porosity, also depicted in Figure 6. 5(b), shows that the porosity of the membrane increased from 60.5% (pristine PVDF) to 84.6% (modified membrane). This correlates with the increment observed in the EWC and the enhanced finger-like pores seen in the SEM image (Figures 6. 3(e) and (f)) of the modified membrane. The improvement in the membrane's porosity is due to the fast liquid-liquid exchange during the phase inversion process, which is induced by the presence of the modifiers, as explained in section 6.5.3.

6.5.5 Membrane surface charge, thermal and mechanical stability

The surface charge of a membrane is one of the major determinants of its performance because the electrostatic interaction between a membrane and the contaminants influences the membrane's behaviour, such as its fouling phenomenon and separation efficiency (Williams, 2016). Zeta potential measurements are often used to determine the membrane surface charge, and this is performed at various pH since the surface charge of membranes is dependent on the pH of the solution (Childress & Elimelech, 2000). Figure 6. 6(a) shows the zeta potential values of the pristine and modified membranes measured over a pH range of 1.8-11.7. Both membranes have positive zeta potentials at low pH between 1.8 and 4.0, however, the zeta potentials of the modified membrane were less positive than that of the pristine membrane at this pH range. In addition, the isoelectric point (IEP) of the modified membrane is 4.09, while

that of the pristine membrane was detected at 4.3. The protonation of the surface groups of the membranes could explain the positive zeta potentials of the membranes at low pH. With the modified membrane having a more oxygen-containing group on its surface, more H^+ is required to neutralize the surface negative charge and achieve a point of zero charge, hence the less positive zeta potential and IEP obtained for the modified membrane at this range. As the pH was further increased, the zeta potentials of both membranes changed to negative, with the modified membrane exhibiting more negative values. This is attributed to the deprotonation of the membranes' surface groups at higher pH, and the presence of more oxygen-containing groups in the modified membrane is also responsible for its observed higher negative zeta potential. This result of the zeta potentials of the modified membrane is imperative in predicting or understanding its behaviour in the treatment of BTEX wastewater at any of the studied pH.

Figure 6. 6(b) shows the TGA curves of the membranes, which represent the effect of the modifiers on the thermal stability of the modified membrane. The pristine PVDF started to decompose at 445ºC owing to the good thermal stability of the polymer itself, and the PVA-Fe_3O_4-PVDF membrane began to decompose at 459ºC. This positive shift of the TGA curve of the modified membrane signifies that an enhancement of the thermal stability of the membrane was achieved by incorporating the modifiers in the membrane. A plausible explanation for the improvement in the thermal stability of the modified membrane is that there was good interaction and binding between the Fe_3O_4-NPs, PVA, and PVDF, which reinforced the membrane's molecular chain. In addition, the PVA-Fe_3O_4-PVDF membrane exhibited a one-step degradation process, which indicates that there was good entanglement of the molecular chains of the PVA and PVDF, thereby suggesting that the blend amounts of the two polymers used for the membrane fabrication produced a compatible polymer blend.

There was also an improvement in the mechanical strength of the PVA-Fe_3O_4-PVDF membrane, as illustrated by the stress-strain curve in Figure 6. 6(c). With the incorporation of the modifiers into the PVDF matrix, the ultimate tensile strength increased from 3.17 MPa (pristine membrane) to 6.62 MPa (modified membrane). Thus, its mechanical strength was doubled. This improved mechanical feature of the modified membrane can be ascribed to the good mechanical stability of the Fe_3O_4-NPs (Martínez-Cabanas et al., 2016b), and the efficient entanglement of the molecular chains of the PVA and PVDF during the fabrication process. The synergistic impact of both modifiers resulted in the significant improvement of the ultimate tensile strength of the modified membrane. With the improved mechanical strength, the modified membrane can withstand more stress during its usage. Conversely, the elongation

tendency of the PVA-Fe_3O_4-PVDF membrane was reduced to about half when compared with that of the pristine membrane, as indicated by the reduced tensile strain of the modified membrane. This decline in the tensile strain of the modified membrane could be attributed to the improved rigidity introduced into the membrane by the Fe_3O_4-NPs, as well as the restraining of the molecular chains of the membrane due to the entanglement of the PVA and PVDF. These effects of the modifiers on the membrane limit its stretching ability, resulting in the observed decline in the membrane's tensile strain.

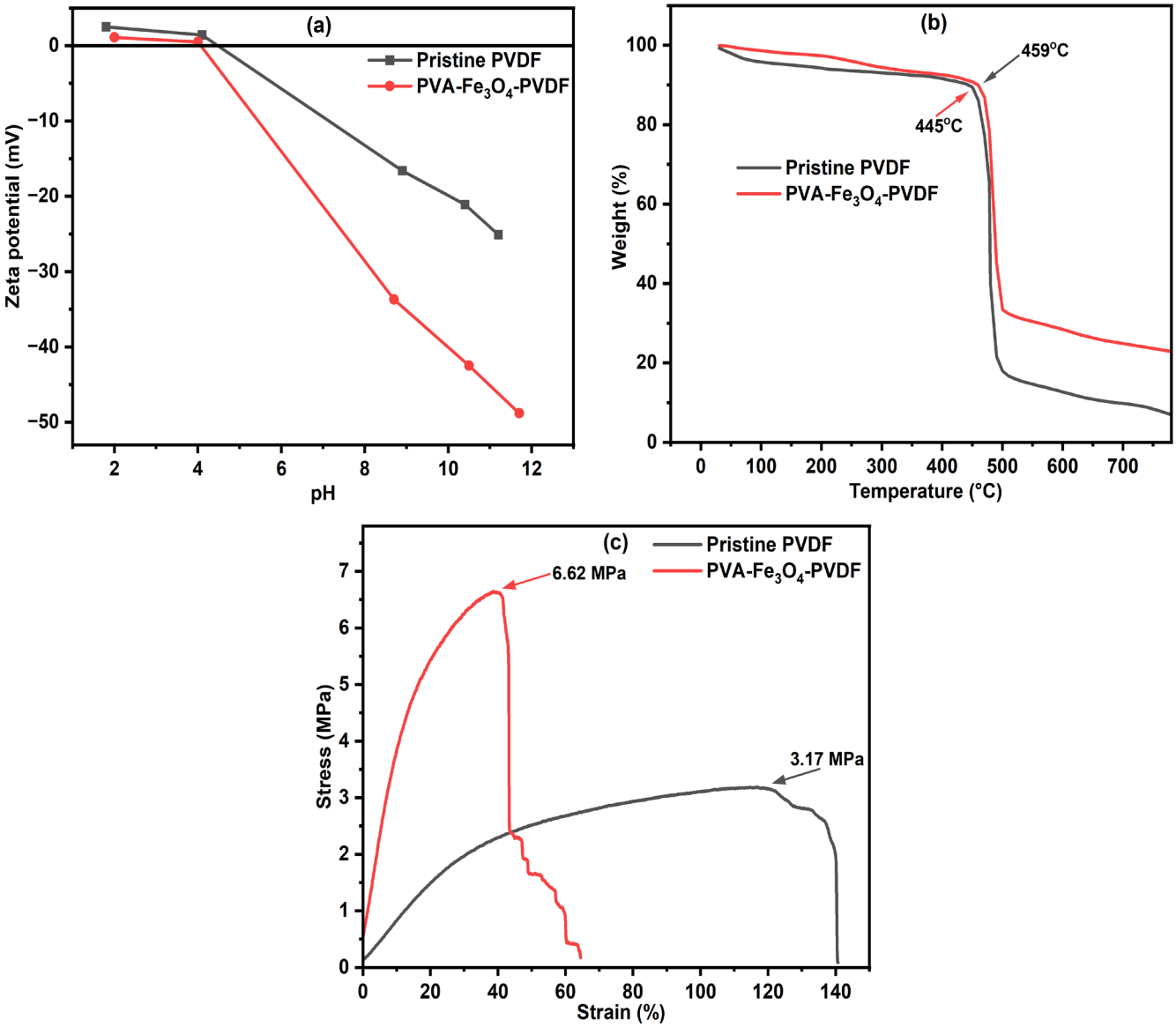


Figure 6. 6: (a) surface zeta potentials, (b) TGA curves, and (c) stress-strain curves of the pristine PVDF and PVA-Fe_3O_4-PVDF membrane.

6.5.6 Permeance flux, separation, and antifouling performance of the membrane

The short-term permeation, separation, and antifouling performance of the modified membrane was investigated using a dead-end stirred filtration cell. Filtration was performed for 180 min using DI water or synthetic BTEX water to determine the pure water flux or BTEX flux of the membrane. Figure 6. 7(a) shows that the pure water flux of the pristine membrane was 165 L/m^2h while that of the PVA-Fe_3O_4-PVDF membrane was 313 L/m^2h which signifies that the pure water flux of the modified membrane was nearly doubled. This improvement can be linked to the enhanced hydrophilicity and pore structure of the modified membrane, as previously discussed. With the modified membrane being more hydrophilic and exhibiting better pore structure, it has more affinity for water, and the water permeation resistance was reduced.

On filtering the synthetic BTEX water through the membranes, a reduced flux was obtained compared with their counterpart pure water flux. The pristine membrane has a BTEX flux of 85 L/m^2h and the BTEX flux of the PVA-Fe_3O_4-PVDF membrane was 256 L/m^2h. However, the modified membrane has a lesser flux decline of 18% while the reduction in flux for the pristine membrane was 48%. Formation of the hydration layer is a known phenomenon that occurs on the hydrophilic membrane surface during filtration and it limits the adsorption of organic contaminants on the membrane (Xiong et al., 2022). Thus, the lesser flux decline seen with the modified membrane could be attributed to the formation of a hydration layer on the membrane's surface, which minimizes the adsorption of the BTEX on the membrane, resulting in the lesser flux reduction during the BTEX water filtration. There may have been an initial deposition of the BTEX contaminants on the membrane before the formation of a stable hydration layer, which explains the decline in the BTEX flux of the modified membrane compared with its pure water flux.

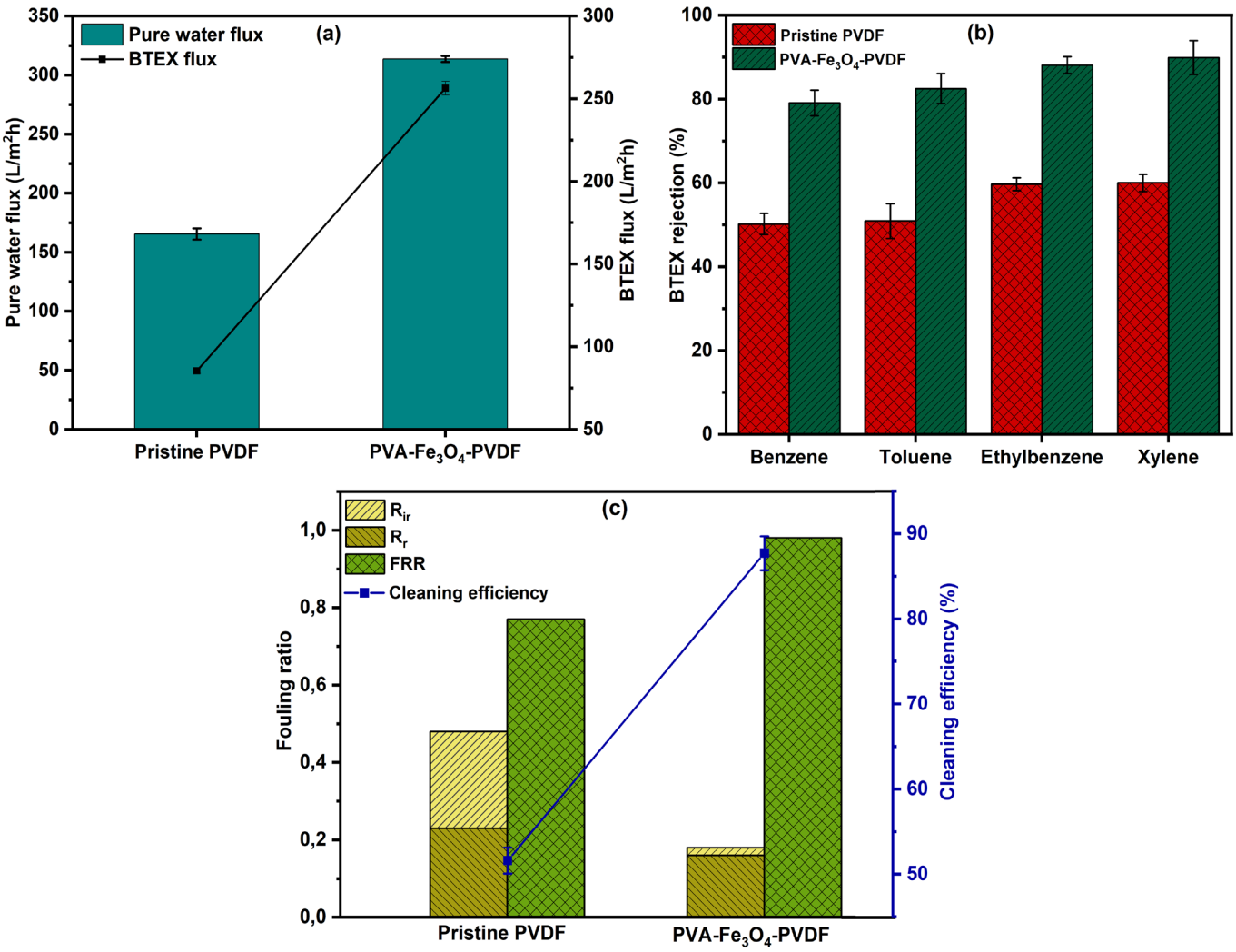


Figure 6. 7: (a) Permeate fluxes, (b) BTEX rejections, and (c) fouling ratios and cleaning efficiency of the membranes.

An improvement in the BTEX rejection was also observed for the PVA-Fe_3O_4-PVDF membrane, as depicted in Figure 6. 7(b). The hydration layer that formed on the surface of the hydrophilic-modified membrane prevented the BTEX contaminants from reaching and penetrating through the surface of the membrane, while few of the contaminants were deposited on the membrane before the formation of a stable hydration layer. Hence, the observed improvement in the BTEX rejection of the modified membrane. In addition, the BTEX rejection was observed to increase in the order of B<T<E<X, which suggests that some of the contaminants that reached the membrane might have been removed through size exclusion. This is inferred from the fact that molecular diameters of B, T, E, and X are 0.58, 0.60, 0.63, and 0.63nm, respectively (Su et al., 2016), and the rejection trend seems to correlate with the molecular size of the BTEX contaminants. Therefore, it is postulated that the hydration layer

and steric exclusion are the main separation routes that facilitated the removal of the BTEX using the modified membrane.

Figure 6. 7(c) shows the antifouling performance of the modified membrane. Compared with the pristine membrane, there was a significant improvement in the ability of the modified membrane to suppress the non-specific adsorption of the organic BTEX contaminants on the membrane, as indicated by its lesser total fouling ratio, R_t. The membrane's R_t is the sum of its reversible fouling (R_r) and irreversible fouling (R_{ir}) ratio, and the modified membrane exhibited an R_t of 0.18, of which the R_r was 0.16 while the R_{ir} was 0.02. The R_t of the pristine membrane was 0.48, of which the Rr was 0.23, and the Rir was 0.25. Thus, the antifouling propensity of the membrane improved by about 62.5% with the addition of the modifiers to the membrane. The formation of a hydration layer due to the improved hydrophilicity of the modified membrane forms a barrier between the BTEX and membrane thereby limiting the attachment of the BTEX contaminants on the membrane. When fouled, there was better ease of removing the foulants on the modified membrane through physical cleaning as indicated by its lesser R_{ir} of 0.02, compared with the R_{ir} of 0.25 for the pristine membrane. This is further established by the higher cleaning efficiency, η_c, of the modified membrane, which was found to have improved by 70% through physical cleaning using water and ultrasonic agitation of the membrane. This antifouling result can be used to make a conclusive inference that, under short-term filtration, the modified membrane can significantly resist fouling from BTEX contaminants which invariably enhances the membrane's performance.

6.5.7 Crossflow filtration performance

The long-term filtration performance of the PVA-Fe_3O_4-PVDF membrane was tested using a crossflow system to determine its operational stability in terms of the climax or limits of the membrane in regards to its BTEX flux, BTEX rejection, and reusability. Before these parameters were tested, the first crossflow experiment was conducted to determine that a stable pure water flux was achieved after compacting the membrane for 2 h. Figure 6. 8(a) depicts the pure water flux of the membrane after compaction, which shows that the pure water flux remained relatively constant throughout the 18 h filtration of DI water. Hence, any decline in BTEX flux in the subsequent BTEX filtration could be attributed to membrane fouling, as the

attachment of foulants on membranes results in a decline in their permeability (Tan et al., 2017).

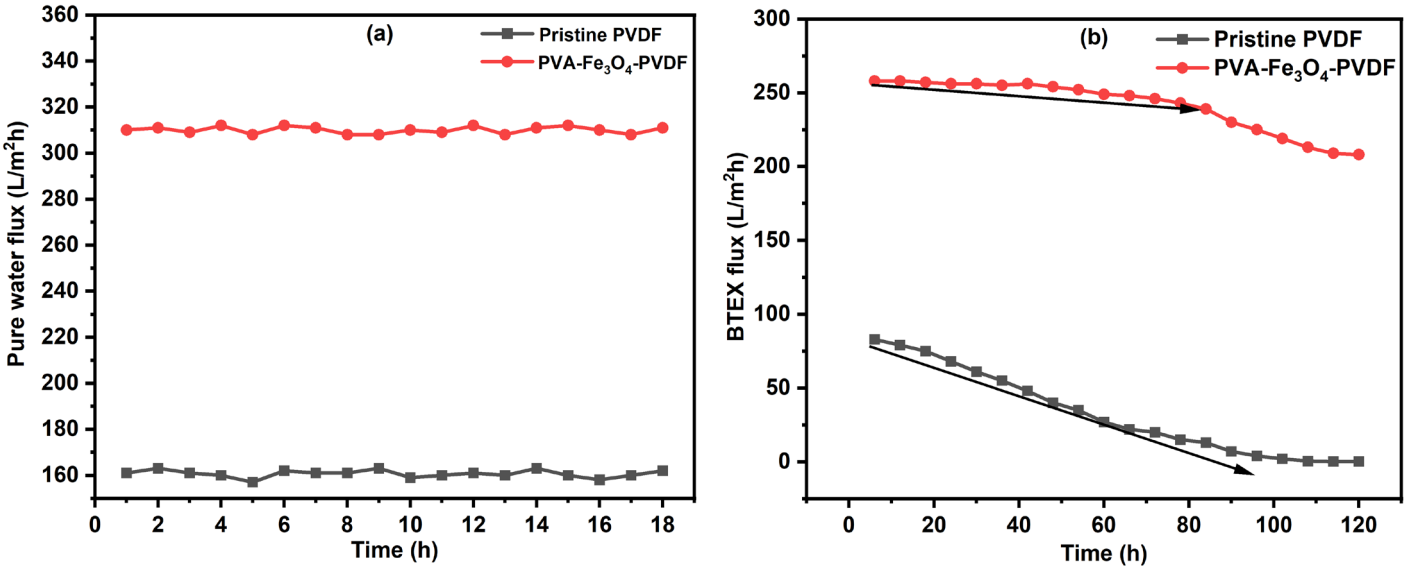


Figure 6. 8: Variation of (a) pure water flux, and (b) BTEX flux during the long-term filtration tests.

Figure 6. 8(b) shows the BTEX flux of the membrane over a 120 h filtration which indicates that the modified membrane maintained moderately the same BTEX flux for the first 84 h during the crossflow filtration, after which a steep decline in the BTEX flux is observed. This contradicts the performance of the pristine membrane, whose BTEX flux started declining from the initial stage of the filtration. The ability of the modified membrane to maintain its BTEX flux for 84 h could be ascribed to the formation of the hydration layer on the membrane surface, which prevented the deposition of the BTEX on the membrane. However, after 84 h of filtration, the feed solution might have been more saturated, resulting in more BTEX breaking through the hydration layer and depositing on the membrane. This led to the blockage or narrowing of the membrane pores by the BTEX resulting in the flux decline.

The modified membrane maintained fairly stable and high BTEX rejection throughout the long filtration process, with a slight decline in rejection as the filtration progressed, as shown in Figure 6. 9 (a-d). Considering that the rejection capacity of the modified membrane was higher than that of the pristine membrane for the entire duration, the role of the hydration layer informing an extra separation barrier on the surface of the modified membrane is further established. Thus, while the pristine membrane might have removed the BTEX through only adsorption and steric exclusion, the modified membrane used the hydration layer on its surface

as an extra barrier to achieve higher rejection. However, due to the saturation of the feed with time, the BTEX may break through the hydration layer, which results in the slight decline in rejection with time.

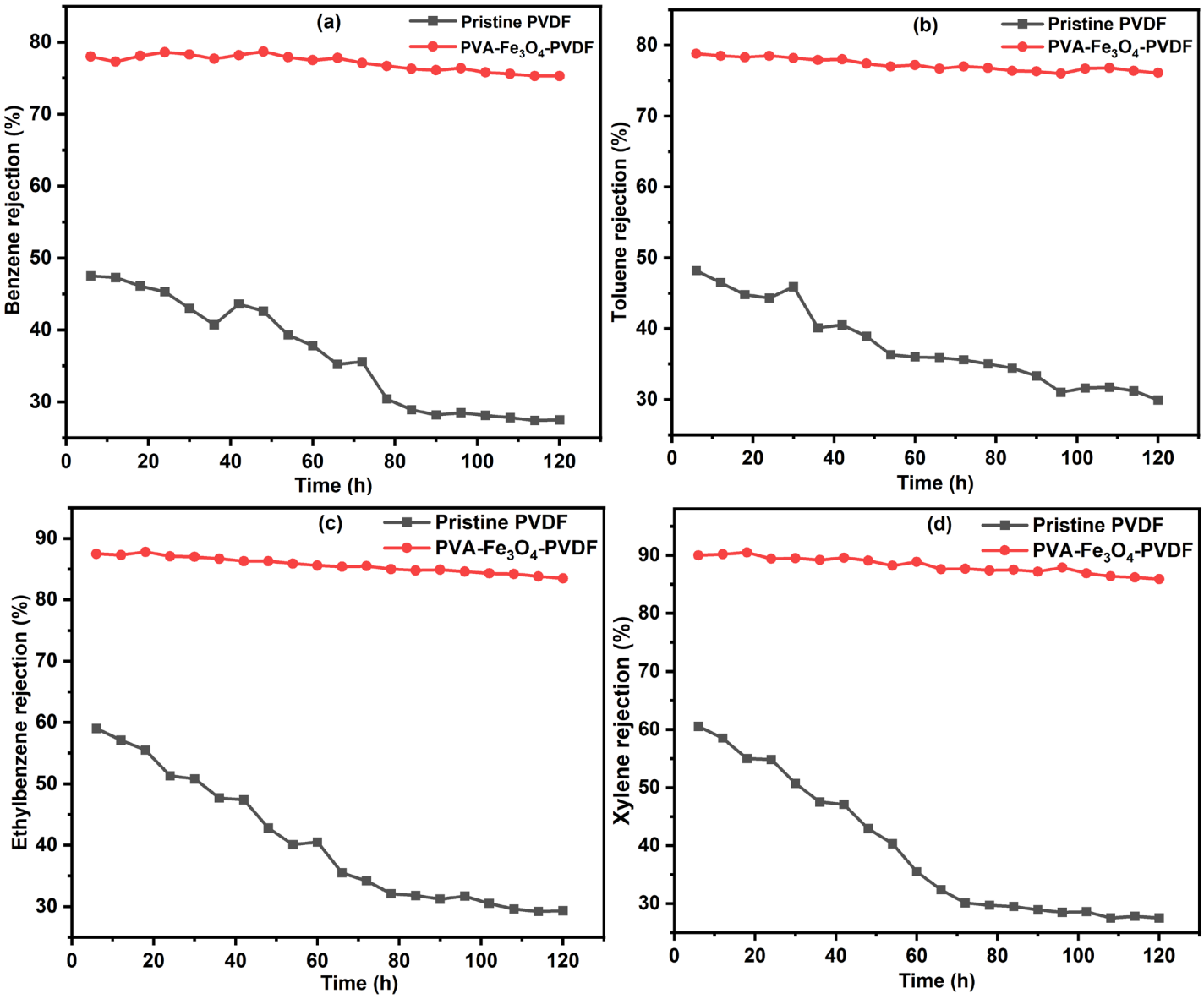


Figure 6. 9: Variation of the rejection of (a) benzene, (b) toluene, (c) ethylbenzene, and (d) xylene over long-term crossflow filtration.

The reusability of the membrane after being subjected to long-term use was assessed by physically cleaning the membrane and subjecting the cleaned membrane to another cycle of long-term BTEX filtration. The cleaning of the membrane was done by washing and backwashing with DI water for 1 h and mild ultrasonication for another 30 min. As depicted in Figure 6. 10, the BTEX flux of the modified membrane in the first cycle started at 258 L/m^{2}h, while the flux in the second cycle, after cleaning, started at 224 L/m2h, which indicates that

there was a 13% decline in BTEX flux of the membrane after performing physical cleaning of the membrane after long-term use. The decline in BTEX flux of the pristine membrane was obtained to be 47%, thus implying that the modified membrane has a lesser BTEX flux decline than the pristine membrane. Adsorption of the BTEX on the pristine membrane made its physical cleaning less effective in removing the adsorbed BTEX, meanwhile, the modified membrane had less adsorbed BTEX due to the formation of a hydration layer that reduced BTEX adsorption on the membrane. Hence, physical cleaning of the modified membrane was more effective, although the 13% BTEX flux decline shows that there is irreversible fouling that would require chemical cleaning.

Overall, the results of the long-term assessment of the membrane performance showed that the modified membrane has fairly good operational stability in the treatment of BTEX-contaminated wastewater.

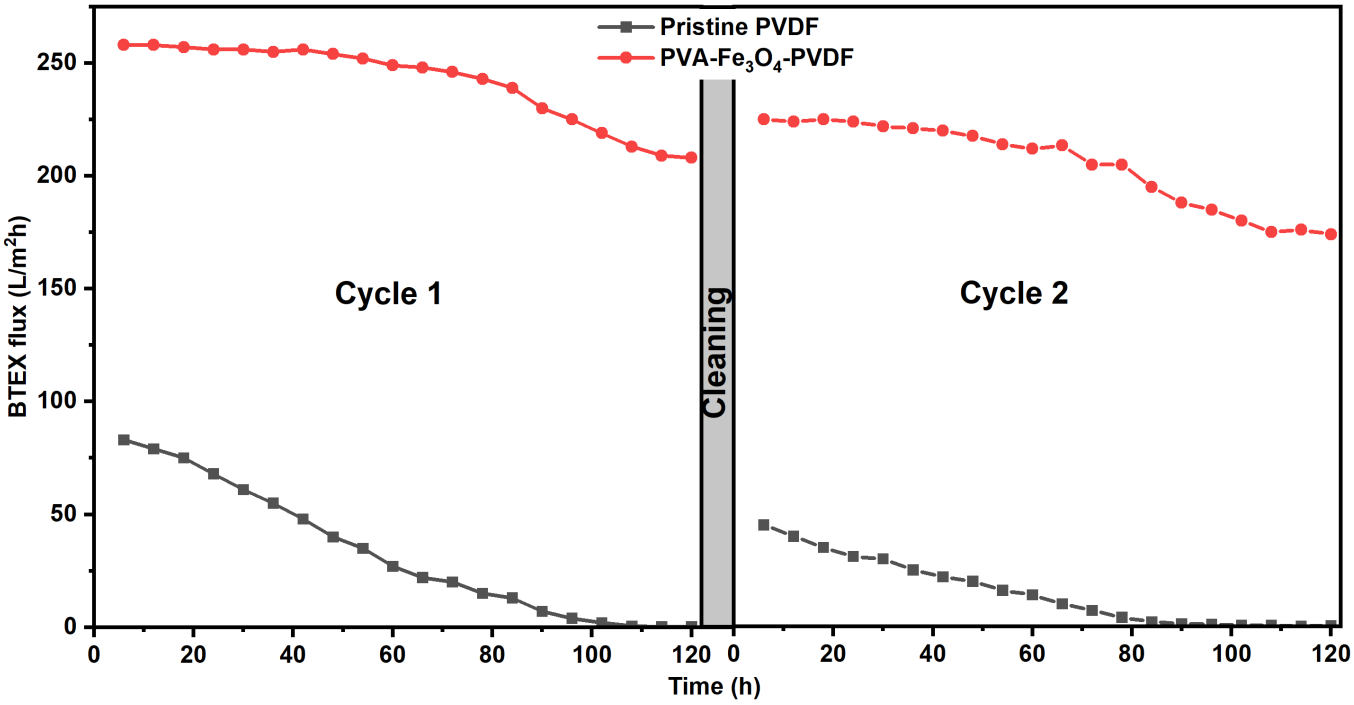


Figure 6. 10: Reusability of the membrane.

6.5.8 Stability of the modifiers in the membrane matrix

The leaching of the Fe_3O_4-NPs from the modified membrane during wastewater filtration could constitute secondary contamination of the treated water and even reduce the membrane separation performance (Esfahani et al., 2019). Thus, the stability of the Fe_3O_4-NPs in the membrane matrix was ascertained by performing the iron leaching test by measuring the concentration of iron in the filtrates collected during the long-term filtration tests. The results

indicate that the concentration of iron in the filtrates was lower than 50 ppb. Although the World Health Organization (WHO) did not provide a definitive guideline value for the permissible limit of iron in drinking water, it stated that a concentration of about 2 ppm and below poses no health risk (WHO, 2017). Hence, the results of the iron leaching test suggest that the amount of iron in the filtrate is way below the amount that could be of any health risk. This implies that the incorporated Fe_3O_4-NPs were fairly stable in the membrane matrix thereby indicating that the use of this modifier to improve the PVDF membrane poses no health concerns that could emanate from its leaching.

Figure 6. 11 (a) depicts the SEM image of the membrane after the long-term filtration test, which shows the presence of the Fe_3O_4-NPs in the membrane matrix, thus indicating that a considerable amount of the NPs remained in the membrane after the long-term filtration test. This further establishes the fairly good stability of the Fe_3O_4-NPs in the membrane matrix.

To assess the stability of the PVA in the membrane matrix, the membrane used for the long-term filtration test was thoroughly washed, dried, and analyzed using FTIR to determine its chemical composition. As depicted in Figure 6. 11(b), there was a broad peak at 3369 cm^{-1}, which is due to the O-H stretching, which confirms the presence of the hydrophilic hydroxyl group in the membrane. This suggests the presence of PVA in the membrane after the long-term filtration, thus affirming the good stability of the PVA in the membrane matrix.

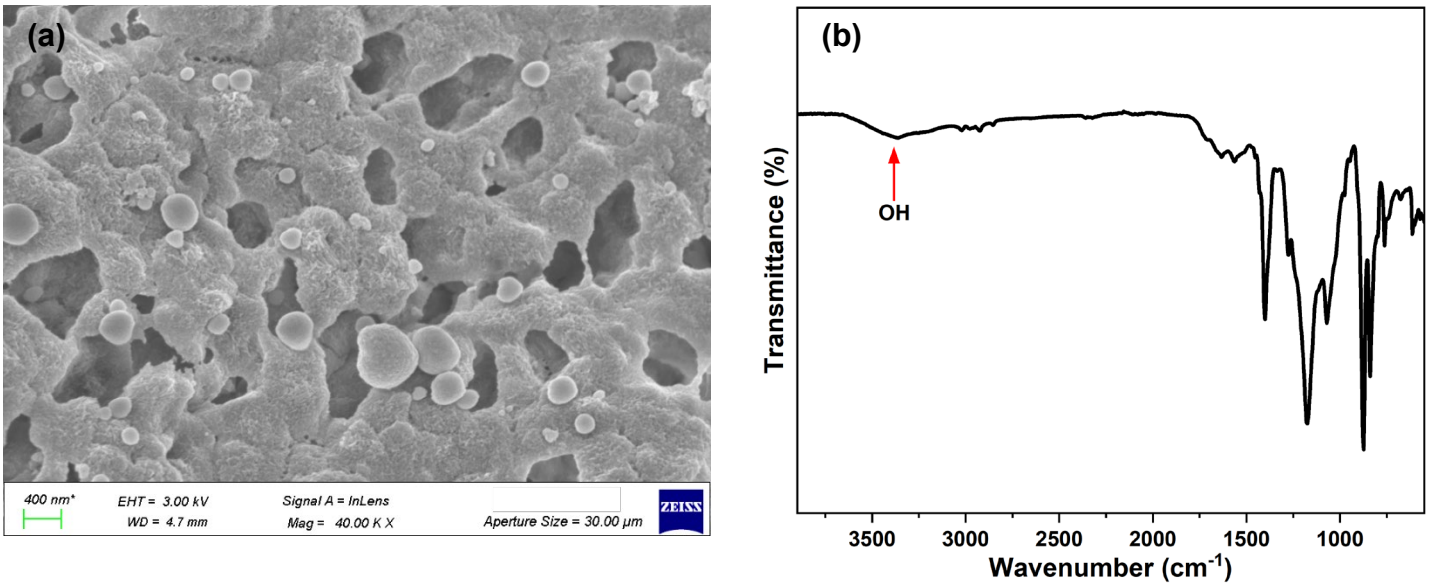


Figure 6. 11: (a) SEM image, and (b) FTIR spectrum of the PVA-Fe_3O_4-PVDF membrane after long-term filtration test.

6.6 Comparison with similar studies

Table 6.1 depicts the comparison of the performance of the PVA-Fe_3O_4-PVDF membrane with other modified membranes employed for the treatment of BTEX wastewater. Although the operating parameters used in the various studies differ, an idea of the relative performance of the membranes is outlined. The PVA-Fe_3O_4-PVDF membrane displayed a high PWF compared to the other modified membranes. In addition, the %R and FRR of the PVA-Fe_3O_4-PVDF membrane are comparatively high. Note that the %R described in Table 6.1 is the reported highest %R of any or all of the components of BTEX, that is benzene, toluene, ethylbenzene, and xylene. Summarily, the PVA-Fe_3O_4-PVDF membrane exhibited high membrane performance compared to the other studies, thereby identifying the modified membrane as a potential alternative for the treatment of BTEX-contaminated wastewater.

Table 6. 1: Comparison of the performance of the PVA-Fe_3O_4-PVDF membrane with other similar studies in the literature.

Membrane composition	PWF (L/m^2h)	%R	FRR	Ref.
Carbon nanotube/PVDF	7.1	≈ 90%	-	(Su et al., 2016)
Fe-NPs/ PES	84.73	≈ 60%	-	(Unuigbe et al., 2020b)
TA-Fe^{III}/PES	150.0	≈ 90%	-	(Makhani et al., 2022)
Fe_3O_4-NPs/PVDF	266.0	≈ 80%	≈ 80%	(Enemuo et al., 2024)
PVA/Fe_3O_4/PVDF	313.0	≈ 90%	≈ 98%	This study

6.7 Conclusion

Hybrid modifiers consisting of Biogenic-synthesized Fe_3O_4-NPs and PVA were used to modify a PVDF membrane to improve the membrane hydrophilicity and endow the membrane with antifouling ability. Subsequently, the performance of the modified membrane was enhanced as indicated by its PWF of 313 L/m^2h, BTEX flux of 256 L/m^2h, and BTEX rejection of approximately 90%. The membrane also exhibited good operational stability under long-term use, and there was no significant leaching of the incorporated modifiers from the membrane during the filtration tests. In addition, the physical features of the membrane were also improved, as shown by its higher ultimate tensile strength and thermal resistance compared to

the pristine membrane. Overall, the PVA-Fe_3O_4-PVDF membrane showed enhanced filtration, separation, and antifouling performance, thereby establishing the membrane as a potential alternative for removing BTEX from contaminated water.

References

Alzahrani, S., & Mohammad, A. W. (2014). Challenges and trends in membrane technology implementation for produced water treatment: A review. *Journal of Water Process Engineering*, *4*, 107–133. https://doi.org/10.1016/j.jwpe.2014.09.007

Amiri, S., Asghari, A., Harifi-Mood, A. R., Rajabi, M., He, T., & Vatanpour, V. (2022). Polyvinyl alcohol and sodium alginate hydrogel coating with different crosslinking procedures on a PSf support for fabricating high-flux NF membranes. *Chemosphere*, *308*, 136323. https://doi.org/10.1016/j.chemosphere.2022.136323

Barati, N., Husein, M. M., & Azaiez, J. (2021). Modifying ceramic membranes with in situ grown iron oxide nanoparticles and their use for oily water treatment. *Journal of Membrane Science*, *617*, 118641. https://doi.org/10.1016/j.memsci.2020.118641

Bulatović, S., Ilić, M., Šolević Knudsen, T., Milić, J., Pucarević, M., Jovančićević, B., & Vrvić, M. M. (2022). Evaluation of potential human health risks from exposure to volatile organic compounds in contaminated urban groundwater in the Sava river aquifer, Belgrade, Serbia. *Environmental Geochemistry and Health*, *44*(10), 3451–3472. https://doi.org/10.1007/s10653-021-01119-2

Bustillo-Lecompte, C. F., Kakar, D., & Mehrvar, M. (2018). Photochemical treatment of benzene, toluene, ethylbenzene, and xylenes (BTEX) in aqueous solutions using advanced oxidation processes: Towards a cleaner production in the petroleum refining and petrochemical industries. *Journal of Cleaner Production*, *186*, 609–617. https://doi.org/10.1016/j.jclepro.2018.03.135

Chew, N. G. P., Zhao, S., Malde, C., & Wang, R. (2017). Superoleophobic surface modification for robust membrane distillation performance. *Journal of Membrane Science*, *541*, 162–173. https://doi.org/10.1016/j.memsci.2017.06.089

Childress, A. E., & Elimelech, M. (2000). Relating Nanofiltration Membrane Performance to Membrane Charge (Electrokinetic) Characteristics. *Environmental Science & Technology*, *34*(17), 3710–3716. https://doi.org/10.1021/es0008620

Deleanu, I., Stoica, A., M., S., Dobre, L., Dobre, T., Jinga, S., & Tardei, C. (2012). Potassium sorbate release from poly(vinyl alcohol)–bacterial cellulose films. *Chemical Papers*, *66*, 138–143. https://doi.org/10.2478/s11696-011-0068-4

Delunardo, F. A. C., Paulino, M. G., Medeiros, L. C. C., Fernandes, M. N., Scherer, R., & Chippari-Gomes, A. R. (2020). Morphological and histopathological changes in seahorse (Hippocampus reidi) gills after exposure to the water-accommodated fraction of diesel oil. *Marine Pollution Bulletin*, *150*, 110769. https://doi.org/10.1016/j.marpolbul.2019.110769

Drioli, E., Ali, A., Lee, Y. M., Al-Sharif, S. F., Al-Beirutty, M., & Macedonio, F. (2016). Membrane operations for produced water treatment. *Desalination and Water Treatment*, *57*(31), 14317–14335. https://doi.org/10.1080/19443994.2015.1072585

Enemuo, N., Richards, H., & Daramola, M. O. (2024). Evaluation of the performance of Fe3O4-NPs/PVDF nanocomposite membrane for removal of BTEX from contaminated water. *Journal of Water Process Engineering*, *60*, 105185. https://doi.org/10.1016/j.jwpe.2024.105185

Esfahani, M. R., Aktij, S. A., Dabaghian, Z., Firouzjaei, M. D., Rahimpour, A., Eke, J., Escobar, I. C., Abolhassani, M., Greenlee, L. F., Esfahani, A. R., Sadmani, A., & Koutahzadeh, N. (2019). Nanocomposite membranes for water separation and purification: Fabrication, modification, and applications. *Separation and Purification Technology*, *213*, 465–499. https://doi.org/10.1016/j.seppur.2018.12.050

Ghaemi, N., Madaeni, S. S., Daraei, P., Rajabi, H., Zinadini, S., Alizadeh, A., Heydari, R., Beygzadeh, M., & Ghouzivand, S. (2015). Polyethersulfone membrane enhanced with iron oxide nanoparticles for copper removal from water: Application of new functionalized Fe3O4 nanoparticles. *Chemical Engineering Journal*, *263*, 101–112. https://doi.org/10.1016/j.cej.2014.10.103

Gissi, F., Strzelecki, J., Binet, M. T., Golding, L. A., Adams, M. S., Elsdon, T. S., Robertson, T., & Hook, S. E. (2021). A Comparison of Short-Term and Continuous Exposures in Toxicity Tests of Produced Waters, Condensate, and Crude Oil to Marine Invertebrates and Fish. *Environmental Toxicology and Chemistry*, *40*(9), 2587–2600. https://doi.org/10.1002/etc.5129

Gu, J., Ji, L., Xiao, P., Zhang, C., Li, J., Yan, L., & Chen, T. (2021). Recent Progress in Superhydrophilic Carbon-Based Composite Membranes for Oil/Water Emulsion Separation.

ACS Applied Materials & Interfaces, *13*(31), 36679–36696. https://doi.org/10.1021/acsami.1c07737

Hansen, B. H., Sørensen, L., Størseth, T. R., Nepstad, R., Altin, D., Krause, D., Meier, S., & Nordtug, T. (2019). Embryonic exposure to produced water can cause cardiac toxicity and deformations in Atlantic cod (Gadus morhua) and haddock (Melanogrammus aeglefinus) larvae. *Marine Environmental Research*, *148*, 81–86. https://doi.org/10.1016/j.marenvres.2019.05.009

Ismail, N. H., Salleh, W. N. W., Ismail, A. F., Hasbullah, H., Yusof, N., Aziz, F., & Jaafar, J. (2020). Hydrophilic polymer-based membrane for oily wastewater treatment: A review. *Separation and Purification Technology*, *233*, 116007. https://doi.org/10.1016/j.seppur.2019.116007

Ju, H., Sagle, A. C., Freeman, B. D., Mardel, J. I., & Hill, A. J. (2010). Characterization of sodium chloride and water transport in crosslinked poly(ethylene oxide) hydrogels. *Journal of Membrane Science*, *358*(1), 131–141. https://doi.org/10.1016/j.memsci.2010.04.035

Kim, J., & Van der Bruggen, B. (2010). The use of nanoparticles in polymeric and ceramic membrane structures: Review of manufacturing procedures and performance improvement for water treatment. *Environmental Pollution*, *158*(7), 2335–2349. https://doi.org/10.1016/j.envpol.2010.03.024

Kim, S., Chu, K. H., Al-Hamadani, Y. A. J., Park, C. M., Jang, M., Kim, D.-H., Yu, M., Heo, J., & Yoon, Y. (2018). Removal of contaminants of emerging concern by membranes in water and wastewater: A review. *Chemical Engineering Journal*, *335*, 896–914. https://doi.org/10.1016/j.cej.2017.11.044

Kusworo, T. D., Susanto, H., Aryanti, N., Rokhati, N., Widiasa, I. N., Al-Aziz, H., Utomo, D. P., Masithoh, D., & Kumoro, A. C. (2021). Preparation and characterization of photocatalytic PSf-TiO2/GO nanohybrid membrane for the degradation of organic contaminants in natural rubber wastewater. *Journal of Environmental Chemical Engineering*, *9*(2), 105066. https://doi.org/10.1016/j.jece.2021.105066

Kusworo, T. D., Yulfarida, M., Kumoro, A. C., Sumardiono, S., Djaeni, M., Kurniawan, T. A., Othman, M. H. D., & Budiyono, B. (2023). A highly durable and hydrophilic PVDF-MoS2/WO3-PVA membrane with visible light driven self-cleaning performance for pollutant-

burdened natural rubber wastewater treatment. *Journal of Environmental Chemical Engineering*, *11*(2), 109583. https://doi.org/10.1016/j.jece.2023.109583

Lee, S.-T., Vu, C. T., Lin, C., & Chen, K.-S. (2018). High occurrence of BTEX around major industrial plants in Kaohsiung, Taiwan. *Environmental Forensics*, *19*(3), 206–216. https://doi.org/10.1080/15275922.2018.1475432

Leusch, D. F., & Bartkow, D. M. (2010). *A short primer on benzene, toluene, ethylbenzene and xylenes (BTEX) in the environment and in hydraulic fracturing fluids*.

Li, S., Huang, X., Wan, Z., Liu, J., Lu, L., Peng, K., Schmidt-Ott, A., & Bhattarai, R. (2020). Green synthesis of ultrapure La(OH)3 nanoparticles by one-step method through spark ablation and electrospinning and its application to phosphate removal. *Chemical Engineering Journal*, *388*, 124373. https://doi.org/10.1016/j.cej.2020.124373

Li, X., Sotto, A., Li, J., & Van der Bruggen, B. (2017). Progress and perspectives for synthesis of sustainable antifouling composite membranes containing in situ generated nanoparticles. *Journal of Membrane Science*, *524*, 502–528. https://doi.org/10.1016/j.memsci.2016.11.040

Lin, Y.-C., Tseng, H.-H., & Wang, D. K. (2021). Uncovering the effects of PEG porogen molecular weight and concentration on ultrafiltration membrane properties and protein purification performance. *Journal of Membrane Science*, *618*, 118729. https://doi.org/10.1016/j.memsci.2020.118729

Liu, A., Hong, N., Zhu, P., & Guan, Y. (2018). Understanding benzene series (BTEX) pollutant load characteristics in the urban environment. *Science of The Total Environment*, *619–620*, 938–945. https://doi.org/10.1016/j.scitotenv.2017.11.184

Liu, C., Guo, Y., Zhou, Y., Yang, B., Xiao, K., & Zhao, H.-Z. (2022). High-hydrophilic and antifouling reverse osmosis membrane prepared based an unconventional radiation method for pharmaceutical plant effluent treatment. *Separation and Purification Technology*, *280*, 119838. https://doi.org/10.1016/j.seppur.2021.119838

Liu, H., Yu, H., Yuan, X., Ding, W., Li, Y., & Wang, J. (2019). Amino-functionalized mesoporous PVA/SiO2 hybrids coated membrane for simultaneous removal of oils and water-soluble contaminants from emulsion. *Chemical Engineering Journal*, *374*, 1394–1402. https://doi.org/10.1016/j.cej.2019.05.161

Liu, M.-L., Li, L., Sun, Y.-X., Fu, Z.-J., Cao, X.-L., & Sun, S.-P. (2021). Scalable conductive polymer membranes for ultrafast organic pollutants removal. *Journal of Membrane Science*, *617*, 118644. https://doi.org/10.1016/j.memsci.2020.118644

Lu, Q., Li, N., & Zhang, X. (2022). Supramolecular recognition PVDF/PVA ultrafiltration membrane for rapid removing aromatic compounds from water. *Chemical Engineering Journal*, *436*, 132889. https://doi.org/10.1016/j.cej.2021.132889

Lu, Q., Zhang, X., Hing Wong, N., Sunarso, J., & Li, N. (2022). Anti-biofouling polyvinylidene fluoride/quaternized polyvinyl alcohol ultrafiltration membrane selectively separates aromatic contaminants from wastewater by host–guest interactions. *Separation and Purification Technology*, *296*, 121387. https://doi.org/10.1016/j.seppur.2022.121387

Ma, L., Hurtado, A., Eguilior, S., & Llamas Borrajo, J. F. (2024). Acute and chronic risk assessment of BTEX in the return water of hydraulic fracturing operations in Marcellus Shale. *Science of The Total Environment*, *906*, 167638. https://doi.org/10.1016/j.scitotenv.2023.167638

Makhani, T., Sadare, O. O., Wagenaar, S., Moothi, K., Moutloali, R. M., & Daramola, M. O. (2022). Fabrication and performance evaluation of tannin iron complex (TA-FeIII/PES) UF membrane in treatment of BTEX wastewater. *Water SA*, *48*(4), Article 4.

Mamah, S. C., Goh, P. S., Ismail, A. F., Suzaimi, N. D., Yogarathinam, L. T., Raji, Y. O., & El-badawy, T. H. (2021). Recent development in modification of polysulfone membrane for water treatment application. *Journal of Water Process Engineering*, *40*, 101835. https://doi.org/10.1016/j.jwpe.2020.101835

Martínez-Cabanas, M., López-García, M., Barriada, J. L., Herrero, R., & Sastre de Vicente, M. E. (2016). Green synthesis of iron oxide nanoparticles. Development of magnetic hybrid materials for efficient As(V) removal. *Chemical Engineering Journal*, *301*, 83–91. https://doi.org/10.1016/j.cej.2016.04.149

Medeiros, L. C. C., Delunardo, F. A. C., Simões, L. N., Paulino, M. G., Vargas, T. S., Fernandes, M. N., Scherer, R., & Chippari-Gomes, A. R. (2017). Water-soluble fraction of petroleum induces genotoxicity and morphological effects in fat snook (Centropomus parallelus). *Ecotoxicology and Environmental Safety*, *144*, 275–282. https://doi.org/10.1016/j.ecoenv.2017.06.031

Mukherjee, R., & De, S. (2016). Novel carbon-nanoparticle polysulfone hollow fiber mixed matrix ultrafiltration membrane: Adsorptive removal of benzene, phenol and toluene from aqueous solution. *Separation and Purification Technology*, *157*, 229–240. https://doi.org/10.1016/j.seppur.2015.11.015

Muneron Mello, J. M., Brandão, H. L., Valério, A., de Souza, A. A. U., de Oliveira, D., da Silva, A., & de Souza, S. M. A. G. U. (2019). Biodegradation of BTEX compounds from petrochemical wastewater: Kinetic and toxicity. *Journal of Water Process Engineering*, *32*, 100914. https://doi.org/10.1016/j.jwpe.2019.100914

Munirasu, S., Haija, M. A., & Banat, F. (2016). Use of membrane technology for oil field and refinery produced water treatment—A review. *Process Safety and Environmental Protection*, *100*, 183–202. https://doi.org/10.1016/j.psep.2016.01.010

Ng, L. Y., Mohammad, A. W., Leo, C. P., & Hilal, N. (2013). Polymeric membranes incorporated with metal/metal oxide nanoparticles: A comprehensive review. *Desalination*, *308*, 15–33. https://doi.org/10.1016/j.desal.2010.11.033

Ng, Z. C., Lau, W. J., & Ismail, A. F. (2020). GO/PVA-integrated TFN RO membrane: Exploring the effect of orientation switching between PA and GO/PVA and evaluating the GO loading impact. *Desalination*, *496*, 114538. https://doi.org/10.1016/j.desal.2020.114538

Padaki, M., Surya Murali, R., Abdullah, M. S., Misdan, N., Moslehyani, A., Kassim, M. A., Hilal, N., & Ismail, A. F. (2015). Membrane technology enhancement in oil–water separation. A review. *Desalination*, *357*, 197–207. https://doi.org/10.1016/j.desal.2014.11.023

Purushothaman, M., Arvind, V., Saikia, K., & Vaidyanathan, V. K. (2022). Fabrication of highly permeable and anti-fouling performance of Poly(ether ether sulfone) nanofiltration membranes modified with zinc oxide nanoparticles. *Chemosphere*, *286*, 131616. https://doi.org/10.1016/j.chemosphere.2021.131616

Qu, J., Liu, Y., Cheng, L., Jiang, Z., Zhang, G., Deng, F., Wang, L., Han, W., & Zhang, Y. (2021). Green synthesis of hydrophilic activated carbon supported sulfide nZVI for enhanced Pb(II) scavenging from water: Characterization, kinetics, isotherms and mechanisms. *Journal of Hazardous Materials*, *403*, 123607. https://doi.org/10.1016/j.jhazmat.2020.123607

Rene, E. R., Jo, M. S., Kim, S. H., & Park, H. S. (2007). Statistical analysis of main and interaction effects during the removal of BTEX mixtures in batch conditions, using wastewater

treatment plant sludge microbes. *International Journal of Environmental Science & Technology*, *4*(2), 177–182. https://doi.org/10.1007/BF03326271

Saeedi-Jurkuyeh, A., Jonidi Jafari, A., Kalantary, R. R., & Esrafili, A. (2021). Preparation of a thin-film nanocomposite forward osmosis membrane for the removal of organic micro-pollutants from aqueous solutions. *Environmental Technology*, *42*(19), 3011–3024. https://doi.org/10.1080/09593330.2020.1720307

Saini, B., Vaghani, D., Khuntia, S., Sinha, M. K., Patel, A., & Pindoria, R. (2020). A novel stimuli-responsive and fouling resistant PVDF ultrafiltration membrane prepared by using amphiphilic copolymer of poly(vinylidene fluoride) and Poly(2-N-morpholino)ethyl methacrylate. *Journal of Membrane Science*, *603*, 118047. https://doi.org/10.1016/j.memsci.2020.118047

Sakarkar, S., Muthukumaran, S., & Jegatheesan, V. (2020). Evaluation of polyvinyl alcohol (PVA) loading in the PVA/titanium dioxide (TiO2) thin film coating on polyvinylidene fluoride (PVDF) membrane for the removal of textile dyes. *Chemosphere*, *257*, 127144. https://doi.org/10.1016/j.chemosphere.2020.127144

Samuel, O., Othman, M. H. D., Kamaludin, R., Sinsamphanh, O., Abdullah, H., Puteh, M. H., Kurniawan, T. A., Li, T., Ismail, A. F., Rahman, M. A., Jaafar, J., El-badawy, T., & Chinedu Mamah, S. (2022). Oilfield-produced water treatment using conventional and membrane-based technologies for beneficial reuse: A critical review. *Journal of Environmental Management*, *308*, 114556. https://doi.org/10.1016/j.jenvman.2022.114556

Savage, N., & Diallo, M. S. (2005). Nanomaterials and water purification: Opportunities and challenges. *Journal of Nanoparticle Research*, *7*(4), 331–342. https://doi.org/10.1007/s11051-005-7523-5

Shores, A., Laituri, M., & Butters, G. (2017). Produced water surface spills and the risk for BTEX and naphthalene groundwater contamination. *Water, Air, & Soil Pollution*, *228*(11), 435. https://doi.org/10.1007/s11270-017-3618-8

Su, F., Lu, C., & Tai, J.-H. (2016). Separation of benzene, toluene, ethylbenzene and p-xylene from aqueous solutions by carbon nanotubes/polyvinylidene fluoride nanocomposite membrane. *Journal of Water Resource and Protection*, *8*(10), Article 10. https://doi.org/10.4236/jwarp.2016.810075

Subasi, Y., & Cicek, B. (2017). Recent advances in hydrophilic modification of PVDF ultrafiltration membranes – a review: Part II. *Membrane Technology*, *2017*(11), 5–11. https://doi.org/10.1016/S0958-2118(17)30233-1

Sun, Y., Zong, Y., Yang, N., Zhang, N., Jiang, B., Zhang, L., & Xiao, X. (2020). Surface hydrophilic modification of PVDF membranes based on tannin and zwitterionic substance towards effective oil-in-water emulsion separation. *Separation and Purification Technology*, *234*, 116015. https://doi.org/10.1016/j.seppur.2019.116015

Tan, Y. H., Goh, P. S., Ismail, A. F., Ng, B. C., & Lai, G. S. (2017). Decolourization of aerobically treated palm oil mill effluent (AT-POME) using polyvinylidene fluoride (PVDF) ultrafiltration membrane incorporated with coupled zinc-iron oxide nanoparticles. *Chemical Engineering Journal*, *308*, 359–369. https://doi.org/10.1016/j.cej.2016.09.092

Unuigbe, C. F., Fayemiwo, O. M., & Daramola, M. O. (2020). Performance evaluation of iron nanoparticles infused polyethersulphone (Fe-NPs/PES) membrane during treatment of BTEX-contaminated wastewater. *Water and Environment Journal*, *34*(S1), 74–86. https://doi.org/10.1111/wej.12506

WHO. (2017). *Guidelines for drinking-water quality, 4th edition, incorporating the 1st addendum*. https://www.who.int/publications-detail-redirect/9789241549950

Williams, P. M. (2016). Membrane Charge (Zeta Potential) Effect. In E. Drioli & L. Giorno (Eds.), *Encyclopedia of Membranes* (pp. 1–2). Springer. https://doi.org/10.1007/978-3-642-40872-4_1003-1

Xiong, Z., Liu, J., Yang, Y., Lai, Q., Wu, X., Yang, J., Zeng, Q., Zhang, G., & Zhao, S. (2022). Reinforcing hydration layer on membrane surface via nano-capturing and hydrothermal crosslinking for fouling reduction. *Journal of Membrane Science*, *644*, 120076. https://doi.org/10.1016/j.memsci.2021.120076

Yalcinkaya, F., Siekierka, A., & Bryjak, M. (2017). Surface modification of electrospun nanofibrous membranes for oily wastewater separation. *RSC Advances*, *7*(89), 56704–56712. https://doi.org/10.1039/C7RA11904F

Ying, S., Guan, Z., Ofoegbu, P. C., Clubb, P., Rico, C., He, F., & Hong, J. (2022). Green synthesis of nanoparticles: Current developments and limitations. *Environmental Technology & Innovation*, *26*, 102336. https://doi.org/10.1016/j.eti.2022.102336

Ying, Y., Ying, W., Li, Q., Meng, D., Ren, G., Yan, R., & Peng, X. (2017). Recent advances of nanomaterial-based membrane for water purification. *Applied Materials Today*, *7*, 144–158. https://doi.org/10.1016/j.apmt.2017.02.010

Yu, B., Yuan, Z., Yu, Z., & Xue-song, F. (2022). BTEX in the environment: An update on sources, fate, distribution, pretreatment, analysis, and removal techniques. *Chemical Engineering Journal*, *435*, 134825. https://doi.org/10.1016/j.cej.2022.134825

Zarghami, S., Mohammadi, T., Sadrzadeh, M., & Van der Bruggen, B. (2019). Superhydrophilic and underwater superoleophobic membranes—A review of synthesis methods. *Progress in Polymer Science*, *98*, 101166. https://doi.org/10.1016/j.progpolymsci.2019.101166

Zhang, J., Wang, Q., Wang, Z., Zhu, C., & Wu, Z. (2014). Modification of poly(vinylidene fluoride)/polyethersulfone blend membrane with polyvinyl alcohol for improving antifouling ability. *Journal of Membrane Science*, *466*, 293–301. https://doi.org/10.1016/j.memsci.2014.05.006

Zhang, J., Wang, Z., Wang, Q., Ma, J., Cao, J., Hu, W., & Wu, Z. (2017). Relationship between polymers compatibility and casting solution stability in fabricating PVDF/PVA membranes. *Journal of Membrane Science*, *537*, 263–271. https://doi.org/10.1016/j.memsci.2017.05.041

Zhang, L.-P., Liu, Z., Faraj, Y., Zhao, Y., Zhuang, R., Xie, R., Ju, X.-J., Wang, W., & Chu, L.-Y. (2019). High-flux efficient catalytic membranes incorporated with iron-based Fenton-like catalysts for degradation of organic pollutants. *Journal of Membrane Science*, *573*, 493–503. https://doi.org/10.1016/j.memsci.2018.12.032

Zhang, N., Yang, N., Zhang, L., Jiang, B., Sun, Y., Ma, J., Cheng, K., & Peng, F. (2020). Facile hydrophilic modification of PVDF membrane with Ag/EGCG decorated micro/nanostructural surface for efficient oil-in-water emulsion separation. *Chemical Engineering Journal*, *402*. https://doi.org/10.1016/j.cej.2020.126200

Zhang, R., Liu, Y., He, M., Su, Y., Zhao, X., Elimelech, M., & Jiang, Z. (2016). Antifouling membranes for sustainable water purification: Strategies and mechanisms. *Chemical Society Reviews*, *45*(21), 5888–5924. https://doi.org/10.1039/C5CS00579E

Zhao, X., Zhang, R., Liu, Y., He, M., Su, Y., Gao, C., & Jiang, Z. (2018). Antifouling membrane surface construction: Chemistry plays a critical role. *Journal of Membrane Science*, *551*, 145–171. https://doi.org/10.1016/j.memsci.2018.01.039

Zheng, L., Tang, M., Wang, Y., Hou, D., Li, X., & Wang, J. (2022). A novel Cu-BTC@PVA/PVDF Janus membrane with underwater-oleophobic/hydrophobic asymmetric wettability for anti-fouling membrane distillation. *Separation and Purification Technology*, *299*, 121807. https://doi.org/10.1016/j.seppur.2022.121807

Zhong, Q., Shi, G., Sun, Q., Mu, P., & Li, J. (2021). Robust PVA-GO-TiO2 composite membrane for efficient separation oil-in-water emulsions with stable high flux. *Journal of Membrane Science*, *640*, 119836. https://doi.org/10.1016/j.memsci.2021.119836

Zuo, C., Wang, L., Tong, Y., Shi, L., Ding, W., & Li, W. (2021). Co-deposition of pyrogallol/polyethyleneimine on polymer membranes for highly efficient treatment of oil-in-water emulsion. *Separation and Purification Technology*, *267*, 118660. https://doi.org/10.1016/j.seppur.2021.118660

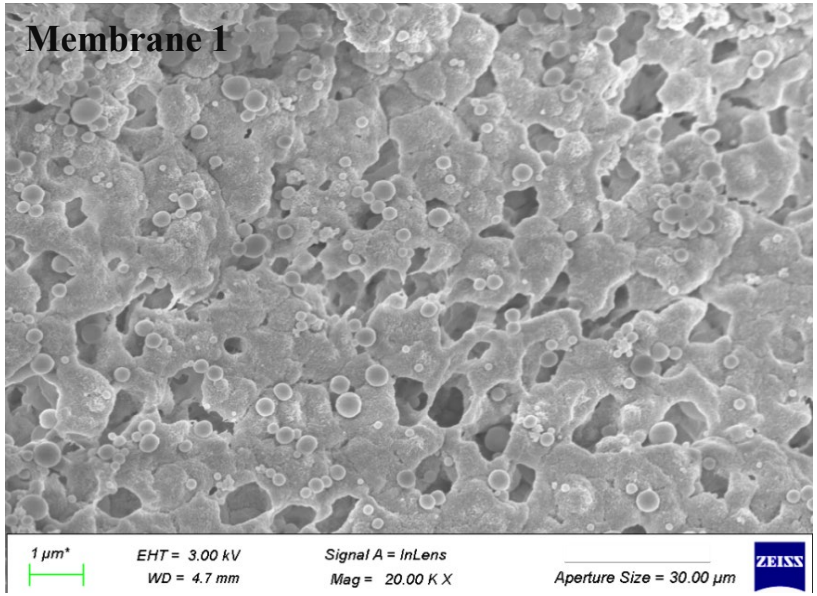
Chapter 7: Reproducibility study

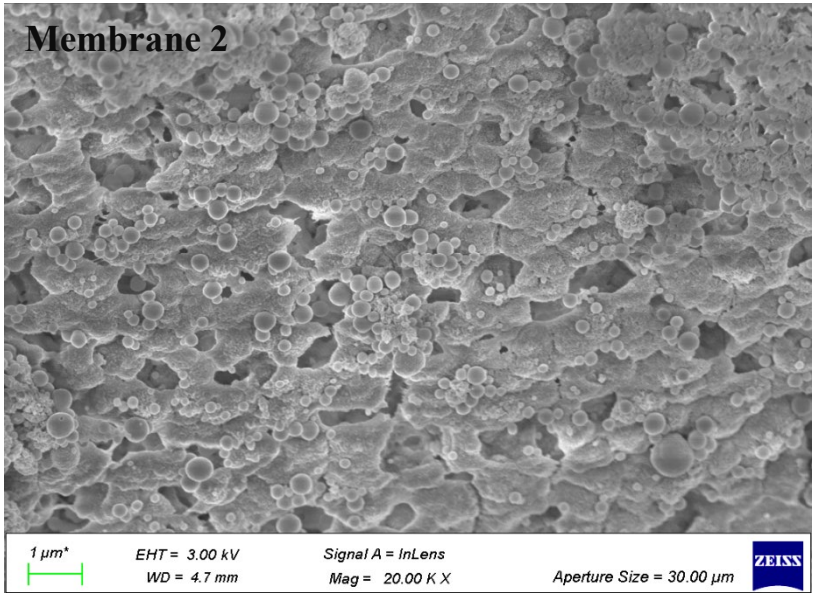
This chapter details the study performed to assess if the observed properties and performance of the PVA-Fe_3O_4-PVDF membrane can be reproduced. Hence, the results presented in this chapter highlight the possibility of obtaining the same properties and performance of the membrane as compared to the original experiments in Chapter 6.

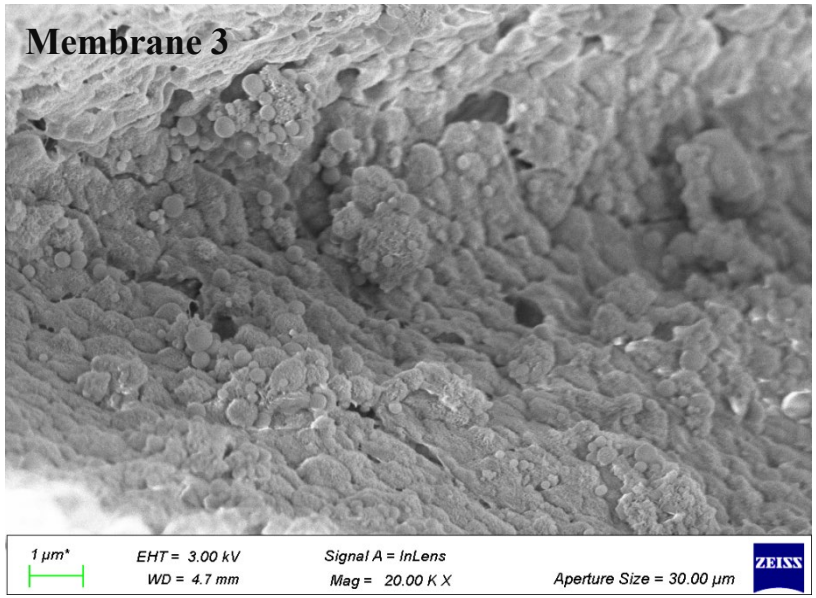
7.1 Reproducibility studies of the properties and performance of the PVA-Fe_3O_4-PVDF membrane.

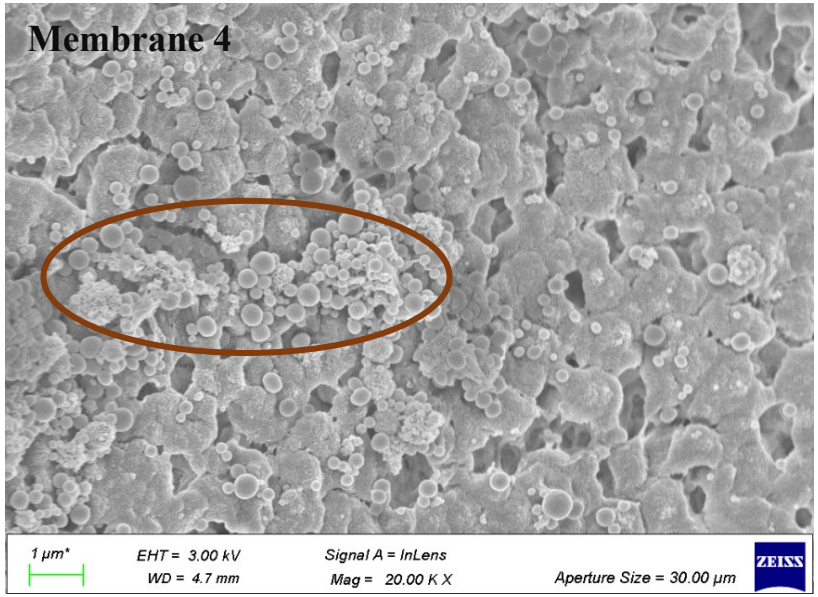
To assess the reproducibility of some of the features and performance of the PVA-Fe_3O_4-PVDF membrane, ten more of the PVA-Fe_3O_4-PVDF membrane were fabricated. Each of the membranes was fabricated at different times using the same fabrication conditions as stated in **Paper 3**, Chapter 6. The cross-section morphology of the membranes was investigated using SEM to determine the dispersion of the Fe_3O_4-NPs in the membrane. The BTEX flux and rejection were also determined for all ten membranes to compare the reproducibility of their performance.

As depicted in Figure 7. 1, the Fe_3O_4-NPs were well dispersed in the membrane matrix except for membrane 4, membrane 6, and membrane 9. Thus, out of the ten membranes tested for reproducibility in terms of the Fe_3O_4 nanoparticles dispersion, seven membranes exhibit good dispersion of the nanoparticles in the membrane matrix. This reaffirms that blending 1 wt.% of the Fe_3O_4-NPs into the PVDF membrane results in a modified membrane with fairly good dispersed nanoparticles. Agglomeration of nanoparticles in a membrane matrix negatively affects the membrane features and performance (Méricq et al., 2015). Hence, the proper dispersion of the Fe_3O_4-NPs is necessary to achieve the intended improvement in the performance of the modified membrane.

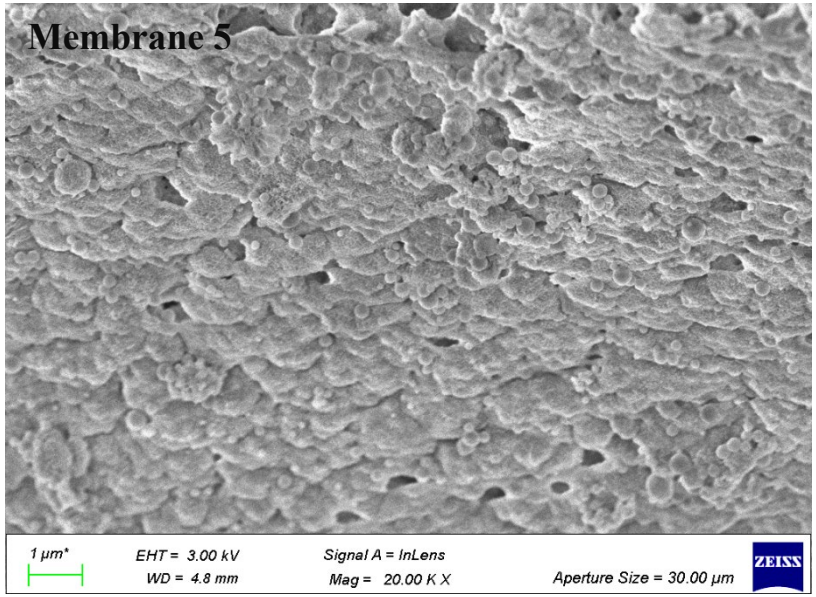

Membrane 1
1 µm*
EHT = 3.00 kV
WD = 4.7 mm
Signal A = InLens
Mag = 20.00 K X
Aperture Size = 30.00 µm
ZEISS

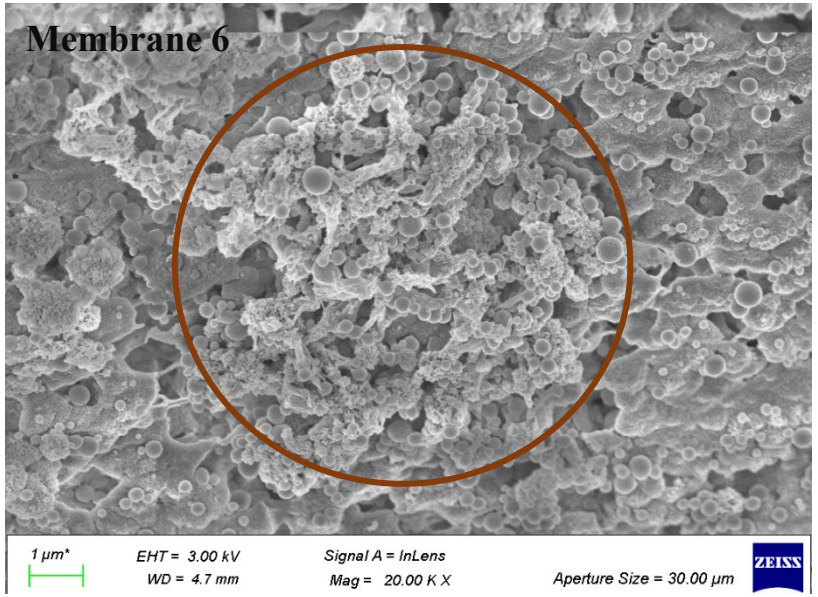

Membrane 2
1 µm*
EHT = 3.00 kV
WD = 4.7 mm
Signal A = InLens
Mag = 20.00 K X
Aperture Size = 30.00 µm
ZEISS

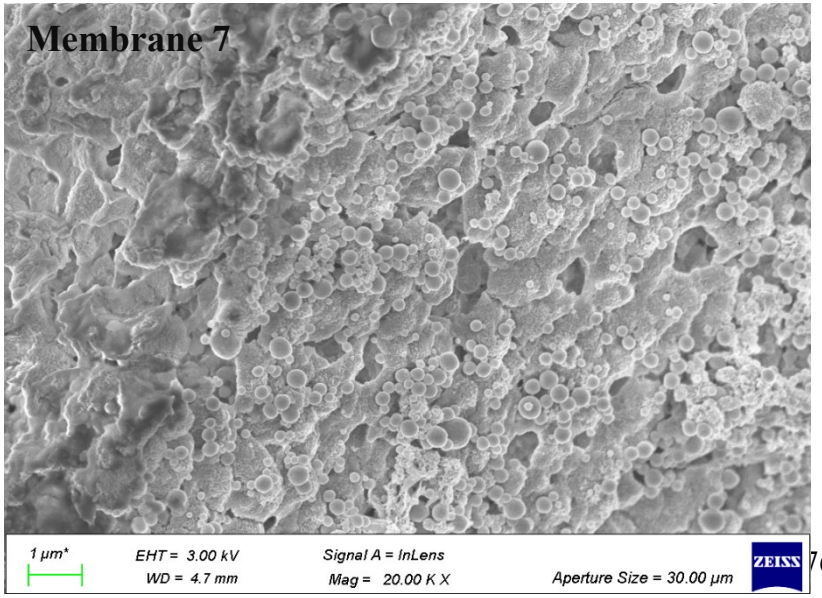

Membrane 3
1 µm*
EHT = 3.00 kV
WD = 4.7 mm
Signal A = InLens
Mag = 20.00 K X
Aperture Size = 30.00 µm
ZEISS

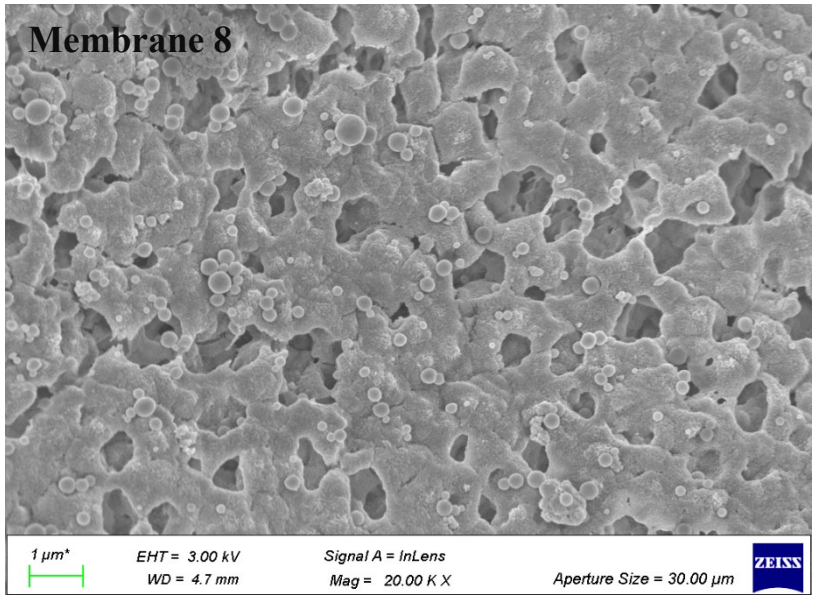

Membrane 4
1 µm*
EHT = 3.00 kV
WD = 4.7 mm
Signal A = InLens
Mag = 20.00 K X
Aperture Size = 30.00 µm
ZEISS

]


Membrane 5
1 µm*
EHT = 3.00 kV
WD = 4.8 mm
Signal A = InLens
Mag = 20.00 K X
Aperture Size = 30.00 µm
ZEISS


Membrane 6
1 µm*
EHT = 3.00 kV
WD = 4.7 mm
Signal A = InLens
Mag = 20.00 K X
Aperture Size = 30.00 µm
ZEISS


Membrane 7
1 µm*
EHT = 3.00 kV
WD = 4.7 mm
Signal A = InLens
Mag = 20.00 K X
Aperture Size = 30.00 µm
ZEISS


Membrane 8
1 µm*
EHT = 3.00 kV
WD = 4.7 mm
Signal A = InLens
Mag = 20.00 K X
Aperture Size = 30.00 µm
ZEISS

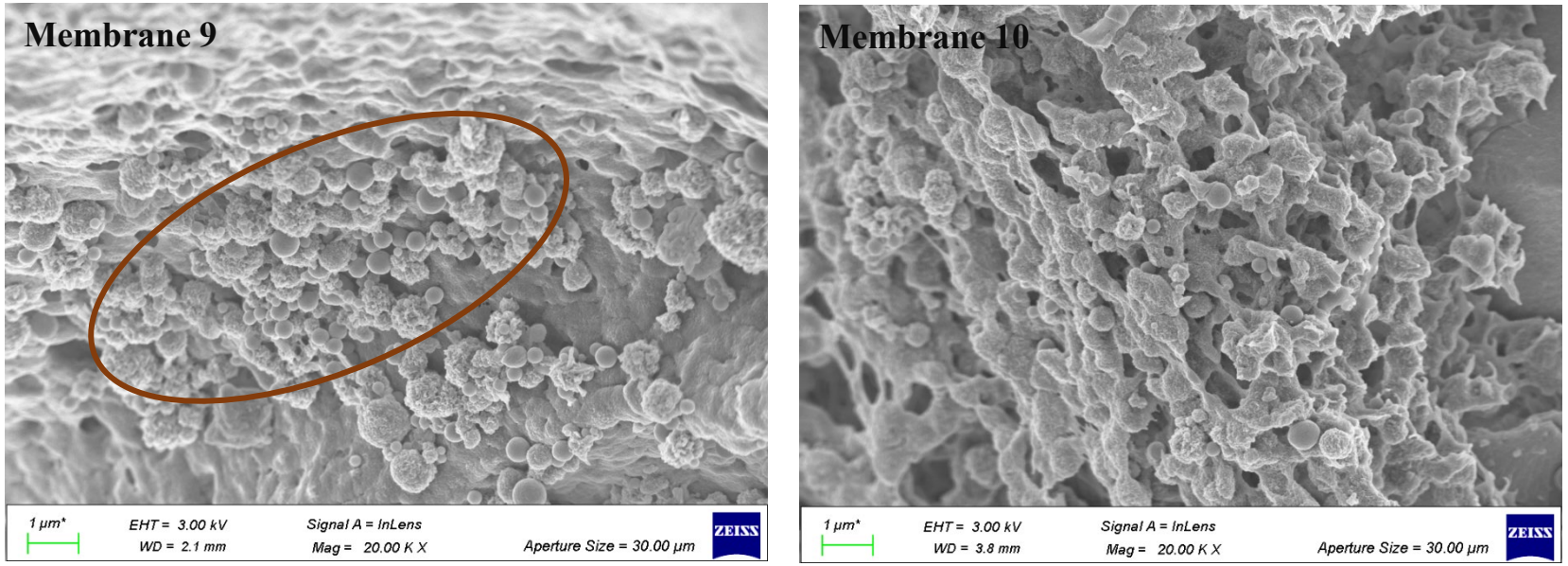


Figure 7. 1: The SEM image of the inner structure of the membranes shows the dispersion of the Fe_3O_4-NPs in the membrane matrix.

Table 7.1 shows the BTEX flux and rejection of the ten membranes tested for performance reproducibility. The BTEX flux of the PVA-Fe_3O_4-PVDF membrane used in this study was 256.33 Lm^2/h, as reported in Paper 3. As shown in Table 7.1, the ten membranes exhibit BTEX flux ranging from 205.67 Lm^2/h to 250.67 Lm^2/h, which is fairly close to the BTEX flux of the studied PVA-Fe_3O_4-PVDF membrane, which was 256.33 Lm^2/h. Membrane 3 and membrane 9 have the lowest BTEX flux of 205.67 Lm^2/h and 210.33 Lm^2/h respectively. Comparing the BTEX flux of the ten membranes, a standard deviation of 18.11 was obtained, and the coefficient of variation was 7.60%, which indicates a low variability of the obtained BTEX flux of the ten membranes.

The BTEX rejections reported in the study, as presented in Paper 3, are benzene, 79.1%, toluene, 82.5%, ethylbenzene, 88.1%, and xylene, 89.9%. A comparison of the BTEX rejection of the ten membranes depicted in Table 7.1 with the BTEX rejection of the membrane used in the study shows that the BTEX rejections are fairly close, with few exceptions. This confirms that the performance of the membranes is relatively reproducible.

Table 7. 1: The reproducibility of the performance of the membranes

Membrane ID	BTEX flux (Lm^2/h)	BTEX rejection (%)			
		Benzene	Toluene	Ethylbenzene	Xylene
Membrane 1	247.67 ± 2.52	71.2	80.1	82.6	83.9
Membrane 2	250.67 ± 3.68	67.8	80.5	81.2	81.5
Membrane 3	205.67 ± 5.69	75.7	78.0	86.5	79.2
Membrane 4	223.33 ± 2.52	77.2	76.3	80.2	83.5
Membrane 5	249.67 ± 3.06	73.5	77.0	78.3	79.7
Membrane 6	250.67 ± 3.79	76.3	81.2	80.6	89.2
Membrane 7	249.67 ± 5.86	65.6	71.5	77.5	80.3
Membrane 8	250.00 ± 2.65	69.3	73.8	80.9	82.8
Membrane 9	210.33 ± 4.16	76.1	79.2	86.6	88.4
Membrane 10	248.33 ± 3.06	78.9	79.5	81.4	82.6

CHAPTER 8: Conclusions and Recommendations

8.1 General conclusions

This study explored the development of a new antifouling nanocomposite membrane for the removal of BTEX from contaminated water by utilizing sustainable biogenic-synthesized Fe_3O_4-NPs and PVA to improve the hydrophilicity of PVDF membrane and enhanced its performance in the removal of BTEX from contaminated water. The impact of the biogenic-synthesized Fe_3O_4-NPs in BTEX removal was comprehensively studied, followed by the hydrophilic modification of PVDF membranes with the biogenic-synthesized Fe_3O_4-NPs and PVS. As a result of the modification, the hydrophilicity of the PVA-Fe_3O_4-PVDF membrane was significantly improved, which consequently minimizes the hydrophobic interaction between the membrane and the BTEX, thereby enhancing the antifouling ability of the membrane during the filtration of BTEX wastewater. Compared with the pristine membrane, the Rt of the modified membrane was reduced by about 62.5%, while the Rir was reduced by about 92%. This proves that the biogenic-synthesized Fe_3O_4-NPs and PVA are potential modifiers to fabricate an antifouling PVDF membrane in BTEX wastewater treatment. The improvement in the antifouling ability of the membrane led to improved performance of the modified membrane under both short-term use and longer-term application. The longer-term application of the membrane shows that the PVA-Fe_3O_4-PVDF membrane has relatively good operational stability as the membrane can maintain its BTEX flux for 84 h without any significant flux decline.

Testing the reproducibility of some of the features and performance of the modified membrane indicates that the membrane has good reproducibility. This was inferred from the SEM images of the membrane, which showed that most of the refabricated membranes have good dispersion of the Fe_3O_4-NPs in the membrane matrix. Thus, out of the ten re-fabricated membranes, only three showed agglomeration of the Fe_3O_4-NPs in the membrane matrix. The BTEX flux and BTEX rejection of the re-fabricated membranes also showed that there is a fairly good correlation between their performance results.

Overall, the biogenic-synthesized Fe_3O_4-NPs proved to be potential materials for enhancing a PVDF membrane, and the synergistic impact of both biogenic-synthesized Fe3O4-NPs and PVA results in an antifouling and operationally stable PVDF membrane.

8.2 Recommendations

With reference to the procedures and outcomes of this study, the following recommendations are made:

Biogenic synthesis of nanoparticles could provide an easier and more sustainable approach to generating hydrophilic modifiers for membrane modifications; hence, it is recommended that bio-reductants should be mainly used for the synthesis of nanoparticles for membrane modifications.

Although the PVA-Fe_3O_4-PVDF membrane is promising for treating synthetic BTEX wastewater, it is vital that its performance is tested using real wastewater containing BTEX contaminants, especially petroleum-based wastewater. By doing so, the membrane's applicability for commercial purposes will be established.

This study was conducted using lab-scale operations settings. To commercialize the membrane, the fabrication should be scaled up, and large-scale membrane performance assessments should be conducted to determine its possible use in industries as a BTEX wastewater treatment alternative.

Appendix

Author copyright permissions.

All copyright permissions of the images used in this thesis were obtained from Copyright Clearance Center.

A.1: Copyright Clearance Center permission for Figure 2.4.

ELSEVIER LICENSE
TERMS AND CONDITIONS

Aug 20, 2024

This Agreement between Ngozi Enemuo ("You") and Elsevier ("Elsevier") consists of your license details and the terms and conditions provided by Elsevier and Copyright Clearance Center.

License Number	5853320324382
License date	Aug 20, 2024
Licensed Content Publisher	Elsevier
Licensed Content Publication	Journal of Molecular Liquids
Licensed Content Title	A review on adsorptive removal of oil pollutants (BTEX) from wastewater using carbon nanotubes
Licensed Content Author	Hirra Anjum,Khairiraihanna Johari,Nirmala Gnanasundaram,Magesh Ganesapillai,Appusamy Arunagiri,Iyyaswami Regupathi,Murugesan Thanabalan
Licensed Content Date	Mar 1, 2019
Licensed Content Volume	277
Licensed Content Issue	n/a
Licensed Content Pages	21
Start Page	1005
End Page	1025
Type of Use	reuse in a thesis/dissertation

A.2: Copyright Clearance Center permission for Figure 2.5.

ELSEVIER LICENSE
TERMS AND CONDITIONS

Aug 20, 2024

This Agreement between Ngozi Enemuo ("You") and Elsevier ("Elsevier") consists of your license details and the terms and conditions provided by Elsevier and Copyright Clearance Center.

License Number	5853340316345
License date	Aug 20, 2024
Licensed Content Publisher	Elsevier
Licensed Content Publication	Desalination
Licensed Content Title	A comprehensive review on anti-fouling nanocomposite membranes for pressure driven membrane separation processes
Licensed Content Author	Jainesh H. Jhaveri,Z.V.P. Murthy
Licensed Content Date	Feb 1, 2016
Licensed Content Volume	379
Licensed Content Issue	n/a
Licensed Content Pages	18
Start Page	137
End Page	154
Type of Use	reuse in a thesis/dissertation

A.3: Copyright Clearance Center permission for Figure 2.6.

ELSEVIER LICENSE
TERMS AND CONDITIONS

Aug 20, 2024

This Agreement between Ngozi Enemuo ("You") and Elsevier ("Elsevier") consists of your license details and the terms and conditions provided by Elsevier and Copyright Clearance Center.

License Number	5853350432306
License date	Aug 20, 2024
Licensed Content Publisher	Elsevier
Licensed Content Publication	Separation and Purification Technology
Licensed Content Title	Nanocomposite membranes for water separation and purification: Fabrication, modification, and applications
Licensed Content Author	Milad Rabbani Esfahani,Sadegh Aghapour Aktij,Zoheir Dabaghian,Mostafa Dadashi Firouzjaei,Ahmad Rahimpour,Joyner Eke,Isabel C. Escobar,Mojtaba Abolhassani,Lauren F. Greenlee,Amirsalar R. Esfahani,Anwar Sadmani,Negin Koutahzadeh
Licensed Content Date	Apr 15, 2019
Licensed Content Volume	213
Licensed Content Issue	n/a
Licensed Content Pages	35
Start Page	465
End Page	499